Novel Reactivity at Iron Centers Supported by Poly(phosphino)borate Ligands

Thesis by

Christine Marie Thomas

In partial fulfillment of the requirements for the degree of Doctor of Philosophy

California Institute of Technology

Pasadena, California

2006

(Defended May 8, 2006)

Acknowledgements

First and foremost I would like to thank my research advisor, Professor Jonas C. Peters, without whom I never would have made it this far. Over the years Jonas has managed to push me above and beyond what I thought I was capable of as a scientist. His enthusiasm for chemistry, his creativity (see below), and his talent and intuition as a synthetic chemist have helped me to become the "synthetic all-star" that I am. Through his guidance I have truly grown immensely both as a scientist and as a person. I thank him for continuing to have confidence in me even when I lacked confidence in myself and for giving me a chance when times were tough. I would also like to thank the other members of my committee–Professor Brian M. Stoltz, Professor Robert H. Grubbs, and Professor Jacqueline K. Barton–for keeping me on track and helping me prepare for my own independent academic career. In addition, I am forever indebted to Professor Chip Nataro for introducing me to the field of inorganic chemistry and for preparing me for my graduate studies in this field.

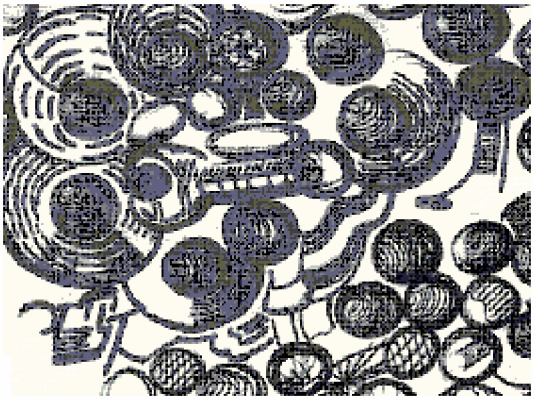

I have had the pleasure of working with some fantastic people in the Peters Group over the years. Graduate school would not have been the same without the support and camaraderie of this unique group of individuals. First, I would like to say thank you to

Kathleen Hand for keeping her candy dish full, for displaying my fine artwork on her refrigerator, and for keeping the group functioning on a daily basis. I wish her, Russell, and "Knight Rider" all the best in the years to come. The original Peters Group played the most integral part in my first few years at Caltech. Ted Betley, Seth "Powder" Harkins and Steve Brown were, and still are, always willing to help keep me on track both inside and outside of the lab. I don't have older brothers, but they're probably the closest thing. Chris "The Curmudgeon" Thomas was a fantastic mentor during my first few years and was always willing to help out "Chris Thomas the girl" (our names were always a good source of amusement, too). I'm forever grateful to Cora Macbeth for her positive attitude, her confidence in me, and her career advice. David Jenkins and Claire Jacobs were always a pleasure to have around in the office. Connie Lu has truly been there with me through it all, and I wish her all the best as she finishes up and moves on to "a better place." Although I was sad to see her go, I'm very grateful to Erin Daida–many of her preliminary results served to jump-start my graduate career. Matt "Sister" Whited has been a great friend to have around and is personally responsible for keeping the Peters Group caffeinated. For both, I am very grateful and I wish him all the best success in the rest of his graduate career and beyond. I would also like to thank the post-docs who have come through the group and helped to greatly broaden the group's knowledge and expertise: Dr. Bruce MacKay, Dr. Mark Mehn, Dr. Phillip Collier, Dr. Eric Rivard, Dr. Xile "E-xile" Hu, and Dr. Arjun Mendiratta. To the newest members of Team Peters–Valerie Scott, Alex Miller, Caroline Saouma and Jillian Dempsey–it's been wonderful getting to know you, I wish you all the best, and please don't hesitate to call or e-mail me

if you need to talk chemistry. To Valerie: I hope that we can continue to enjoy rubber policemen and 3-way stopcocks even when I'm far away from the cockpit.

Last, but certainly not least, I would like to thank the best person I've ever shared my box with (that's what she said), Neal Mankad: I idolize you to nuts. I still have no idea what this means, but working with such a talented and responsible person has truly been a pleasure. Thanks for all the time and effort you spent mounting my unruly, thermally unstable crystals (see above). It's been great sharing both lab and office space with someone who I get along with so well. I've found very few people over the years that I can tolerate for long periods of time, and I'm certainly glad you're one of them. "I'm not going to lie to you"… you've played a major role in making my last two years in the lab both productive and enjoyable.

Several individuals have provided technical assistance during my graduate career. I would like to acknowledge Neal Mankad, Larry Henling, Mike Day, and Ted Betley for their help with X-ray crystallography. Dr. Angelo Di Bilio and Dr. Mark Mehn assisted with EPR spectroscopy. Although my time working in the NMR facility with Dr. Scott Ross was brief, he taught me quite a bit about NMR maintenance and advanced techniques, and I am grateful to him for that. For insightful discussions about chemistry and for assisting in the collection of fluorescence data, I would like to thank Brian Leigh.

Lastly, thank you to Eleno, Mateo, George, and Aurelia (the wait-staff at Amigos') for providing ample libations.

For making my life outside of the lab (gasp!) enjoyable, I would like to thank all of my friends outside of the Peters Group: all three of them. In addition to providing some unforgettable memories, I thank Jason "The Texas Teacup" Keith, Nathan "The Dread Pirate" Lundblad, and Sarah "Drags" Dragsten for being there for me during some of my most trying years. Thank you Ben Roethlisberger for returning my e-mails, for leading the Steelers to victory, and for making a "got milk" ad so that you could watch over me while I wrote my thesis. In addition I'm grateful to the women of the Oxy Olde Girls Rugby Club and the men of the Caltech Rugby Football Club for providing an outlet for the pent-up aggression that comes naturally in the later years of graduate school.

Lastly, I need to thank my family for their love and support. I am particularly grateful to my parents, John and Nancy Thomas, for raising me with some sort of innate work ethic and sense of ambition and for giving me the independence to follow the path I've chosen. And thanks Mom for sending care packages!

Abstract

The reactivity of the iron(II) alkyl species $[PhBP^{iPr}_3]FeMe$ ($[PhBP^{iPr}_3]$ = $PhB(CH_2P^iPr_2)_3^-$) towards Si-H bonds is presented. Reaction of $[PhBP^{iPr}_3]FeMe$ with primary aryl silanes results in the unusual η^3 silane adducts $[PhBP^{iPr}_3]Fe(H)(\eta^3\text{-}H_2SiMeR)$. X-ray crystallography, Mössbauer spectroscopy, and theoretical calculations confirm this structural assignment; however, solution NMR experiments suggest a degree of fluxionality in solution.

Low valent, tris(phosphino)borate iron platforms have been shown to facilitate the activation of white phosphorus, P_4. The iron(I) precursors $\{[PhBP^{iPr}_3]Fe\}_2(\mu\text{-}N_2)$ and $[PhBP^{Ph}_3]Fe(PPh_3)$ react with P_4 to quantitatively generate $\{[PhBP^{iPr}_3]Fe\}_2(\mu\text{-}P_4)$ and $\{[PhBP^{Ph}_3]Fe\}_2(\mu\text{-}P_4)$, respectively. These unique iron(II) dimers bridged by square P_4^{2-} units have been characterized structurally and spectroscopically, and their reactivity has been examined. A simplified electronic structure calculation is presented to aid in discussion of bonding within these complexes.

Motivated by the versatility of the tris(phosphino)borate ligands, a new family of tripodal hybrid bis(phosphino)pyrazolylborate ligands, $[PhBP^{tBu}_2(pz')]^-$ ($[PhBP^{tBu}_2(pz')]^-$ = $PhB(CH_2P^tBu_2)_2(pz')^-$), has been prepared and characterized. The synthesis, spectroscopy, and solid-state structures of four-coordinate, pseudo-tetrahedral iron(II) and cobalt(II) halide complexes supported by these ligands is presented. To compare the electron-releasing ability of these ligands with their $[PhBP^R_3]$ analogues, the cyclic voltammetry of these complexes is introduced. Potential routes to a terminal cobalt or iron nitride complex via extrusion of N_2 from coordinated azide and metathesis with the N-atom transfer reagent Li(dbabh) are investigated.

Reduction of the [PhBP$^{tBu}_2$(pz')]MX halide complexes in the presence of excess phosphine generates low valent [PhBP$^{tBu}_2$(pz')]M^{I}(PMe$_3$) precursors. These precursors react with organic azides to generate cobalt(III) and iron(III) imides. Initial reactivity studies indicate that these imides are more moderately more reactive than the corresponding tris(phosphino)borate complexes. The electrochemistry of the [PhBP$^{tBu}_2$(pz')]Fe^{III}(NR) imides features a quasi-reversible to fully reversible oxidation event, dependent on choice of pyrazolyl substituents and scan rate. This oxidation can be achieved chemically to generate the isolable cationic iron(IV) imides, [PhBP$^{tBu}_2$(pz')]Fe^{IV}(NR)$^{+}$. The structural and spectroscopic characterization of these highly unusual complexes is discussed.

Table of Contents

List of Figures

Chapter 1.

Chapter 2.

Chapter 3.

Chapter 4.

List of Tables

Chapter 2.

Chapter 3.

Chapter 4.

Chapter 5.

Appendix A.

Appendix B.

List of Abbreviations and Nomenclature

$[PhBP^{Ph}_3]$	$[PhB(CH_2PPh_2)_3]^-$
$[PhBP^{iPr}_3]$	$[PhB(CH_2P^iPr_2)_3]^-$
$[PhBP^{R}_3]$	$[PhB(CH_2PR_2)_3]^-$ where R is the phosphine substituents
$[PhBP^{tBu}_2(pz)]$	$[PhB(CH_2PR_2)_2(pz)]^-$
$[PhBP^{tBu}_2(pz^{tBuPh})]$	$[PhB(CH_2PR_2)_2(pz^{tBuPh})]^-$
$[PhBP^{tBu}_2(pz^{Me2})]$	$[PhB(CH_2PR_2)_2(pz^{Me2})]^-$
$[PhBP^{tBu}_2(pz')]$	general bis(phosphino)pyrazolylborate ligand
Cp	cyclopentadienyl
Cp^*	pentamethylcyclopentadienyl
$[PhTt^{tBu}]$	$PhB(CH_2S^tBu)_3$
[Tp]	general hydrotris(pyrazolyl)borate ligand
[Tp*]	$[HB(3,5\text{-}Me_2pz)_3]^-$
$[(4\text{-}BPh_3)bpy]$	2,2'-bipyridylborate
$[Ph_2B(pz)_2]$	diphenylbis(pyrazolyl)borate
$[Ph_2BP_2]$	$[Ph_2B(CH_2PPh_2)_2]^-$
$[Ph_2SiP_2]$	$Ph_2Si(CH_2PPh_2)_2$
$[Ph_3BP^{p\text{-}iPr}_2]$	$[Ph_3B(p\text{-}C_6H_4P^iPr_2)]^-$
$[Ph_3BP^{m\text{-}iPr}_2]$	$[Ph_3B(m\text{-}C_6H_4P^iPr_2)]^-$
$[Ph_3BP^{p\text{-}Ph}_2]$	$[Ph_3B(p\text{-}C_6H_4PPh_2)]^-$
$[Ph_3BP^{m\text{-}Ph}_2]$	$[Ph_3B(m\text{-}C_6H_4PPh_2)]^-$
$[Ph_3BP']$	general monodentate triphenyl(arylphosphino)borate
$Ph_3SiP^{p\text{-}iPr}_2$	$Ph_3Si(p\text{-}C_6H_4P^iPr_2)$

$Ph_3SiP^{p\text{-}Ph}{}_2$	$Ph_3Si(p\text{-}C_6H_4PPh_2)$
$PhBP^{iPr}{}_2$	$PhB(CH_2P^iPr_2)_2$
$PhBP^{tBu}{}_2$	$PhB(CH_2P^tBu_2)_2$
$\{^1H\}$	hydrogen-1 decoupled
°	degrees, in measure of angles
°C	degrees Celsius
^1H	hydrogen-1
^{11}B	boron-11
^{19}F	fluorine-19
^{29}Si	silicon-29
^{31}P	phosphorus-31
Å	Angstrom, 10^{-10} m
Ac	acetate, $-COCH_3$
ACN	acetonitrile
Ad	1-adamantyl
ADP	adenosine diphosphate
Anal. Calcd.	elemental analysis calculated
Ar_F	$3,5\text{-}(CF_3)_2\text{-}C_6H_3$
av	average
ASN	5-azonia-spiro[4.4]nonane
atm	atmosphere
ATP	adenosine triphosphate
B	magnetic field strength

B3LYP	Becke three-parameter function with Lee-Yang-Parr correlation
bpy	2,2'-bipyridine
br	broad
^{n}Bu	*n*-butyl
^{t}Bu	*tert*-butyl
C_{3v}, C_s	Schoenflies symmetry designations
C_6D_6	benzene-d_6
$CDCl_3$	chloroform-*d*
C_6H_6	benzene
cm	centimeter(s)
cm^{-1}	inverse centimeters or wavenumbers
cm^3	cubic centimeters
COD	cyclooctadiene
cont'd.	continued
CV	cyclic voltammetry or cyclic voltammogram
Cy	cyclohexyl
d	doublet
d^n	d-electron count of n-electrons for a transition metal
d_n	metal d-orbital of n-symmetry
D_{calcd}	calculated density
dba	dibenzylideneacetone
dbabh	2,3:5,6-dibenzo-7-aza bicycle[2.2.1]hepta-2,5-diene
dd	doublet of doublets

deg	degree(s)
DFT	density functional theory
dt	doublet of triplets
e	pair of degenerate metal d orbitals
e^-	electron(s)
E	an atom or functional group forming a metal-ligand multiple bond
EPR	electron paramagnetic resonance
equiv	equivalents
Et	ethyl, $–CH_2CH_3$
ESI/MS	electrospray ionization mass spectrometry
etriphos	$CH_3C(CH_2PEt_2)_3$
eV	electron volt(s)
EXAFS	Extended X-ray Absorption Fine Structure spectroscopy
Fc	ferrocene, Cp_2Fe
Fc^+	ferrocenium, Cp_2Fe^+
Fw	formula weight
g	gram(s)
G	Gauss
GC/MS	gas chromatography mass spectrometry
GHz	gigahertz
g	g-factor
h	hour(s)
H	applied magnetic field

HF	Hartree-Fock
HMQC	Heteronuclear Multiple Quantum Coherence
HOMO	highest occupied molecular orbital
Hz	hertz
IR	infrared
$^{n}J_{A\text{-}Z}$	in NMR spectroscopy, coupling constant between nuclei A and Z over n bonds (n, A, or Z omitted if not known)
J_{obs}	in NMR spectroscopy, observed coupling constant
K	degrees in Kelvin
k_H/k_D	kinetic isotope effect
L	dative ligand for a transition metal
LACVP	Los Alamos core valence potential
LUMO	lowest unoccupied molecular orbital
m-	*meta* position of an aryl ring
m	multiplet
M	general transition metal
M^n	general transition metal in the n oxidation state
Me	methyl, $-CH_3$
Mes	mesityl, $-C_6H_2(CH_3)_3$
mg	milligram(s)
MHz	megahertz, 10^6 Hertz
min	minute(s)
mL	milliliter(s)

MLCT	metal to ligand charge transfer
mm	millimeter(s)
mmol	millimole(s)
MO	molecular orbital
mol	mole(s)
MS	mass spectrometry
mT	millitesla(s)
mV	millivolt(s)
m/z	mass per charge
NBD	norbornadiene
NBO	natural bond orbital
nm	nanometer(s)
NMR	nuclear magnetic resonance
NOESY	Nuclear Overhauser Enhancement Spectroscopy
np_3	$N(CH_2CH_2PPh_2)_3$
o-	*ortho* position of an aryl ring
OTf	$-OSO_2CF_3$
P_x	cluster of x phosphorus atoms
p-	*para* position of an aryl ring
Ph	phenyl
ppm	parts per million
^{i}Pr	*iso*-propyl
pz	pyrazolyl

pz^{tBuPh}	3,5-*p*-*tert*-butylphenyl pyrazolyl
pz^{Me2}	3,5-dimethyl pyrazolyl
pzH	pyrazole
q	quartet
R	general alkyl or aryl substituents
rt	room temperature
s	second(s)
S	spin
SOMO	singly occupied molecular orbital
SQUID	superconducting quantum interference device
sqrt	square root
t	triplet
T	temperature
THF	tetrahydrofuran
THF-d_8	tetrahydrofuran-d_8
TMEDA	tetramethylethylenediamine
TMS	trimethylsilyl
tolyl	$-C_6H_4CH_3$
triphos	$H_3CC(CH_2PPh_2)_3$
UV-vis	ultraviolet-visible
V	volume
V	volt(s)
X	monoanionic atom or group, such as halide

XRD	X-ray diffraction
δ	delta, isomer shift in Mössbauer spectroscopy
δ	delta, chemical shift in NMR spectroscopy
ε	extinction coefficient in M^{-1} cm^{-1}
Δ	difference between two values
ΔE_Q	quadrupole splitting in Mössbauer spectroscopy
η^n	hapticity of order n
κ^n	denticity of order n
λ	wavelength
λ_{max}	wavelength of maximum absorption
μ	absorption coefficient (XRD)
μ-A	bridging atom
μ_B	Bohr magnetons
μ_{eff}	effective magnetic moment
μL	microliter(s)
υ	frequency
χ	magnetic susceptibility
χ_M	molar magnetic susceptibility

Chapter 1: Introduction and Background to the Coordination Chemistry of Late Transition Metal Poly(phosphino)borates

1.1 Tris(phosphino)borate Ligands

A major focus of the Peters Group has been the use of poly(phosphino)borate ligands to stabilize low-coordinate mid-to-late transition metal complexes.[1] A number of these ligands have been synthesized, including variants with one,[2] two,[3] and three[4] phosphine arms tethered to an anionic borate moiety. It has been shown that the sterics and electronics of these ligand frameworks can be modified substantially by using different phosphine substituents.[3b] This is true in particular for the tris(phosphino)borate ligands [$PhBP^R_3$] ([$PhBP^R_3$] = [$PhB(CH_2PR_2)_3$]$^-$, where R = Ph or ^{i}Pr) which are of interest due to their *facially* coordinating nature, similar to other well-studied L_2X-type ligands such as the tris(pyrazolyl)borate (Tp),[5] tris(thioether)borate,[6] and cyclopentadienyl[7] ligand families. The electron-releasing phosphine donors of [$PhBP^R_3$] render it more electron-rich than many other L_2X ligands,[8] and the anionic borate backbone of [$PhBP^R_3$] also provides a more electron-releasing coordination environment than its neutral analogue triphos (triphos = $CH_3C(CH_2PPh_2)_3$).[9]

The three-fold symmetric tris(phosphino)borate ligands give rise to a molecular orbital diagram featuring a splitting pattern with two high-energy anti-bonding orbitals and three predominantly non-bonding orbitals as a result of an axial distortion from a rigorously tetrahedral geometry to a geometry in which the angles between the phosphines become close to 90°, reminiscent of three vertices of an octahedron (Figure 1.1). If we define the z axis as the metal-boron vector, the a_1 orbital, d_{z^2}, drops in energy as a result of this distortion, approaching the *e* set of non-bonding orbitals d_{xy} and $d_{x^2-y^2}$. The other *e* set of orbitals, d_{xz} and d_{yz}, are of ideal symmetry to engage in multiple bonds to a ligand in the fourth coordination site.[10] A particularly interesting consequence of this

electronic structure is the observation that the d^7 cobalt(II) complex [PhBP$^{Ph}_3$]CoI adopts a low spin (S =1/2) ground state, even in the absence of a π-basic donor ligand.[11] The presence of a single unpaired electron in the orbitals of *e* symmetry leads to a noticeable Jahn-Teller distortion to C_s symmetry in the solid-state structure of [PhBP$^{Ph}_3$]CoI. Removal of one electron from this cobalt(II) species leads to a highly stabilized low-spin, d^6 electron configuration that is amenable to the stabilization of complexes featuring metal-ligand bonds such as the cobalt(III) imide complex [PhBP$^{Ph}_3$]Co^{III}≡N(*p*-tolyl).[12]

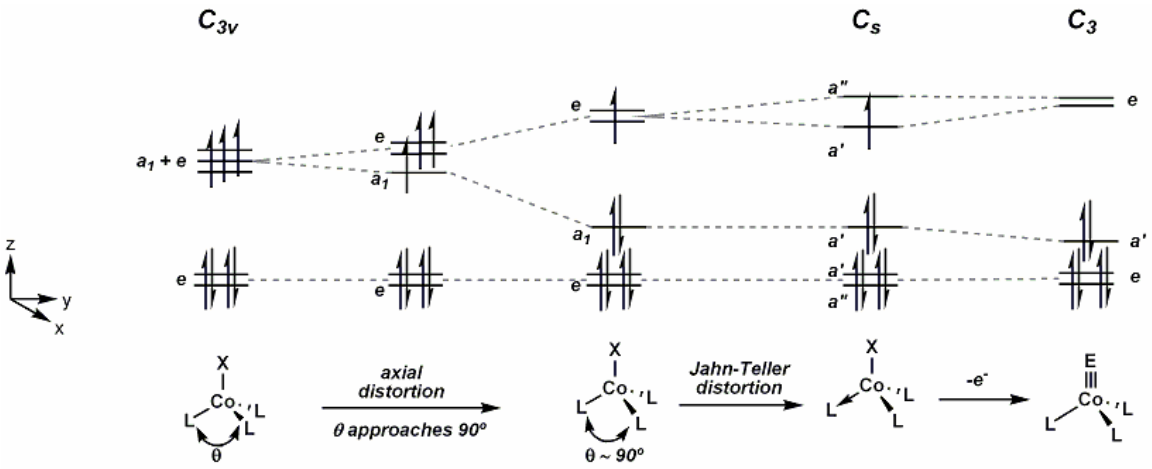

Figure 1.1 Molecular orbital diagram for [PhBP$_3$]Co complexes. Figure is adapted from reference 12.

1.2 Iron-Nitrogen Multiple Bonds–Imides and Nitrides

Transition metal complexes containing metal-to-ligand multiple bonds, M=E or M≡E (where E = N^{3-}, NR^{2-}, O^{2-}, CR^{3-}, CR^{2-} for example) are of fundamental importance as intermediates in atom and group transfer reactions in catalytic transformations such as epoxidation, cyclopropanation, and aziridination.[13] More specifically, iron-nitrogen multiple bonds are of particular interest as mechanistically relevant to biological and industrial nitrogen fixation processes. Industrially, dinitrogen is reduced to ammonia via

the Haber-Bosch process, in which nitrogen and hydrogen are combined at high temperatures (400-500 ºC) and high pressures (100-300 atm) over a solid-supported catalyst (typically Fe or Ru).[14] It is thought that surface-bound nitrides play a role, but due to the harsh heterogeneous conditions required for this process, the mechanism is not well understood. Low coordinate iron nitride and/or imide complexes may serve as small molecule models of such surface bound species and may lead to a more rigorous mechanistic understanding of the catalytic hydrogenation process.

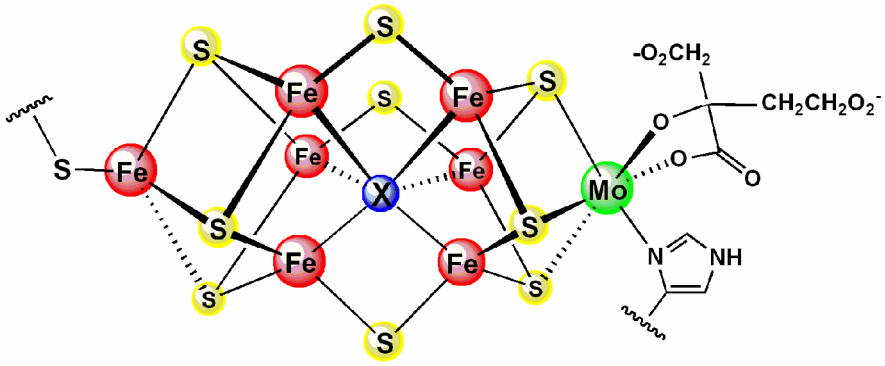

Figure 1.2 Cyrstallographically determined structure of the FeMo-cofactor of nitrogenase.

Biologically, nitrogen fixation is accomplished at ambient pressures and temperatures by the metalloenzyme nitrogenase via the overall reaction: $N_2 + 8H^+ + 8e^- + 16MgATP \rightarrow 2NH_3 + H_2 + 16MgADP + 16P_i$.[15] Although the mechanism of this reaction is not well understood, high resolution X-ray data have revealed that the active site of nitrogenase, known as the FeMo-cofactor, is composed of a cluster of sulfur-ligated pseudo-tetrahedral iron centers linked by a central light atom X and tethered to a molybdenum homocitrate moiety (Figure 1.2).[16] The identity of X, which is most likely carbon, nitrogen, or oxygen, can not be determined from the X-ray diffraction data and is still under debate.[17]

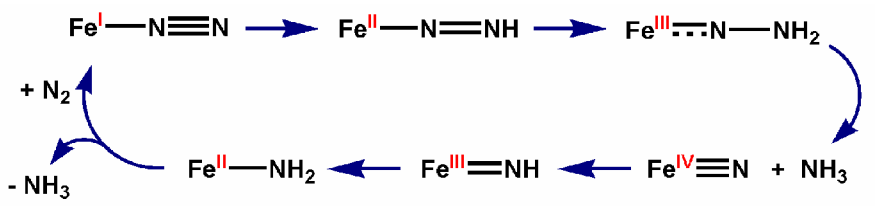

Figure 1.3 Proposed catalytic cycle for the reduction of nitrogen at a single iron site.

One particular area of uncertainty is whether iron or molybdenum serves as the site of nitrogen binding and reduction.[18] In light of this, a number of molybdenum model complexes bearing nitrogenous ligands relevant to nitrogen reduction have been synthesized,[19] and catalytic reduction of nitrogen to ammonia at a single molybdenum site has been realized.[20] However, since iron is the only metal ubiquitous to all forms of nitrogenase, it seems plausible that iron plays an integral role in the nitrogen fixation process, and a number of spectroscopic studies suggest that iron is the binding site for other substrates such as H^+, acetylene, CO, and propargyl alcohol.[21] A potential pathway for nitrogen reduction at a single iron site via stepwise addition of protons and electrons is shown in Figure 1.3, and a number of models of the potential intermediates in this cycle have been isolated using $[PhBP^R_3]Fe$ platforms.[22]

Of particular interest are the iron(III) imide and iron(IV) nitride intermediates proposed in this catalytic cycle. Although high valent iron complexes containing multiple bonds to nitrogen are still quite rare, several examples of terminal imide and nitride complexes have appeared in the recent literature, and some examples are shown in Figure 1.4.[23] To date, the most effective ligands for supporting these types of metal-nitrogen multiply-bonded complexes have been the tris(phosphino)borate ligands. Although iron imides in the +2 and +3 oxidation states are now known, the only example of an isolable iron(IV) terminal imide is part of the cluster shown in Figure 1.4.[23c] In Figure 1.4, the

terminal imide linkage in the $[Fe_4(\mu_3\text{-}N^tBu)_4(N^tBu)Cl_3]$ cluster is represented as a double bond as described by Lee, et al. However, based on the short Fe-N bond length (1.635(4)Å) and analogy to the pseudo-tetrahedral $[PhBP^R_3]Fe{\equiv}NR$ complexes, a triple bond is likely more accurate. Mononuclear iron(IV) imides have only been postulated as intermediates and no isolable examples have been reported.[24] Such compounds could potentially serve as models for intermediates between the iron(IV) nitride and iron(III) imide species in the catalytic nitrogen reduction cycle (Scheme 1.1).

Scheme 1.1

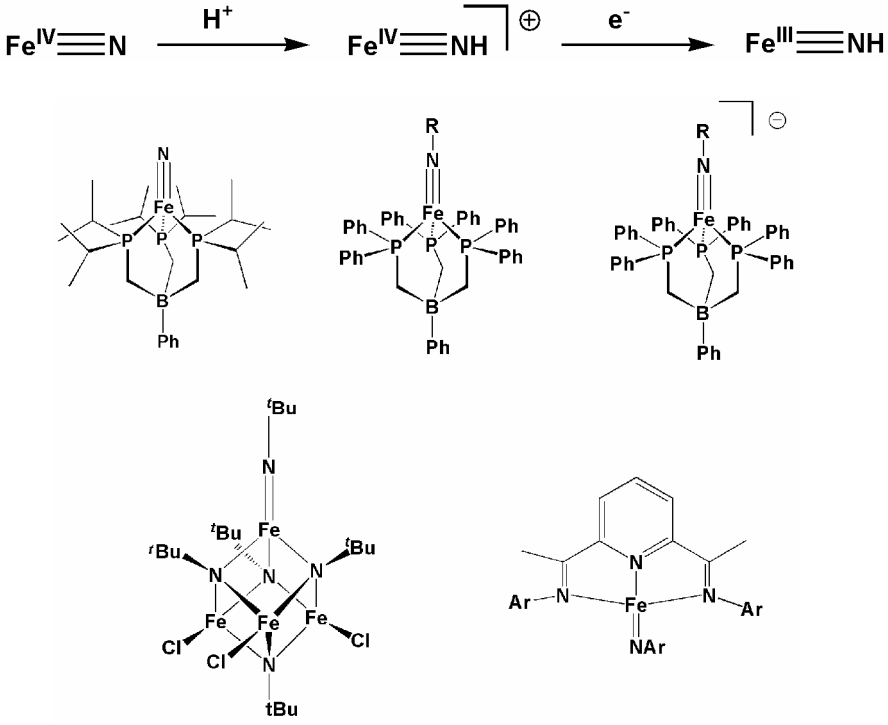

Figure 1.4 Some recent examples of terminal iron imide and nitride complexes.

1.3 Small Molecule Activation

In addition to their ability to stabilize M≡E linkages, the unique capacity of the tris(phosphino)borate iron platforms to accommodate both π-acidic (e.g., N_2, CO) and π-basic (e.g., NR^{2-}, N^{3-}) ligands makes them particularly intriguing candidates for the

activation of small molecule substrates. Such processes could ultimately lead to the transformation of common unreactive substrates into more useful organic compounds.

One example of such a transformation is the activation of Si-H bonds. Oxidative addition of X-H bonds (X = H, C, Si) to a metal center is often implicated in both stoichiometric and catalytic reactions. While oxidative addition of H_2 is thermodynamically favorable, the addition of C-H bonds is typically more difficult. The addition of hydrosilanes to transition metal centers, on the other hand, occurs much more readily.[25] These types of reactions are particularly interesting as a result of their implication in catalytic hydrosilation as well as their relevance to other, less facile oxidative addition processes. Since it has been established that [$PhBP^{iPr}_3$]Fe alkyl species react with H_2 to form highly reactive iron hydrides, leading to the catalytic hydrogenation of olefins,[26] the activation of Si-H bonds should also be accessible using this plaform.

Another interesting, less common, small molecule activation process is the reaction of elemental phosphorus (P_4) with coordinatively unsaturated transition metal centers.[27] The ultimate goal of this type of chemistry is to use the resulting transition metal P_x complexes as a medium for functionalizing white phosphorus, leading to new P-H and P-C bonds.[28] Although a number of transition metal P_x complexes have been generated,[29] the factors governing the stepwise activation of P_4 are not well understood. For this reason, the synthesis and reactivity of unique transition metal complexes incorporating partially activated P_4 moieties is of interest.

1.4 Chapter Summaries

In Chapter 2, the reaction of [$PhBP^{iPr}_3$]FeMe with primary aryl silanes ($RSiH_3$) to generate structurally unprecedented η^3-H_2SiR_2 adducts is discussed. The assignment of

$[PhBP^{iPr}_3]Fe^{II}(H)(\eta^3\text{-}H_2SiMeR)$ as an η^3 silane adduct rather than an iron(IV) silylene trihydride is cemented by theoretical calculations as well as structural (X-ray) and spectroscopic data (NMR, Mössbauer). A discussion of the mechanism by which Si-H activation occurs to form this product is presented.

Chapter 3 discusses the activation of elemental phosphorus, P_4, by $[PhBP^R_3]Fe^I$ complexes to generate unique iron(II) dimers bridged by square P_4^{2-} units. Structural and spectroscopic characterization of $\{[PhBP^{iPr}_3]Fe\}_2(\mu\text{-}P_4)$ and $\{[PhBP^{Ph}_3]Fe\}_2(\mu\text{-}P_4)$ is described. A simplified electronic structure calculation is provided to aid in discussion of bonding within these complexes. The reactivity of $\{[PhBP^{Ph}_3]Fe\}_2(\mu\text{-}P_4)$ towards one-electron reduction and characterization of the resulting product is described. Thermolysis of $\{[PhBP^{iPr}_3]Fe\}_2(\mu\text{-}P_4)$ leads to clean formation of a P_3-bridged dimer.

Chapter 4 introduces a new family of tripodal hybrid bis(phosphino)pyrazolylborate ligands, $[PhBP^{tBu}_2(pz')]^-$, and the preparation and characterization of these ligands is discussed. The synthesis, spectroscopy, and solid-state structures of four-coordinate, pseudo-tetrahedral iron(II) and cobalt(II) halide complexes supported by these ligands is presented. The cyclic voltammetry of these complexes is introduced and compared to data reported for the analogous $[PhBP^R_3]FeCl$ and $[PhBP^R_3]CoI$ complexes to show that the new $[PhBP^{tBu}_2(pz')]^-$ ligands are more electron-releasing than their tris(phosphino)borate congeners. Potential routes to a terminal cobalt or iron nitride complex via extrusion of N_2 from coordinated azide and metathesis with the N-atom transfer reagent Li(dbabh) are investigated.

Chapter 5 describes the preparation of iron(III), cobalt(III), and iron(IV) terminal imide complexes supported by $[PhBP^{tBu}_2(pz')]^-$ ligands. These complexes are prepared

first by reduction of the corresponding metal(II) halide in the presence of excess phosphine to generate low valent $[PhBP^{tBu}_2(pz')]M^{I}(PMe_3)$ precursors. These precursors react with organic azides to generate cobalt(III) and iron(III) imides. Initial reactivity studies indicate that these imides are more moderately more reactive than the corresponding tris(phosphino)borate complexes. Of particular interest is the electrochemistry of the $[PhBP^{tBu}_2(pz')]Fe^{III}(NR)$ imides, which features a quasi-reversible to fully reversible oxidation event, dependent on choice of pyrazolyl substituents and scan rate. This oxidation can be achieved chemically to generate the isolable cationic iron(IV) imides, and the structural and spectroscopic characterization of these complexes is discussed.

References Cited

[1] Thomas, J. C.; Peters, J. C. *Inorg. Synth.* **2004**, *34*, 8.

[2] Thomas, C. M.; Peters, J. C. *Inorg. Chem.* **2004,** *43,* 8.

[3] (a) Thomas, J. C.; Peters, J. C. *J. Am. Chem. Soc.*; **2001**, *123*, 5100–5101. (b) Thomas, J. C.; Peters, J. C. *Inorg. Chem.* **2003,** *42,* 5055.

[4] (a) Barney, A. A.; Heyduk, A. F.; Nocera, D. G. *Chem. Commun.* **1999**, 2379. (b) Shapiro, I. R.; Jenkins, D. M.; Thomas, J. C.; Day, M. W.; Peters, J. C. *Chem. Commun.* **2001**, 2152–2153.

[5] (a) Trofimenko, S. *Scorpionates: The Coordination Chemistry of Polypyrazolylborate Ligands*; Imperial College Press: London, 1999. (b) Trofimenko, S. *Chem. Rev.* **1993**, *93*, 943. (c) Trofimenko, S. *Polyhedron* **2004**, *23*, 197.

[6] (a) Schebler, P. J.; Riordan, C. G.; Guzei, I. A.; Rheingold, A. L. *Inorg. Chem.* **1998**, *37,* 4754. (b) Schebler, P. J.; Riordan, C. G.; Liable-Sands, L.; Rheingold, A. L. *Inorg.*

Chim. Acta **1998,** *270,* 543. (c) Ohrenberg, C.; Ge, P.; Schebler, P.; Riordan, C. G.; Yap, G. P. A.; Rheingold, A. L. *Inorg. Chem.* **1996,** *35,* 749. (d) Ge, P.; Haggerty, B. S.; Rheingold, A. L.; Riordan, C. G. *J. Am. Chem. Soc.* **1994,** *116,* 8406.

[7] Crabtree, R. H. *The Organometallic Chemistry of the Transition Metals*, 2nd ed., Wiley: New York, 1994, pp 120-128.

[8] Feldman, J. D.; Peters, J. C.; Tilley, T. D. *Organometallics* **2002,** *21,* 4050.

[9] Dapporto, P.; Midollini, S.; Sacconi, L. *Inorg. Chem.* **1975**, *14*, 1643.

[10] Harris, D. C.; Bertolucci, M. D. *Symmetry and Spectroscopy: An Introduction to Vibrational and Electronic Spectroscopy;* Dover Publications, Inc.: New York, 1989.

[11] Jenkins, D. M.; Di Bilio, A. J.; Allen, M. J.; Betley, T. A.; Peters, J. C. *J. Am. Chem. Soc.* **2002**, *124*, 15336.

[12] Jenkins, D. M.; Betley, T. A.; Peters, J. C. *J. Am. Chem. Soc.* **2002**, *124*, 11238.

[13] (a) Costas, M.; Mehn, M. P.; Jensen, M. P.; Que, L., Jr. *Chem. Rev.* **2004**, *104*, 939. (b) Doyle, M. P. *Acc. Chem. Res.* **1986**, *19*, 348-356. (c) Müller, P.; Fruit, C. *Chem. Rev.* **2003**, *103*, 2905. (d) Woo, L. K. *Chem. Rev.* **1993**, *93*, 1125. (e) Nugent, W. A.; Mayer, J. M. *Metal-ligand multiple bonds, the chemistry of transition metal complexes containing oxo, nitride, imido, alkylidene, or alkylidyne ligands*. Wiley New York, 1988. (e) Lane, B. S.; Burgess, K. *Chem. Rev.* **2003**, *103*, 2457.

[14] (a) Ertl, G. *Chem. Rec.* **2001**, *1*, 33. (b) Ertl, G. In *Catalytic Ammonia Synthesis*; Jennings, J. R., Ed.; Plenum Press: New York, 1991. (c) Appl, M. *Ammonia*; Wiley-VCH: Weinheim, 1999. (d) Postgate, J. *Nitrogen Fixation*; Cambridge Press: Cambridge, 1990.

[15] (a) Seefeldt, L. C.; Dean, D. R. *Acc. Chem. Res.* **1997**, *30*, 260. (b) Rees, D. C.; Howard, J. C. *Current Opinion in Chemical Biology* **2000**, *4*, 559. (c) Burgess, B. K.; Lowe, D. J. *Chem. Rev.* **1996**, *96*, 2963.

[16] Einsle, O.; Tezcan, F. A.; Andrade, S. L. A.; Schmid, B.; Yoshida, M.; Howard, J. B.; Rees, D. C. *Science* **2002**, *297*, 1696.

[17] (a) Dance, I. *Chem. Commun.* **2003**, 324. (b) Lee, H. I.; Benton, P. M.; Laryukhin, M.; Igarashi, R. Y.; Dean, D. R.; Seefeldt, L. C.; Hoffman, B. M. *J. Am. Chem. Soc.* **2003**, *125*, 5604. (c) Lovell, T.; Liu, T.; Case, D. A.; Noodleman, L. *J. Am. Chem. Soc.* **2003**, *125*, 8377. (d) Hinnemann, B.; Norskov, J. K. *J. Am. Chem. Soc.* **2003**, *125*, 1466. (e) Yang, T. C.; Maeser, N. K.; Laryukhin, M.; Lee, H. I.; Dean, D. R.; Seefeldt, L. C.; Hoffman, B. M. *J. Am. Chem. Soc.* **2005**, *127*, 12804.

[18] Seefeldt, L. C.; Dance, I. G.; Dean, D. R. *Biochemistry* **2004**, *43*, 1401.

[19] (a) Chatt, J.; Dilworth, J. R.; Richards, R. L. *Chem. Rev.* **1978**, *78*, 589. (b) Laplaza, C. E.; Cummins, C. C. *Science* **1995**, *269*, 861. (b) Laplaza, C. E.; Johnson, M. J. A.; Peters, J. C.; Odom, A. L.; Kim, E.; Cummins, C. C.; George, G. N.; Pickering, I. J. *J. Am. Chem. Soc.* **1996**, *118*, 8623. (c) Chatt, J. *J. Less Common Metals* **1974**, *36*, 429. (d) Seino, H.; Ishii, Y.; Hidai, M. *J. Am. Chem. Soc.* **1994**, *116*, 7433. (e) Ishii, Y.; Kawaguchi, M.; Ishino, Y.; Aoki, T.; Hidai, M. *Organometallics* **1994**, *13*, 5062. (f) George, T. A.; Kaul, B. B.; Chen, Q.; Zubieta, J. *Inorg. Chem.* **1993**, *32*, 1706. (g) Seino, H.; Ishii, Y.; Sasagawa, T.; Hidai, M. *J. Am. Chem. Soc.* **1995**, *117*, 12181. (h) Peters, J. C.; Cherry, J. P. F.; Thomas, J. C.; Baraldo, L.; Mindiola, D. J.; Davis, W. M.; Cummins, C. C. *J. Am. Chem. Soc.* **1999**, *121*, 10053.

[20] Yandulov, D. V.; Schrock, R. R. *Science* **2003**, *301*, 76.

[21] (a) Mayer, S. M.; Niehaus, W. G.; Dean, D. R. *J. Chem. Soc., Dalton Trans.* **2002**, *5*, 802. (b) Ryle, M. J.; Lee, H. L.; Seefeldt, L. C.; Hoffman, B. M. *Biochemistry* **2000**, *39*, 1114. (c) Sørlie, N.; Christiansen, J.; Dean, D. R.; Hales, B. J. *J. Am. Chem. Soc.* **1999**, *121*, 9457. (d) Lee, H. I.; Sorlie, M.; Christiansen, J.; Song, R.; Dean, D. R.; Hales, B. J.; Hoffman, B. M. *J. Am. Chem. Soc.* **2000**, *122*, 5582. (e) Lee, H. I.; Cameron, L. M.; Hales, B. J.; Hoffman, B. M. *J. Am. Chem. Soc.* **1997**, *119*, 10121. (d) Christie, P. D.; Lee, H. I.; Cameron, L. M.; Hales, B. J. *J. Am. Chem. Soc.* **1996**, *118*, 8707.

[22] (a) Brown, S. D.; Betley, T. A.; Peters, J. C. *J. Am. Chem. Soc.* **2003**, *125*, 322. (b) Betley, T. A.; Peters, J. C. *J. Am. Chem. Soc.* **2003**, *125*, 10782. (c) Brown, S. D.; Peters, J. C. *J. Am. Chem. Soc.* **2004**, *126*, 4538. (d) Betley, T. A.; Peters, J. C. *J. Am. Chem. Soc.* **2004**, *126*, 6252. (e) Brown, S. D.; Peters, J. C. *J. Am. Chem. Soc.* **2005**, *127*, 1913. (f) Brown, S. D.; Mehn, M. P.; Peters, J. C. *J. Am. Chem. Soc.* **2005**, *127*, 13146.

[23] (a) Mehn, M. P.; Peters, J. C. *J. Inorg. Biochem.* **2006**, *100*, 634-643. (b) Bart, S. C.; Lobkovsky, E.; Bill, E.; Chirik, P. J. *J. Am. Chem. Soc.* **2006**, *128*, 5302. (c) Verma, A. K.; Nazif, T. N.; Achim, C.; Lee, S. C. *J. Am. Chem. Soc.* **2000**, *122*, 11013. (d) Grapperhaus, C.A.; Mienert, B.; Bill, E.; Weyhermuller, T.; Weighardt, K. *Inorg. Chem.* **2000**, *39*, 5306. (e) Aliaga-Alcalde, M.; George, S. D.; Mienert, B.; Bill, E.; Weighardt, K.; Neese, F. *Angew. Chem. Int. Ed.* **2005**, *44*, 2908.

[24] (a) Lucas, R. L; Powell, D. R; Borovik, A. S. *J. Am. Chem. Soc.* **2005**, *127*, 11596. (b) Jensen, M. P.; Mehn, M. P.; Que, L., Jr. *Angew. Chem. Int. Ed.* **2003**, *42*, 4357.

[25] Corey, J. Y.; Braddock-Wilking, J. *Chem. Rev.* **1999**, *99*, 175.

[26] Daida, E. J.; Peters, J. C. *Inorg. Chem.* **2004**, *43*, 7474.

[27] (a) Ehses, M.; Romerosa, A.; Peruzzini, M. *Topics in Current Chem.* **2002**, *220*, 107. (b) Whitmire, K. H. *Adv. Organomet. Chem.* **1998**, *42*, 1.

[28] (a) Peruzzini, M.; de los Rios, I.; Romerosa, A.; Vizza, F. *Eur. J. Inorg. Chem.* **2001**, 593. (b) Scherer, O. J. *Acc. Chem. Res.* **1999**, *32*, 751.

[29] (a) Scheer, M. *Coord. Chem. Rev.* **1997**, *163*, 271. (b) Scherer, O. J. *Comments Inorg. Chem.* **1987**, *6*, 1.

Chapter 2: An η^3-H_2SiR_2 Adduct of $[PhB(CH_2P^iPr_2)_3]Fe^{II}(H)$

The text in this chapter is reproduced in part with permission from:

Thomas, C. M.; Peters, J. C. *Angew. Chem. Int. Ed.* **2006,** *45,* 776.

2.1 Introduction

The tripodal tris(phosphino)borate ligand $[PhB(CH_2P^iPr_2)_3]^-$ (abbreviated $[PhBP^{iPr}_3]$) stabilizes iron complexes in a wide range of oxidation states, including high-valent Fe^{IV}.[1] $[PhBP^{iPr}_3]FeL_n$ systems are, moreover, known to mediate a number of 2-electron redox transformations, including $Fe^{II/IV}$ oxidative group transfer and oxidative addition/reductive elimination processes.[1a,c] In the latter context, it was recently demonstrated that 4-coordinate iron alkyl species of the type $[PhBP^{iPr}_3]Fe^{II}$-R undergo facile hydrogenolysis to generate iron(IV) trihydrides of the type $[PhBP^{iPr}_3]Fe(H)_3(PR_3)$ that can be likewise generated by H_2 addition to $[PhBP^{iPr}_3]Fe^{II}(H)(PR_3)$ precursors.[1c] These complexes mediate catalytic olefin hydrogenation, most likely via uncommon $Fe^{II/IV}$ oxidative addition/reductive elimination steps.[1c]

Motivated by these findings the reactivity of these 4-coordinate $[PhBP^{iPr}_3]Fe^{II}$-R alkyl species with silane substrates has been examined for comparison to their reactivity towards H_2, anticipating that structurally distinctive iron silylene species might be generated. In this chapter, the structural and spectroscopic characterization of unusual η^3-silane adducts of iron(II), $[PhBP^{iPr}_3]Fe^{II}(H)(\eta^3\text{-}H_2SiR_2)$ is reported. As described below, the available structural, spectroscopic, and theoretical data also suggest the possibility that the $[PhBP^{iPr}_3]Fe^{II}(H)(\eta^3\text{-}H_2SiR_2)$ systems described herein equilibrate via silylene intermediates of the type $[PhBP^{iPr}_3]Fe^{IV}(H)_3(SiR_2)$.[2] Such silylene intermediates would be isoelectronic to the previously reported $[PhBP^{iPr}_3]Fe^{IV}(H)_3(PR_3)$ but appear to be too high energy relative to their ground state $[PhBP^{iPr}_3]Fe^{II}(H)(\eta^3\text{-}H_2SiR_2)$ isomers to be directly observed.

While transition metal complexes that exhibit η^2-$HSiR_3$ interactions are ubiquitous,[3,4] those that exhibit well-characterized interactions between two or more metal hydrides and a coordinated silicon atom are much less common. They have nevertheless been described in certain cases, including the dinuclear complex $[(PR_3)_2H_2Ru]_2(\eta^4\text{-}SiH_4)$ of Sabo-Etienne and coworkers[5] and the mononuclear complexes $Re(H)_4(PPh_3)(\eta^3\text{-}H_2SiR_3)$,[6] $(PCy_3)_2Ru(H)(\eta^2\text{-}H_2)(\eta^3\text{-}H_2SiPh_3)$,[7] $Ru(PPh_3)_3(H)_3SiMeCl_2$,[8] and $Cp^*Ru(PPh_3)(\eta^3\text{-}H_2SiMeCl_2)$.[9] Metal hydride/silyl systems of these types are often described as lying somewhere along the continuum to oxidative addition, the limit being full oxidative addition with earlier, 'arrested' addition stages also being common.[4a] To the best of our knowledge, the $[PhBP^{iPr}_3]Fe^{II}(H)(\eta^3\text{-}H_2SiR_2)$ complexes described here are the first thoroughly characterized examples of arrested silane adducts of iron that exhibit an η^3 binding mode (i.e., $Fe(\eta^3\text{-}H_2SiR_2)$). The only other example of such a bonding mode for a silane ligand of any transition metal complex appears to be the aforementioned dinuclear ruthenium system of Sabo-Etienne.[5]

2.2 Results and Discussion

2.2.1 Synthesis and Structural Characterization of $[PhBP^{iPr}_3]Fe^{II}(H)(\eta^3\text{-}H_2SiMeR)$ (R = Ph, Mes)

Access to a $[PhBP^{iPr}_3]Fe^{II}(H)(\eta^3\text{-}H_2SiR_2)$ species is accomplished by the reaction between $[PhBP^{iPr}_3]$Fe-Me (**2.1**) and $PhSiH_3$, leading to the quantitative formation of a single diamagnetic red product (**2.2**) (^{1}H NMR) (Scheme 2.1). In contrast to the previously reported reaction of **2.1** with H_2,[1c] methane loss is not detected by ^{1}H NMR. The $^{31}P\{^1H\}$ NMR spectrum of **2.2** reveals a broad singlet at δ 76 ppm, consistent with a C_{3v}-symmetric structure. All three phosphorus nuclei remain magnetically equivalent in

the $^{31}P\{^{1}H\}$ NMR spectra at temperatures as low as -80 ˚C. The ^{1}H NMR spectrum of **2.2** reveals a hydride signal at -13.5 ppm with a complicated splitting pattern. This data initially led us to postulate complex **2.2** to be an Fe^{IV} silylene trihydride, $[PhBP^{iPr}_3]Fe^{IV}(H)_3(SiPhMe)$ (structure B in Scheme 2.1).

Scheme 2.1

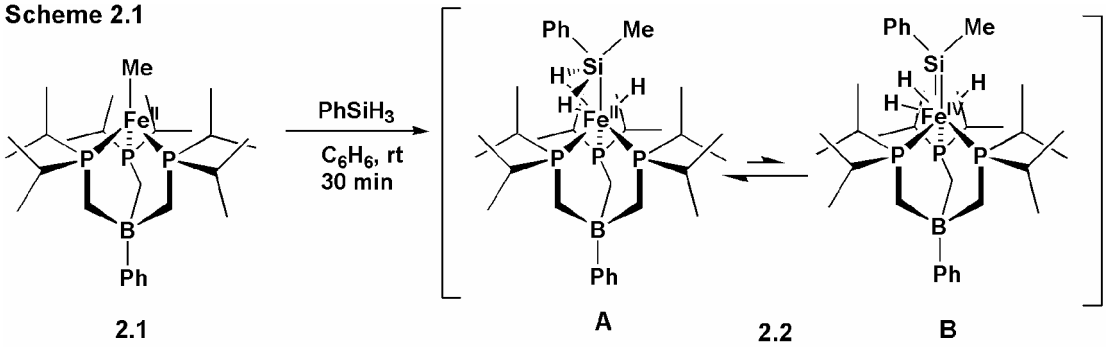

To assess the structure of complex **2.2** in the solid state, X-ray quality single crystals were grown by cooling a concentrated ethereal solution of **2.2** to -35 ˚C. High resolution X-ray diffraction analysis provided the solid state structure shown in Figure 2.1. The structure confirms that a 1,2-methyl migration occurs from the iron center to the silicon center during the transformation. A remarkably short Fe-Si distance of 2.1280(7) Å is present. This distance is very similar to the Fe-Si distance of 2.154(1) Å reported for the only structurally characterized example of an iron silylene species, $[Cp^{*}Fe(CO)(SiMes_2)SiMe_3]$.[10] Moreover, the geometry of the silicon atom of **2.2** is rigorously planar (C2-Si-Fe + C2-Si-C1 + C1-Si-Fe = 360˚) if one considers its connectivity to the phenyl, methyl, and iron substituents only. All three hydride positions could be located in the difference Fourier map and refined, revealing that two of the hydrides (H1 and H3) are located within bonding distance of both the iron and the silicon centers (Fe-H1: 1.55 Å; Fe-H3: 1.57 Å; Si-H1: 1.46 Å; Si-H2: 1.55 Å). The third hydride (H2) is located outside the typical bonding radius of the silicon atom (2.00 Å) and resides

appreciably closer to the Fe center (1.48 Å). These structural data warranted more careful consideration of the silylene assignment.

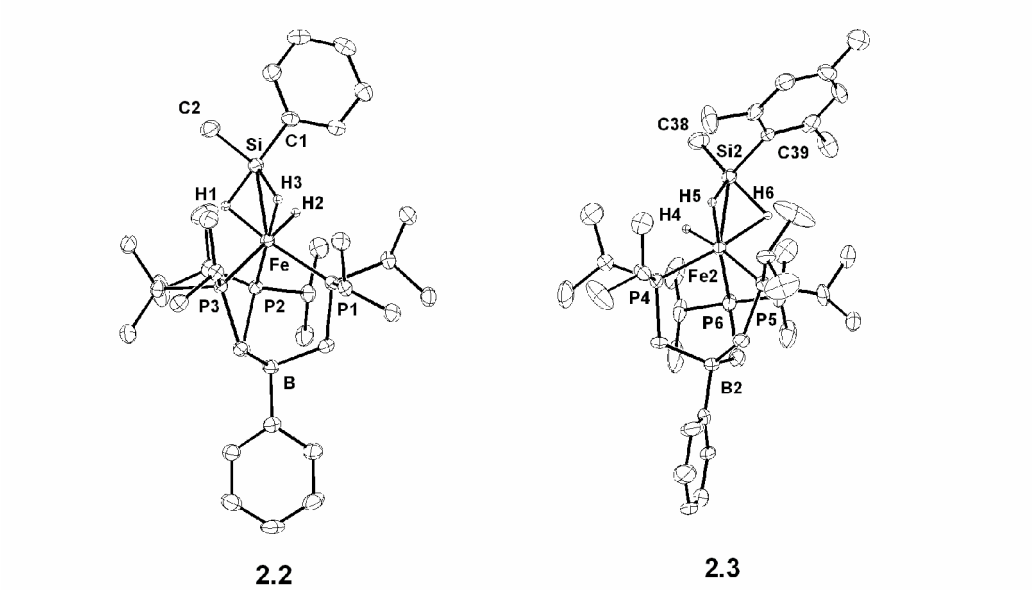

Figure 2.1. Solid state molecular structure of [PhBP$^{i\text{Pr}}_3$]Fe$^{\text{II}}$(H)(H_2SiPhMe) (**2.2**) and [PhBP$^{i\text{Pr}}_3$]Fe$^{\text{II}}$(H)(H_2SiMesMe) (**2.3**) showing 50% displacement ellipsoids. In the case of **2.3,** only one of the two independent molecules present in the asymmetric unit cell is shown. Hydrogen atoms other than the hydrides of interest have been omitted for clarity.

Because there is inevitable uncertainty in accurately locating the positions of hydrogen atoms close to heavier atoms such as Si and Fe by X-ray crystallography, a related complex was prepared for additional support of the structural assignment. In an analogous reaction to that shown in Scheme 2.1, complex **2.1** reacts with one equivalent of mesitylsilane (H_3SiMes; Mes = 2,4,6-$Me_3C_6H_2$) to generate a diamagnetic red product (**2.3**) in quantitative yield. Complex **2.3** displays analogous NMR data to that for **2.2**, with a $^{31}P\{^1H\}$ shift at 79 ppm and a hydride-type ^1H NMR resonance at -13.4 ppm, also suggestive of a highly symmetric structure in solution. X-ray quality crystals could be similarly obtained, and one of the two independent molecules present in the asymmetric

unit cell is shown in Figure 2.1. As in the case of complex **2.2**, two of the three hydrides are located within bonding distance of the silicon atom in each molecule (Si-H5/H6 = 1.56/1.62 and 1.67/1.74 Å) while the third hydride appears to be outside the bonding radius of the Si atom (Si-H4 = 2.14 and 1.97 Å). The Fe-Si distances in both molecules for **2.3** (2.131(1) / 2.141(1) Å) are essentially identical to that of **2.2** (2.1280(7) Å). Regardless of the inevitable uncertainty in the specific Fe-H and Si-H bond distances, the gross similarity between the structures of **2.2** and **2.3** strongly suggests the presence of two 3-centered Fe-H-Si interactions in the solid state and one Fe-H hydride interaction.

For additional structural examination of the hydride positions, a density functional (DFT) geometry optimization of the structure of **2.2** was performed using the Jaguar package (B3LYP/LACVP**).[11,12] All of the atoms of **2.2** were used in the calculation, and the structure was minimized using the experimentally determined X-ray coordinates as an initial guess. The resulting Fe-H and Si-H bond lengths were very similar to those determined by crystallography (Table 2.1). Interestingly, perturbing the crystallographic coordinates to provide a more three-fold symmetric structure without Si-H interactions as a starting point led to the same structural minimum. It is gratifying to note that the DFT model locates two short and one much longer Si-H distance, in accord with the η^3-H_2SiR_2 adduct formulation. Accordingly, a natural bond orbital (NBO) analysis predicts only two Si-H bonding orbitals (Si-H1, Si-H3).[13] Likewise, only one Fe-H bonding orbital is predicted (Fe-H2) and no bonding orbital is located between Si and Fe. It thus appears that complexes **2.2** and **2.3** are better described as η^3 silane adducts of an iron(II) hydride (structure type A in Scheme 2.1) than as iron(IV) silylene trihydrides (structure type B).

Table 2.1. Interatomic distances for complex **2.2** as determined by X-ray crystallography and a DFT (JAGUAR: B3LYP/LACVP**) geometry optimization.

	Experimental (Å)	Calculated (Å)
Fe-Si	2.1280(7)	2.166
Fe-H1	1.553(1)	1.555
Fe-H2	1.482(1)	1.484
Fe-H3	1.566(2)	1.569
Si-H1	1.464(1)	1.469
Si-H2	2.001(2)	2.073
Si-H3	1.552(2)	1.554

2.2.2 Characterization of $[PhBP^{iPr}_3]Fe^{II}(H)(\eta^3\text{-}H_2SiMeR)$ by ^1H and ^{29}Si NMR Spectroscopy

Further inspection of the solution state NMR data available for **2.2** confirms that a significant Si-H interaction is also maintained in the solution phase. A T_{1min} measurement of 177 ms (-30 ˚C, toluene-d_8) was determined for the hydride resonance of the ^1H NMR spectrum. This large value would appear to rule out the presence of a non-classical dihydrogen adduct species (η^2-H_2) but does not help to distinguish between a classical hydride formulation versus the η^2 Si-H-Fe interaction suggested by the crystallographic and DFT data.[14,15] Simulation of the hydride signal (Figure 2.2) reveals that its complicated splitting pattern arises from first order coupling of each equivalent hydride to one *trans* phosphorus ($|^2J_{P\text{-}H}|$ = 27 Hz) and two *cis* phosphorus atoms ($|^2J_{P\text{-}H}|$ = 3 Hz). The coupling pattern is complicated by second order effects that result from phosphorus-phosphorus coupling ($^2J_{P\text{-}P}$ = 62 Hz). Accordingly, the hydride signal appears as a singlet in the $^1H\{^{31}P\}$ NMR spectrum. The second order splitting pattern of the hydride signal in

the ^{1}H NMR changes as the temperature of the solution decreases, indicating a fluxional process (Figure 2.3). However, decoalescence of the signal likely occurs at temperatures well below those examined (-80 ˚C).

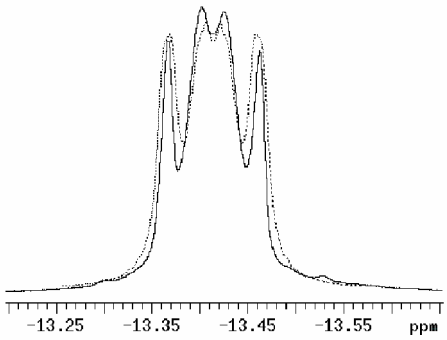

Figure 2.2. Experimental (black) and simulated (gray) ^{1}H NMR data (500 MHz, 295 K, C_6D_6) for the hydride region of complex **2.2**.

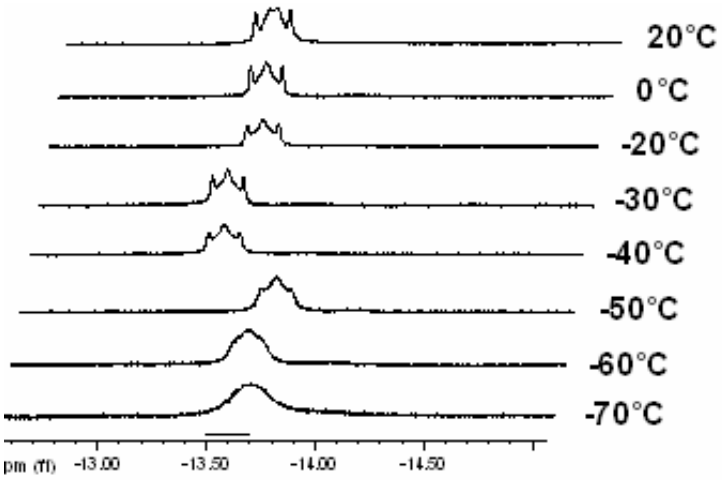

Figure 2.3. Variable temperature ^{1}H NMR (20˚C to -70˚C, 300 MHz, toluene-d_8) of the hydride signal of [PhBP$^{i\text{Pr}}_3$]Fe(H)(η^3-H_2SiPhMe) (**2.2**).

The $^{29}Si\{^{1}H\}$ NMR data obtained for **2.2** and **2.3** reveal signals at 162 ppm and 160 ppm, respectively (Figure 2.4). These values are significantly downfield of known classical transition metal silyl adducts (-120 to 90 ppm) but are somewhat upfield of reported transition metal silylenes (> 200 ppm).[4a,2] Although monomeric complexes containing η^2-$HSiR_3$ interactions display a wide range of chemical shifts in the $^{29}Si\{^{1}H\}$ NMR (from -28 to 55 ppm),[3,4a] the shifts observed for **2.2** and **2.3** are much further downfield and closer to resonances observed for silylenes, likely reflective of the η^3 nature of the ligand and the very close Fe-Si contact that results, as is evident from the solid state structures. Interestingly, coupling to the three ^{31}P nuclei of the $[PhBP^{iPr}_3]$ ligand is observed in the $^{29}Si\{^{1}H\}$ spectrum of complex **2.3** ($^{2}J_{Si\text{-}P}$ = 61 Hz), while the signal observed for **2.2** remains a broad singlet.

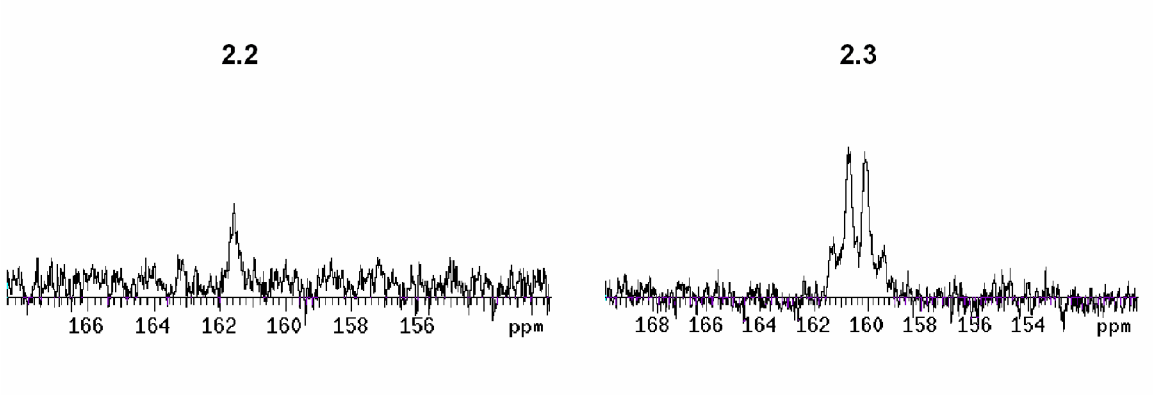

Figure 2.4. $^{29}Si\{^{1}H\}$ NMR of **2.2** and **2.3,** illustrating the difference in their respective coupling patterns. $^{2}J_{Si\text{-}P}$ = 61 Hz for **2.3**.

Closer inspection of the hydride signals for both **2.2** and **2.3** reveals the presence of ^{29}Si satellites that provide $J_{Si\text{-}H}$ coupling values of 68 and 70 Hz, respectively. Due to the rapid exchange of the hydrides in solution, the actual ^{29}Si coupling can be determined by the following equation: $J_{obs} = 1/3[2J_{Si\text{-}H(\eta 2)} + J_{Si\text{-}H(terminal)}]$.[16] Assuming that $J_{Si\text{-}H(terminal)}$

is negligible, this provides maximum $J_{Si\text{-}H(\eta 2)}$ values of 102 Hz and 105 Hz for **2.2** and **2.3**, respectively. In order to confirm these coupling constants, and to definitively assign the solution structures of complexes **2.2** and **2.3**, an HMQC experiment was undertaken for each species (Figure 2.5).[17] The data obtained reveals a direct correlation between the ^{29}Si NMR signals of **2.2** and **2.3** and the corresponding hydride signals in their ^{1}H NMR spectra. This data further confirms that Si-H interactions exist for **2.2** and **2.3** both in solution and in the solid state.

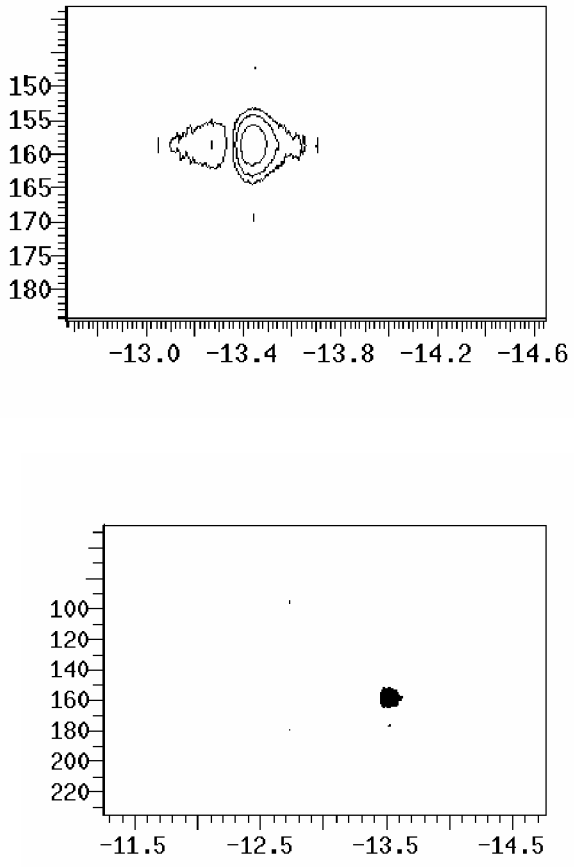

Figure 2.5. ^{29}Si/^{1}H HMQC data recorded for complex **2.2** (top) and **2.3** (bottom) (273 K, 99 MHz/500 MHz, toluene-d_8).

2.2.3 Confirmation of the Structural Assignment of [PhBP$^{iPr}_3$]Fe^{II}(H)(η^3-H$_2$SiMeR) Using Mössbauer Spectroscopy

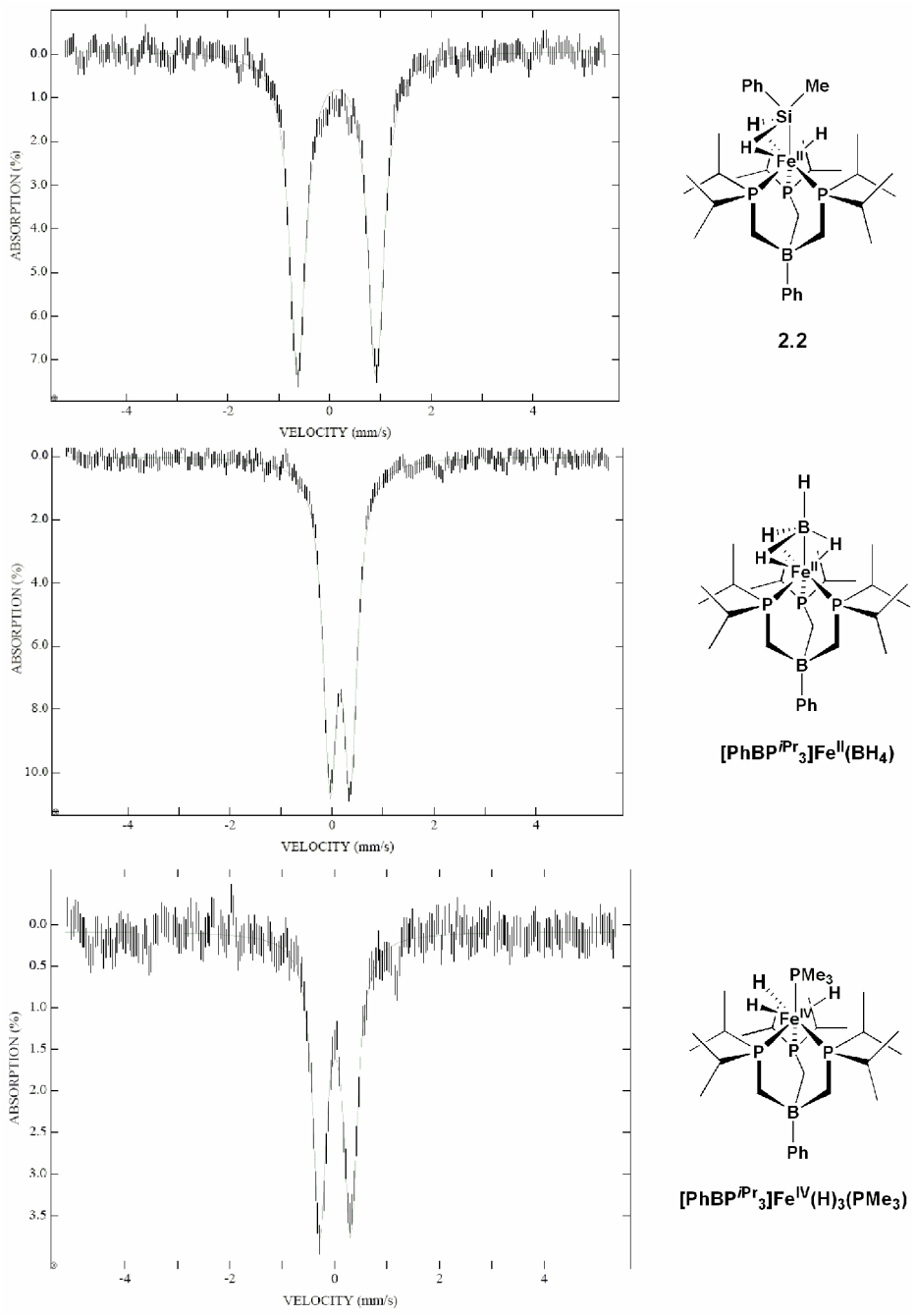

Figure 2.6 Mössbauer spectra of **2.2**, [PhBP$^{iPr}_3$]Fe^{II}(BH$_4$),[19] and [PhBP$^{iPr}_3$]Fe^{IV}(H)$_3$(PMe$_3$)[1c] at 4.2 K recorded in zero field.

To confirm the assignment of an iron(II) oxidation state in complex **2.2**, a zero-field Mössbauer spectrum was collected (4.2 K, frozen toluene solution) for comparison with similar iron complexes of known oxidation state (Figure 2.6).[18] The Mössbauer spectrum of **2.2** exhibits a quadrupole doublet with an isomer shift (δ, vs. Fe metal at 298 K) of 0.14 mm/s. This is in very good agreement with the isomer shift observed for the bona fide low spin iron(II) borohydride complex $[PhBP^{iPr}_3]Fe^{II}(BH_4)$,[19] for which δ = 0.16 mm/s is observed. It is noteworthy that the quadrupole splitting (ΔE_Q) of 1.54 mm/s observed for **2.2** is significantly larger than the ΔE_Q = 0.40 mm/s observed in the spectrum of $[PhBP^{iPr}_3]Fe^{II}(BH_4)$. This is presumably attributed to the greater deviation from spherical symmetry around the iron center in **2.2.** For comparison, Mössbauer data were collected for $[PhBP^{iPr}_3]Fe^{IV}(H)_3(PMe_3)$, a complex whose oxidation state is unequivocally iron(IV).[1c] In this case the isomer shift, δ = 0.01 mm/s, is significantly smaller than that observed for either **2.2** or $[PhBP^{iPr}_3]Fe^{II}(BH_4)$. Due to the symmetry of the three hydrides around the iron center, a relatively small quadrupole splitting (ΔE_Q = 0.59 mm/s) is observed, as seen for $[PhBP^{iPr}_3]Fe^{II}(BH_4)$. This similarity in isomer shift between **2.2** and $[PhBP^{iPr}_3]Fe^{II}(BH_4)$ confirms the assignment of **2.2** as a low spin, iron(II) hydride.

Based upon the structural, spectroscopic, and DFT data, **2.2** and **2.3** are therefore best assigned as iron(II) hydride complexes featuring two η^2-Si-H interactions that give rise to η^3-H_2SiR_2 adducts of $[PhBP^{iPr}_3]Fe^{II}(H)$. It is important to note that although there is no sigma bond between the Fe-H and the silicon atom, a weak attractive interaction can not be ruled out.[4d] While three-centered, two-electron bonding interactions in **2.2** and **2.3** are apparent in their solid state structures, in solution all three hydrides undergo rapid

exchange and appear to be chemically equivalent. It seems to us likely that an iron(IV) silylene trihydride, shown as structure type B in Scheme 2.1, could be responsible for interconverting the hydride positions rapidly on the NMR time scale. As noted above, isolobal $[PhBP^{iPr}_3]Fe^{IV}(H)_3(PR_3)$ species are chemically stable within this system, and the extremely short Fe-Si bond distance, in addition to the planar nature of the Si center with respect to the methyl, phenyl, and iron substituents, suggests that virtually no structural reorganization at the Si center would be required under such a scenario.

2.2.4 Mechanistic Considerations

Scheme 2.2

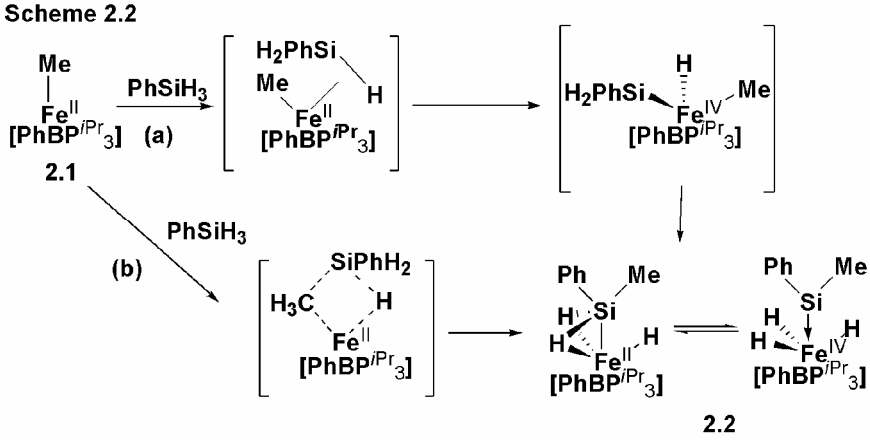

A number of mechanistic pathways to account for the formation of **2.2** and **2.3** can be envisioned. Two plausible mechanisms are shown in Scheme 2.2. Given the propensity for the $[PhBP^{iPr}_3]Fe$ scaffold to undergo two-electron redox processes, it is perhaps most reasonable to propose an oxidative addition/reductive elimination mechanism as shown in (a).[1] In this scenario, the first step is coordination of silane followed by an oxidative addition to the Fe^{II} center. Reductive 1,2-methyl migration from iron to silicon then affords an isomer of **2.2** (or **2.3**). A sigma-bond metathesis pathway (b) also provides a convenient and potentially low-energy methyl migration pathway. No

intermediates could be detected when the reaction between **2.1** and $PhSiH_3$ was monitored by ^1H NMR spectroscopy at low temperature (-50 ˚C, toluene-d_8).

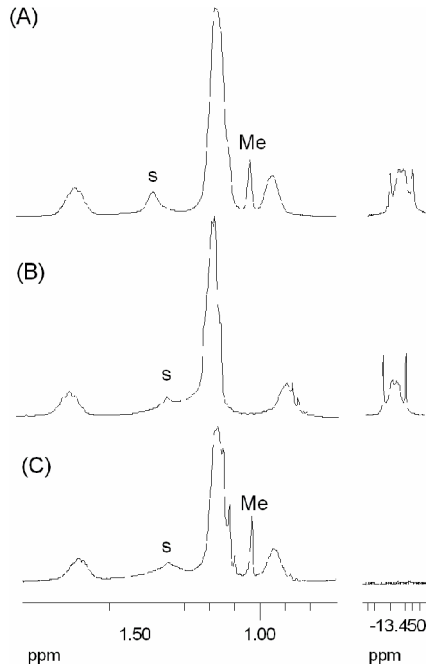

Figure 2.7. ^1H NMR spectra of (A) **2.2**, (B) **2.5**, and (C) **2.6,** illustrating the disappearance of diagnostic peaks upon deuterium labeling. Resonances attributable to residual solvent (THF) are labeled "s."

Methane loss does not occur during the course of the reaction between **2.1** and phenylsilane or mesitylsilane, whereas such loss occurs readily when **2.1** is exposed to H_2.[1c] To probe the possibility that reversible methane loss and reactivation might be occurring prior to methyl migration, a deuterium labeling study was undertaken. The deuterated methyl species, [PhBP$^{i\text{Pr}}_3$]Fe-CD_3 (**2.4**), was generated via addition of d_3-MeLi to [PhBP$^{i\text{Pr}}_3$]Fe-Cl. Reaction between **2.4** and $PhSiH_3$ results in the sole formation of [PhBP$^{i\text{Pr}}_3$]Fe(H)($H_2SiPhCD_3$) (**2.5**) based on ^1H NMR data (Figure 2.7). Likewise, the reaction between **2.1** and $PhSiD_3$ results in the formation of [PhBP$^{i\text{Pr}}_3$]Fe(D)($D_2SiPhMe$)

(**2.6**). These experiments appear to rule out any incipient methane formation prior to methyl migration.

As a final point of interest we note the selectivity **2.1** exhibits for primary silane substrates. For example, **2.1** does not react at all with secondary or tertiary (e.g., Ph_2SiH_2 and Et_3SiH) silane substrates over extended periods, presumably because such silanes cannot lead to the thermodynamically stable η^3-silane adduct structures. Secondary silane substrates do react, however, if **2.1** is exposed to H_2 in their presence. For instance, **2.1** reacts with $MePhSiH_2$ to produce **2.2** quantitatively under a blanket of hydrogen (Scheme 2.3). Examination of this reaction sequence at low temperature (-20 ˚C, toluene-d_8) reveals methane loss and the initial formation of the previously reported trihydride species $[PhBP^{iPr}_3]Fe(H)_3$ prior to product formation.[1c] $[PhBP^{iPr}_3]Fe(H)_3$ gradually decays as **2.2** appears. This sequence suggests that **2.1** reacts with H_2 to generate a reactive hydride source that is then trapped by silane, analogous to the trapping of such hydride species by the addition of a phosphine donor.[1c]

Scheme 2.3

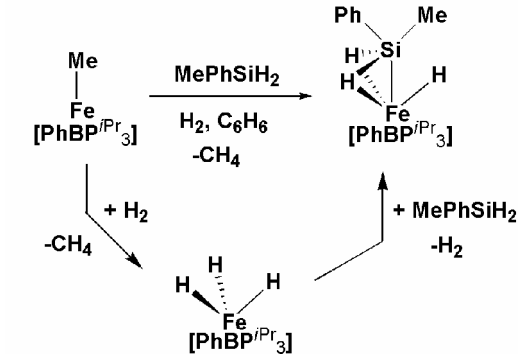

2.3 Conclusions

In summary, it has been found that the $[PhBP^{iPr}_3]$Fe-Me complex reacts with primary aryl silanes to mediate Si-H bond activation and 1,2-methyl migration to generate unusual η^3-H_2SiRMe silane adducts of $[PhBP_3]Fe^{II}$-H (R = Ph, Mes). These iron

complexes serve as relatives to the numerous group VIII complexes now known of the general type $L_3M(ER_3)H_3$ (E = Si, Sn; M = Fe, Ru, Os).[20] The key distinction to be drawn is that the complexes described herein feature a less-substituted Si atom that consequently attracts two Fe-H bonds–hence the formation of a $[PhBP^{iPr}_3]Fe(H)(\eta^3\text{-}H_2SiR_2)$ bonding mode is preferred with a very short Fe-Si distance that is distinct from, but closely associated to, its silylene isomer $[PhBP^{iPr}_3]Fe(H)_3(SiR_2)$.

2.4 Experimental Section

2.4.1 General Considerations

All syntheses reported were carried out using standard glovebox and Schlenk techniques in the absence of water and dioxygen, unless otherwise noted. Benzene, petroleum ether, diethyl ether, acetonitrile, dichloromethane, tetrahydrofuran, and toluene were degassed and dried by sparging with N_2 gas followed by passage through an activated alumina column. Hexamethyldisiloxane was dried over CaH and distilled prior to use. All solvents were stored over 3-Å molecular sieves. Deuterated benzene, dichloromethane, acetone, acetonitrile, and toluene were purchased from Cambridge Isotope Laboratories, Inc., degassed via repeated freeze-pump-thaw cycles, and dried over 3-Å molecular sieves. Deuterated THF was purchased from Cambridge Isotope Laboratories, Inc., sparged, and dried over 3-Å molecular sieves prior to use. Solvents were frequently tested using a standard solution of sodium benzophenone ketyl in tetrahydrofuran to confirm the absence of oxygen and moisture. NMR spectra were recorded at ambient temperature unless otherwise stated on Varian Mercury 300 MHz and Varian Inova 500 MHz instruments. ^1H and ^{13}C NMR chemical shifts were referenced to residual solvent. ^{31}P NMR chemical shifts were referenced to 85% H_3PO_4.

^{29}Si NMR was referenced to tetraethylsilane. IR spectra were recorded on a Bio-Rad Excalibur FTS 3000 spectrometer controlled by Win-IR Pro software. Elemental Analyses were performed by Desert Analytics, Tuscon, AZ.

2.4.2 DFT Calculations

A hybrid density functional calculation and natural bond orbital (NBO) analysis was performed for **2.2** using the Jaguar package (version 5.0, release 20). The calculation employed B3LYP with LACVP** as the basis set. A geometry optimization was carried out starting from coordinates based on the solid state structure of **2.2** as the initial HF guess. No symmetry constraints were imposed and the calculation was performed assuming a singlet ground electronic state. Geometry optimizations were also performed using a slightly perturbed starting structure in which the three hydrides were placed in symmetry equivalent positions (pseudo three-fold) at typical Fe-H distances but beyond bonding distance to the Si atom. This perturbed starting point provided the same minimized geometry as when the crystallographic coordinates were used as the initial guess. Natural atomic charges and bond orders obtained from the NBO calculation are summarized in Table 2.2 below.

Table 2.2. Natural atomic charges and bond orders from NBO analysis of **2.2**.

Atomic Charges		**Bond Orders**	
Fe	-0.37	Fe-H2	0.65
Si	1.38	Si-H1	0.80
H2	-0.13	Si-H3	0.83
H1	-0.13		
H3	-0.14		

2.4.3 Starting Materials and Reagents

Complex **2.1**,[1c] $[PhBP^{iPr}_3]FeCl$,[21] $[PhBP^{iPr}_3]Fe(H)_3(PMe_3)$,[1c] and $PhSiD_3$[22] were prepared using literature methods. The generation of $[PhBP^{iPr}_3]Fe\text{-}CD_3$ (**2.4**) followed the same protocol reported for **2.1** using CD_3Li instead of CH_3Li. All other chemicals were purchased from Aldrich, Strem, or Gelest and used without further purification.

2.4.4 NMR Simulation

NMR simulations were performed using gNMR V4.0.1 assuming three equivalent protons, each coupling to one *trans* phosphorus atom and two *cis* phosphorus atoms. A linewidth of 8.0 Hz achieved the most accurate simulation. Second order effects were taken into account by using a P-P coupling constant of 62 Hz.

2.4.5 Synthesis of Compounds

(2,4,6-trimethylphenyl)silane ($MesSiH_3$). Neat $SiCl_3H$ (3.72 mL, 36.9 mmol) was dissolved in Et_2O (250 mL). To this stirring solution was added 2,4,6-trimethylphenylmagnesium bromide (36.9 mL, 1.0M in Et_2O, 36.9 mmol) over 30 minutes at room temperature, resulting in the precipitation of white solids. The mixture was stirred for 6 hours at room temperature. The solution was cooled to -35 ˚C and stirred while $LiAlH_4$ (4.19 g, 111 mmol) was added in small portions over the course of 1 hour. The mixture was allowed to warm to room temperature and stirred for 12 hours, then filtered through Celite to remove salts. The filtrate was slowly poured over ice (50 g). The E_2O layer was separated and washed with water (2 x 20 mL). The remaining solution was dried over Mg_2SO_4 and volatiles were removed in vacuo. Distillation (45 ˚C, full vacuum) provided the product as a clear liquid (3.5 g, 63%). The NMR spectroscopic data was identical to that reported previously for this silane.[23]

[PhBP$^{iPr}_3$]Fe(H)(η^3-SiH$_2$MePh) (2.2). Solid **2.1** (0.0828 g, 0.150 mmol) was dissolved in C_6H_6 (3 mL). To this solution was added neat $PhSiH_3$ (18.5 μL, 0.150 mmol). The resulting solution immediately became deep red in color. After stirring for 30 minutes at room temperature, the volatiles were removed in vacuo. The red solids were redissolved in minimal Et_2O (1 mL) and cooled to -35 ^oC for 12 hours. The resulting red crystals were dried in vacuo to yield analytically pure product (0.0641, 65%). ^1H NMR (300 MHz, C_6D_6): δ 8.05 (m, 2H, *o*-PhB), 7.97 (m, 2H, *o*-PhSi), 7.62 (m, 2H, *m*-PhB), 7.35 (m, 2H, *m*-PhSi), 7.24 (m, 2H, *p*-PhSi, PhB), 1.72 (m, 6H, C*H*$(CH_3)_2$), 1.16 (m, 36H, CH(C*H*$_3)_2$), 1.03 (m, 3H, SiMe), 0.94 (m, 6H, CH_2), -13.45 (m, 3H, Si/Fe-H, $^1J_{Si\text{-}H}$ = 68 Hz). $^{31}P\{^1H\}$ NMR (121 MHz, C_6D_6): δ 76.2. $^{29}Si\{^1H\}$ NMR (99.3 MHz, C_6D_6): δ 161.6. $^{13}C\{^1H\}$ NMR (75.5 MHz, C_6D_6): δ 159(br), 152 (br), 134.9, 132.4, 131.4, 127.8, 126.1, 124.0, 33.3, 23.2, 20.1, 16.6. UV-Vis (C_6H_6) λ_{max}, nm (ε, $M^{-1}cm^{-1}$): 500 (sh). IR (KBr/C_6H_6): ν(Fe-H) 2034 cm^{-1}. Anal. Calcd. for $C_{34}H_{64}BFeP_3Si$: C, 61.82; H, 9.77. Found: C, 61.51; H, 9.49.

[PhBP$^{iPr}_3$]Fe(H)(η^3-H$_2$SiMesMe) (2.3). Solid **2.1** (0.0275 g, 0.0498 mmol) was dissolved in C_6H_6 and to this solution was added $MesSiH_3$ (10 μL, 0.0747 mmol). The resulting mixture was stirred for one hour and the solution gradually became bright red. Volatiles were removed in vacuo and the resulting solids were washed with petroleum ether (2 x 3 mL). The solids were then dissolved in minimal Et_2O (0.5 mL) and cooled to -35 ˚C over 12 hours to yield spectroscopically pure, X-ray-quality crystals (0.0301 g, 86.0 %). ^1H NMR (300 MHz, toluene-d_8): δ 7.94 (m, 2H, *o*-PhB), 7.52 (m, 2H, *m*-PhSi), 7.27 (m, 1H, *p*-PhB), 6.62 (s, 2H, *m*-Mes), 2.45 (s, 6H, *o*-MesCH_3), 2.10 (s, 3H, *p*-MesCH_3), 1.66 (m, 6H, C*H*$(CH_3)_2$), 1.39 (s, 3H, Si-Me), 1.15 (m, 36H, CH(C*H*$_3)_2$), 0.85

(m, 6H, CH_2), -13.40 (m, 3H, $^1J_{Si\text{-}H}$ = 70 Hz). $^{31}P\{^1H\}$ NMR (121 MHz, C_6D_6): δ 79.5 (s). $^{29}Si\{^1H\}$ NMR (99.32 MHz, toluene-d_8): 160.4 (q, $^2J_{Si\text{-}P}$ = 59 Hz). Anal. Calcd. for $C_{37}H_{70}BFeP_3Si$: C, 63.25; H, 10.04. Found: C, 63.25; H, 9.66.

[PhBP$^{iPr}_3$]Fe(H)(H_2SiCD_3Ph) (2.5). Complex **2.5** was prepared analogously to **2.2** using **2.4.** ^1H NMR (300 MHz, C_6D_6): δ 8.05 (m, 2H, *o*-PhB), 7.94 (m, 2H, *o*-PhSi), 7.48 (m, 2H, *m*-PhB), 7.31 (m, 2H, *m*-PhSi), 7.22 (m, 2H, *p*-PhSi, PhB), 1.74 (m, 6H, C*H*$(CH_3)_2$), 1.18 (m, 36H, CH(C*H*$_3)_2$), 0.89 (m, 6H, CH_2), -13.42 (m, 3H, Fe-H). $^{31}P\{^1H\}$ NMR (121 MHz, C_6D_6): δ 76.2.

[PhBP$^{iPr}_3$]Fe(D)(η^3-D_2SiMePh) (2.6). Complex **2.6** was prepared analogously to **2.2** using $PhSiD_3$. ^1H NMR (300 MHz, C_6D_6): δ 8.04 (m, 2H, *o*-PhB), 7.98 (m, 2H, *o*-PhSi), 7.61(m, 2H, *m*-PhB), 7.32 (m, 2H, *m*-PhSi), 7.25 (m, 2H, *p*-PhSi, PhB), 1.72 (m, 6H, C*H*$(CH_3)_2$), 1.17 (m, 36H, CH(C*H*$_3)_2$), 1.03 (s, 3H, Me), 0.95 (m, 6H, CH_2). $^{31}P\{^1H\}$ NMR (121 MHz, C_6D_6): δ 79.2. IR (C_6H_6): ν = 1445 cm^{-1} (Fe-D) (calculated ν = 1440 cm^{-1}).

2.4.6 X-ray Experimental Data

X-ray diffraction studies were carried out in the Beckman Institute Crystallographic Facility on a Bruker Smart 1000 CCD diffractometer under a stream of dinitrogen. Data were collected using the Bruker SMART program, collecting ω scans at 5 ϕ settings. Data reduction was performed using Bruker SAINT v6.2. Structure solution and structure refinement were performed using SHELXS-97 (Sheldrick, 1990) and SHELXL-97 (Sheldrick, 1997). All structural representations were produced using the Diamond software program. Crystallographic data are summarized in Table 2.3.

Table 2.3. Crystallographic data for [PhBP$^{i\mathrm{Pr}}_3$]Fe(H)(η^3-SiH$_2$MePh), **2.2**; and [PhBP$^{i\mathrm{Pr}}_3$]Fe(H)(η^3-H$_2$SiMesMe), **2.3**.

	2.2	**2.3**
chemical formula	$C_{34}H_{64}BFeP_3Si$	$C_{37}H_{70}BFeP_3Si$
fw	660.51	702.59
T (°C)	-173	-173
λ (Å)	0.71073	0.71073
a (Å)	11.3852(12)	18.1126(13)
b (Å)	12.0036(13)	20.3251(14)
c (Å)	16.1029(17	21.6417(16)
α (°)	95.172(2)	90
β (°)	107.352(2)	90
γ (°)	95.805(2)	90
V (Å^3)	2072.9(4)	7967.2(10)
space group	P-1	P2(1)2(1)2(1)
Z	2	8
D_{calc} (g/cm^3)	1.058	1.171
μ(cm^{-1})	5.28	5.53
R1, wR2[a] ($I > 2\sigma(I)$)	0.0309, 0.0816	0.0609, 0.0920

[a] $R1 = \Sigma||F_o| - |F_c||/\Sigma|F_o|$, $wR2 = \{\Sigma[w(F_o^2 - F_c^2)^2]/\Sigma[w(F_o^2)^2]\}^{1/2}$

References Cited

[1] (a) Betley, T. A.; Peters, J. C. *J. Am. Chem. Soc.* **2004,** *108*, 6252. (b) Betley, T. A.; Peters, J. C. *J. Am. Chem. Soc.* **2003**, *125*, 10782. (c) Daida, E. J.; Peters, J. C. *Inorg. Chem.* **2004**, 7474.

[2] Relevant examples of transition metal silylene complexes: (a) Peters, J. C.; Feldman, J. D.; Tilley, T. D. *J. Am. Chem. Soc.* **1999**, *121*, 9871. (b) Mork, B. V.; Tilley, T. D. *J.*

Am. Chem. Soc. **2004**, *126*, 4385. (c) Feldman, J. D.; Peters, J. C.; Tilley, T. D. *Organometallics* **2002**, *21*, 4065. (d) Glaser, P. B.; Wanandi, P. W.; Tilley, T. D. *Organometallics* **2004**, *23*, 693. (e) Beddie, C.; Hall, M. B. *J. Am. Chem. Soc.* **2004**, 13564. (f) Glaser, P.; Tilley, T. D. *J. Am. Chem. Soc.* **2003**, *125*, 13640.

[3] For examples of group 8 η^2-silane adducts, see: (a) Bart, S. C.; Lobkovsky, E.; Chirik, P. J. *J. Am. Chem. Soc.* **2004**, *126*, 13794. (b) Ohki, Y.; Kojima, T.; Oshima, M.; Suzuki, H. *Organometallics* **2001**, *20*, 2654. (c) Simons, R. S.; Tessier, C. A. *Organometallics* **1996**, *15*, 2604. (d) Scharrer, E.; Brookhart, M. *J. Organomet. Chem.* **1995**, *497*, 61. (e) Schubert, U.; Gilbert, S.; Mock, S. *Chem. Ber.* **1992**, *125*, 835. (f) Scharrer, E.; Chang, S.; Brookhart, M. *Organometallics* **1995**, *14*, 5686. (g) Delpech, F.; Sabo-Etienne, S.; Daran, J.-C.; Chaudret, B.; Hussein, K.; Marsden, C. J.; Barthelat, J.–C. *J. Am. Chem. Soc.* **1999**, *121*, 6668-6682. (h) Atheaux, I.; Delpech, F.; Donnadieu, B.; Sabo-Etienne, S.; Chaudret, B.; Hussein, K.; Barthelat, J.–C.; Braun, T.; Duckett, S. B.; Perutz, R. N. *Organometallics* **2002**, *21*, 5347-5357. (i) Lachaize, S.; Sabo-Etienne, S.; Donnadieu, B.; Chaudret, B. *Chem. Comm.* **2003**, 214.

[4] Reviews that cover η^2 Si-H interactions: (a) Corey, J. Y.; Braddock-Wilking, J. *Chem. Rev.* **1999**, *99*, 175. (b) Schubert, U. *Adv. Organomet. Chem.* **1990**, *30*, 151. (c) Nikonov, G. I. *J. Organomet. Chem.* **2001**, *635*, 24. (d) Lin, Z. *Chem. Soc. Rev.* **2002**, *31*, 239. (e) Kubas, G. J. *Metal Dihydrogen and Sigma Bond Complexes: Structure, Theory and, Reactivity.* Kluwer Academic: New York, 2001.

[5] (a) Atheaux, I.; Donnadieu, B.; Daran, J.-C.; Sabo-Etienne, S.; Chaudret, B.; Hussein, K.; Barthelat, J.-C. *J. Am. Chem. Soc.* **2000**, *122*, 5664. (b) Ben Said, R.; Hussein, K.;

Barthelat, J.-C.; Atheaux, I.; Sabo-Etienne, S.; Grellier, M.; Donnadieu, B.; Chaudret, B. *Dalton Trans.* **2003**, 4139.

[6] Luo, X.-L.; Baudry, D.; Boydell, P.; Charpin, P.; Nierlich, M.; Ephritikhine, M.; Crabtree, R. H. *Inorg. Chem.* **1990**, *29*, 1511.

[7] Hussein, K.; Marsden, C. J.; Barthelat, J.-C.; Rodriguez, V.; Conejero, S.; Sabo-Etienne, S.; Donnadieu, B.; Chaudret, B. *Chem. Commun.* **1999**, 1315.

[8] Yardy, N. M.; Lemke, F. R. *Organometallics* **2001**, *20*, 5670.

[9] Osipov, A. L.; Gerdov, S. M.; Kuzmina, L. G.; Howard, J. A. K.; Nikonov, G. I. *Organometallics* **2005**, *24,* 587.

[10] Tobita, H.; Matsuda, A.; Hashimoto, H.; Ueno, K.; Ogino, H. *Angew. Chem. Int. Ed.* **2004**, *43*, 221.

[11] Jaguar 5.0, Schrodinger, LLC, Portland, Oregon, 2002.

[12] Lee, C.; Yang, W.; Parr, R. G. *Phys. Rev. B.* **1988**, *37*, 785.

[13] NBO 5.0. Glendening, E. D.; Badenhoop, J. K.; Reed, A. E.; Carpenter, J. E.; Bohmann, J. A.; Morales, C. M.; Weinhold, F. (Theoretical Chemistry Institute, University of Wisconsin, Madison, WI, 2001); http://www.chem.wisc.edu/~nbo5.

[14] Crabtree, R. H.; Lavin, M.; Bonneviot, L. *J. Am. Chem. Soc.* **1986**, *108*, 4032.

[15] For comparison, [PhBP$^{i\mathrm{Pr}}_3$]Fe(H)$_3$(PMe$_3$) exhibits a T_{1min} of 140 ms.[1c]

[16] Taw, F. L.; Bergman, R. G.; Brookhart, M. *Organometallics* **2004**, *23*, 886-890.

[17] Silverstein, R. M.; Webster, F. X. *The Spectrometric Identification of Organic Compounds*, 6th ed., John Wiley & Sons, Inc,: New York, NY, **1998**, Ch. 6, pp 262.

[18] Collaboration with Bill Gunderson and Prof. Michael Hendrich, Carnegie Mellon University, Pittsburgh, PA.

[19] Masters of Science Thesis of Erin J. Daida, 2005.

[20] For examples see: (a) Gilbert, S.; Knorr, M.; Mock, S.; Schubert, U. *J. Organomet. Chem*. **1994**, *480*, 241. (b) Procopio, L. J.; Berry, D. H. *J. Am. Chem. Soc*. **1991**, *113*, 4039. (c) Rickard, C. E. F.; Roper, W. R.; Woodgate, S. D.; Wright, L. J. *J. Organomet. Chem*. **2000**, *609*, 177. (d) Hubler, K.; Hubler, U.; Roper, W. R.; Schwerdtfeger, P.; Wright, L. J. *Chemistry–A European Journal* **1997**, *10*, 1608-1616.

[21] Betley, T. A.; Peters, J. C. *Inorg. Chem.* **2003**, *42*, 5074-5084.

[22] Benkeser, R. A.; Landesman, H.; Foster, D. J. *J. Am. Chem. Soc.* **1952**, *74*, 648-650.

[23] Minge, O.; Nogai, S.; Schmidbaur, H. *Z. Naturforsch*. **2004**, 153-160.

Chapter 3: P_4 Activation by Iron(I) Affords a Diiron(II) Complex Bridged by a P_4 Square

3.1 Introduction

The transition metal chemistry of elemental phosphorus, P_4, has been explored thoroughly over the past several decades and metal-catalyzed P_4 activation is integral to the ultimate goal of generating organophosphorus compounds directly from P_4.[1] Accordingly, complexes containing P_x ligands are known for nearly all transition metals.[2] While transition metal complexes that contain an intact, tetrahedral P_4 moiety are limited,[3] there are numerous examples of complexes in which one or more of the P-P bonds of P_4 have been cleaved, including many examples of both mono- and dinuclear *cyclo*-P_3 metal complexes.[4,5] In addition, the square planar P_4^{2-} unit, in which two P-P bonds have been cleaved, is well represented in complexes of both early and late transition metals.[6] In most of these examples, the P_4^{2-} unit requires stabilization by additional metal fragments that coordinate to the phosphorus lone pairs. Two interesting exceptions in which P_4^{2-} is sandwiched between two crown-ether supported alkali metal cations were recently reported.[7] To the best of our knowledge, only one example of a structurally characterized transition metal complex featuring a substituent-free P_4^{2-} moeity, $Cp^*(CO)_2Nb(\eta^4\text{-}P_4)$, has been reported.[8]

Recently, we have found that tris(phosphino)borate ($[PhB(CH_2PR_2)_3]^-$, R = Ph, ^{i}Pr) ligands are uniquely capable of stabilizing both high and low valent Fe.[9] This versatility allows Fe complexes supported by these ligands to bind both π acids (e.g., N_2, CO) and π bases (e.g., NR^{2-}, N^{3-}) in the apical coordination site. Among the unique complexes that can be isolated using these ligands are a number of iron(I) complexes with labile L-donors (e.g., PR_3, N_2).[10] Motivated by the intriguing reactivity patterns these tris(phosphino)borate iron systems display, we have begun to explore the reactivity of tris(phosphino)borate-

supported iron(I) complexes with small molecule substrates.[11] Herein, we report a fascinating activation of P_4 by reactive iron(I) precursors to generate unusual diiron(II) complexes bridged by planar η^4-P_4^{2-} moieties. This type of unsubstituted planar P_4^{2-} moiety is extremely rare and the complexes described are, to the best of our knowledge, the first reported examples of P_4 squares symmetrically bridged between two transition metal centers.

3.2 Results and Discussion

The iron(I) complex $\{[PhBP^{iPr}_3]Fe\}_2(\mu\text{-}N_2)$ ($[PhBP^{iPr}_3]$ = $PhB(CH_2P^iPr_2)_3^-$) is a particularly good candidate for small molecule activation chemistry as a result of the lability of the N_2 ligand.[10] Reaction of $\{[PhBP^{iPr}_3]Fe\}_2(\mu\text{-}N_2)$ with one equivalent of P_4 leads to displacement of N_2 and quantitative formation of a diamagnetic green product, $\{[PhBP^{iPr}_3]Fe\}_2(\mu\text{-}P_4)$ (**3.1**) (97% isolated yield) (Scheme 3.1). Similarly, $[PhBP_3]Fe^I(PPh_3)$[10] reacts with 0.5 equivalents of P_4 to liberate PPh_3 and generate $\{[PhBP_3]Fe\}_2(\mu\text{-}P_4)$ (**3.2**) in high yield (93%). In both cases, when excess P_4 is used, the same products are generated exclusively. The diamagnetic nature of **3.1** and **3.2** suggests that both iron centers of the dimeric units can be assigned an iron(II) oxidation state and that the P_4^{2-} unit has been formally reduced by two electrons.

Scheme 3.1

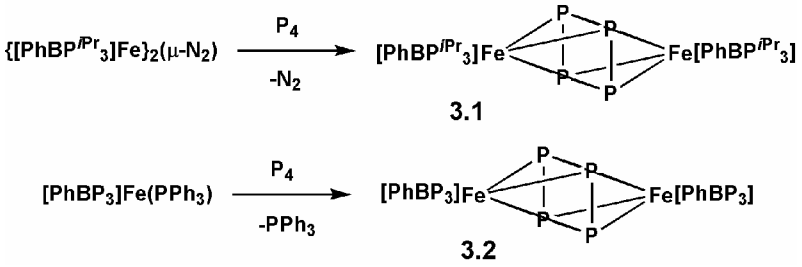

We were fortunate to obtain X-ray-quality crystals of both **3.1** and **3.2**. The solid state structures reveal that the bridging P_4^{2-} unit adopts a planar, η^4-P_4 conformation (Figure

3.1). In both structures, two of the P-P bonds are modestly elongated but all four corners of the P_4 moiety are within reasonable bonding distance of each other (**3.1** : P7-P8: 2.192(2) Å; P10-P7 2.211(3) Å; P8-P9: 2.137(4) Å; P9-P10: 2.137(3) Å; **3.2** : P4-P5: 2.251(1) Å; P5-P6: 2.155(1) Å). In addition, each of the four bridging phosphorus atoms in **3.1** and **3.2** are bonded to both iron centers (**3.1 :** Fe1-P7: 2.301(2) Å; Fe2-P7: 2.303(2) Å; Fe1-P8: 2.389(2) Å; Fe2-P8: 2.362(2); Fe1-P9: 2.517(2) Å; Fe2-P9: 2.515(2) Å; Fe1-P10: 2.371(2) Å; Fe2-P10: 2.399(2) Å; **3.2 :** Fe-P4: 2.2735(8) Å; Fe-P5: 2.3759(9) Å; Fe-P6: 2.553(9) Å). On average, the Fe-P and P-P bond lengths of complexes **3.1** and **3.2** are remarkably similar despite the electronic differences imparted by variation of the phosphine ligand substituents.

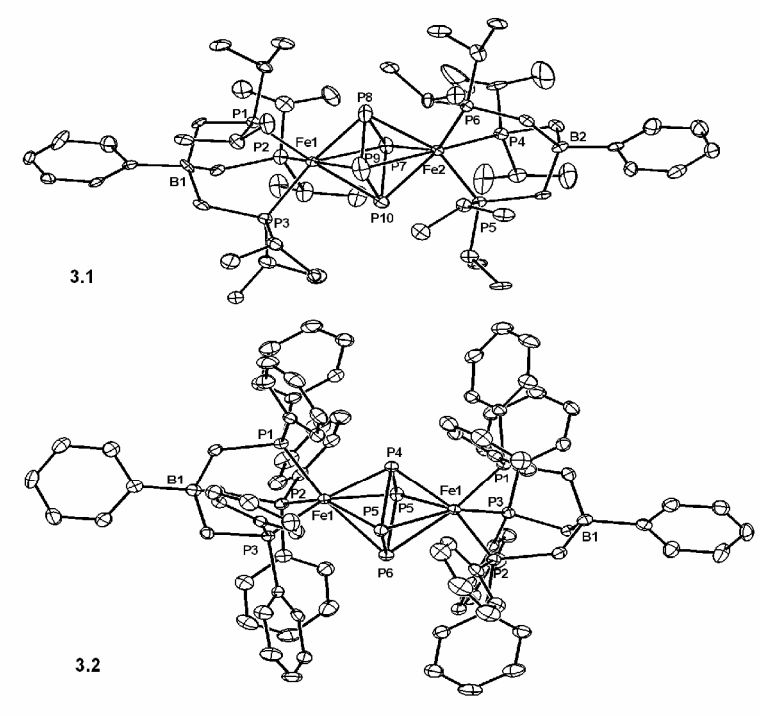

Figure 3.1 50% displacement ellipsoid representation of **3.1** and **3.2**. In the case of **3.2**, the right half of the molecule has been generated via symmetry operations. Hydrogen atoms have been omitted for clarity.

The electronic differences between **3.1** and **3.2** are, however, manifested in their spectroscopic properties. The $^{31}P\{^{1}H\}$ NMR spectrum of **3.1** exhibits two singlets at 131.7 ppm and 45.6 ppm that integrate in a 2:3 ratio and correspond to the phosphorus nuclei of the P_4 moiety and (phosphino)borate ligand, respectively. Similarly, complex **3.2** also exhibits two singlets in the $^{31}P\{^{1}H\}$ NMR. The chemical shift corresponding to the phosphorus atoms of the (phosphino)borate ligand in **3.2** (44.6 ppm) is nearly identical to that observed for **3.1**. The ^{31}P signal of the P_4 unit in **3.2**, however, is much farther downfield to 214.9 ppm. This dramatic difference can most likely be attributed to a more activated P_4 unit in **3.2** as a result of the more electron-releasing [$PhBP^{iPr}_3$] ligand. As a result of their more covalent character, the ^{31}P signals for the P_4^{2-} unit in complexes **3.1** and **3.2** are shifted significantly upfield from the shift of 322 ppm reported for the (K-18-crown-6)$_2P_4 \cdot 2NH_3$.[7] It is likely that the absence of coupling between the phosphorus nuclei of the borate ligand and that of the P_4 unit in both **3.1** and **3.2,** even at low temperatures (toluene-d_8, -80 ˚C), is due to the dominant π-bonding between the iron centers and the P_4 unit.

The optical absorption spectra of **3.1** and **3.2** show relatively similar bands in the 350-800 nm range. The optical spectrum of **3.1** has two intense features at 641 nm (ε = 7800 M^{-1} cm^{-1}) and 766 nm (ε = 5900 M^{-1} cm^{-1}) that contribute to its green color. The corresponding optical features for complex **3.2** are observed at 628 nm (ε = 8000 M^{-1} cm^{-1}) and 766 nm (ε = 5000 M^{-1} cm^{-1}). These bands can likely be attributed to LMCT transitions based on their intensity and the similarity between the complexes. The higher energy feature is presumably red-shifted in complex **3.1** as a result of the more reduced metal center.

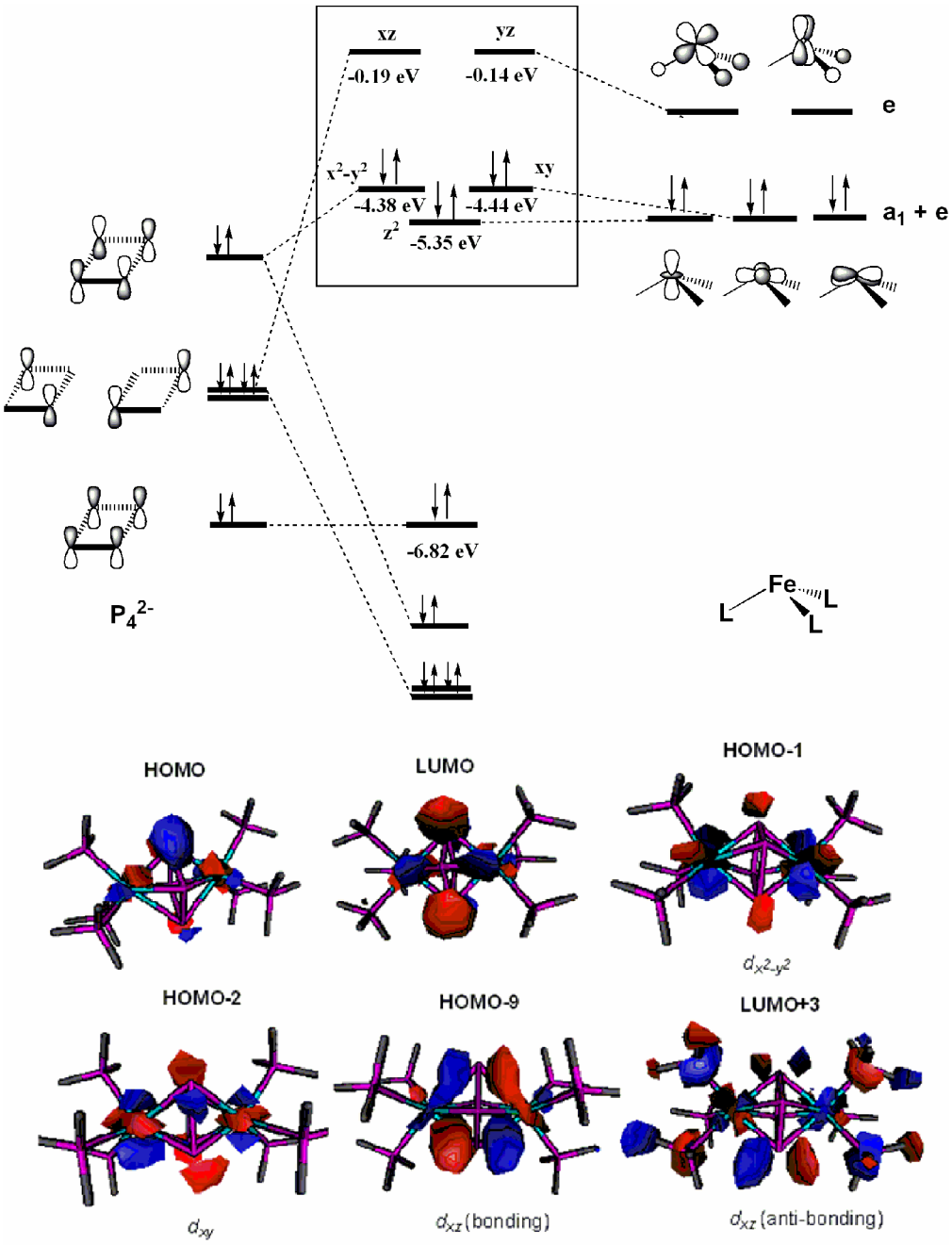

Figure. 3.2 Simplified MO diagram theoretically calculated for $(PH_3)_3Fe(\mu\text{-}P_4)Fe(PH_3)_3$ using DFT. For clarity only one set of Fe d orbitals is shown (left). Selected frontier orbitals calculated for $(PH_3)_3Fe(\mu\text{-}P_4)Fe(PH_3)_3$ displaying bonding and anti-bonding interactions between the Fe centers and P_4^{2-}.

The planar, symmetric geometry of the dianionic P_4^{2-} unit is a result of its aromaticity, and its electronic structure is quite similar to cyclobutadiene.[12] It has been suggested that the P_4^{2-} unit can best be desribed as "lone pair aromatic," meaning that the electrons are delocalized primarily through the lone pairs.[7] To better understand the bonding in our new diiron structure types, calculations were performed using DFT (Jaguar, B3LYP, LACVP).[13] For the purpose of simplifying calculations, the (phosphino)borate ligands were replaced with PH_3 groups. Our theoretical results are consistent with the low-spin Fe^{II} formulation and suggest that the Fe d_{z^2} orbitals are essentially non-bonding with respect to the P_4 unit due to poor overlap with the fully symmetric combination of P_4 p_z orbitals (Figure 3.2). The strongest orbital overlap exists between the Fe d_{xz} and d_{yz} orbitals and the P_4 *e* set of p_z orbitals, while the Fe d_{xy} and $d_{x^2-y^2}$ overlap with the P_4 orbitals to a much lesser extent. Interestingly, both the HOMO and the LUMO reside predominantly on the P_4 phosphorus atoms.

Upon examining the reactivity of **3.1** and **3.2**, we found that although **3.2** is thermally stable to temperatures as high as 120 ˚C, complex **3.1** undergoes thermolysis (80 ˚C, toluene, 24 h) to lead to clean formation of a single diamagnetic product $\{[PhBP^{iPr}_3]Fe\}_2(\mu\text{-}P_3)$ (**3.3**) initially identified by electrospray ionization MS (m/z = 1067 (M^+)). The connectivity of **3.3** was determined by X-ray diffraction of single crystals; however, an anisotropically refined structure could not be obtained due to disorder in both the isopropyl groups and the P_3 unit (Figure 3.3). The $^{31}P\{^1H\}$ NMR spectrum of **3.3** exhibits a triplet at -271 ppm ($^2J_{P\text{-}P}$ = 420 Hz) corresponding to the P_3 unit and a doublet at 56 ppm ($^2J_{P\text{-}P}$ = 420 Hz) for the $[PhBP^{iPr}_3]$ ligand. The coupling pattern is simplified by the absence of coupling between phosphorus nuclei *cis* to each other.

This product is analogous to a number of iron and cobalt species containing *cyclo*-P_3 units, most notably (triphos)Co(P_3), (np_3)Co(P_3), [(triphos)Co(μ-P_3)Fe(etriphos)][PF_6]$_2$, and [(triphos)Co(μ-P_3)Co(etriphos)][BPh_4]$_2$ (triphos = $CH_3C(CH_2PPh_2)_2$, etriphos = $CH_3C(CH_2PEt_2)_2$, np_3 = $N(CH_2CH_2PPh_2)_3$).[4] These complexes are synthesized in a one-pot reaction of the metal salt, ligand, and elemental phosphorus, and so the mechanism by which the final product forms is ambiguous. In the case of the more controlled generation of **3.3**, the mechanism, as well as the fate of the expelled phosphorus atom, is more intriguing. A recent kinetic and computational study by Cummins et al. suggests several possible mechanistic pathways to generate similar *cyclo*-P_3 Mo species via phosphide extrusion from a coordinated P_4 fragment.[5] In light of this study, as well as the previously reported iron(IV) nitride supported by the [$PhBP^{iPr}_3$] ligand, it is possible to consider that the formation of **3.3** is accompanied by transient formation of a terminal [$PhBP^{iPr}_3$]Fe^{IV}≡P intermediate. A full DFT study would be required to examine this and other potential mechanistic possibilities.

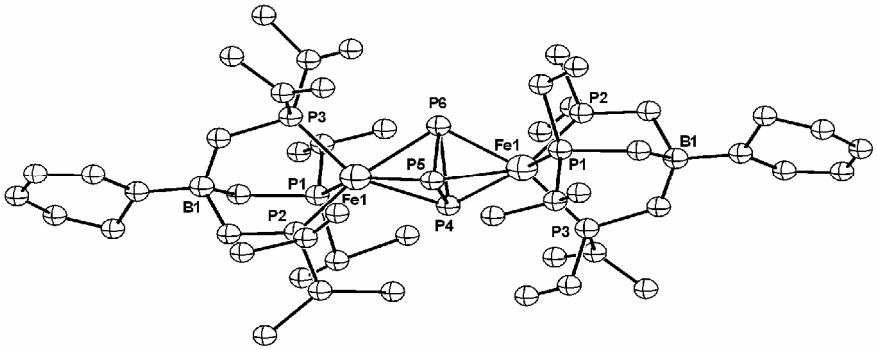

Figure 3.3 Isotropically refined structure of complex **3.3,** confirming its connectivity. Only one of two independent molecules in the asymmetric unit cell is shown. The right half of the molecule has been generated using symmetry operations.

In addition to their differences in thermal stability, cyclic voltammetry reveals that complex **3.1** and **3.2** have very different electrochemical properties. While complex **3.1** does not appear to undergo any facile, reversible redox processes,[14] electrochemistry of **3.2** reveals several distinct features (Figure 3.4). The cyclic voltammagram of **3.2** exhibits a reversible reduction at -1.48 V, assigned as the one electron reduction of the Fe centers. The irreversible reduction at -2.32 V is likely attributed to further reduction of the P_4 unit, leading to disruption of its planar structure. Redox activity centered at the P_4 unit is consistent with the predicted location of the LUMO (*vide supra*). The quasi-reversible oxidation that occurs at +0.14 V is likely metal-centered, but, in out hands, this oxidation process can not be achieved chemically.

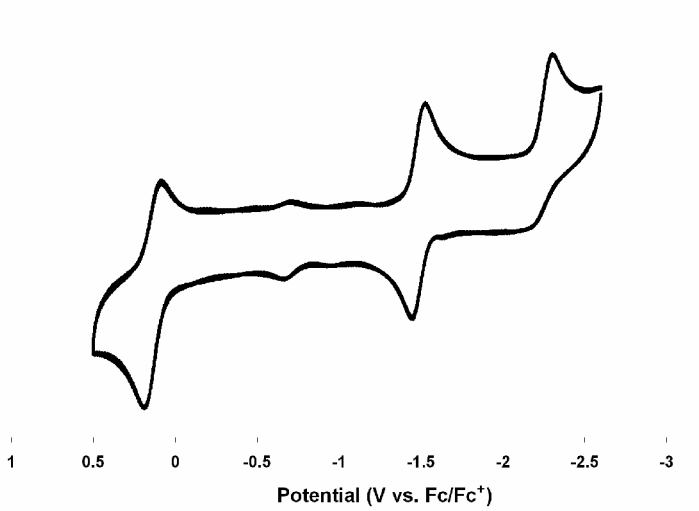

Figure 3.4 Cyclic voltammetry of **3.2** (0.4 M $[^{n}Bu_4N]PF_6$ electrolyte in THF, scan rate = 100 mV/s).

As predicted by cyclic voltammetry, complex **3.2** can be chemically reduced by one equivalent of KC_8 or Cp^*_2Co (Cp* = pentamethylcyclopentadienyl) to generate paramagnetic, brown $[\{[PhBP_3]Fe\}_2\text{-}(\mu\text{-}P_4)]^-$ (**3.4**) quantitatively. Solution magnetic data and ESI-MS (m/z = 865 (M^-)) confirmed the complex's formulation. Determination of the

magnetic moment of **3.4** in solution by Evans' method revealed a μ_{eff} value of 1.82 μ_B, corresponding to one unpaired electron (spin-only value = 1.73 μ_B).[15] X-ray quality crystals of [**3.4**][Cp*$_2$Co] were obtained, but a high quality structure could not be obtained. Nonetheless, an isotropically refined structure confirmed the connectivity of **3.4** and verifies that the P_4 unit remains intact (Figure 3.5). EPR spectroscopy of **3.4**[K(THF)$_4$] shows a rhombic signal at g_{avg} = 2.05 (Figure 3.6), consistent with an S = ½ spin state. Interestingly, the signal is nearly isotropic, and the three g values are very similar (g_1 = 2.08, g_2 = 2.05, and g_3 = 2.02), indicating that the unpaired electron resides in a very symmetric orbital. The absence of hyperfine coupling to phosphorus in the EPR signal, even at low temperature, is likely indicative that the unpaired electron resides primarily on iron.

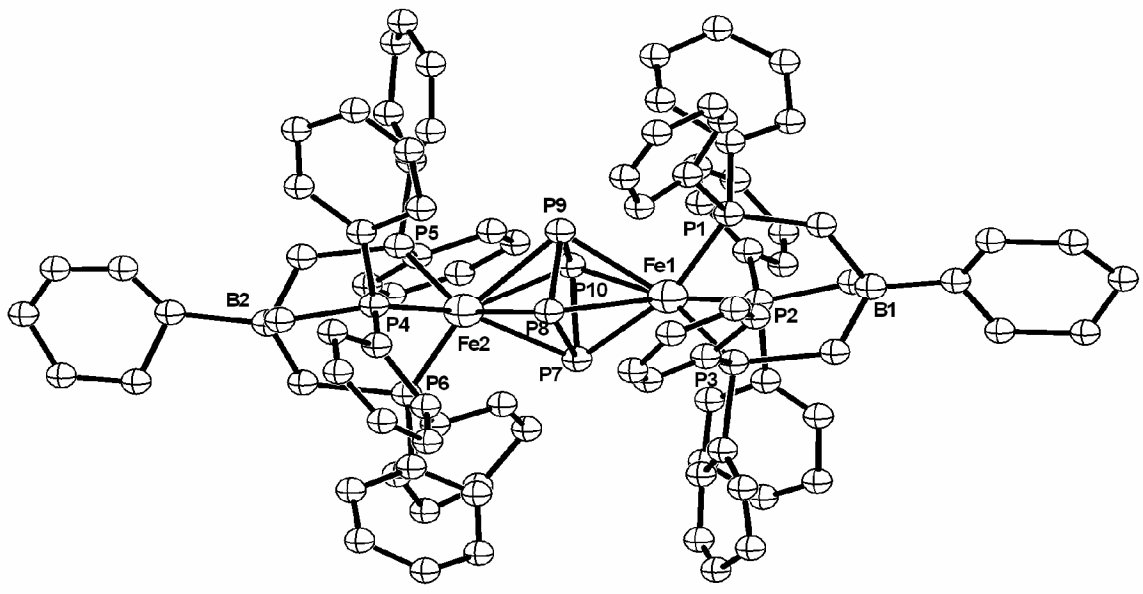

Figure 3.5 Isotropically refined structure of complex **3.4**[Cp*$_2$Co], confirming its connectivity. The [Cp*$_2$Co] countercation, hydrogen atoms, and a THF molecule in the solvent lattice are not shown.

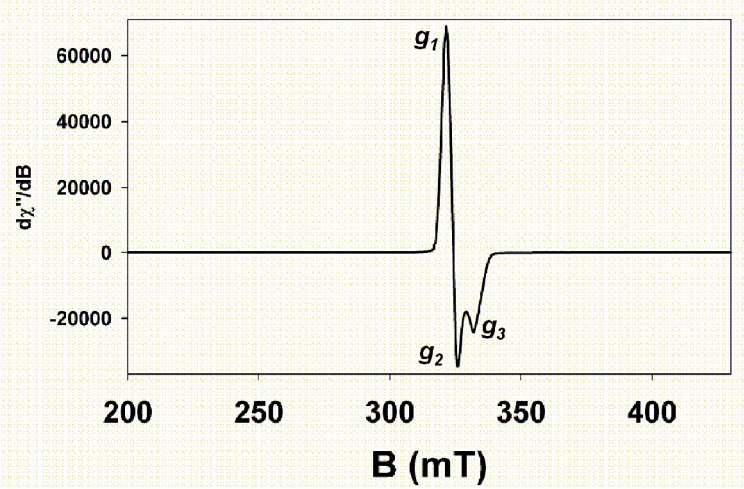

Figure 3.6 EPR spectrum of **3.4** (methytetrahydrofuran at 20K, X band, 9.474 GHz).

3.3 Conclusions

In summary, low-valent Fe(I) tris(phosphino)borate precursors activate elemental phosphorus, P_4, at room temperature to generate unprecedented low-spin dinuclear Fe(II) complexes, $\{[PhBP^{iPr}_3]Fe\}_2$-(μ-P_4) (**3.1**) and $\{[PhBP_3]Fe\}_2$-(μ-P_4) (**3.2**), bridged by planar P_4^{2-} moieties. Complex **3.1** undergoes P-P bond cleavage under thermolytic conditions to generate a *cyclo*-P_3 bridged species. Complex **3.2**, on the other hand, is thermolytically stable, but can be reduced by one electron to generate a highly delocalized anionic P_4-bridged complex. These complexes are the first reported examples of dinuclear transition metal centers bridged by a planar P_4^{2-} moiety.

3.4 Experimental Section

3.4.1 General Considerations

General considerations are outlined in Section 2.4.1.

3.4.2 Starting Materials and Reagents

$\{[PhBP^{iPr}_3]Fe\}_2(\mu\text{-}N_2)$,[10b] $[PhBP_3]Fe(PPh_3)$,[10a] and KC_8[16] were prepared using literature methods. White phosphorous, P_4, was recrystallized from toluene prior to use.

All other chemicals were purchased from Aldrich or Strem and used without further purification.

3.4.3 DFT Calculations

A hybrid density functional calculation was performed for $(PH_3)_3Fe(\mu\text{-}P_4)Fe(PH_3)_3$ using the Jaguar package (version 5.0, release 20).[13a] The calculation employed B3LYP with LACVP** (LACVP**$^{++}$ for B) as the basis set.[13b] No symmetry constraints were imposed, and the calculation was performed assuming a singlet electronic ground state. Pictorial representations of the resulting molecular orbitals were generated using the Molden software program.

3.4.4 EPR Measurements

X-band EPR spectra were obtained on a Bruker EMX spectrometer equipped with a rectangular cavity working in the TE_{102} mode. Variable temperature measurements were conducted with an Oxford continuous-flow helium cryostat (temperature range 3.6 - 300 K). Accurate frequency values were provided by a frequency counter built in the microwave bridge. Solution spectra were acquired in 2-methyltetrahydrofuran and sample preparation was performed under a nitrogen atmosphere. Simulation of EPR data was performed using the WinEPR program.

3.4.5 Synthesis of Compounds

{[PhBP$^{iPr}_3$]Fe}$_2$(μ-P$_4$) (3.1). Solid {[PhBP$^{iPr}_3$]Fe}$_2$(μ-N$_2$) (0.0649 g, 0.0589 mmol) was dissolved in THF (5 mL). To this was added a solution of solid P_4 (0.0073 g, 0.0589 mmol) in THF (2 mL). The resulting mixture gradually became dark green while stirring for one hour. Solvent was removed from the resulting solution *in vacuo*. The resulting green solids were dissolved in minimal benzene, filtered through Celite, and lyophilized

to yield analytically pure product (0.0678 g, 96.1%). Crystals suitable for X-ray diffraction were grown from a toluene / hexamethyldisiloxane mixture at -35 °C. ^{1}H NMR (300 MHz, C_6D_6): δ = 8.22 (d, 4H, $^{3}J_{H\text{-}H}$ = 6.9 Hz, *o*-Ph), 7.72 (t, 4H, $^{3}J_{H\text{-}H}$ = 6.9 Hz, *m*-Ph), 7.43 (m, 2H, $^{3}J_{H\text{-}H}$ = 6.9 Hz, *p*-Ph), 2.31 (m, 12H, C*H*$(CH_3)_2$), 1.30 (br m, 12H, CH_2), 1.19 (br m, 72H, CH(C*H*$_3)_2$). ^{31}P NMR (121 MHz, C_6D_6): δ = 131.67 (s, 4P, P_4), 45.6 (s, 6P, PhBP$^{i\text{Pr}}_3$). ^{13}C NMR (75.5 MHz, C_6D_6): δ = 165 (br), 132, 128, 124, 51, 33, 21, 14 (m). ES-MS$^-$ (Electrospray): m/z 661 ([PhBP$^{i\text{Pr}}_3$]Fe-P_4^-). UV-Vis (C_6H_6) λ_{max}, nm (ε): 434 (14,000), 641 (7,800), 766 (5,900). Anal. Calcd. for $C_{54}H_{106}B_2Fe_2P_{10}$: C, 54.12; H, 8.91. Found: C, 53.04; H, 7.81.

{[PhBP$_3$]Fe}$_2$(μ-P$_4$) (3.2). Solid [PhBP$_3$]Fe(PPh$_3$) (0.2590 g, 0.2583 mmol) was dissolved in THF (10 mL). To this was added a solution of P_4 (0.0320 g, 0.258 mmol) in THF (2 mL). After stirring for one hour, the solution had become dark green. The resulting solution was filtered through Celite and dried in vacuo. The green solids were then extracted with C_6H_6 (10 mL) and filtered through Celite. Petroleum ether (10 mL) was added and the mixture was stirred for 1 hour. The green, microcrystalline precipitate was collected on a sintered glass frit and washed with petroleum ether (2 x 5 mL) to yield analytically pure **3.2** (0.1924 g, 92.8%). Crystals suitable for X-ray diffraction were grown via vapor diffusion of Et_2O into a concentrated CH_2Cl_2 solution. ^{1}H NMR (300 MHz, C_6D_6): δ = 8.27 (d, 4H, $^{3}J_{H\text{-}H}$ = 6.6 Hz, *o*-PhB), 7.71 (t, 4H, $^{3}J_{H\text{-}H}$ = 6.9 Hz, *m*-PhB), 7.44 (t, 2H, $^{3}J_{H\text{-}H}$ = 6.9 Hz, *o*-PhB), 6.94 (m, 24H, *o*-PhP), 6.82 (t,12, $^{3}J_{H\text{-}H}$ = 7.2 Hz, *p*-PhP), 6.62 (t, 24H, $^{3}J_{H\text{-}H}$ = 7.2 Hz, *m*-PhP), 2.23 (m,12, CH_2). ^{31}P NMR (121 MHz, C_6D_6): δ = 214.9 (s, 4P, P_4), 44.6 (s, 6P, PhBP$_3$). ^{13}C NMR (75.5 MHz, C_6D_6): δ = 164 (br), 145.0, 142.1, 136.2, 133.0, 132.7, 126.5, 125.5, 22.6. UV-Vis (C_6H_6) λ_{max}, nm

(ε): 431 (sh), 628 (8,000), 766 (5,000). Anal. Calcd. for $C_{90}H_{82}B_2Fe_2P_{10}$: C, 67.28; H, 5.14. Found: C, 66.68; H, 5.39.

{[PhBP$^{iPr}_3$]Fe}$_2$(μ-P$_3$) (3.3). Solid **3.1** (0.4588 g, 0.3830 mmol) was dissolved in toluene (15 mL) and heated to 80 °C for 18 hours in a sealed reaction vessel. The green/brown solution was then filtered through Celite, and the resulting filtrate was dried in vacuo. The remaining green/brown solids were extracted with benzene (5 mL), filtered through Celite, and then dried in vacuo. Vapor diffusion of petroleum ether into a concentrated benzene solution resulted in spectroscopically pure, crystalline product (0.3468 g, 77.6%). Crystals grown by this method were used for X-ray diffraction. ^{1}H NMR (300 MHz, C_6D_6): δ = 7.71 (d, 4H, $^3J_{H\text{-}H}$ = 6.9 Hz, *o*-Ph), 7.40 (t, 4H, $^3J_{H\text{-}H}$ = 6.9 Hz, *m*-Ph), 7.21 (t, 2H, $^3J_{H\text{-}H}$ = 6.9 Hz, *p*-Ph), 2.20 (br m, 12H, CH_2), 1.93 (m, 6H, C*H*$(CH_3)_2$) 1.68 (m, 6H, C*H*$(CH_3)_2$) 0.8-1.20 (m, 72H, CH(C*H*$_3$)$_2$), ^{31}P NMR (121 MHz, C_6D_6): δ = 55.6 (d, 6P, $^2J_{P\text{-}P}$ = 420 Hz, PhBP$^{iPr}_3$), -271.3 (t, 3P, $^2J_{P\text{-}P}$ = 420 Hz, P_3). ^{13}C NMR (75.5 MHz, C_6D_6): δ = 165 (br), 129.6, 129.3, 126.0, 42.1, 34.8, 23.1, 14 (m). ES-MS$^+$ (Electrospray): m/z 1167 (M^+). ES-MS$^-$ (Electrospray): m/z 630 ([PhBP$^{iPr}_3$]Fe-P$_3^-$). UV-Vis (C_6H_6) λ_{max}, nm (ε): 646 (3,100). Anal. Calcd. for $C_{54}H_{106}B_2Fe_2P_9$: C, 55.55; H, 9.15. Found: C, 54.12; H, 8.73.

[{[PhBP$_3$]Fe}$_2$(μ-P$_4$)][K(THF)$_4$] (3.4). Solid **3.2** (0.0186 g, 0.0116 mmol) was dissolved in THF (1 mL). To this was added a THF (0.5 mL) solution of KC_8 (0.0016 g, 0.0116 mmol) and the mixture immediately became brown. After stirring for 1 hour, the volatiles were removed from the reaction mixture *in vacuo*. The brown solids were redissolved in THF (1 mL) and filtered through Celite. Vapor diffusion of petroleum ether into this concentrated THF solution resulted in analytically pure, needle-like

crystals of **3.4** (0.0132 g, 69%). ^{1}H NMR (300 MHz, C_6D_6): δ = 7.71, 7.39, 7.21, 6.92, 5.99 (br), 5.21, 4.98. UV-Vis (C_6H_6) λ_{max}, nm (ε): 431 (sh), 631 (4900), 752 (sh). Evans' method (THF-d_8): 1.82 μ_B. ES-MS$^-$ (Electrospray): m/z 865 ([$PhBP_3$]Fe-P_4^-). Anal. Calcd. for $C_{106}H_{114}B_2Fe_2KO_4P_{10}$: C, 65.82; H, 5.94. Found: C, 63.48; H, 5.51.

3.4.6 X-ray Experimental Data

Crystallographic procedures are outlined in Section 2.4.6. **3.2** cocrystallized with two different solvent molecules occupying the same site. This disorder was best modeled with 30% dichloromethane and 70% diethyl ether. Half of **3.2** was generated via symmetry operations. The structures of **3.3** and **3.4** were both of poor quality and only isotropic refinement could be achieved. The structure of **3.3** contained two independent molecules in the asymmetric unit cell–one of which was only half of a dimer from which the other half was generated via symmetry operations. In both cases, the phosphorus atoms of the P_3 unit were all disordered over two positions. The structure of complex **3.4** contained one molecule of THF in the unit cell. Crystallographic data are summarized in Table 3.1.

Table 3.1. Crystallographic data for {[PhBP$^{iPr}_3$]Fe}$_2$(μ-P$_4$), **3.1**; {[PhBP$_3$]Fe}$_2$(μ-P$_4$), **3.2**; {[PhBP$^{iPr}_3$]Fe}$_2$(μ-P$_3$)**, 3.3**; and [{[PhBP$_3$]Fe}$_2$(μ-P$_4$)][Cp*$_2$Co], **3.4**.

	3.1	**3.2**·0.3CH_2Cl_2,0.7Et_2O
chemical formula	$C_{27}H_{52}BFeP_5$	$[C_{90}H_{82}B_2Fe_2P_{10}]$·0.3$[CH_2Cl_2]$,0.7$[C_4H_{10}O]$
Fw	598.20	1765.62
T (°C)	-173	-173
λ (Å)	0.71073	0.71073
a (Å)	11.350(3)	24.349(4)
b (Å)	22.458(5)	13.541(2)
c (Å)	12.184(3)	26.482(4)
α (°)	90	90
β (°)	96.004(4)	95.201(4)
γ (°)	90	90
V (Å^3)	3088.6(12)	8696(2)
space group	P2(1)	C2/c
Z	4	4
D_{calc} (g/cm^3)	1.286	1.349
μ(cm^{-1})	7.63	6.27
R1, wR2[a] ($I > 2\sigma(I)$)	0.0663, 0.1253	R1 = 0.0392, wR2 = 0.0775

[a] $R1 = \Sigma||F_o| - |F_c||/\Sigma|F_o|$, $wR2 = \{\Sigma[w(F_o^2 - F_c^2)^2]/\Sigma[w(F_o^2)^2]\}^{1/2}$

Table **3.1** cont'd

	3.3	**3.4**[Cp*$_2$Co]•THF
chemical formula	$C_{82}H_{106}B_3Fe_3P_{12}$	$C_{114}H_{120}B_2CoFe_2OP_{10}$
Fw	1663.29	2008.05
T (°C)	-173	-173
λ (Å)	0.71073	0.71073
a (Å)	13.469(3)	24.0222(16)
b (Å)	17.838(4)	12.5617(9)
c (Å)	21.376(4)	33.940(3)
α (°)	112.652(4)°.	90
β (°)	92.471(4)°.	95.545(3)
γ (°)	100.363(4)°.	90
V (Å^3)	4626.5(16)	10193.8(12)
space group	P-1	C2/c
Z	3	8
D_{calc} (g/cm^3)	1.791	2.617
μ(cm^{-1})	10.65	12.97
R1, wR2[a] ($I > 2\sigma(I)$)	0.2852, 0.4102	0.1283, 0.1758

[a] $R1 = \Sigma||F_o| - |F_c||/\Sigma|F_o|$, $wR2 = \{\Sigma[w(F_o^2 - F_c^2)^2]/\Sigma[w(F_o^2)^2]\}^{1/2}$

References Cited

[1] (a) Barbaro, P.; Ienco, A.; Mealli, C.; Peruzzini, M.; Scherer, O.; Schmitt, G.; Vizza, F.; Wolmershauser, G. *Chem. Eur. J.* **2003**, *9*, 5195. (b) Peruzzini, M.; de los Rios, I.; Romerosa, A.; Vizza, F. *Eur. J. Inorg. Chem.* **2001**, 593.

[2] (a) Ehses, M.; Romerosa, A.; Peruzzini, M. *Top. Curr. Chem.* **2002**, *20*, 107. (b) Scherer, O. J. *Acc. Chem. Res.* **1999**, *32*, 751. (c) Whitmire, K. H. *Adv. Organomet.*

Chem. **1998**, *42*, 1. (d) Urnėžius, E.; Brennessel, W. W.; Cramer, C. J.; Ellis, J. E.; Schleyer, P. v. R. *Science* **2002**, *295*, 832.

[3] (a) Dapporto, P.; Midollini, S.; Sacconi, L. *Angew. Chem. Int. Ed.* **1979**, *18*, 469. (b) Dapporto, P.; Sacconi, L.; Stoppioni, P.; Zanobini, F. *Inorg. Chem.* **1981**, *20*, 3834. (c) de los Rios, I.; Hamon, J.–R.; Hamon, P.; Lapinte, C.; Toupet, L.; Romerosa, A.; Peruzzini, M. *Angew. Chem. Int. Ed.* **2001**, *40*, 3910.

[4] (a) Dapporto, P.; Sacconi, L.; Stoppioni, P.; Zanobini, F. *Inorg. Chem.* **1981**, *20*, 3834. (b) Ghildardi, C. A.; Midollini, S.; Orlandini, A.; Sacconi, L. *Inorg. Chem.* **1980**, *19*, 301. (c) Cecconi, F.; Dapporto, P.; Midollini, S.; Sacconi, L. *Inorg. Chem.* **1978**, *17*, 3292. (d) Di Vaira, M.; Ghilardi, C. A.; Midollini, S.; Sacconi, L. *J. Am. Chem. Soc.* **1978**, *100*, 2550. (e) Bianchini, C.; Di Vaira, M.; Sacconi, L. *Inorg. Chem.* **1981**, *20*, 1169.

[5] Stephens, F. H.; Johnson, M. J. A.; Cummins, C. C.; Kryatova, O. P.; Kryatov, S.V.; Rybak-Akimova, E. V.; McDonough, J. E.; Hoff, C. D. *J. Am. Chem. Soc.* **2005**, *127*, 15191.

[6] (a) Scheer, M.; Becker, U.; Chisholm, M. H.; Huffman, J. C.; Lemoigno, F.; Eisenstein, O. *Inorg. Chem.* **1995**, *34*, 3117. (b) Barr, M. E.; Smith, S. K.; Spencer, B.; Dahl, L. E. *Organometallics* **1991**, *10*, 3983. (c) Scheer, M.; Troitzsch, C.; Jones, P. G. *Angew. Chem. Int. Ed.* **1992**, *31*, 1377. (d) Scheer, M.; Becker, U. *J. Organomet. Chem.* **1997**, 451. (e) Scheer, M.; Becker, U.; Huffman, J. C.; Chisholm, M. H. *J. Organomet. Chem.* **1993**, *461*, C1. (f) Scherer, O. J.; Volmecke, T.; Wolmershauser, G. *Eur. J. Inorg. Chem.* **1999**, 945. (g) Scherer, O. J.; Schwarz, G.; Wolmershauser, G. *Z. Anorg.*

Allg. Chem. **1996**, *622*, 951. (h) Heberhold, M.; Frohmader, G.; Milius, W. *J. Organomet. Chem.* **1996**, *522*, 185.

[7] (a) Kraus, F.; Hanauer, T.; Korber, N. *Inorg. Chem.* **2006,** *45*, 1117. (b) Kraus, F.; Korber, N. *Chemistry: A European Journal* **2005**, *11*, 5945.

[8] Scherer, O. J.; Vondung, J.; Wolmershauser, G. *Angew. Chem. Int. Ed.* **1989**, *28*, 1355.

[9] (a) Brown, S. D.; Peters, J. C. *J. Am. Chem. Soc.* **2004**, *126*, 4538. (b) Betley, T. A.; Peters, J. C. *J. Am. Chem. Soc.* **2004**, *126*, 6252. (c) Brown, S. D.; Peters, J. C. *J. Am. Chem. Soc.* **2005**, *127*, 1913.

[10] (a) Brown, S. D.; Betley, T. A.; Peters, J. C. *J. Am. Chem. Soc.* **2003**, *125*, 322. (b) Betley, T. A.; Peters, J. C. *J. Am. Chem. Soc.* **2003**, *125*, 10782.

[11] (a) Daida, E. J.; Peters, J. C. *Inorg. Chem.* **2004**, *43*, 7474. (b) Thomas, C. M.; Peters, J. C. *Angew. Chem. Int. Ed.* **2006**, *45*, 776.

[12] (a) Maier, G. *Angew. Chem. Int. Ed.* **1988**, ***6***, 351. (b) Ohanessian, G.; Hiberty, P. C.; Lefour, J.–M.; Flament, J.–P.; Shaik, S. S. *Inorg. Chem.* **1988**, *27*, 2219. (c) Hess, B. A., Jr.; Ewig, C. S.; Schaad, L. J. *J. Org. Chem.* **1985**, *50*, 5869.

[13] (a) Jaguar 5.0, Schrodinger, LLC, Portland, Oregon, 2002. (b) Lee, C.; Yang, W.; Parr, R. G. *Phys. Rev. B.* **1988**, *37*, 785.

[14] Electrochemistry conditions: THF, range: 0.75 V to -3.0 V vs Fc/Fc^{+}.

[15] (a) Sur, S. K. *J. Magn Reson.* **1989**, *82*, 169. (b) Evans, D. F. *J. Chem. Soc.* **1959**, 2003.

[16] Evans, W. J.; Lee, D. S.; Ziller, J. W. *J. Am. Chem. Soc.* **2004**, *126*, 454.

Chapter 4: Design of Hybrid Bis(phosphino)pyrazolylborate Ligands, $[PhBP^{tBu}_2(pz')]^-$, and Their Coordination Chemistry with Respect to Iron and Cobalt

The text in this chapter is reproduced in part with permission from:

Thomas, C. M.; Mankad, N. P.; Peters, J. C. *J. Am. Chem. Soc.* **2006,** *128*, 4956.

4.1 Introduction

The coordination chemistry of tridentate borato ligands such as tris(pyrazolyl),[1] tris(phosphino),[2] and tris(thioether)borates[3] has been explored using a wide variety of transition metals for applications such as homogeneous catalysis, small molecule activation, and modeling biological active sites. A number of hybrid borato ligands that incorporate two pyrazolyl moieties with a third donor have been designed,[4,5] including the most recent example: a bis(pyrazolyl)phosphinoborate, reported by Casado and coworkers.[4a] The transition metal coordination chemistry of these anionic, mixed donor ligands, however, remains unexplored.

Our group has found that the strong field tris(phosphino)borate ligands, $[PhBP^{R}_{3}]$ (R = Ph, ^{i}Pr), can support a wide range of mid-to-late transition metal complexes. The versatile nature of these ligands allows them to support a wide range of metal oxidation states with both π-acidic (e.g., N_2, CO) and π-basic (e.g., NR^{2-}, N^{3-}) ligands.[6] In addition, $[PhBP^{R}_{3}]$ iron complexes have been shown to be competent for small molecule activation.[7] Motivated by the unique and versatile late transition metal chemistry of the $[PhBP^{R}_{3}]$ ligands, we have designed a new type of hybrid ligand, $[PhB(CH_2P^{t}Bu_2)_2(pz')]^-$ (pz' = pyrazolyl derivative), in which one of the phosphine arms has been replaced with a pyrazolyl moiety. In this chapter, the synthetic methodology providing access to this ligand and its derivatives is discussed, and their coordination chemistry with respect to iron and cobalt is explored.

4.2 Results and Discussion

4.2.1 Synthesis and Characterization of [PhBP$^{tBu}_2$(pz')]Tl

Access to the bis(phosphino)pyrazolylborate ligands is achieved by initial preparation of the bis(phosphino)borane precursor PhB($CH_2P^tBu_2$)$_2$ (**4.1**) via metathesis between $PhBCl_2$ and two equivalents of $LiCH_2P^tBu_2$ (Scheme 4.1). Reaction of [pz]Li with **4.1**, followed immediately by salt metathesis with $TlPF_6$, leads to the clean formation of solid white [PhBP$^{tBu}_2$(pz)]Tl (**4.2**, where [PhBP$^{tBu}_2$(pz)] = [PhB($CH_2P^tBu_2$)$_2$(pz)]$^-$) in 66% isolated yield. The use of the bulky $LiCH_2P^tBu_2$ carbanion is critically important in the preparation of this type of hybrid borate ligand because (i) effective di- rather than tri-substitution at boron can be achieved, which could not be realized using less-hindered carbanions such as $LiCH_2P^iPr_2$ and $LiCH_2PPh_2$; (ii) the borane product, PhB($CH_2P^tBu_2$)$_2$ (**4.1**), does not appear to dimerize to an appreciable degree in solution. Such dimerization, resulting from the phosphine donors weakly intermolecularly coordinating to the Lewis acidic boron atoms, is evident from the $^{11}B\{^1H\}$ NMR spectrum of **4.1**.[8] Although shifted downfield from the typical values observed for four-coordinate borates, the chemical shift at 3.8 ppm is diagnostic of 4-coordinate boron. In addition, this signal is a broad doublet and displays significant boron-phosphorous coupling ($^1J_{B\text{-}P}$ = 112 Hz). The weakness of this interaction, however, allows the efficient introduction of a third donor arm.

Scheme 4.1

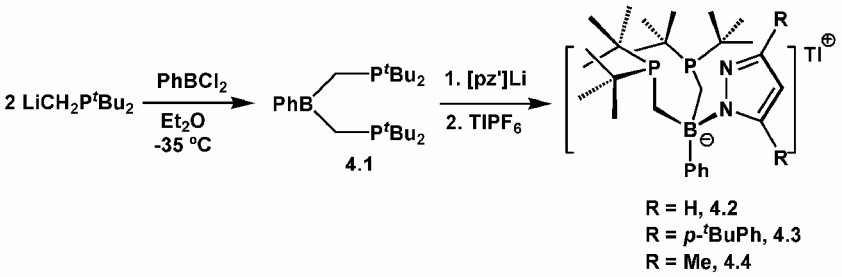

Due to the modularity of this ligand synthesis, derivatives of pyrazole can also be used to generate more sterically hindered and/or more electron-releasing ligands. For example, lithiation of 3,5-(*p*-^{t}BuPh)$_2$pzH followed by reaction with **4.1** and metathesis with $TlPF_6$ leads to formation of [PhBP$^{t\text{Bu}}_2$(pz$^{t\text{BuPh2}}$)][Tl] (**4.3**, where [PhBP$^{t\text{Bu}}_2$(pz$^{t\text{BuPh2}}$)]= [PhB(CH$_2$P^{t}Bu$_2$)$_2$(3,5-(^{t}BuPh)$_2$pz)]$^-$) in 81% yield. Similarly, addition of [3,5-(Me$_2$)pz]Li generated *in situ* to **4.1** yields [PhBP$^{t\text{Bu}}_2$(pz$^{\text{Me2}}$)][Tl] (**4.4**, where [PhBP$^{t\text{Bu}}_2$(pz$^{\text{Me2}}$)] = [PhB(CH$_2$P^{t}Bu$_2$)$_2$(3,5-(Me)$_2$pz)]$^-$.

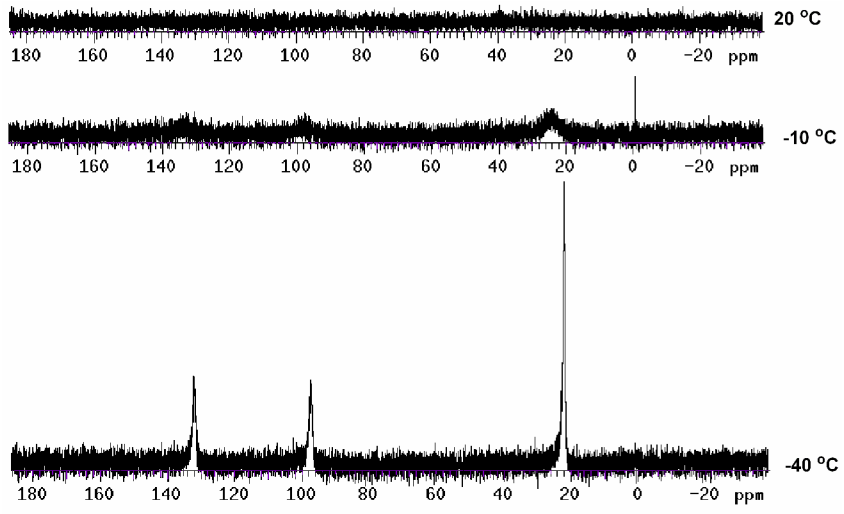

Figure 4.1. Variable temperature $^{31}P\{^1H\}$ NMR spectra of **4.2** at 20 °C, -10 °C, and -40 °C (121.5 MHz, toluene).

Interestingly, while ligands **4.2**, **4.3**, and **4.4** display diagnostic resonances in their ^{1}H NMR spectra, their $^{31}P\{^1H\}$ spectra reveal a degree of fluxionality in solution. For example, while the ^{31}P NMR spectra of the [PhBP$^R_3$] (R = Ph, ^{i}Pr) ligands display a doublet due to coupling of all three phosphorus nuclei to Tl,[2b,2g] the ^{31}P spectra of ligands **4.2** and **4.4** are silent at room temperature. Variable temperature ^{31}P NMR spectra of **4.2** and **4.4** (Figure 4.1) reveal two sharp signals of equal size at low temperatures (-40 °C, toluene): a doublet (**4.2**: 114 ppm, $^1J_{\text{P-Pt}}$ = 3890 Hz; **4.4**: 131 ppm, $^1J_{\text{P-Pt}}$ = 3770 Hz) corresponding to a

phosphorous atom bound to Tl and a singlet (**4.2**: 22 ppm; **4.4**: 92 ppm) corresponding to a dangling phosphorous arm. The bulkier ligand **4.3**, on the other hand, displays a room temperature ^{31}P spectrum containing a doublet (113 ppm, $^{1}J_{\text{Tl-P}}$ = 3790 Hz) and a singlet (28 ppm). This indicates that the bulkier ligand **4.3** is likely locked into bidentate coordination to Tl due to its more sterically encumbered pyrazole substituents.

4.2.2 Synthesis and Structural Characterization of [PhBP$^{t\text{Bu}}_2$(pz')]M(X) Complexes (M = Fe, Co)

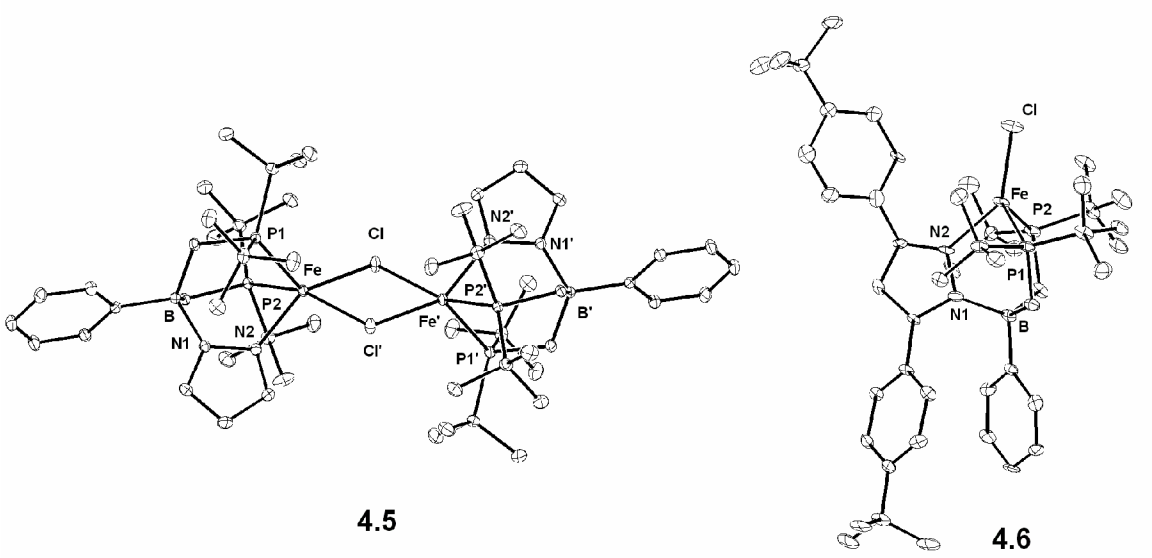

Figure 4.2 Displacement ellipsoid (50%) representation of **4.5** and **4.6**. Complex **4.5** is dimeric in the solid state and the right half of the molecule has been generated using symmetry operations. Selected interatomic distances and angles: **4.5**, Fe-P1, 2.4684(4) Å; Fe-P2, 2.6385(4) Å; Fe-N2, 2.091(1) Å; P1-Fe-P2, 101.58(1)°; P1-Fe-N2, 86.69(4)°; P2-Fe-N2, 87.30(3)°. **4.6**, Fe-P1, 2.469(2) Å; Fe-P2, 2.462(2) Å; Fe-N2, 2.114(5) Å; P1-Fe-P2, 114.33(7)°; P1-Fe-N2, 87.8(1)°; P2-Fe-N2, 88.5(2)°; Cl-Fe-N2, 139.3(2)°.

Although ligands **4.2**, **4.3**, and **4.4** seem reluctant to coordinate Tl in a κ^3 fashion, pseudotetrahedral iron and cobalt halide complexes in which all three donors coordinate

can be generated. Metathesis of **4.2**, **4.3**, and **4.4** with $FeCl_2$ leads to clean formation of [PhBP$^{t\text{Bu}}_2$(pz)]FeCl (**4.5**), [PhBP$^{t\text{Bu}}_2$(pz$^{t\text{BuPh}}$)]FeCl (**4.6**), and [PhBP$^{t\text{Bu}}_2$(pz$^{\text{Me}}$)]FeCl (**4.7**), isolated in good yield as yellow crystalline solids. Evans' method (C_6H_6, 295 K)[9] confirms that all three iron chloride complexes are high spin (S = 2): **4.5**, μ_{eff} = 5.20 μ_B; **4.6**, μ_{eff} = 4.87 μ_B; **4.7**, μ_{eff} = 5.05 μ_B. While solution magnetic data indicates that complex **4.5** adopts a monomeric, 4-coordinate pseudo-tetrahedral geometry, the X-ray crystal structure reveals that **4.5** is dimeric in the solid state (Figure 4.2). The sterically hindered substituents of complex **4.6**, on the other hand, favor a monomeric geometry in both solution and the solid state.

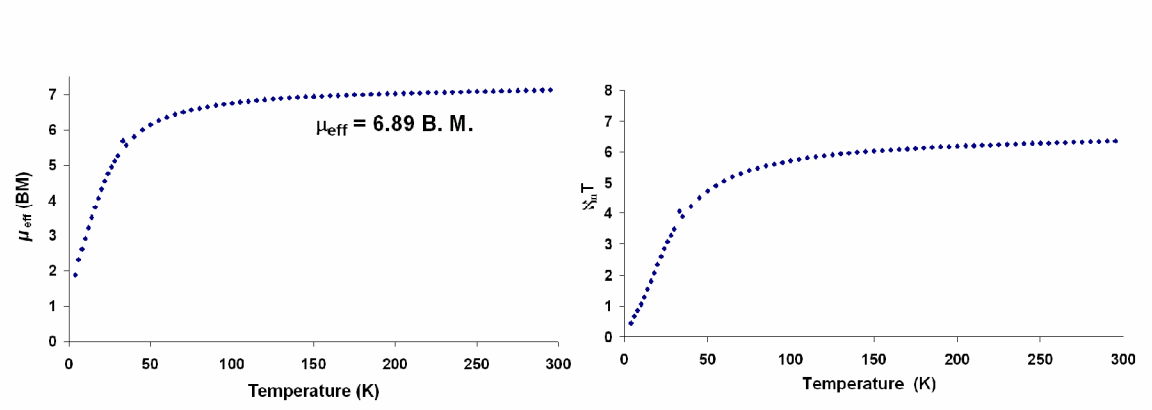

Figure 4.3 SQUID magnetization data per dimeric unit of **4.5** shown as a plot of μ_{eff} (BM) versus T (K) (left) and $\chi_m T$ (cm^3 / mol K) versus T (K)**.** *A* μ_{eff} value is reported for the average of the data over the temperature range 60-300 K. Magnetic field strength = 5000 G.

Solid state magnetic susceptibility data for **4.5** were obtained via SQUID magnetometry. The plot of $\chi_m T$ versus temperature (K) features a decrease in $\chi_m T$ as the temperature is lowered, consistent with antiferromagnetic coupling between the two iron centers of the chloride-bridged dimer (Figure 4.3). The plot of μ_{eff} versus temperature

reveals an effective magnetic moment of 6.89 BM over the temperature range of 60-300 K, corresponding to six unpaired electrons per dimer.

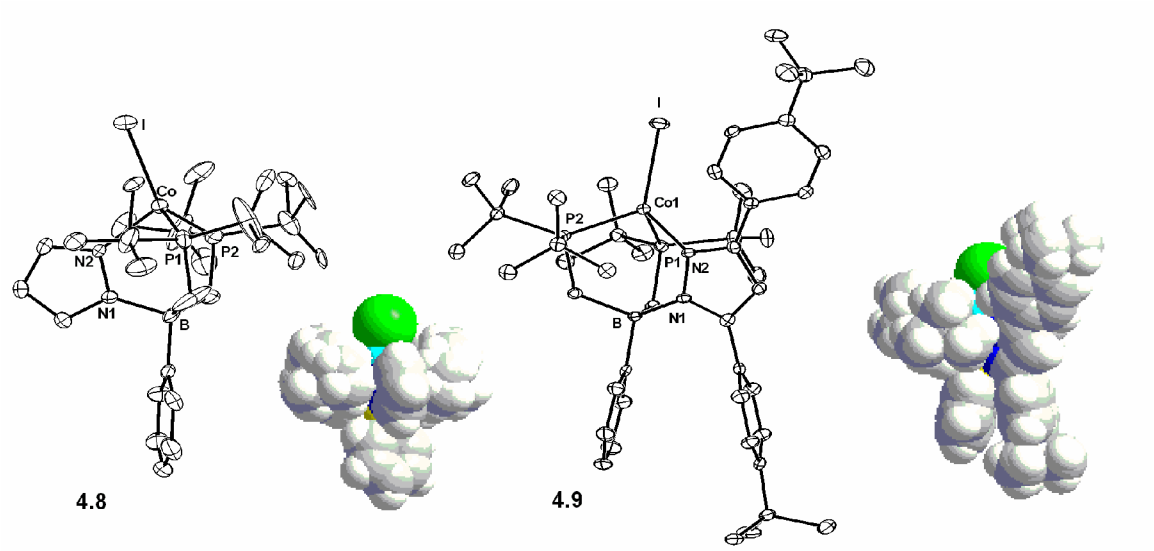

Figure 4.4 Displacement ellipsoid representations (50%) and space-filling models of **4.8** and **4.9.** Selected interatomic distances and angles: **4.8**, Co-P1, 2.377(1) Å; Co-P2, 2.385(1) Å; Co-N2, 1.993(3) Å; P1-Co-P2, 110.99(4)°; P1-Co-N2, 92.17(9)°; P2-Co-N2, 94.81(9)°; I-Co-N2, 110.90(8)°. **4.9**, Co-P1, 2.4227(8) Å; Co-P2, 2.3540(8) Å; Co-N2, 2.032(2) Å; P1-Co-P2, 111.69(3)°; P1-Co-N2, 95.18(6)°; P2-Co-N2, 91.88(6)°; I-Co-N2, 124.32(6)°.

Similarly, reaction of CoI_2 with **4.2** and **4.3** generates the high spin (S = 3/2) green complexes [PhBP$^{t\text{Bu}}_2$(pz)]CoI (**4.8**) and [PhBP$^{t\text{Bu}}_2$(pz$^{t\text{BuPh}}$)]CoI (**4.9**) with solution magnetic moments of 4.35 μ_B and 4.10 μ_B (Evans' method, C_6H_6, 295 K), respectively. XRD analysis of single crystals of **4.8** and **4.9** reveal that both complexes adopt a monomeric pseudo-tetrahedral geometry. The structures and corresponding space-filling models of complexes **4.8** and **4.9** shown in Figure 4.4 reveal that modifying the substituents at the pyrazolyl 3 position incorporates significant steric bulk above the apical coordination site of the cobalt

center. This is also manifested in some noteable structural distortions in **4.9**. For example, while the Co-P distances in **4.8** are relatively similar (2.377(1) Å and 2.385(1) Å), the Co-P distances in **4.9** differ by nearly 0.1 Å (2.4227(8) Å and 2.3540(8) Å). In addition, the iodide in both complexes is slightly bent with respect to the axis containing the B and Co atoms (~15° for **4.8** and ~7° for **4.9**). In complex **4.8**, the iodide ligand bends towards the pyrazole ring–the least sterically crowded part of the cobalt coordination sphere–resulting in a very small N2-Co-I angle of 110.90(8)°. This distortion is not as pronounced in **4.9** due to the additional sterics on the pyrazole moiety, resulting in a larger N2-Co-I angle of 124.32(6)°.

The glassy toluene EPR spectrum of complex **4.8** was collected at 4 K (Figure 4.5). The resulting rhombic signal is consistent with a high spin ($S = 3/2$) cobalt(II) species with estimated g values of 5.6, 2.3, and 2.1. This is similar to the previously reported EPR spectrum of the high spin ($S = 3/2$) cobalt(II) complex [PhBP$^{i\text{Pr}}_3$]CoI.[2b] In contrast, the EPR spectrum reported for the low-spin ($S = 1/2$) cobalt(II) complex [PhBP$_3$]CoI features an isotropic signal at $g = 2.0$.

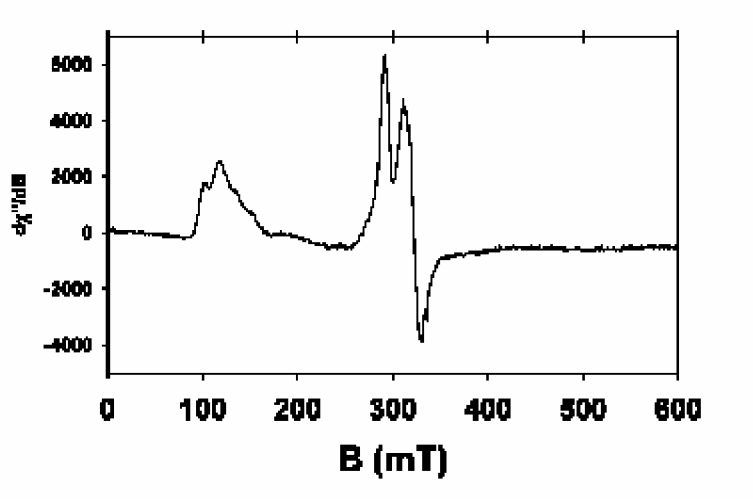

Figure 4.5 EPR spectrum of **4.8** in glassy toluene solution (4 K, 9.474 GHz).

4.2.3 Electrochemistry of [PhBP$^{tBu}_2$(pz')]M(X) Complexes (M = Fe, Co)

Interestingly, complexes **4.5**, **4.6**, and **4.7** display electrochemical properties that are very different from their tris(phosphine) analogues (Figure 4.6A). While cyclic voltammetry of the [PhBP$^R_3$]FeCl complexes reveals fully reversible reductions (-2.03 V for R = ^{i}Pr, -1.65 V for R = Ph),[2b] the cyclic voltammograms of **4.5**, **4.6**, and **4.7** show irreversible reductions at -2.25 V, -3.05 V, and -2.48 V, respectively, vs. Fc/Fc$^+$.[10] The oxidative features located at ~0.3-0.5 V in the cyclic voltammograms of **4.5** and **4.6** can likely be attributed to oxidation of the anionic borate moiety. In contrast, electrochemistry of the cobalt complex **4.8** reveals a fully reversible Co$^{II/I}$ couple at -1.61 V vs. Fc/Fc$^+$ (Figure 4.6B). This potential is 350 mV more negative than the corresponding reduction observed for [PhBP$^{iPr}_3$]CoI at -1.26 V.

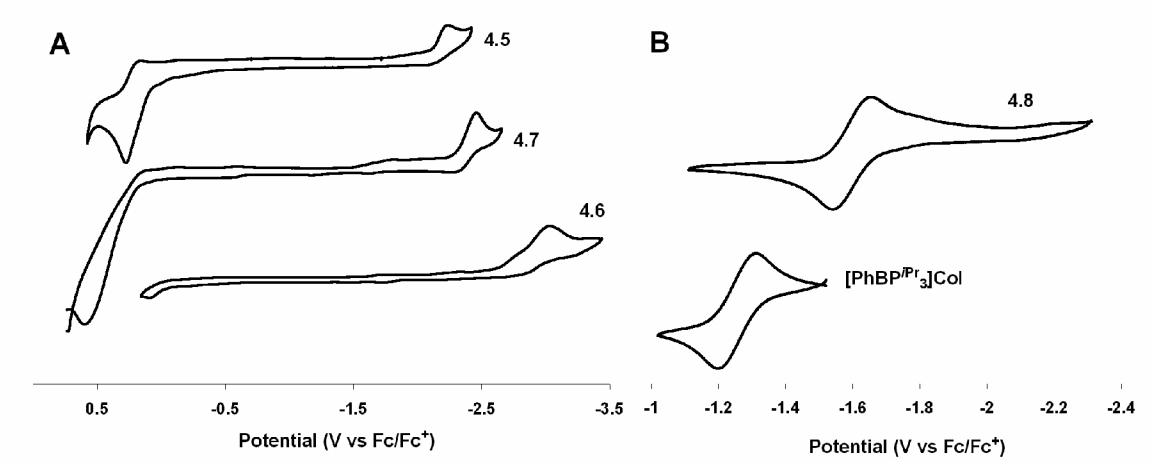

Figure 4.6 Cyclic voltammetry of **4.5**, **4.6**, and **4.7** (A) and **4.8** and [PhBP$^{iPr}_3$]CoI (B). Experimental parameters: 0.40 M [^{n}BuN$_4$][PF$_6$] in THF, scan rate = 100 mV/s.

4.2.4 Exploring Routes to a Terminal Nitride Complex, [PhBP$^{tBu}_2$(pz')]M≡N (M = Fe, Co)

Our group recently discovered that the [PhBP$^{iPr}_3$] ligand is capable of stabilizing a rare iron(IV) nitride in solution at low temperatures.[6a] Upon concentration or warming to

ambient temperature, the [PhBP$^{iPr}_3$]Fe^{IV}≡N complex accesses a decomposition pathway in which it reductively couples to form the {[PhBP$^{iPr}_3$]Fe^{I}}$_2$(μ-N$_2$) dimer, making this species difficult to isolate. Motivated by this finding, routes to similar nitride species supported by hybrid [PhBP$^{tBu}_2$(pz')]$^-$ ligands were explored. It was initially postulated that ligand **4.3** would be particularly suited for this goal due to its bulky substituents protruding above the iron coordination sphere and, thus, blocking dimerization.

Scheme 4.2

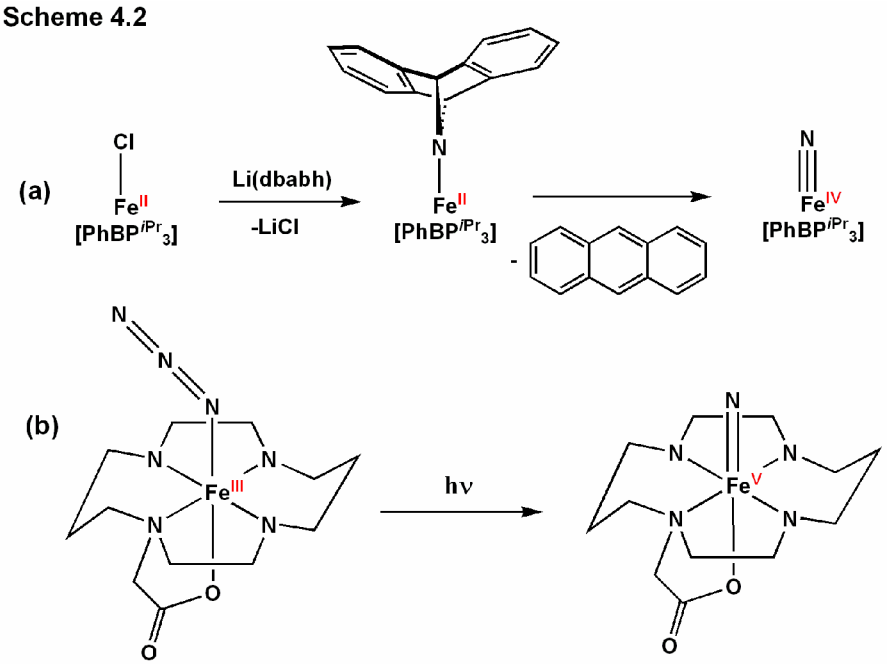

Two well-precedented routes to terminal metal nitride species have proven particularly successful with respect to iron. The [PhBP$^{iPr}_3$]Fe^{IV}≡N complex was generated via low temperature metathesis of the lithium amide reagent Li(dbabh) (dbabh = 2,3:5,6-dibenzo-7-aza bicycle[2.2.1]hepta-2,5-diene)[11] with [PhBP$^{iPr}_3$]Fe^{II}-Cl (Scheme 4.2a).[6a] At low temperature (-35 °C), the intermediate [PhBP$^{iPr}_3$]Fe^{II}(dbabh) species is observed spectroscopically. Upon warming to 0 °C, the [PhBP$^{iPr}_3$]Fe^{IV}≡N complex is formed with concomitant loss of anthracene. Another synthetic route has proven useful for the generation of iron(V) nitride species at low temperature. The groups of both Nakamoto[12]

and Wieghardt[13] have generated terminal iron nitrides via photolytic N_2 expulsion from a coordinated azide ligand (Scheme 4.2b). In addition, a bridging iron nitride, [{[PhBP$^{Ph}_3$]Fe}$_2$(μ-N)][Na(THF)$_n$)], can be generate via reduction of an iron azide complex.[14] The above routes have been explored using the [PhBP$^{tBu}_2$(pz')]$^-$ ligands.

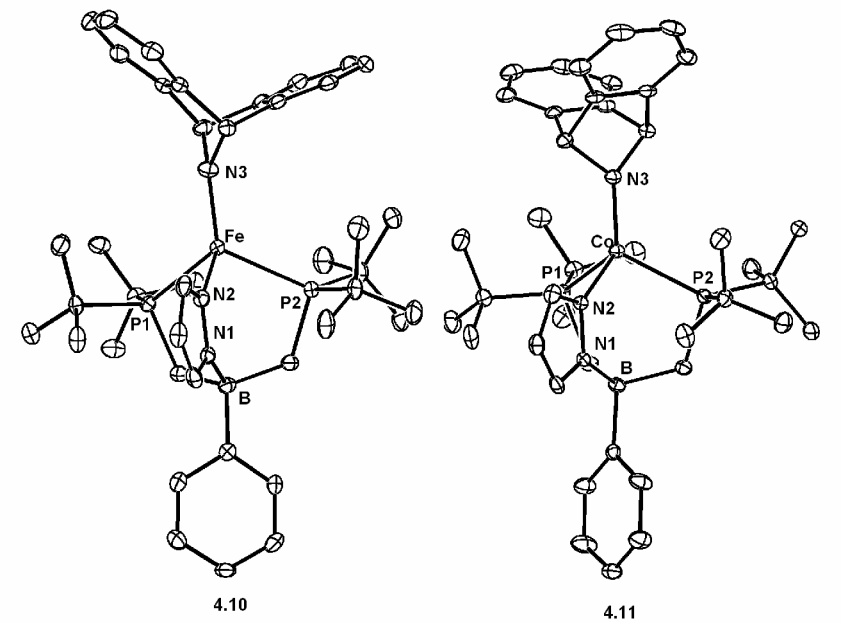

Figure 4.7 Displacement ellipsoid representations (50 %) of **4.10** and **4.11**. Hydrogen atoms have been omitted for clarity. Relevant interatomic distances: **4.10**, Fe-N3, 1.882(3) Å; **4.11**, Co-N3, 1.854(4) Å.

Reaction of **4.5** with Li(dbabh) at low temperature (-35 °C) results in an immediate color change from yellow to red with concomitant precipitation of LiCl. The major product formed in this reaction is the iron(II) amide complex [PhBP$^{tBu}_2$(pz)]Fe(dbabh) (**4.10**). Complex **4.10** is high spin in solution with a solution magnetic moment of 4.61 μ_B (Evans' method, benzene). Unlike the [PhBP$^{iPr}_3$]Fe(dbabh) complex, **4.10** does not extrude anthracene when warmed to room temperature. Moreover, complex **4.10** is thermally stable at temperatures up to 80 °C. XRD analysis of

crystals of **4.10** confirmed its formulation as an iron(II) anthracenyl amide complex (Figure 4.7). The Fe-N distance is comparable to that observed in other known iron(II) amides (1.882(3) Å).[7d] Photolysis of complex **4.10** for 12 hours resulted in no observable reaction (^{1}H NMR). Prolonged heating of **4.10** in toluene at 80 °C for one week results solely in ligand decomposition products, although free anthracene is observed. Attempts to trap a potential nitride intermediate with PMe_3 or morpholine resulted in the same distribution of products. Reaction of the more sterically hindered iron chloride complex **4.6** with Li(dbabh) at room temperature resulted in a mixture of products, including an iron(II) amide complex and several diamagnetic ligand decomposition products. Extrusion of anthracene was not observed in this reaction. Presumably the amide complex is far less stable in this case as a result of steric crowding.

Since known examples of cobalt nitrides are absent from the literature, the cobalt iodide complex **4.8** was also treated with Li(dbabh) at ambient temperature, resulting in a gradual color change from forest green to dark red and formation of a single paramagnetic product. This product was identified as the cobalt amide complex [PhBP$^{t\text{Bu}}_2$(pz)]Co(dbabh) (**4.11**) via X-ray crystallography (Figure 4.7). Complex **4.11** has a solution magnetic moment of 4.05 μ_B, confirming that it is a high spin, cobalt(II) complex. Thermolysis and photolysis of **4.11** did not result in a clean transformation, and anthracene was not extruded under either of these conditions. On the other hand, reduction of **4.11** with sodium napthelenide at low temperature (-35 °C) resulted in an immediate color change from dark red to indigo blue. This blue color may be attributed to an anthracenyl radical anion. Upon warming to room temperature and stirring for several hours, this blue color faded to deep red/purple. The product of this reaction was identified

as $\{[\kappa^2\text{-PhBP}^{t\text{Bu}}_2(\text{pz})]\text{Co}^{\text{I}}\text{NH}(\text{C}_{14}\text{H}_9)\}\{\text{Na}(\text{THF})_3\}$ (**4.12**) (Figure 4.8) via X-ray crystallography. The low coordination number and low oxidation state of this product make it a particularly unusual complex. In fact, **4.12** is the first structurally characterized example of a trigonally coordinated cobalt amide.[15] This product results from H-atom transfer from the anthracenyl moiety to the amide nitrogen, accompanied by cleavage of an N-C bond. The pyrazolyl arm of the borate ligand remains unbound to cobalt and instead binds to the sodium countercation. In the crystal lattice, the sodium ion also appears to coordinate to the phenyl ring located on the borate. The Co-N distance is 1.993(3) Å, elongated from that of complex **4.11** (1.854(4) Å). Reduction of **4.11** with a milder reductant, such as Na/Hg amalgam, resulted in a color change to purple, loss of one equivalent of anthracene, and formation of several diamagnetic products with ^{31}P NMR resonances at 111, 108, and 62 ppm. Thus far, the identity of these diamagnetic products has not been established.

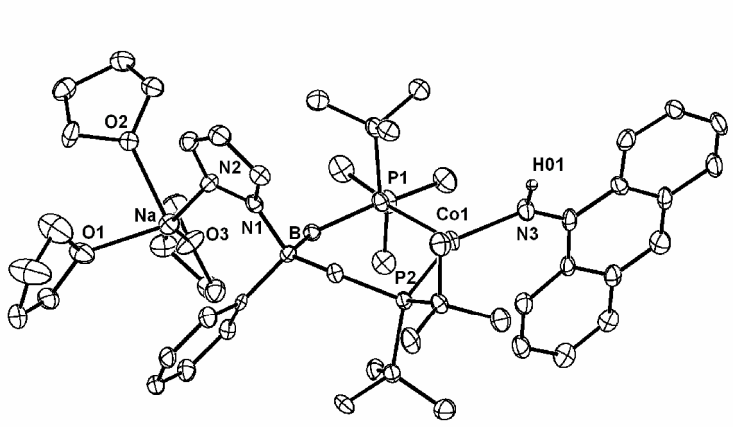

Figure 4.8 Displacement ellipsoid representation (50%) of **4.12**. The amide hydrogen was located in the difference Fourier map and refined. Hydrogen atoms other than the amide hydrogen have been omitted for clarity. Relevant interatomic distances and angles: Co-N3, 1.993(3) Å; Co-P1, 2.255(1) Å; Co-P2, 2.263(1) Å; Co-N3-C1 130.7(3) °.

The synthetic route to an iron nitride via nitride elimination from a coordinated azide was also explored. An iron(II) azide complex, $[PhBP^{tBu}_2(pz)]Fe(N_3)$ (**4.13**), was synthesized via reaction of **4.5** with 20 stoichiometric equivalents of sodium azide. The resulting yellow compound was found to have a characteristic infrared azide stretching frequency of 2068 cm^{-1}. Photolysis of **4.13** for 1 h resulted in quantitative consumption of starting material; however, this resulted in a number of ligand decomposition products (MeP^tBu_2, $Ph(CH_2P^tBu_2)_2$, and others), and no evidence for dinitrogen elimination was observed. Similarly, heating **4.13** to 65 °C in toluene results solely in ligand decomposition with no evidence for nitride formation. Reduction of **4.13** with one equivalent of Na/Hg amalgam resulted in several unidentified paramagnetic products. No iron-containing diamagnetic products as would be expected for either a terminal[6a] or bridging nitride[14] were observed.

4.3 Discussion

4.3.1 Relative Electron-Releasing Character of $[PhBP^{tBu}_2(pz')]^-$ Ligands Compared to the Tris(phosphino)borates, $[PhBP^R_3]^-$

The cyclic voltammetry data for the $[PhBP^{tBu}_2(pz')]FeCl$ and $[PhBP^{tBu}_2(pz')]CoI$ complexes provide a mechanism for comparing the relative electron-releasing character of these ligands with their tris(phosphine) analogues. As shown in Table 4.1, the reduction potential of complex **4.5** is shifted 0.22 V more negative than the corresponding reduction potential for $[PhBP^{iPr}_3]FeCl$ and 0.60 V more negative than that for $[PhBP^{Ph}_3]FeCl$.[2b] The reduction potentials of **4.6** and **4.7** are shifted to even lower potentials. Although these values cannot be rigorously compared due to the differences in their reversibility, a comparison of the cobalt halide complexes is in agreement with this

trend. The cyclic voltammograms of both **4.8** and [PhBP$^{iPr}_3$]CoI reveal reversible reductive events, with the potential for **4.8** shifted cathodically by 0.36 V.[2b]

Table 4.1 Reversibility and potentials of the reduction events observed in the cyclic voltammograms of **4.5**, **4.6**, **4.7**, [PhBP$^{iPr}_3$]FeCl, [PhBP$^{Ph}_3$]FeCl, **4.8**, and [PhBP$^{iPr}_3$]CoI.

Complex	reversibility	Reduction potential (vs. Fc/Fc^+)
[PhBP$^{tBu}_2$(pz)]FeCl, **4.5**	Irreversible	-2.25 V
[PhBP$^{tBu}_2$(pz^{tBuPh})]FeCl, **4.6**	Irreversible	-3.05 V
[PhBP$^{tBu}_2$(pz^{Me2})]FeCl, **4.7**	Irreversible	-2.48 V
[PhBP$^{iPr}_3$]FeCl[a]	Quasi-reversible	-2.03 V
[PhBP$^{Ph}_3$]FeCl[a]	Reversible	-1.65 V
[PhBP$^{tBu}_2$(pz)]CoI, **4.8**	Reversible	-1.62 V
[PhBP$^{iPr}_3$]CoI[a]	Reversible	-1.26 V

[a] Previously reported.[2b]

These data indicate that the bis(phosphino)pyrazolyl borate ligands provide more electron-rich coordination environments than either of the tris(phosphino)borate ligands. Unlike the tris(phosphino)borate ligands, the mixed donor ligands possess potential resonance contributors that can delocalize the borate's negative charge throughout the pyrazole ring and towards the metal center (Scheme 4.3). This delocalization, combined with the electron-rich di-*tert*-butylphosphine donors, results in hybrid ligands that can contribute more overall electron density to transition metal centers than either Tp or [PhBP$^R_3$] ligands themselves.

Scheme 4.3

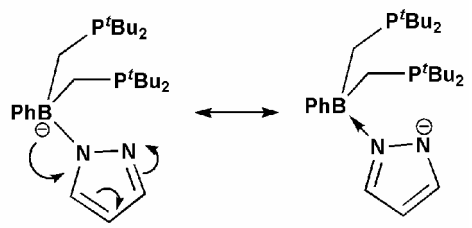

4.3.2 The Effects of Perturbing the C_3 Symmetry of a Tripodal Ligand on the Relative Energies of d Orbitals.

It has been noted previously that the [PhBP$^{Ph}_3$]CoI complex adopts an unusual low-spin electron configuration,[2a] while similar cobalt(II) halide complexes such as [Tp]CoI[16] and [PhTt^{tBu}]CoCl[17] have been shown to be rigorously high-spin. This phenomenon was attributed to an axial distortion away from typical tetrahedral bond angles, resulting in average P-Co-P angles of ~90° (Scheme 4.4). This distortion lowers the energy of the d_{z^2} orbital and results in a more favorable low-spin configuration. The complex must then undergo a Jahn-Teller distortion to break the degeneracy of the singly occupied e set of orbitals. This is manifested in a significant elongation of one of the Co-P bonds to a C_s symmetric structure, as seen in the solid state structure.[2a] Interestingly, the [PhBP$^{iPr}_3$]CoX analogues are rigorously high-spin.[2b] This paradox has been attributed to several factors: (i) the incompatibility of the more sterically hindered [PhBP$^{iPr}_3$] ligand with the shorter Co-P distances expected in a low-spin environment, and (ii) the differences in relative π-acceptor character between alkyl and aryl phosphines.

Scheme 4.4

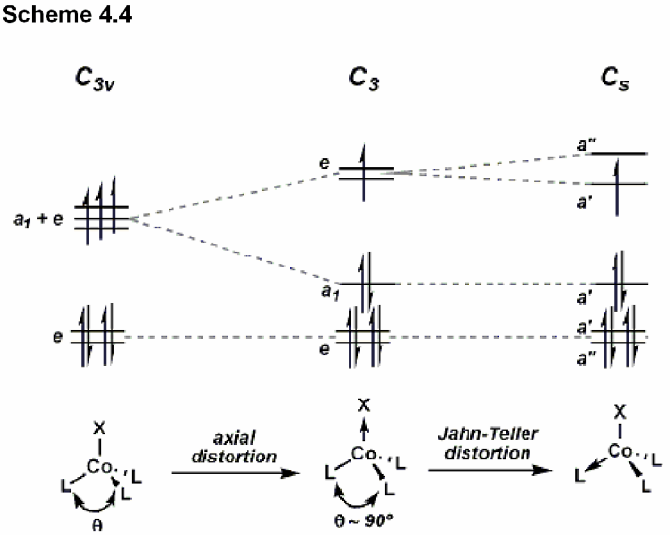

Since the bis(phosphino)pyrazolylborate ligands provide a C_s symmetric geometry to cobalt(II) halide complexes, it is interesting to consider the origin of the spin state of complex **4.8**. As noted in section 4.2.2, complex **4.8** adopts a high-spin (S = 3/2) configuration in solution. Since the complex is C_s-symmetric much like the distorted [PhBP$^{Ph}_3$]CoI, one might have expected **4.8** to be low-spin, especially given the strong-field nature of its ligands. However, the difference in energy between high- and low-spin ground states in pseudo-tetrahedral d^7 systems is presumably relatively small, as has been noted in several other cases.[2a,b,16] The low-spin state in **4.8** can presumably be attributed to the same factors leading to a low-spin configuration in [PhBP$^{iPr}_3$]CoI, namely the poor π-accepting abilities of the alkyl phosphine donors and the steric congestion around the metal center.

4.4 Conclusions

In summary, new hybrid bis(phosphino)pyrazolylborate ligands, [PhBP$^{tBu}_2$(pz')]$^-$, have been synthesized. Although the phosphine substituents are limited to *tert*-butyl groups, the presence of a pyrazole ring makes the synthesis of a family of these ligands quite modular. High-spin pseudo-tetrahedral [PhBP$^{tBu}_2$(pz')]M-X complexes (M = Fe, Co; X = Cl, I) have been synthesized and characterized structurally and spectroscopically. The cyclic voltammetry of these species has been described, and this data implies that these hybrid ligands are more electron-releasing than their tris(phosphino)borate congeners. Despite their similarities to the tris(phosphino)borate ligand scaffolds, these ligands do not appear to be capable of stabilizing an iron(IV) nitride. Conventional routes to such a species, such as (1) anthracene extrusion from an anthracenyl amide complex and (2) N_2 extrusion from coordinated azide, have proven unsuccessful.

4.5 Experimental Section

4.5.1 General Considerations

General considerations are outlined in Section 2.4.1.

4.5.2 Magnetic Measurements

Magnetic measurements on [PhBP$^{t\text{Bu}}_2$(pz)]FeCl (**4.5**) were recorded using a Quantum Designs SQUID magnetometer running Magnetic Property Measurement System Rev. 2 software. Data were recorded at 5000 G. The sample was suspended in the magnetometer in a plastic straw sealed under nitrogen with Lilly No. 4 gel caps. The sample was placed in liquid nitrogen immediately upon transfer out of the glovebox. The sample was attached to the sample rod while under liquid nitrogen and quickly transferred into the SQUID magnetometer. The chamber was cycled repeatedly prior to introducing the sample to the chamber. The loaded sample was centered within the magnetometer using the DC centering scan at 35 K and 5000 G. Data were acquired at 3-29 K (one data point every 2 K) and 30-300 K (one data point every 5 K). At the end of the run the temperature was returned to 35K to ensure that the response was similar.

The magnetic susceptibility was adjusted for diamagnetic contributions using the constitutive corrections of Pascal's constants. The molar magnetic susceptibility (χ_M) was calculated by converting the calculated magnetic susceptibility (χ) obtained from the magnetometer to a molar susceptibility (using the multiplication factor {(molecular weight)/[(sample weight)*(field strength)]}).

4.5.3 EPR Measurements

EPR measurements were carried out as outlined in Section 3.4.4.

4.5.4 Electrochemical Measurements

Electrochemical measurements were carried out as outlined in section 3.4.3.

4.5.5 Starting Materials and Reagents

. $^{t}Bu_2PCl$,[18] $^{t}Bu_2PMe$,[19] $LiCH_2P^{t}Bu_2$,[20] 3,5-(p-$^{t}BuPh)_2$pyrazole,[21] and Li(dbabh)[11] were prepared using literature methods. All other chemicals were purchased from commercial vendors and used without further purification.

4.5.6 Synthesis of Compounds

$PhB(CH_2P^{t}Bu_2)_2$ (4.1). Solid $LiCH_2P^{t}Bu_2$ (2.1008 g, 12.6 mmol) was suspended in Et_2O (150 mL) and cooled to -78°C with vigorous stirring. To this stirring solution was added neat $PhBCl_2$ (1.0043 g, 6.33 mmol) dropwise over 5 minutes. The resulting mixture was allowed to stir and warm to room temperature. After 1 hour, the mixture was filtered over Celite to remove the lithium chloride salts. Solvent was removed from the resulting yellow solution to yield analytically pure product (2.2838 g, 88.9 %). ^{1}H NMR (300 MHz, C_6D_6): δ = 8.02 (m, 2H, *o*-Ph), 7.27 (m, 3H, *m, p*-Ph), 2.27 (d, $^{2}J_{P\text{-}H}$ = 5.7 Hz, CH_2), 1.12 (d, $^{2}J_{P\text{-}H}$ = 10.5 Hz, 36 H, ^{t}Bu). ^{31}P NMR (300 MHz, C_6D_6): δ = 38.4 (s). ^{13}C NMR (126.7 MHz, C_6D_6): δ = 143.1 (br, *ipso*-BPh), 134.5 (s, *o*-BPh), 131.7 (s, *m*-BPh), 128.9 (s, *p*-BPh), 31.9 (d, $C(CH_3)_3$), 29.8 (s, $C(CH_3)_3$), 19.4 (m, CH_2). ^{11}B NMR (160.4 MHz, C_6D_6): δ = 3.8 (d, $^{1}J_{B\text{-}P}$ = 112 Hz). Anal. Calcd. for $C_{24}H_{45}BP_2$: C, 70.93; H, 11.16. Found: C, 69.32; H, 10.60.

$[PhBP^{tBu}_2(pz)]Tl$ (4.2). Solid pyrazole (0.4713 g, 6.932 mmol) was dissolved in Et_2O (100 mL) and cooled to -35 °C. To this stirring solution was added $^{n}BuLi$ (4.33 mL, 1.6 M solution in hexanes, 7.6 mmol) dropwise over 10 minutes. The resulting mixture was allowed to warm to room temperature and stir for 1 hour, and then **4.1** (2.8142 g, 6.9

mmol) was added as a THF solution (50 mL). After 12 hours, $TlPF_6$ (2.42 g, 6.93 mmol) in THF (20 mL) was added to the homogeneous, yellow reaction mixture. The resulting cloudy solution was stirred for 1 hour, and then filtered through Celite. Solvent was removed from the filtrate in vacuo. The remaining solids were extracted with petroleum ether (100 mL) and filtered through Celite, and the filtrate was dried in vacuo. The remaining solids were suspended in hexamethyldisiloxane (75 mL), stirred for 30 minutes, and then cooled to -35 °C for 12 hours. The solids that crashed out of solution were collected on a sintered glass frit, washed with cold hexamethyldisiloxane (10 mL), and dried in vacuo to afford analytically pure **4.2** (3.0875 g, 66%). ^{1}H NMR (300 MHz, C_6D_6): δ = 8.17 (s, 1H, pz-5), 7.42 (br m, 2H, *o*-Ph), 7.31 (s, 1H, pz-3), 7.17 (t, 2H, $^3J_{H\text{-}H}$ = 7.5 Hz, *m*-Ph), 7.05 (t, 1H, $^3J_{H\text{-}H}$ = 7.2 Hz, *o*-Ph), 6.36 (s, 1H, pz-4), 1.47 (m, 4H, CH_2), 1.27 (d, 18H, $^3J_{P\text{-}H}$ = 10.8 Hz, ^{t}Bu), 0.80 (d, 18H, $^3J_{P\text{-}H}$ = 10.5 Hz, ^{t}Bu). ^{31}P{^{1}H} NMR (121.5 MHz, C_6D_6): 35 (very broad). ^{13}C{^{1}H} NMR (75.5 MHz, C_6D_6): δ = 161.1 (br, *ipso*-BPh), 137.4 (s, pz-5), 135.9 (s, pz-3), 135.7 (s, *o*-BPh), 126.6 (s, *m*-Ph), 126.1 (s, *p*-Ph), 104.7 (s, pz-4), 34.2 (m, $C(CH_3)_3$), 31.4 (d, $C(CH_3)_3$), 30.2 (d, $C(CH_3)_3$), 17.6 (m, CH_2). Anal. Calcd. for $C_{27}H_{48}BN_2P_2Tl$: C, 46.84; H, 7.14; N, 4.13. Found: C, 46.78; H, 6.90; N, 3.98.

[PhBP$^{tBu}_2$(pz^{tBuPh})]Tl (4.3). Solid 3,5-(*p*-^{t}BuPh)$_2$pyrazole (1.45 g, 4.36 mmol) was dissolved in Et_2O (50 mL) and cooled to -35 °C. To this stirring solution was added ^{n}BuLi (3.0 mL, 1.6 M solution in hexanes, 4.8 mmol) dropwise over 10 minutes. The resulting mixture was allowed to warm to room temperature and stir for 1 hour, and then **4.1** (1.77 g, 4.36 mmol) was added as a THF solution (20 mL). After 12 hours, $TlPF_6$ (1.53 g, 4.36 mmol) in THF (10 mL) was added to the homogeneous, yellow reaction

mixture. The resulting cloudy solution was stirred for 1 hour, and then filtered through Celite. Solvent was removed from the filtrate in vacuo. The remaining solids were extracted with petroleum ether (50 mL) and filtered through Celite, and the filtrate was dried in vacuo. The remaining solids were suspended in $(TMS)_2O$ (20 mL) and stirred for 30 minutes. The solids were collected on a sintered glass frit, washed with cold $(TMS)_2O$ (5 mL), and dried in vacuo to afford analytically pure **4.3** (3.33 g, 81.1%). ^{1}H NMR (300 MHz, C_6D_6): δ = 8.09 (br m, 2H, *o*-PhB), 7.65 (d, 2H, $^3J_{H\text{-}H}$ = 8.1 Hz, pz-Ar), 7.59 (d, 2H, $^3J_{H\text{-}H}$ = 8.1 Hz, pz-Ar), 7.34 (d, 2H, $^3J_{H\text{-}H}$ = 8.7 Hz, pz-Ar), 7.32 (m, 1H, *p*-PhB), 7.29 (d, 2H, $^3J_{H\text{-}H}$ = 8.7 Hz, pz-Ar), 7.00 (t, 2H, $^3J_{H\text{-}H}$ = 7.2 Hz, *m*-PhB), 6.58 (s, 1H, pz-4), 1.79 (m, 2H, CH_2), 1.31 (s, 9H, ^{t}Bu-Ar), 1.26 (m, 18H, ^{t}Bu-P), 1.20 (s, 9H, ^{t}Bu-Ar), 1.04 (d, 9H, $^3J_{P\text{-}H}$ = 11.4 Hz, ^{t}Bu-P), 0.72 (d, 9H, $^3J_{P\text{-}H}$ = 9.6 Hz, ^{t}Bu-P), 0.56 (m, 1H, CH_2), 0.35 (m, 1H, CH_2). ^{31}P{^{1}H} NMR (121.5 MHz, C_6D_6): δ = 113.0 (d, 1P, $^1J_{Tl\text{-}P}$ = 3790 Hz, coordinated), 27.5 (s, 1P, uncoordinated). ^{13}C{^{1}H} NMR (75.5 MHz, C_6D_6): δ = 160 (*ipso*-BPh), 150.8 (pz-*o*-Ar), 150.6 (pz-*o*-Ar), 137.2 (pz-5), 135.5 (pz-3), 135.0 (pz-*m*-Ar), 133.2 (pz-*m*-Ar), 130.9 (*o*-BPh), 129.9 (*ipso*-pz-Ar), 129.4 (*ipso*-pz-Ar), 129.2 (*ipso*-pz-Ar), 126.7 (*m*-BPh), 125.2 (*p*-BPh), 107.9 (pz-4), 38.0 (P*C*$(CH_3)_3$), 35.8 (P*C*$(CH_3)_3$), 35.0 (Ar*C*$(CH_3)_3$), 34.9 (Ar*C*$(CH_3)_3$), 32.6 (P*C*$(CH_3)_3$), 32.2 (PC(*C*$H_3)_3$), 31.8 (ArC(*C*$H_3)_3$), 31.7 (ArC(*C*$H_3)_3$), 30.5 (PC(*C*$H_3)_3$), 30.3 (PC(*C*$H_3)_3$), 21.2 (CH_2), 19.0 (CH_2). Anal. Calcd. for $C_{47}H_{72}BN_2P_2Tl$: C, 59.91; H, 7.70; N, 2.97. Found: C, 60.00; H, 7.45; N, 2.84.

[PhBP$^{tBu}_2$(pz^{Me})]Tl (4.4). Solid 3,5-dimethylpyrazole (0.4850 g, 5.049 mmol) was dissolved in Et_2O (25 mL) and cooled to -78 °C. To this stirring solution was added ^{n}BuLi (3.5 mL, 1.6 M solution in hexanes, 5.5 mmol) dropwise over 10 minutes. The

resulting cloudy mixture was allowed to warm to room temperature and stir for 1 hour, and then **4.1** (2.0499 g, 5.049 mmol) was added as an Et_2O solution (10 mL). After 12 hours, $TlPF_6$ (1.76 g, 5.05 mmol) in THF (10 mL) was added to the yellow reaction mixture. The resulting cloudy solution was stirred for 1 hour, and then filtered through Celite. Solvent was removed from the filtrate in vacuo. The remaining solids were washed with acetonitrile (2 x 10 mL), collected on a sintered glass frit, and washed with minimal petroleum ether (5 mL) to yield analytically pure product as a white solid (0.9378 g, 26.3%). ^{1}H NMR (300 MHz, C_6D_6): δ = 7.53 (br, 2H, *o*-PhB), 7.21 (t, 2H, $^3J_{H\text{-}H}$ = 6.6 Hz, *m*-PhB) 7.05 (m, 1H, $^3J_{H\text{-}H}$ = 6.6 Hz, *p*-PhB), 5.82 (br s, 1H, pz-4), 2.59 (s, 3H, pz-Me), 2.03 (s, 3H, pz-Me), 1.51 (m, 4H, CH_2), 1.32 (d, 18H, $^3J_{P\text{-}H}$ = 11.1 Hz, ^{t}Bu), 0.80 (d, 18H, $^3J_{P\text{-}H}$ = 11.1 Hz, ^{t}Bu). ^{31}P{^{1}H} NMR (121.5 MHz, C_6D_6): δ = 35 (very broad). ^{13}C{^{1}H} NMR (75.5 MHz, C_6D_6): δ = 160 (br, *ipso*-BPh), 136.8 (s, pz-5), 136.0 (s, pz-3), 134.6 (s, *o*-BPh), 126.5 (s, *m*-Ph), 125.7 (s, *p*-Ph), 108.2 (s, pz-4), 32.6 (m, $C(CH_3)_3$), 31.5 (d, $C(CH_3)_3$), 30.4 (d, $C(CH_3)_3$), 18.0 (m, CH_2), 16.7 (s, pz-Me), 2.4 (s, pz-Me). Anal. Calcd. for $C_{29}H_{52}BN_2P_2Tl$: C, 49.34; H, 7.43; N, 3.97. Found: C, 49.10; H, 7.15; N, 3.78.

[PhBP$^{tBu}_2$(pz)]FeCl (4.5). Solid **4.2** (0.6935 g, 1.023 mmol) was dissolved in THF (10 mL). To this was added a slurry of $FeCl_2$ (0.130 g, 1.03 mmol) in THF (5 mL), and the resulting mixture was stirred for 2 hours. The resulting cloudy yellow solution was filtered through Celite to remove TlCl, and the filtrate was dried in vacuo. The remaining yellow solids were extracted with benzene (10 mL), filtered through Celite, and dried in vacuo. The resulting solids were extracted with toluene (5 mL), filtered through Celite, and cooled to -35 ˚C for 12 hours, yielding analytically pure, yellow product as a

crystalline solid (0.398 g, 68.9%). Crystals suitable for X-ray diffraction were chosen from crystals grown in this fashion. ^{1}H NMR (300 MHz, C_6D_6): δ = 277.5 (br s, CH_2), 45.3 (br s, *o*-Ar), 29.1 (s, pz-3), 27.2 (br s, pz-4), 17.1 (br s, pz-5), 14.2 (s, *m*-Ar), 14.1 (s, *p*-Ar), 9.4 (br s, ^{t}Bu), -6.2 (br s, ^{t}Bu). UV-vis (C_6H_6) λ_{max}, nm (ε): 380 (250), 430 (sh). Evans method (C_6D_6, 295 K): 5.20 μ_B. Anal. Calcd. for $C_{27}H_{48}BClFeN_2P_2$: C, 57.42; H, 8.57; N, 4.96. Found: C, 57.13; H, 8.27; N, 4.81.

[PhBP$^{tBu}_2$(pz^{tBuPh})]FeCl (4.6). Solid **4.3** (0.3652 g, 0.3880 mmol) was dissolved in THF (5 mL). To this was added a slurry of $FeCl_2$ (0.0492 g, 0.388 mmol) in THF (5 mL), and the resulting mixture was stirred for 2 hours. The resulting cloudy yellow solution was filtered through Celite to remove TlCl, and the filtrate was dried in vacuo. The remaining yellow solids were extracted with benzene (10 mL), filtered through Celite, and dried in vacuo. The resulting solids were extracted with toluene (5 mL), filtered through Celite, and cooled to -35 ˚C for 12 hours, yielding analytically pure, yellow product as a crystalline solid (0.1035 g, 33.2%). ^{1}H NMR (300 MHz, C_6D_6): δ = 272 (br s, CH_2), 56.1 (br s, *o*-Ar), 24.9 (br s, pz-4), 15.2 (s), 14.4 (s, ^{t}Bu-P), 12.2 (s, *m*-Ar), 11.8 (s, *p*-Ar), 4.0 (s), 2.8 (br, overlapping signals), -3.18 (br s, ^{t}Bu-Ar), -3.8 (br s, ^{t}Bu-P). UV-vis (C_6H_6) λ_{max}, nm (ε, $M^{-1}cm^{-1}$): 392 (250). Evans method (C_6D_6): 4.87 μ_B. Anal. Calcd. for $C_{47}H_{72}BClFeN_2P_2$: C, 68.08; H, 8.75; N, 3.38. Found: C, 68.19; H, 8.60; N, 3.30.

[PhBP$^{tBu}_2$(pz^{Me})]FeCl (4.7). Solid **4.4** (0.5553 g, 0.7872 mmol) was dissolved in THF (15 mL). To this was added a slurry of $FeCl_2$ (0.0998 g, 0.7872 mmol) in THF (5 mL), and the resulting mixture was stirred for 2 hours. The resulting cloudy yellow solution was filtered through Celite to remove TlCl, and the filtrate was dried in vacuo. The remaining yellow solids were extracted with benzene (10 mL), filtered through Celite,

and dried in vacuo. The resulting solids were then extracted with toluene (5 mL), filtered through Celite, and cooled to -35 ˚C for 12 hours, yielding analytically pure product as a crystalline white solid (0.2705 g, 58.0%). ^{1}H NMR (300 MHz, C_6D_6): δ = 285.5 (br s, CH_2), 93.8 (s, pz-3-Me), 49.2 (s, *o*-Ar), 29.1, 25.8 (s, pz-5-Me), 23.2 (br s, pz-4), 13.1 (s, *m*-Ar), 12.3 (s, *p*-Ar), 13.0 (br s, ^{t}Bu), -2.8 (br s, ^{t}Bu). UV-vis (C_6H_6) λ_{max}, nm (ε, $M^{-1}cm^{-1}$): 372 (1000). Evans method (C_6D_6, 295 K): 5.05 μ_B. Anal. Calcd. for $C_{29}H_{52}BClFeP_2N_2$: C, 58.76; H, 8.84; N, 4.73. Found: C, 58.36; H, 8.64; N, 4.88.

[PhBP$^{tBu}_2$(pz)]CoI (4.8). Solid **4.2** (0.4117 g, 0.608 mmol) was dissolved in THF (10 mL). To this was added a slurry of CoI_2 (0.1900 g, 0.608 mmol) in THF (5 mL), and the resulting mixture was stirred for 2 hours. The resulting cloudy green solution was filtered through Celite to remove yellow TlI, and the filtrate was dried in vacuo. The remaining green solids were extracted with benzene (10 mL), filtered through Celite, and dried in vacuo. The resulting solids were extracted with toluene (5 mL), filtered through Celite, and cooled to -35 ˚C for 12 hours, yielding analytically pure, green product as a crystalline solid (0.1823 g, 45.5 %). ^{1}H NMR (300 MHz, C_6D_6): δ = 60.2 (s, pz-5), 45.3 (s, pz-4), 44.9 (br s, pz-3), 19.1 (s, ^{t}Bu), 16.5 (s, Ar), 10.7(s, tBu), 10.0 (Ar), 8.4 (Ar). UV-vis (C_6H_6) λ_{max}, nm (ε): 450 (420), 627 (570), 659 (640), 697 (590). Evans method (C_6D_6): 4.35 μ_B. Anal. Calcd. for $C_{27}H_{48}BCoIN_2P_2$: C, 49.19; H, 7.34; N, 4.25. Found: C, 49.00; H, 7.11; N, 4.22.

[PhBP$^{tBu}_2$(pz^{tBuPh})]CoI (4.9). Solid **4.3** (0.1529 g, 0.1620 mmol) was dissolved in THF (10 mL). To this was added a slurry of CoI_2 (0.0508 g, 0.162 mmol) in THF (5 mL), and the resulting mixture was stirred for 2 hours. The resulting cloudy green solution was filtered through Celite to remove yellow solids (TlI), and the filtrate was dried in vacuo.

The remaining green solids were extracted with benzene (10 mL), filtered through Celite, and dried in vacuo. The resulting solids were extracted with toluene (5 mL), filtered through Celite, and cooled to -35 ˚C for 12 hours, yielding analytically pure, green product as a crystalline solid (0.0955 g, 76.4 %). ^{1}H NMR (300 MHz, C_6D_6): δ = 70.0 (br), 25.2 (br s, ^{t}Bu-P), 20.2 (s, B-Ar), 13.1 (s, B-Ar), 13.4 (s, B-Ar), 10.6 (s, pz-Ar), 8.9 (s, pz-Ar), 3.5 (br s, ^{t}Bu-P), 3.1 (s, ^{t}Bu-Ar), -2.8 (s, pz-Ar), -4.5 (s, ^{t}Bu-Ar), -37.2. UV-vis (C_6H_6) λ_{max}, nm (ε): 588 (610), 653 (690), 693 (650), 734 (sh), 776 (330). Evans method (C_6D_6): 4.10 μ_B. Anal. Calcd. for $C_{47}H_{72}BCoI_2N_2P_2$: C, 53.73; H, 6.91; N, 2.67. Found: C, 53.60; H, 6.67; N, 2.69.

[PhBP$^{tBu}_2$(pz)]Fe(dbabh) (4.10). Solid **4.5** (0.0547 g, 0.0969 mmol) was dissolved in THF (5 mL) and cooled to -35 °C. To this was added a cold solution of Li(dbabh) (0.0193 g, 0.0969 mmol) in THF (1 mL). The resulting red/orange mixture was allowed to stir for 4 hours at -35 °C. Volatiles were removed from the solution in vacuo, and the remaining solids were dissolved in C_6H_6 and filtered through Celite. Solvent was removed from the filtrate in vacuo, and the resulting red/orange solids were extracted with toluene (2 mL), filtered through Celite, and cooled to -35 °C for 12 hours, yielding analytically pure product as red/orange crystals (0.0295 g, 42.2%). ^{1}H NMR (300 MHz, C_6D_6): δ = 288 (br s, CH_2), 39.8 (br s, *p*-Ar), 36.0 (br s, dbabh), 31.3 (s, pz-5), 29.6 (br s, pz-3), 19.1, 16.9, 15.3 (s, *o*-Ar), 15.0 (s, *m*-Ar), 3.7, 1.5, -8.7 (br s, ^{t}Bu). UV-vis (C_6H_6) λ_{max}, nm (ε): 350 (2700), 452 (sh). Evans method (C_6D_6): 4.61 μ_B. Anal. Calcd. for $C_{41}H_{58}BFeN_3P_2$: C, 68.25; H, 8.10; N, 5.82. Found: C, 67.84; H, 7.81; N, 5.51.

[PhBP$^{tBu}_2$(pz)]Co(dbabh) (**4.11**). Solid **4.8** (0.1588 g, 0.2410 mmol) was dissolved in THF (5 mL) and cooled to -35 °C. To this was added a cold solution of Li(dbabh)

(0.0726 g, 0.265 mmol) in THF (2 mL). The resulting red/brown mixture was allowed to stir for 2 hours at room temperature. Volatiles were removed from the solution in vacuo, and the remaining solids were washed with petroleum ether (2 x 10 mL). Solvent was removed from the filtrate in vacuo, and the resulting red/brown solids were extracted with toluene (2 mL), filtered through Celite, and cooled to -35 °C for 12 hours, yielding analytically pure product as red/brown crystals (0.0942 g, 54.0%). ^{1}H NMR (300 MHz, C_6D_6): δ = 68.0, 48.4, 46.1, 18.6, 13.8, 13.4, 11.0, 9.9, 8.3 (br s, ^{t}Bu), 4.9 (br s, ^{t}Bu), UV-vis (C_6H_6) λ_{max}, nm (ε): 409 (2700), 479 (sh), 692 (1300). Evans method (C_6D_6): 4.05 μ_B. Anal. Calcd. for $C_{41}H_{58}BCoN_3P_2$: C, 67.96; H, 8.07; N, 5.80. Found: C, 67.83; H, 7.80; N, 5.57.

Generation of {[κ^2-PhBP$^{tBu}_2$(pz)]Co^{I}NH(C$_{14}$H$_9$)}{Na(THF)$_3$} (**4.12**). Napthalene (0.0142 g, 0.0783 mmol) was dissolved in THF (2 mL) and added to a vial containing solid Na (0.0082 g, 0.36 mmol). This mixture was stirred for 30 minutes, and the resulting intense green solution was cooled to -35 °C. This solution was then filtered through Celite directly into a cold (-35 °C) solution of **4.11** in THF (2 mL). The resulting intense blue solution was kept at -35 °C for 2 hours with occasional agitation. Cold petroleum ether (10 mL) was layered on top of this solution, and after 12 hours, a purple precipitate had formed. The supernatant was decanted, and the remaining purple solids were washed with petroleum ether (2 x 2 mL) and dried in vacuo. Crystals suitable for X-ray diffraction were obtained via vapor diffusion of petroleum ether into a concentrated THF solution of **4.12**. ^{1}H NMR (300 MHz, C_6D_6): δ = 26.9, 10.6, 8.6, 7.8, 6.0, 4.8, 4.3 (THF), 1.9 (THF), -26.2, -39.9, -87.8. UV-vis (C_6H_6) λ_{max}, nm: 378, 392, 520. Evans method (C_6D_6): 3.41 μ_B.

[PhBP$^{tBu}_2$(pz)]Fe(N$_3$) (4.13). Solid **4.5** (0.0625 g, 0.111 mmol) was dissolved in THF (5 mL). To this was added a slurry of NaN_3 (0.144 g, 2.21 mmol) in THF (2 mL), and the resulting mixture was stirred for 12 hours. The resulting cloudy yellow solution was filtered through Celite to remove excess NaN_3 and NaCl, and the filtrate was dried in vacuo. The remaining yellow solids were extracted with benzene (10 mL), filtered through Celite, and dried in vacuo. The solids were then extracted with toluene (5 mL), filtered through Celite, and cooled to -35 ˚C for 12 hours, yielding analytically pure product as yellow crystals (0.0386 g, 93.7 %). ^{1}H NMR (300 MHz, C_6D_6): δ = 276.8 (br s, CH_2), 43.7 (br s, *p*-Ar), 30.5 (br s, pz-3), 29.2 (s, pz-5), 15.2 (br s, pz-4), 14.2 (s, *o*-Ar), 14.1 (s, *m*-Ar), 9.0 (br s, ^{t}Bu), -4.8 (br s, ^{t}Bu). IR (cm^{-1}): 2068. UV-vis (C_6H_6) λ_{max}, nm (ε): 381 (200), 460 (sh). Evans method (C_6D_6): 4.91 μ_B. Anal. Calcd. for $C_{27}H_{48}BFeN_5P_2$: C, 56.76; H, 8.47; N, 12.26. Found: C, 56.51; H, 7.69; N, 10.45.

4.5.7 X-ray Experimental Data

Crystallographic procedures are outlined in Section 2.4.6. Crystallographic data are summarized in Table 4.2. The structure of **4.5** sits on a center of symmetry; consequently, half of the atoms are generated via symmetry operations.

Table 4.2. Crystallographic data for [PhBP$^{t\text{Bu}}_2$(pz)]FeCl, **4.5**; [PhBP$^{t\text{Bu}}_2$(pz$^{t\text{BuPh}}$)]FeCl, **4.6**; [PhBP$^{t\text{Bu}}_2$(pz)]CoI, **4.8**; [PhBP$^{t\text{Bu}}_2$(pz$^{t\text{BuPh}}$)]CoI, **4.9**; [PhBP$^{t\text{Bu}}_2$(pz)]Fe(dbabh), **4.10**; [PhBP$^{t\text{Bu}}_2$(pz)]Co(dbabh), **4.11**; and {[η^2-PhBP$^{t\text{Bu}}_2$(pz)]Co$^{\text{I}}$NH($C_{14}H_9$)}{Na(THF)$_3$}, **4.12**.

	4.5	**4.6**	**4.8**
chemical formula	$C_{54}H_{96}B_2Cl_2Fe_2N_4P_2$	$C_{47}H_{72}BClFeN_2P_2$	$C_{27}H_{48}BCoIN_2P_2$
Fw	1067.51	864.57	659.25
T (°C)	-173	-173	-173
λ (Å)	0.71073	0.71073	0.71073
a (Å)	10.3430(4)	10.210(3)	19.145(4)
b (Å)	10.5536(4)	15.710(4)	10.635(2)
c (Å)	14.0707(5)	15.921(5)	16.043(3)
α (°)	87.428(2)	93.498(5)	90
β (°)	83.364(2)	102.945(5)	107.92(3)
γ (°)	73.7360(10)	108.426(5)	90
V (Å^3)	1464.43(9)	2337.2(11)	3107.9(11)
space group	P-1	P-1	P2(1)/c
Z	1	2	4
D_{calc} (g/cm^3)	1.210	1.229	1.409
μ(cm^{-1})	6.78	5.39	16.66
R1, wR2[a] ($I > 2\sigma(I)$)	0.0494, 0.0817	0.0898, 0.1834	0.0474, 0.0704

[a] $R1 = \Sigma||F_o| - |F_c||/\Sigma|F_o|$, $wR2 = \{\Sigma[w(F_o^2 - F_c^2)^2]/\Sigma[w(F_o^2)^2]\}^{1/2}$

Table 4.2 cont.

	4.9	**4.10**	**4.11**
chemical formula	$C_{47}H_{72}BCoIN_2P_2$	$C_{41}H_{58}BFeN_3P_2$	$C_{41}H_{58}BCoN_3P_2$
Fw	923.65	721.50	724.58
T (°C)	-173	-173	-173
λ (Å)	0.71073	0.71073	0.71073
a (Å)	10.1160(9)	10.8950(10	10.901(12)
b (Å)	30.952(3)	19.702(2)	19.51(2)
c (Å)	15.1936(13)	18.4197(19)	18.36(2)
α (°)	90	90	90
β (°)	102.831(2)	96.460(2)	96.45(4)
γ (°)	90	90	90
V (Å^3)	4638.4(7)	3928.7(7)	3879(8)
space group	P2(1)/c	P2(1)/n	P2(1)/n
Z	4	4	4
D_{calc} (g/cm^3)	1.323	1.220	1.241
μ(cm^{-1})	11.38	4.97	5.57
R1, wR2[a] ($I > 2\sigma(I)$)	0.0403, 0.0622	0.0547, 0.0853	0.0530, 0.0750

[a] $R1 = \Sigma||F_o| - |F_c||/\Sigma|F_o|$, $wR2 = \{\Sigma[w(F_o^2 - F_c^2)^2]/\Sigma[w(F_o^2)^2]\}^{1/2}$

Table 4.2 (cont'd)

	4.12
chemical formula	$C_{45}H_{75}BCoN_4NaO_3P_2$
fw	874.76
T (°C)	-173
λ (Å)	0.71073
a (Å)	21.809(3)
b (Å)	10.3991(12)
c (Å)	23.569(3)
α (°)	90
β (°)	100.287(2)
γ (°)	90
V (Å^3)	5259.4(12)
space group	P2(1)/n
Z	5
D_{calc} (g/cm^3)	1.381
μ(cm^{-1})	5.41
R1, wR2[a] ($I > 2\sigma(I)$)	R1 = 0.0554, 0.0831

[a] $R1 = \Sigma||F_o| - |F_c||/\Sigma|F_o|$, $wR2 = \{\Sigma[w(F_o^2 - F_c^2)^2]/\Sigma[w(F_o^2)^2]\}^{1/2}$

References Cited

[1] (a) Trofimenko, S. *Scorpionates: The Coordination Chemistry of Polypyrazolylborate Ligands*; Imperial College Press: London, 1999. (b) Trofimenko, S. *Chem. Rev.* **1993**, *93*, 943. (c) Trofimenko, S. *Polyhedron* **2004**, *23*, 197.

[2] (a) Jenkins, D. M.; Di Bilio, A. J.; Betley, T. A.; Peters, J. C. *J. Am. Chem. Soc.* **2002**, *124*, 15336. (b) Betley, T. A.; Peters, J. C. *Inorg. Chem.* **2003**, *42*, 5074. (c) Thomas, J. C.; Peters, J. C. *Polyhedron* **2004,** *23*, 489. (d) MacBeth, C. E.; Thomas, J. C.; Betley, T. A.; Peters, J. C. *Inorg. Chem.* **2004**, *43*, 4645. (e) Peters, J. C.; Feldman, J. D.; Tilley, T.

D. *J. Am. Chem. Soc.* **1999**, *121*, 9871. (f) Barney, A. A.; Heyduk, A. F.; Nocera, D. G. *Chem. Commun.* **1999**, 2379. (g) Shapiro, I. R.; Jenkins, D. M.; Thomas, J. C.; Day, M. W.; Peters, J. C. *Chem. Commun.* **2001**, 2152.

[3] (a) Ohrenberg, C.; Liable-Sands, L. M.; Rheingold, A. L.; Riordan, C. G. *Inorg. Chem.* **2001**, *40*, 4276. (b) Ohrenberg, C.; Ge, P.; Schebler, P.; Riordan, C. G.; Yap, G. P. A.; Rheingold, A. L. *Inorg. Chem.* **1996**, *35*, 749. (c) Ohrenberg, C.; Riordan, C. G.; Liable-Sands, L.; Rheingold, A. L. *Coord. Chem. Rev.* **1998**, *174*, 301.

[4] (a) Casado, M. A.; Hack, V.; Camerano, J. A.; Ciriano, M. A.; Tejel, C.; Oro, L. A. *Inorg. Chem.* **2005**, *44*, 9122. (b) Chiou, S.-J.; Innocent, J.; Riordan, C. G.; Lam, K.-C.; Liable-Sands, L.; Rheingold, A. L. *Inorg. Chem.* **2000**, *39*, 4347. (c) Chiou, S.-J.; Ge, P.; Riordan, C. G.; Liable-Sands, L. M.; Rheingold, A. L. *Chem. Commun.* **1999**, 159. (d) Thompson, J. S.; Zitzmann, J. L.; Marks, T. J.; Ibers, J. A. *Inorg. Chim. Acta* **1980**, *46*, L101. (e) Ghosh, P.; Parkin, G. *Chem. Commun.* **1998**, 413. (f) Niedenzu, K.; Trofimenko, S. *Inorg. Chem.* **1985**, *24*, 4222.

[5] Neutral neopentane-based mixed pyrazolyl/phosphine donor ligands have also been examined; however, in most cases, these ligands adopt a bidentate binding mode with a dangling pyrazolyl arm. See: (a) Jacobi, A.; Huttner, G.; Winterhalter, U.; Cunskis, S. *Eur. J. Inorg. Chem.* **1998**, 675. (b) Faissner, R.; Huttner, G.; Kaifer, E.; Kircher, P.; Rutsch, P.; Zsolnai, L. *Eur. J. Inorg. Chem.* **2003**, 2219. (c) Faissner, R.; Huttner, G.; Kaifer, E.; Rutsch, P. *Eur. J. Inorg. Chem.* **2003**, 1681.

[6] (a) Betley, T. A.; Peters, J. C. *J. Am. Chem. Soc.* **2004**, *126*, 6252. (b) Jenkins, D. M.; Betley, T. A.; Peters, J. C. *J. Am. Chem. Soc.* **2002**, *124*, 11238. (c) Brown, S. D.; Betley,

T. A.; Peters, J. C. *J. Am. Chem. Soc.* **2003**, *125*, 322. (d) Betley, T. A.; Peters, J. C. *J. Am. Chem. Soc.* **2003**, *125*, 10782.

[7] (a) Daida, E. J.; Peters, J. C. *Inorg. Chem.* **2004**, *43*, 7474. (b) Brown, S. D.; Mehn, M. P.; Peters, J. C. *J. Am. Chem. Soc.* **2005**, *127*, 13146. (c) Thomas, C. M.; Peters, J. C. *Angew. Chem. Int. Ed.* **2006**, *45,* 776. (d) Brown, S. D.; Peters, J. C. *J. Am. Chem. Soc.* **2004**, *126*, 4538. (e) Thomas, C. M.; Daida, E. J.; Peters, J. C. *manuscript in preparation.*

[8] For an example of similar 3-coordinate and 4-coordinate boranes and a discussion of their ^{11}B NMR spectra, see: Groshens, T. J.; Higa, K. T.; Nissan, R.; Butcher, R. J.; Freyer, A. J. *Organometallics* **1993**, *12*, 2904.

[9] (a) Sur, S. K. *J. Magn. Reson.* **1989**, *82*, 169. (b) Evans, D. F. *J. Chem. Soc.* **1959**, 2003.

[10] The irreversible reduction observed in the cyclic voltammagram of **4.6** is approaching the solvent (THF) window so the reported potential of -3.05 V is approximate.

[11] (a) Carpino, L. A.; Padykula, R. E.; Barr, D. E.; Hall, F. H.; Krause, J. G.; Dufresne, R. F.; Thoman, C. J. *J. Org. Chem.* **1998**, *53*, 2565. (b) Mindiola, D. J.; Cummins, C. C. *Angew. Chem. Int. Ed.* **1998**, *37*, 945.

[12] Wagner, W. D.; Nakamoto, K. *J. Am. Chem. Soc.* **1988**, *110*, 4044.

[13] (a) Meyer, K.; Bill, E.; Mienert, B.; Weyhermüller, T.; Wieghardt, K. *J. Am. Chem. Soc.* **1999**, *121*, 4859. (b) Grappherhaus, C. A.; Mienert, B.; Bill. E.; Weyhermüller, T.; Wieghardt, K. *Inorg. Chem.* **2000**, *39*, 5306.

[14] Brown, S. D.; Peters, J. C. *J. Am. Chem. Soc.* **2005**, *127*, 1913.

[15] Based on a search of the Cambridge Structural Database for 3-coordinate cobalt NR_2^- complexes.

[16] Detrich, J. L.; Konecny, R.; Vetter, W. M.; Doren, D.; Rheingold, A. L.; Theopold, K. H. *J. Am. Chem. Soc.* **1996**, *118*, 1703.

[17] Schebler, P. J.; Riordan, C. G.; Guzei, I. A.; Rheingold, A. L. *Inorg. Chem.* **1998**, *37*, 4754.

[18] Fild, M.; Stelzer, O.; Schmutzler, R. *Inorg. Synth.* **1973**, *14*, 4.

[19] Kolodiazhnyi, O. I. *Synth. Meth. Organomet. Inorg. Chem.* **1996**, *3*, 88.

[20] Karsch, H. H.; Schmidbaur, H. *Z. Naturforsch.* **1977**, *32B*, 762.

[21] Libertini, E.; Yoon, K.; Parkin, G. *Polyhedron* **1993**, *12*, 2539.

Chapter 5: Synthesis and Characterization of Terminal Iron Imides in the +3 and +4 Oxidation States

The text in this chapter is reproduced in part with permission from:

Thomas, C. M.; Mankad, N. P.; Peters, J. C. *J. Am. Chem. Soc.* **2006,** *128*, 4956.

5.1 Introduction

In this chapter, it is demonstrated that similar to its tris(phosphine) analogues, the bis(phosphino)pyrazolylborate hybrid ligands are capable of stabilizing low valent iron(I) and cobalt(I) complexes as well as high valent iron(III), iron(IV), and cobalt(III) terminal imides. Despite their prominent role in biological systems,[1] examples of coordinatively unsaturated iron(I) complexes such as those described herein are limited.[2] Moreover, although implicated as intermediates in group transfer reactions,[3] mid-to-late first row transition metals (e.g., Mn, Fe, Co, Ni) featuring terminal imido/nitrene functionalities are rare.[4] While a number of cobalt imides have been reported recently,[5] examples of iron imides are far less common.[6,7]

The first examples of structurally characterized mononuclear iron imides were those supported by tris(phosphino)borate ligands.[7] These species have been reported in the iron(III) and iron(II) oxidation states. In the iron(III) state, they have been accessed via oxidative nitrene transfer from organic azides using low valent iron(I) precursors. The $[PhBP^{R}_{3}]Fe^{III}(NR)$ complexes that have been isolated all show electrochemically reversible $Fe^{III/II}$ couples, and chemical reduction typically provides their corresponding d^6 $\{[PhBP^{R}_{3}]Fe^{II}(NR)\}^{-}$ analogues in high yield. Well-defined Fe^{IV}=NR species have proven generally more elusive,[8] though thoroughly characterized examples of isolobal Fe^{IV}=O species are now well known.[9] To the best of our knowledge the single report of a complex that can be formulated as an iron(IV) imide concerns Lee's tetranuclear cluster $Fe_4(\mu_3\text{-}N^tBu)_4(N^tBu)Cl_3$, isolated in only 1-2% yield.[10] Mössbauer data for this species were consistent with a cluster featuring three iron(III) centers and one iron(IV) center, the latter most likely indicative of the terminal Fe^{IV}=N^tBu moiety. In this chapter, it is

demonstrated that the hybrid bis(phosphino)pyrazolylborate ligand supports pseudo-tetrahedral iron in the +1, +2, +3, and +4 oxidation states. The +3 and +4 oxidation states are stabilized by the terminal Fe≡NR imide linkage.

5.2 Results

5.2.1 Synthesis and Characterization of [PhBP$^{tBu}_2$(pz')]M^{I}(PMe$_3$) Complexes (M = Fe, Co)

Scheme 5.1

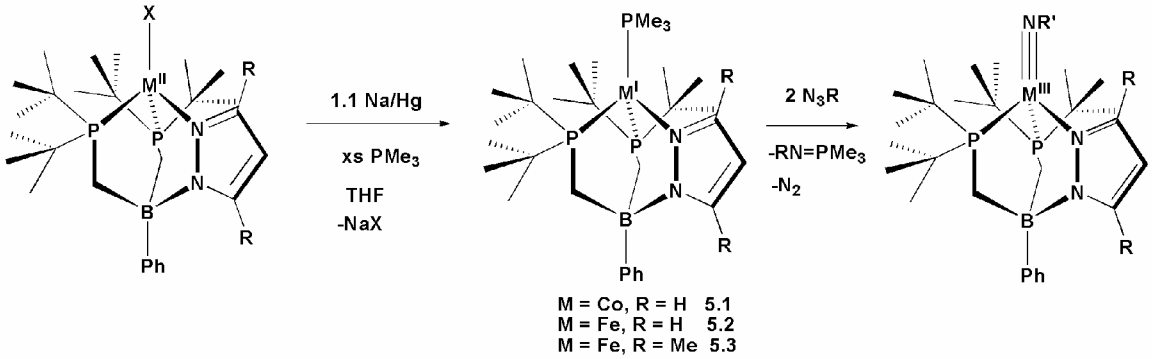

To access metal imides following the overall methodology that proved effective for the synthesis of tris(phosphino)borate iron(III) and cobalt(III) imides,[5a,7] low valent iron(I) and cobalt(I) precursors were synthesized (Scheme 5.1). One-electron reduction of [PhBP$^{tBu}_2$(pz)]CoI (**4.8**) with sodium/mercury amalgam in the presence of excess PMe$_3$ generates [PhBP$^{tBu}_2$(pz)]Co(PMe$_3$) (**5.1**) as a blue/green crystalline solid in 60% isolated yield. The oxidation state of **5.1** is confirmed by its solution magnetic moment of 3.04 μ_B (Evans' method, benzene), indicating a high spin (S = 1) d^8 configuration.[11] Similarly, one-electron reduction of [PhBP$^{tBu}_2$(pz)]FeCl (**4.5**) and [PhBP$^{tBu}_2$(pz^{Me2})]FeCl (**4.7**) in the presence of PMe$_3$ generates [PhBP$^{tBu}_2$(pz)]Fe(PMe$_3$) (**5.2**) and [PhBP$^{tBu}_2$(pz^{Me2})]Fe(PMe$_3$) (**5.3**) as pale green crystalline solids in 65% and 74% isolated yields, respectively. The solution magnetic moments of **5.2** and **5.3** are 4.16 μ_B and 4.06

μ_B, respectively, confirming a high spin (S = 3/2) d^7 electron configuration for each complex. X-ray quality crystals of **5.3** were obtained, and the resulting solid state structure is shown in Figure 5.1.

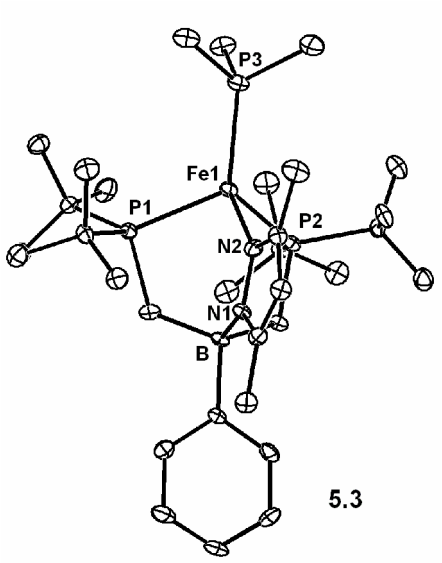

Figure 5.1 Displacement ellipsoid representation (50 %) of **5.3**. Hydrogen atoms have been omitted for clarity. Relevant interatomic distances and angles: Fe1-P1, 2.336(2) Å; Fe1- P2, 2.364(2) Å; Fe1-P3, 2.301(2) Å; Fe1-N2, 2.071(3) Å.

Interestingly, all three low valent phosphine complexes are luminescent to some degree. Emission data for the three complexes (excitation wavelength: 390 nm) is shown in Figure 5.2 along with the corresponding absorption spectrum. Qualitatively, the iron complexes **5.2** and **5.3** are more highly luminescent than the cobalt complex **5.1**, with the most intense luminescence occurring with complex **5.3.** Examinations of the lifetime and quantum yield of these emissions will be the subject of future study.

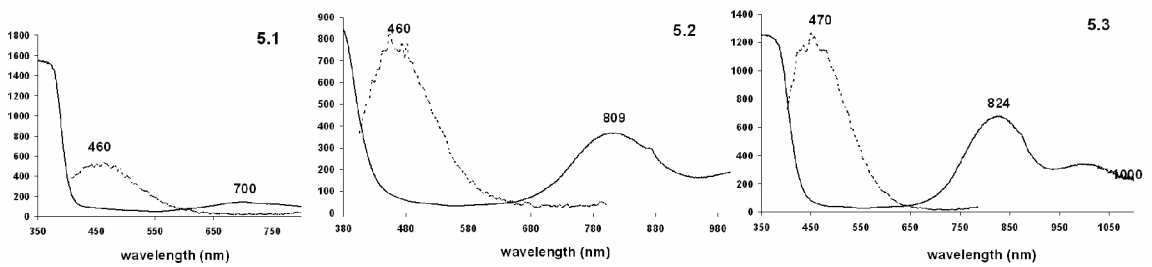

Figure 5.2 Absorption (solid) and emission (dashed) data for **5.1**, **5.2**, and **5.3**. The absorption data is plotted as ε (M^{-1} cm^{-1}) versus wavelength (nm). The emission data is plotted as intensity (arbitrary scale) versus wavelength (nm). Excitation wavelength = 390 nm.

5.2.2 Synthesis and Characterization of [PhBP$^{tBu}_2$(pz')]M^{III}(NR) Complexes (M = Fe, Co; R = ^{t}Bu, Ad, *p*-tolyl)

Terminal imide complexes were synthesized via nitrene transfer from organic azides to the iron(I) and cobalt(I) PMe_3 precursors. Complex **5.1** reacts cleanly with two equivalents of *p*-tolylazide at room temperature to generate the low spin, d^6 cobalt(III) imido complex [PhBP$^{tBu}_2$(pz)]Co≡N(*p*-tolyl) (**5.4**) with concomitant loss of N_2 and a stoichiometric equivalent of (*p*-tolyl)N=PMe_3. Complex **5.4** is diamagnetic and is characterized by a singlet in its $^{31}P\{^1H\}$ NMR spectrum at 90 ppm. X-ray diffraction of single crystals of **5.4** provided the structure shown in Figure 5.3. The short Co-N1 bond distance of 1.655(2) Å and the nearly linear C-N1-Co angle (163.7(2)°) are similar to that observed for the analogous [PhBP$^R_3$]Co≡N(*p*-tolyl) complexes (R = Ph: Co-N, 1.658(2) Å; Co-N-C46, 169.51(2)°; R = ^{i}Pr: Co-N, 1.667(2) Å; Co-N-C, 173.2(2)°).[5a,7b]

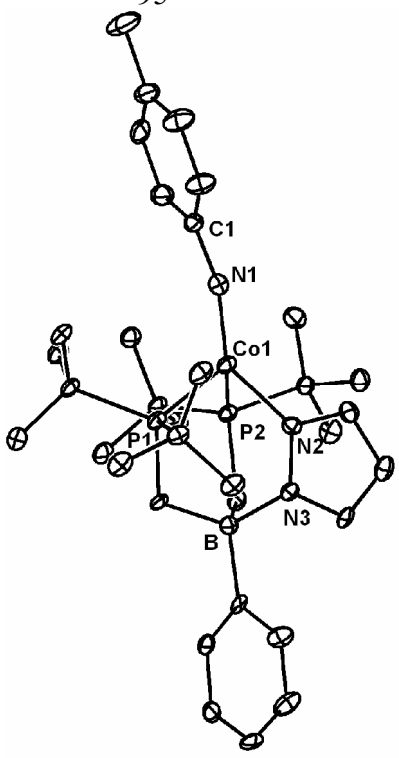

Figure 5.3 Displacement ellipsoid representation of **5.4**. Hydrogen atoms have been omitted for clarity. Relevant interatomic distances and angles: Co1-N1, 1.655(2) Å; Co1-P1, 2.2017(9) Å; Co1-P2, 2.2804(9) Å; Co1-N2, 1.951(2) Å; Co1-N1-C1, 163.7(2)°.

In stark contrast to their tris(phosphino)borate analogues, the iron(I) complexes **5.2** and **5.3** do not react cleanly with *p*-tolylazide or other aryl azides to generate terminal imide complexes. Alternatively, reaction of **5.2** and **5.3** with two equivalents of 1-adamantylazide generates the red-brown iron(III) imides $[PhBP^{tBu}_2(pz)]Fe{\equiv}NAd$ (**5.5**) and $[PhBP^{tBu}_2(pz^{Me2})]Fe{\equiv}NAd$ (**5.6**) and stoichiometric amounts of both N_2 and $AdN{=}PMe_3$. Both **5.5** and **5.6** adopt low spin S = ½ ground states based on solution magnetic data: μ_{eff} = 1.95 μ_B for **5.5** and 1.98 μ_B for **5.6** (Evans' method, C_6D_6). The EPR spectrum of **5.5** (2-methyltetrahydrofuran, 20 K) displays a rhombic signal similar to those of related $[PhBP^R_3]Fe^{III}{\equiv}NR$ imides (Figure 5.4).[7] The EPR data was simulated to

provide the g values g_1 = 2.96, g_2 = 1.95, and g_3 = 1.88, consistent with the S = ½ assignment.

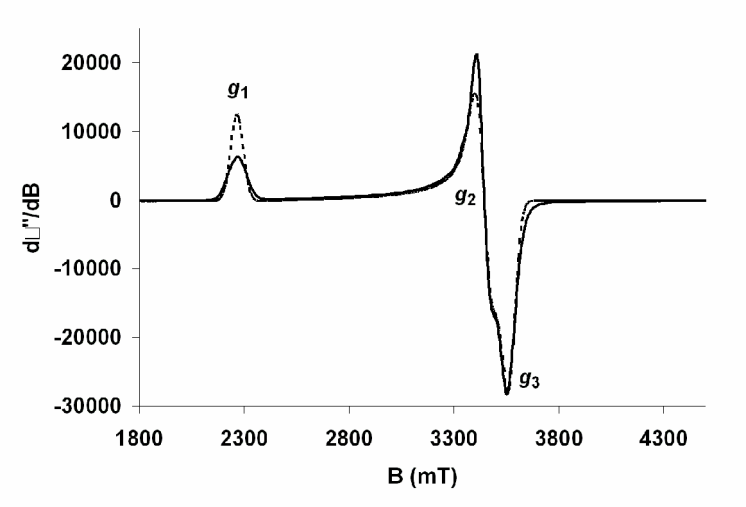

Figure 5.4. Experimental (solid) and simulated (dashed) EPR spectra of **5.5** with g_1 = 2.96, g_2 = 1.95, and g_3 = 1.88 (in 2-methyltetrahydrofuran glass at 20 K, 9.474 GHz).

Other alkyl azides such as *tert*-butylazide react with **5.2** and **5.3** to generate iron imide complexes that are far less stable than **5.5** and **5.6**. For instance, addition of two equivalents of *tert*-butylazide to **5.2** yields [PhBP$^{t\mathrm{Bu}}_2$(pz)]Fe≡N^{t}Bu (**5.7**), a complex that is thermally unstable in solution at room temperature and decomposes substantially in as little as 30 minutes. The analogous imide complex [PhBP$^{t\mathrm{Bu}}_2$(pz$^{\mathrm{Me2}}$)]Fe≡N^{t}Bu (**5.8**) is more stable, but moderate decomposition occurs at room temperature over a 12-hour period. The decomposition pathway of these complexes is thus far unknown.

We undertook a crystallographic investigation of **5.5-5.8** to confirm their connectivities and to examine their Fe-N bond distances and Fe-N$_{\mathrm{imide}}$-C bond angles for comparison with [PhBP$^{\mathrm{R}}_3$]Fe≡NR imides. In all four cases, the crystals obtained were of poor X-ray quality, regardless of the method employed for crystallization (vapor diffusion of petroleum ether into concentrated benzene solutions, slow evaporation of

dichloromethane, and storage in toluene at -35 °C all resulted in very thin plates of identical morphology). The structures of **5.5** and **5.6** could nonetheless be refined isotropically to confirm their connectivity and pseudo-tetrahedral geometry. As anticipated, short Fe-N_{imide} bond distances (average of both molecules in the asymmetric unit cell: **5.5**, 1.63 Å; **5.6**, 1.65 Å) and nearly linear C-N_{imide}-Fe angles (avg: **5.5**, 169°; **5.6,** 172°) are evident from the isotropic structures.[7]

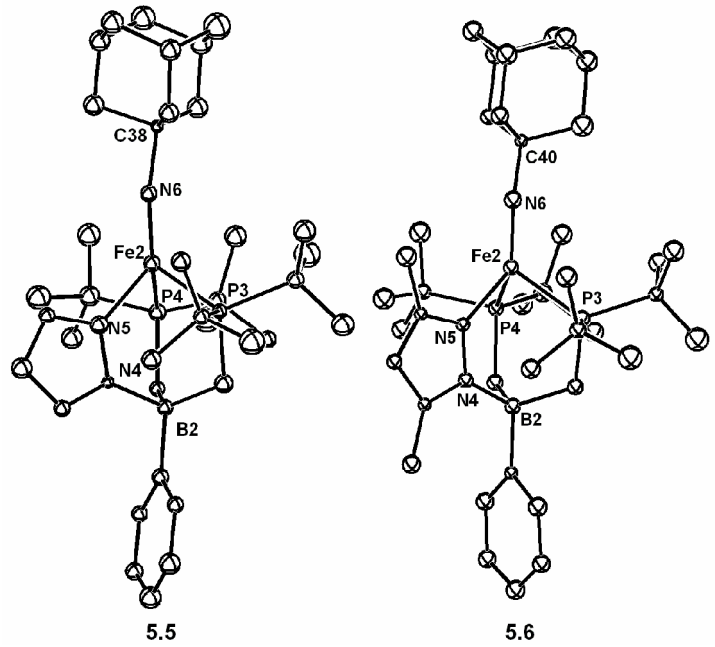

Figure 5.5 Isotropically refined solid-state structures of **5.5** and **5.6**, confirming their connectivity. For both complexes, only one of the two independent molecules in the asymmetric unit cell is shown. Hydrogen atoms have been omitted for clarity. Relevant interatomic distances and angles: **5.5**, Fe2-N6, 1.635(8) Å; Fe1-N3, 1.626(9) Å; Fe2-N6-C38, 170(1)°; Fe1-N3-C1, 175(2)°. **5.6**, Fe2-N6, 1.652(7) Å; Fe1-N3, 1.646(7) Å; Fe2-N6-C40, 172.4(6)°; Fe1-N3-C1, 172.1(6)°.

5.2.3 Reactivity of [PhBP$^{tBu}_2$(pz)]Co≡N(*p*-tolyl) and [PhBP$^{tBu}_2$(pz')]Fe≡N(Ad) Complexes with Carbon Monoxide

As was found for the tris(phosphino)borate iron and cobalt imides, complexes **5.4**-**5.8** are relatively unreactive.[5a,7] Transfer of the nitrene functionality to CO to release isocyanate (RN=C=O) has been demonstrated using imides of iron, cobalt, and nickel.[5a,7,12] Accordingly, the cobalt complex **5.4** is stable under most reaction conditions due to its low spin d^6 ground state, but like [PhBP$^{Ph}_3$]Co≡(*p*-tolyl) it reacts with excess carbon monoxide. The reaction occurs at room temperature over a period of 12 hours to generate the red, diamagnetic cobalt(I) product [PhBP$^{tBu}_2$(pz)]Co(CO)$_2$ (**5.9**) quantitatively (by NMR). Complex **5.9** is characterized by a singlet at 67 ppm in the ^{31}P NMR and two intense ν(CO) stretches at 1983 cm^{-1} and 1923 cm^{-1} in its infrared spectrum. The isocyanate byproduct (*p*-tolyl)N=C=O was identified by GC-MS to confirm that the imide functionality has been transferred to CO. While this reaction is relatively sluggish, it is considerably more facile than the analogous reaction between [PhBP$^{Ph}_3$]Co≡N(*p*-tolyl) and CO, which requires heating to 70 °C for 12 days.[5a]

The iron imide complexes show enhanced reactivity compared to the cobalt imide. For example, **5.5** reacts immediately with CO at room temperature to generate the bright red iron(I) dicarbonyl complex [PhBP$^{tBu}_2$(pz)]Fe(CO)$_2$ (**5.10**) with concomitant loss of the isocyanate AdN=C=O (confirmed by GC-MS). Interestingly, the solution IR spectrum (C_6H_6) of **5.10** features only one CO stretch at 1890 cm^{-1}. Although this initially suggested an iron(I) monocarbonyl complex, X-ray diffraction of single crystals of **5.10** revealed a pentacoordinate dicarbonyl complex (Figure 5.6A). Moreover, the solid state IR spectrum of **5.10** (KBr pellet) features two carbonyl stretches at 1953 cm^{-1} and 1887

cm^{-1}. Similarly, **5.6** reacts rapidly with CO to yield the green dicarbonyl product $[PhBP^{tBu}_2(pz^{Me2})]Fe(CO)_2$ (**5.11**). Complex **5.11** is also characterized by very different solution and solid state IR spectra with one CO stretch at 1883 cm^{-1} in solution and two CO stretches at 1950 cm^{-1} and 1880 cm^{-1} in the solid state. Although this behavior is not well understood, the differences in solution and solid state IR spectra could potentially be a result of hemi-lability of the pyrazolyl donor in solution.

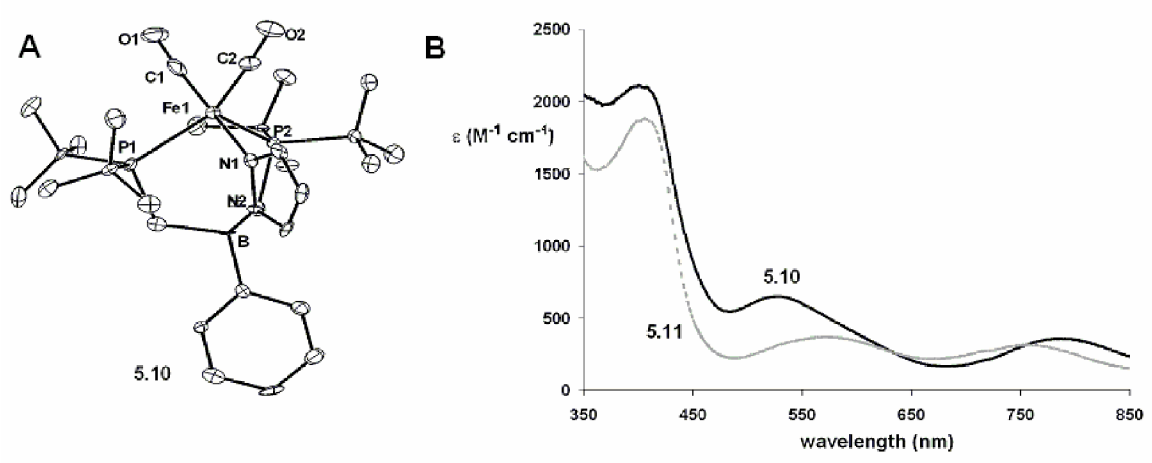

Figure 5.6 (A) Displacement ellipsoid representation (50 %) of **5.10**. Hydrogen atoms have been omitted for clarity. Relevant interatomic distances and angles: Fe1-C1, 1.743(6) Å; Fe1-C2, 1.764(6) Å; Fe1-P1, 2.397(2) Å; Fe1-P2, 2.380(2) Å; Fe1-N1, 1.996(4) Å; Fe1-C1-O1, 174.7(5)°; Fe1-C2-O2, 175.6(5)°. (B) Electronic absorption spectra of **5.10** (black) and **5.11** (gray).

While both **5.10** and **5.11** adopt low spin (S = ½) d^7 ground states based on solution magnetic data (**5.10**, μ_{eff} = 2.06 μ_B; **5.11**, μ_{eff} = 2.07 μ_B), their colors are remarkably different. This difference is apparent in the absorption spectra of the two complexes (Figure 5.6B). Although the feature at ~400 nm is roughly the same for the two complexes, the other two bands shift substantially. The higher energy feature is blue-shifted from 522 nm in **5.10** to 572 nm in **5.11**, while the lower energy feature is red-

shifted from 781 nm in **5.10** to 756 nm in **5.11**. These shifts can be attributed to the more electron-releasing (stronger field) $[PhBP^{tBu}_2(pz^{Me2})]^-$ ligand raising the energy of the anti-bonding d-orbitals.

5.2.4 Electrochemistry of $[PhBP^{tBu}_2(pz')]Fe(NR)$ Complexes (R = ^{t}Bu, Ad)

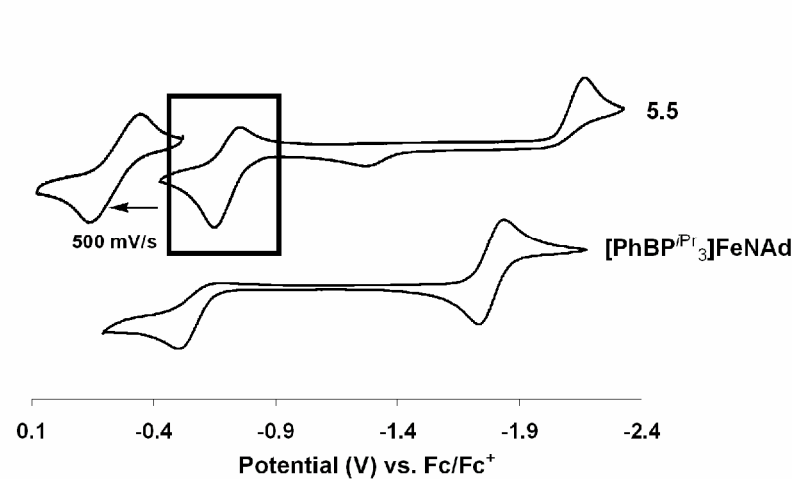

Figure 5.7 Cyclic voltammetry of **5.5** (0.40 M $[^nBu_4N][ClO_4]$ in THF, scan rate = 100 mV/s (full), 500 mV/s (inset)) and $[PhBP^{iPr}_3]Fe{\equiv}NAd$ (0.40 M $[^nBu_4N][PF_6]$ in THF).

The cyclic voltammetry of **5.5** reveals very different features from those observed for $[PhBP^R_3]Fe^{III}(NR)$ imides (Figure 5.7).[7d] For example, the cyclic voltammogram (CV) of previously reported $[PhBP^{iPr}_3]Fe{\equiv}NAd$[7b] features a fully reversible reductive wave at -1.79 V and an irreversible oxidative wave at ca. -0.45 V. This latter process presumably reflects a one-electron oxidation to an unstable Fe(IV) species. By contrast, complex **5.5** exhibits a completely *irreversible* reductive wave at -2.20 V, indicating that the Fe(II) imide anion is, in this case, unstable. The oxidative irreversible wave at -1.26 V appears only after scanning through the -2.20 V wave, indicating that it represents a byproduct of the one-electron reduction of **5.5**. More interesting, however, is the presence of a quasi-reversible feature at -0.72 V for **5.5** (100 mV/s; 295 K). This feature becomes

fully reversible at ambient temperature when the scan rate is increased to 500 mV/s. It represents an $Fe^{IV/III}$ redox couple and suggests that "$\{[PhBP^{tBu}_2(pz)]Fe^{IV}{\equiv}NAd\}^+$" might be modestly stable.

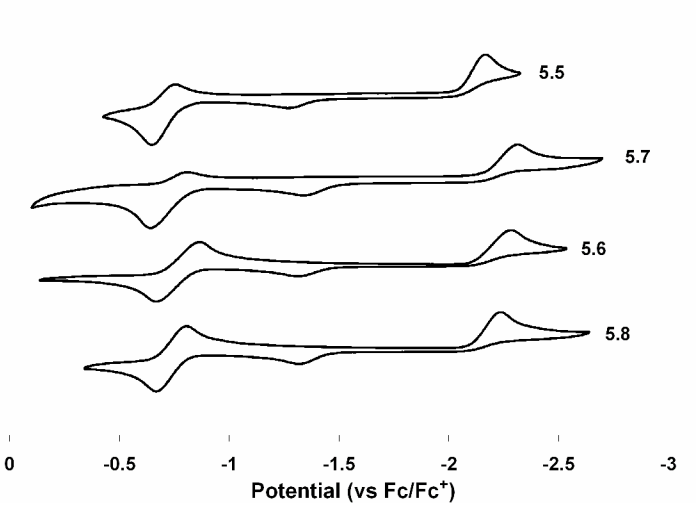

Figure 5.8 Comparison of the cyclic voltammograms of **5.5-5.8** (0.40 M $[^nBu_4N][ClO_4]$ in THF, scan rate = 100 mV/s).

Cyclic voltammetry of **5.6-5.8** was also measured to examine the effects that both the choice of borate ligand and the imide substituent have on the potential and reversibility of the resulting $Fe^{IV/III}$ couple (Figure 5.8). The CV of **5.7** reveals a quasi-reversible oxidation at a potential identical to that observed for **5.5** (-0.72 V), indicating that the choice of alkyl imide substituent does not have a substantial effect on the stability of the putative iron(IV) species or the $Fe^{IV/III}$ potential. However, upon replacing the $[PhBP^{tBu}_2(pz)]^-$ ligand with the more electron-releasing $[PhBP^{tBu}_2(pz^{Me2})]^-$ ligand in complexes **5.6** and **5.8**, the oxidative feature becomes fully reversible, even at slow scan rates (100 mV/s). In both **5.6** and **5.8**, the potential of the $Fe^{IV/III}$ process shifts modestly to more negative potential (-0.77 V for **5.6** and -0.74 V for **5.8**) as a result of the more electron-rich ligand. The reversibility of the oxidation event in the CV of these two

iron(III) imides indicates that an isolable "$\{[PhBP^{tBu}_2(pz^{Me2})]Fe^{IV}{\equiv}NR\}^+$" species may be more stable using the $[PhBP^{tBu}_2(pz^{Me2})]^-$ ligand system.

5.2.5 Synthesis and Characterization of $\{[PhBP^{tBu}_2(pz')]Fe^{IV}(NR)\}\{B(Ar_F)_4\}$ Complexes (R = ^{t}Bu, Ad)

In accord with the electrochemical data, **5.5** can be chemically oxidized with $[Fc][B(Ar_F)_4]$ (Ar_F = 3,5-$(CF_3)_2$-C_6H_3) at low temperature (-78 °C) in THF solution to generate a green, cationic species formulated as $\{[PhBP^{tBu}_2(pz)]Fe^{IV}{\equiv}NAd\}\{B(Ar_F)_4\}$ (**5.12**). A single set of paramagnetic resonances, distinct from the resonances observed for **5.5,** is observed for **5.12** in its ^{1}H NMR spectrum at -50 °C. Using an optical dip-probe assembly, the appearance of absorption bands at 450 nm, 580 nm, and 677 nm are readily observed at low temperature upon addition of the ferrocenium oxidant (Figure 5.10). It was also established that the addition of 1 equiv of $CoCp_2$ to **5.12** generated *in situ* in THF-d_8 solution regenerated **5.5** cleanly, confirming that the oxidation is reversible. The half-life of **5.12** is approximately 50 minutes at -40 °C in THF-d_8, and it must therefore be manipulated and stored at temperatures well below -40 °C. Solution magnetic data collected at low temperature (μ_{eff} = 3.1(2) μ_B in THF-d_8, 222 K; av of 4 runs) indicate two unpaired electrons (S = 1), consistent with the ground state electronic configuration $(d_{z^2})^2(d_{xy})^1(d_{x^2-y^2})^1(d_{xz})^0(d_{yz})^0$.

Owing to the thermal instability of **5.12**, obtaining a solid state structure proved to be a rather challenging experiment. Single green crystals could be obtained by storing a THF/petroleum ether solution at -78 ºC for several days. These crystals had to be manipulated rapidly since, even in crystalline form, **5.12** decomposes to an orange oil after ~2 minutes at room temperature. Rapid manipulation of a single crystal, followed by XRD

analysis confirmed its proposed connectivity (Figure 5.9), but a high quality data set could not be obtained. Nevertheless, the presence of a $\{B(Ar_F)_4\}$ anion in the solid state structure confirmed our assignment of **5.12** as a cationic species.

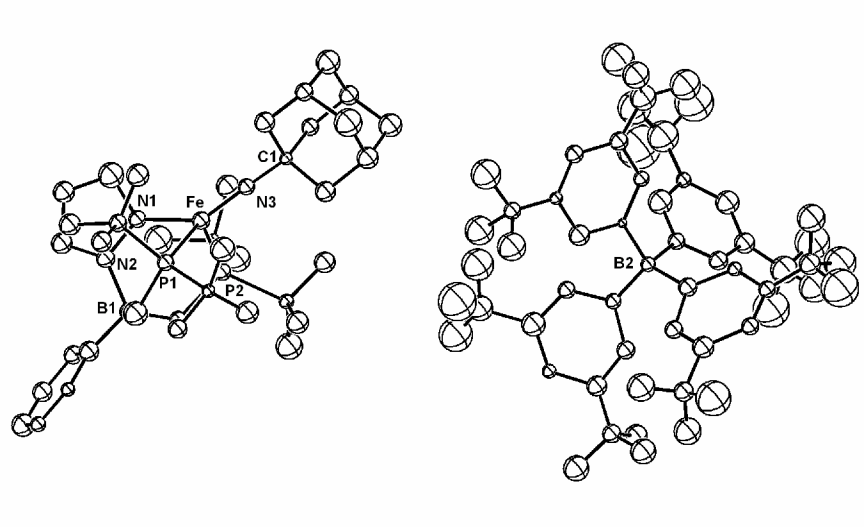

Figure 5.9 Isotropically refined solid-state structure of **5.12**. Three molecules of THF present in the crystal lattice and hydrogen atoms are omitted for clarity. Relevant interatomic distances and angles: Fe1-N3, 1.61(1) Å; Fe1-P1, 2.376(5) Å; Fe1-P2, 2.376(5) Å; Fe1-N1, 1.91(1) Å; Fe1-N3-C1, 174(1)°.

To obtain a better quality data set we set out to prepare an analogue of **5.12** of greater kinetic stability. Oxidation of **5.7** at low temperature also resulted in a rapid color change to dark green, presumably forming "$[PhBP^{tBu}_2(pz)]Fe{\equiv}N^tBu^+$," but this product appeared to be equally unstable at temperatures above -50 ºC so attempts were not made to isolate and characterize this product. Oxidation of **5.6** with $[Fc][B(Ar_F)_4]$, however, led to an imide cation, $\{[PhBP^{tBu}_2(pz^{Me2})]Fe^{IV}{\equiv}NAd\}\{B(Ar_F)_4\}$ (**5.13**), which exhibits far greater thermal stability than **5.12**. Complex **5.13** can even be isolated in pure form at ambient temperature (86.7% yield) and manipulated without appreciable degradation for several hours. Likewise, oxidation of **5.8** with ferrocenium leads to nearly quantitative formation of

the thermally stable imide cation $\{[PhBP^{tBu}_2(pz^{Me2})]Fe^{IV}{\equiv}N^tBu\}\{B(Ar_F)_4\}$ (**5.14**). As with **5.12**, solution magnetic data for both **5.13** and **5.14** confirm an $S = 1$ ground state (μ_{eff} = 3.02 μ_B (**5.13**), 3.13 μ_B (**5.14**)). Comparison of UV-visible absorption spectra for iron(IV) imide complexes **5.12-5.14** reveals relatively similar features, with an intense band around 450 nm and two weaker absorption bands around 580 nm and 700 nm (Figure 5.10).

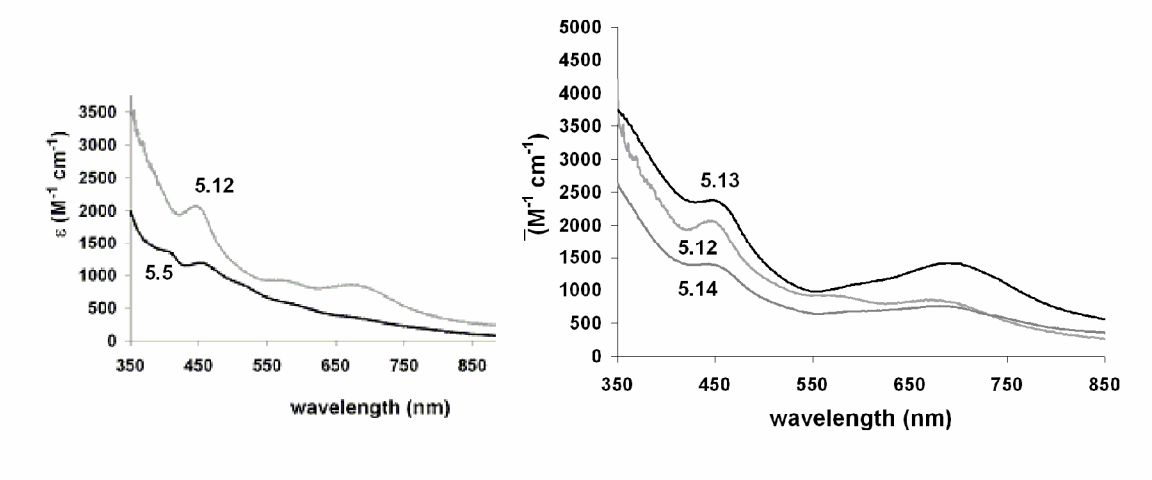

Figure 5.10 (left) UV-visible absorption data collected upon generation of **5.12** *in situ* at -78 °C using an optical dip probe assembly. (right) UV-visible absorption spectra for complexes **5.12-5.14** (C_6H_6, 298 K).

High quality X-ray data sets were obtained for **5.13** and **5.14,** and the anisotropically refined X-ray crystal structures are shown in Figure 5.11. The structures reveal the anticipated pseudo-tetrahedral iron cations and their tetra(aryl)borate counter-anions. The Fe-N3 bond distances (1.634(4) Å (**5.13**) and 1.641(3) Å (**5.14**)) are very similar to the parameters obtained for the corresponding iron(III) imides **5.5** and **5.6** as well as previously reported $[PhBP^R_3]Fe$ imides in the +3 and +2 oxidation states.[7] The Fe-N_{imide}-C bond angles (176.2(3)° (**5.13**) and 178.9(3)° (**5.14**)) are several degrees closer to 180° than in the corresponding angles in the iron(III) imides.

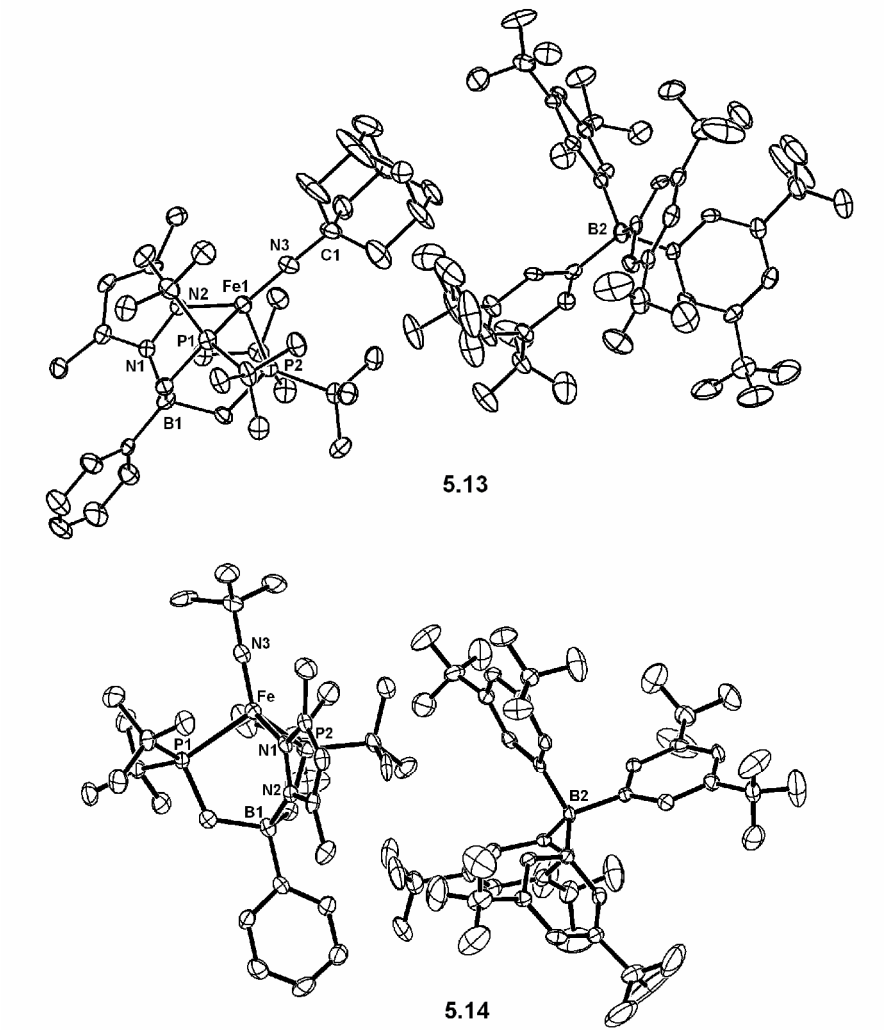

Figure 5.11 Displacement ellispoid representations (50%) of **5.13** and **5.14**. Two THF molecules in the crystal lattice of **5.13** and one THF molecule and one hydrocarbon molecule in the crystal lattice of **5.14** are not shown. The imide ^{t}Bu group in **5.14** was disordered over two positions–only one position is shown for the sake of clarity. Relevant interatomic distances and angles: **5.13**, Fe1-N3, 1.634(4) Å; Fe1-P1, 2.387(2) Å; Fe1-P2, 2.302(2) Å; Fe1-N2, 1.943(4) Å; Fe1-N3-C1, 176.2(3)°. **5.14**, Fe1-N3, 1.641(3) Å; Fe1-P1, 2.377(1) Å; Fe1-P2, 2.311(1) Å; Fe1-N1, 1.921(3) Å; Fe1-N3-C1, 178.9(3)°.

5.3 Discussion

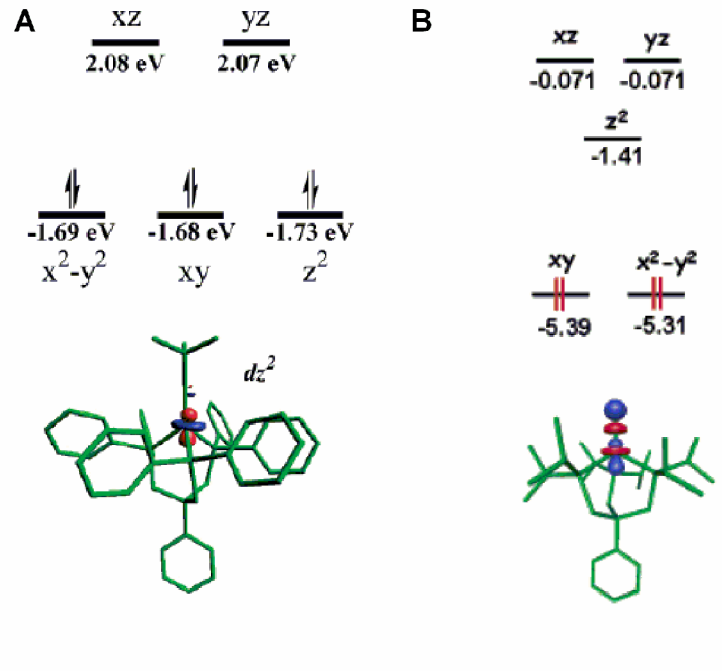

Figure **5.12** Theoretically predicted electronic structure and lobal representations of the d_{z^2} orbitals for $\{[PhBP^{Ph}_3]Fe^{II}{\equiv}N^tBu\}^-$ (A)[7d] and $[PhBP^{iPr}_3]Fe^{IV}{\equiv}N$ (B).[13]

The bonding in the iron(IV) imides "$[PhBP^{tBu}_2(pz')]Fe^{IV}{\equiv}NR^+$" **5.12-5.14** is interesting to consider in light of previously characeterized tris(phosphino)borate complexes featuring iron-nitrogen multiple bonds. The electronic structure and lobal representation of the frontier orbitals were previously calculated for the low spin iron(II) imide anion $\{[PhBP^{Ph}_3]Fe^{II}{\equiv}N^tBu\}^-$ (Figure 5.12A).[7d] These calculations revealed a two-over-three splitting diagram with the orbital of d_{z^2} parentage essentially degenerate with the non-bonding d_{xy} and $d_{x^2-y^2}$ orbitals, resulting in a diamagnetic d^6 ground state. It is thought that the d_{z^2} orbital is lowered in energy as a result of hybridization of the nitrogen p_z orbital towards the imide R group, resulting in an essentially non-bonding interaction with d_{z^2}. Theoretical calculations for the low spin iron(IV) nitride $[PhBP^{iPr}_3]Fe^{IV}{\equiv}N$, however, revealed that in this case d_{z^2} is much higher in energy than the non-bonding d_{xy} and $d_{x^2-y^2}$

orbitals (Figure 5.12B), leading to a diamagnetic d^4 ground state.[13] As seen in the lobal representation, rehybridization of the nitrogen p_z orbital results in a strongly anti-bonding interaction with the d_{z^2} orbital. A set of d orbitals similar to those calculated for $\{[PhBP^{Ph}_3]Fe^{II}{\equiv}N^tBu\}^-$ is consistent with the $S = 1$ ground state observed for the low spin d^4 iron(IV) imides reported in this chapter.

Table 5.1 Iron-nitrogen bond distances for imide and nitride complexes in the +2, +3, and +4 oxidation states.

Complex	**Fe-N distance (Å)**
$\{[PhBP^{Ph}_3]Fe^{II}{\equiv}NAd\}^-$	1.651(3)[7d]
$[PhBP^{Ph}_3]Fe^{III}{\equiv}NAd$	1.641(2)[7d]
$[PhBP^{iPr}_3]Fe^{III}{\equiv}NAd$	1.638(2)[7b]
$[PhBP^{tBu}_2(pz)]Fe^{III}{\equiv}NAd$, **5.5**	1.635(8); 1.626(9)[a]
$[PhBP^{tBu}_2(pz^{Me2})]Fe^{III}{\equiv}NAd$, **5.6**	1.652(7); 1.646(7)[a]
$\{[PhBP^{tBu}_2(pz)]Fe^{IV}{\equiv}NAd\}^+$, **5.12**	1.61(1)
$\{[PhBP^{tBu}_2(pz^{Me2})]Fe^{IV}{\equiv}NAd\}^+$, **5.13**	1.634(4)
$\{[PhBP^{tBu}_2(pz^{Me2})]Fe^{IV}{\equiv}N^tBu\}^+$, **5.14**	1.641(3)
$[PhBP^{iPr}_3]Fe^{IV}{\equiv}N$	1.54[b]

[a] Fe-N distances for both independent molecules in the asymmetric unit cell are reported.
[b] Distance obtained from preliminary EXAFS data.

Assuming that the two unpaired electrons of **5.12-5.14** reside in relatively nonbonding d-orbitals, as predicted from these simple MO considerations, the Fe-N bond should retain its triple bond character (i.e., $Fe^{IV}{\equiv}NR^+$) and the Fe-N distance is therefore not expected to change to a large extent upon oxidation. The Fe-N bond distances for representative iron(II), iron(III), and iron(IV) imide species reported previously or in this work are compiled in Table 5.1. An estimate of the Fe-N distance in the iron(IV) nitride species $[PhBP^{iPr}_3]Fe^{IV}{\equiv}N$ from preliminary EXAFS data is also presented for comparison.

Noteably, across all three iron oxidation states, the Fe-N distance in the imide complexes varies by only ~0.02 Å. This confirms that the Fe-N bond order is maintained and is consistent with the predicted MO diagram for these species. The iron(IV) nitride, on the other hand, features a significantly shorter Fe-N distance (~1.54 Å), consistent with a higher iron-nitrogen bond order.

The cause of the increased stability of the $Fe^{IV}{\equiv}NR$ linkage in the $[PhBP^{tBu}_2(pz')]Fe$ imides in comparison to their $[PhBP^{R}_3]Fe$ congeners is an interesting issue. Based on the increased stability of the iron(IV) complexes upon switching from $[PhBP^{tBu}_2(pz)]^-$ to the more electron-releasing $[PhBP^{tBu}_2(pz^{Me2})]^-$ ligand, the stability of the iron(IV) oxidation state in these complexes is attributed to a more electron-rich iron center. This is manifested in the cathodic shift in the $Fe^{IV/III}$ potential by comparison to previous $[PhBP^{R}_3]Fe$ imide systems. It is also possible that the lower symmetry of the $[PhBP^{tBu}_2(pz')]$ ligand (leading to C_s rather than C_{3v} symmetry) is more compatible with a d^4 triplet electronic configuration.

5.4 Conclusions

To conclude, we have begun to explore the utility of hybrid phosphine/pyrazole borate ligands $[PhBP^{tBu}_2(pz')]^-$ in the context of nitrene group transfer to cobalt and iron. Whereas cobalt imides in the +3 oxidation state and iron imides in the +3 and +2 oxidation states had been previously obtained using $[PhBP^{R}_3]Fe$ systems, we now find that imides in the +3 and +4 oxidation states are accessible using $[PhBP^{tBu}_2(pz')]Fe$ systems. It is remarkable that terminally bonded $L_3Fe{\equiv}NR$ species have now been characterized in three distinct oxidation states using phosphine-borate ligands given the paucity of such species more generally.

5.5 Experimental Section

5.5.1 General Considerations

General considerations are outlined in Section 2.4.1. UV/vis measurements of complex **5.12** were collected using a Cary 50 UV/vis spectrophotometer equipped with a dip probe fitted into an air-tight reaction vessel in a -78 °C bath.

5.5.2 EPR Measurements

EPR measurements were carried out as outlined in Section 3.4.4. EPR data was simulated using WinEPR.

5.5.3 Electrochemical Measurements

Electrochemical measurements were carried out as outlined in section 3.4.3 using 0.40 M [^{n}Bu$_4$N][ClO$_4$] as the supporting electrolyte.

5.5.4 Starting Materials and Reagents

. Complex **4.5**, **4.7,** and **4.8** were prepared as described in section 4.5.6. Fc[B(Ar$_F$)$_4$],[14] *p*-tolylazide,[15] and *tert*-butylazide[16] were prepared using literature methods. All other chemicals were purchased from commercial vendors and used without further purification.

5.5.5 Synthesis of Compounds

[PhBP$^{tBu}_2$(pz)]Co(PMe$_3$) (5.1). Solid **4.8** (0.0488 g, 0.0741 mmol) was combined with PMe$_3$ (15.3 μL, 0.148 mmol) in THF (3 mL). This solution was added to stirring Na/Hg (0.50 mol %, 0.38 g, 0.082 mmol) in THF (2 mL) and the mixture was stirred for 2 hours. The resulting cloudy blue-green solution was filtered through Celite to remove Na salts and amalgam, and the solvent was removed from the filtrate in vacuo. The remaining blue-green solids were extracted with diethyl ether (2 mL), filtered through Celite, and

cooled to -35°C, yielding analytically pure green crystals (0.0272 g, 60.4 %). ^{1}H NMR (300 MHz, C_6D_6): δ = 74.8 (br s), 49.7 (s), 44.7 (br s), 23.6 (s) 13.0 (s), 11.0 (br s), 9.4 (s), 7.6 (s), 2.0 (br s), -4.2 (br s). UV-vis (C_6H_6) λ_{max}, nm (ε): 700 (140). Evans method (C_6D_6): 3.04 μ_B. Anal. Calcd. for $C_{30}H_{57}BCoN_2P_3$: C, 59.22; H, 9.44; N, 4.60. Found: C, 59.20; H, 9.30; N, 4.55.

[PhBP$^{tBu}_2$(pz)]Fe(PMe$_3$) (5.2). Solid **4.6** (0.1890 g, 0.3350 mmol) was combined with PMe_3 (70 μL, 0.67 mmol) in THF (5 mL). This solution was added to stirring Na/Hg (0.50 %, 0.0085 g Na, 1.6 g Hg, 0.37 mmol) in THF, and the mixture was stirred for 1.5 hours. The resulting cloudy yellow-green solution was filtered through Celite to remove Na salts and amalgam, and the solvent was removed from the filtrate in vacuo. The remaining pale green solids were extracted with petroleum ether (5 mL), filtered through Celite, and cooled to -35°C, yielding analytically pure pale green crystals. (0.132 g, 65.2 %). ^{1}H NMR (300 MHz, C_6D_6): δ = 65.0 (br s), 32.2 (s), 11.7 (s), 8.9 (s), 8.2 (br s), 7.3 (s), -10.0 (br s). UV-vis (C_6H_6) λ_{max}, nm (ε): 807 (366). Evans method (C_6D_6, 295 K): 4.16 μ_B. Anal. Calcd. for $C_{30}H_{57}BFeN_2P_3$: C, 59.52; H, 9.49; N, 4.63. Found: C, 58.55; H, 8.94; N, 4.60.

[PhBP$^{tBu}_2$(pz^{Me2})]Fe(PMe$_3$) (5.3). Solid **4.7** (0.2289 g, 0.3864 mmol) was combined with PMe_3 (80 μL, 0.78 mmol) in THF (5 mL). This solution was added to stirring Na/Hg (0.50 %, 0.0098 g Na, 2.0 g Hg, 0.42 mmol) in THF, and the mixture was stirred for 1.5 hours. The resulting cloudy yellow-green solution was filtered through Celite to remove Na salts and amalgam, and the solvent was removed from the filtrate in vacuo. The remaining pale green solids were extracted with petroleum ether (10 mL), filtered through Celite, and cooled to -35°C, yielding analytically pure pale green crystals

(0.1807 g, 73.9%). Crystals suitable for X-ray diffraction were chosen from those grown in this manner. ^{1}H NMR (300 MHz, C_6D_6): δ = 67.8 (br s), 49.3 (s), 36.8 (s), 12.8 (s), 10.1 (br s, ^{t}Bu), 9.1 (s), 7.4 (s), 4.8 (br s, ^{t}Bu), 11.7 (s) -14.2 (br), -17.0 (br s). UV-vis (C_6H_6) λ_{max}, nm (ε, $M^{-1}cm^{-1}$): 1000 (340), 823 (680), 363 (1250). Evans method (C_6D_6, 295 K): 4.06 μ_B. Anal. Calcd. for $C_{32}H_{61}BFeN_2P_3$: C, 60.68; H, 9.71; N, 4.42. Found: C, 59.82; H, 9.33; N, 4.30.

[PhBP$^{tBu}_2$(pz)]Co≡N(*p*-tolyl) (5.4). Solid **5.1** (0.1482 g, 0.2438 mmol) was dissolved in C_6H_6 (5 mL). To this solution, *p*-tolylazide (54 μL, 0.4876 mmol) in C_6H_6 (2 mL) was added. The solution immediately became brown and was stirred for 30 minutes. Solvent was removed in vacuo, and the remaining red-brown solids were extracted with petroleum ether, filtered through Celite, and cooled to -35 °C to yield analytically pure red-brown crystals (0.0466 g, 30 %). ^{1}H NMR (300 MHz, C_6D_6): δ = 9.06 (d, 1H, $^{3}J_{H-H}$ = 1.5 Hz, pz-5), 8.14 (d, 2H, $^{3}J_{H-H}$ = 8.4 Hz, *o*-Ph), 7.87 (d, 2H, $^{3}J_{H-H}$ = 6.9 Hz, *o*-Tol), 7.46 (t, 2H, $^{3}J_{H-H}$ = 7.2 Hz, *m*-Ph), 7.33 (t, 1H, $^{3}J_{H-H}$ = 7.2 Hz, *p*-Ph), 7.25 (d, 1H, $^{3}J_{H-H}$ = 2.1 Hz, pz-3), 6.39 (d, 2H, $^{3}J_{H-H}$ = 7.8 Hz, *m*-Tol) 6.15 (t, 1H, $^{3}J_{H-H}$ = 2.1 Hz, pz-4), 1.43 (d, 18H, $^{3}J_{H-P}$ = 12 Hz. ^{t}Bu), 1.12 (br s, 4H, CH_2), 0.90 (d, 18H, $^{3}J_{H-P}$ = 12 Hz, ^{t}Bu). ^{31}P NMR (121.5 MHz, C_6D_6): δ = 90.2 (br s). $^{13}C\{^{1}H\}$ NMR (75.5 MHz, C_6D_6): δ = 154 (br, *ipso*-BPh), 152.3 (s, *ipso*-N), 137.5 (s, pz-5), 133.9 (s, *o*-BPh), 132.3 (s, pz-3), 130.3 (s, *m*-Ph), 127.5 (s, *m*-Ntol) 127.2 (s, *p*-Ntol), 126.3 (s, *p*-Ph), 110.8 (m, *o*-Ntol), 109.3 (s, pz-4), 34.2 (m, $C(CH_3)_3$), 31.4 (d, $C(CH_3)_3$), 30.2 (d, $C(CH_3)_3$), 17.6 (m, CH_2). UV-vis (C_6H_6) λ_{max}, nm (ε): 431 (560), 638 (190), 793 (130). Anal. Calcd. for $C_{34}H_{55}BCoN_3P_2$: C, 64.06; H, 8.70; N, 6.59. Found: C, 63.62; H, 8.56; N, 6.64.

[PhBP$^{tBu}_2$(pz)]Fe≡NAd (5.5). Solid **5.2** (0.0384 g, 0.0635 mmol) was dissolved in C_6H_6 (5 mL). To this solution, adamantyl azide (0.0226 g, 0.127 mmol) in C_6H_6 (2 mL) was added. The solution immediately became dark purple and was stirred for 30 minutes. Solvent was removed in vacuo, and the remaining purple solids were washed with petroleum ether to remove the Me_3P=NAd byproduct. The remaining solids were dried in vacuo to yield spectroscopically pure product (0.0290 g, 67.3%). Crystals suitable for X-ray diffraction were grown via vapor diffusion of petroleum ether into a concentrated C_6H_6 solution. ^{1}H NMR (300 MHz, C_6D_6): δ = 111.1, 31.3, 25.5, 20.5, 12.1, 11.5, 10.4, 7.3, 4.5, 4.0, 0.9, -7.4, -9.7. UV-vis (C_6H_6) λ_{max}, nm (ε, $M^{-1}cm^{-1}$): 459 (1200), 510 (820), 645 (sh). Evans method (C_6D_6, 295 K): 1.95 μ_B. Anal. Calcd. for $C_{37}H_{63}BFeN_3P_2$: C, 65.49; H, 9.36; N, 6.19. Found: C, 65.10; H, 9.02; N, 6.05.

[PhBP$^{tBu}_2$(pz^{Me2})]Fe≡NAd (5.6). Solid **5.3** (0.0801 g, 0.1266 mmol) was dissolved in C_6H_6 (3 mL). To this solution, adamantyl azide (0.0450 g, 0.253 mmol) in C_6H_6 (2 mL) was added. The solution immediately became dark purple and was stirred for 30 minutes. Solvent was removed in vacuo, and the remaining purple solids were washed with petroleum ether to remove the Me_3P=NAd byproduct. The remaining solids were dried in vacuo to yield spectroscopically pure product (0.0758 g, 84.8%). Crystals suitable for X-ray diffraction were grown via vapor diffusion of petroleum ether into a concentrated C_6H_6 solution. ^{1}H NMR (300 MHz, C_6D_6): δ = 139.9 (br s), 58.9 (s), 24.5 (s), 22.7 (s), 19.1 (s), 11.2 (s), 11.1 (d), 9.4 (d), 8.4 (s), 6.3 (d), -4.2 (br s), -4.7 (s), -8.3 (s). UV-vis (C_6H_6) λ_{max}, nm (ε, $M^{-1}cm^{-1}$): 460 (1100), 503 (1100). Evans method (C_6D_6, 295 K): 1.98 μ_B. Anal. Calcd. for $C_{39}H_{67}BFeN_3P_2$: C, 66.29; H, 9.56; N, 5.95. Found: C, 66.23; H, 9.32; N, 5.85.

[PhBP$^{tBu}_2$(pz)]Fe≡N^{t}Bu (5.7). Solid **5.2** (0.0754 g, 0.125 mmol) was dissolved in THF (3 mL) and cooled to -35 °C. To this was added neat ^{t}BuN$_3$ (0.0247 g, 0.250 mmol). The solution immediately became brown, and bubbles of N_2 were evolved. After stirring at -35 °C for 30 minutes, the volatiles were removed from the solution in vacuo while cold. The remaining solids were extracted with cold petroleum ether (2 mL), filtered through Celite, and recrystallized at -35 °C, resulting in spectroscopically pure product as red-brown crystals (0.0450 g, 63.2%). ^{1}H NMR (300 MHz, C_6D_6): δ = 94.9, 24.3, 23.8, 20.3, 12.1, 11.4, 2.8, -4.3, -7.5, -9.9, -60.9. UV-vis (C_6H_6) λ_{max}, nm (ε, M^{-1}cm^{-1}): 350 (800), 449 (320), 508 (250). 598 (sh). Evans method (C_6D_6, 295 K): 1.71 μ_B.

[PhBP$^{tBu}_2$(pz^{Me2})]Fe≡N^{t}Bu (5.8). Solid **5.3** (0.0368 g, 0.0582 mmol) was dissolved in C_6H_6 (3 mL). To this was added neat ^{t}BuN$_3$ (0.0115 g, 0.116 mmol). The solution immediately became brown, and bubbles of N_2 were evolved. After stirring for 15 minutes, the solution was frozen, and volatiles were removed in vacuo while cold. The remaining solids were extracted with petroleum ether (4 mL), filtered through Celite, and recrystallized at -35 °C, resulting in spectroscopically pure product as red-brown crystals (0.0328 g, 89.8%). ^{1}H NMR (300 MHz, C_6D_6): δ = 126.9, 59.7, 23.5, 22.4, 19.1, 11.3, 11.1, -3.5, -4.9, -8.5. UV-vis (C_6H_6) λ_{max}, nm (ε, M^{-1}cm^{-1}): 411 (sh), 456 (810), 506 (730), 681 (sh). Evans method (C_6D_6, 295 K): 2.08 μ_B.

[PhBP$^{tBu}_2$(pz)]Co(CO)$_2$ (5.9). Solid **5.4** (0.0606 g, 0.104 mmol) was dissolved in C_6H_6 (10 mL) and transferred to a sealed Schlenk tube. The solution was frozen, and the headspace was evacuated. The solution was allowed to thaw, and the headspace of the tube was refilled with CO (g). The resulting mixture was allowed to stir for 12 hours, at which time the solution had become blood red in color. The solvent was removed in

vacuo. The remaining solids were extracted with petroleum ether (15 mL), filtered through Celite, and then cooled to -35 °C for 12 hours, resulting in analytically pure red crystals (0.0361 g, 59.4%). ^{1}H NMR (300 MHz, C_6D_6): δ = 7.99 (d, 2H, $^{3}J_{H\text{-}H}$ = 7.2 Hz, *o*-Ph), 7.81 (m, 1H, pz-5), 7.50 (t, 2H, $^{3}J_{H\text{-}H}$ = 7.2 Hz, *m*-Ph), 7.35 (t, 1H, $^{3}J_{H\text{-}H}$ = 6.9 Hz, *p*-Ph), 7.26 (d, 1H, $^{3}J_{H\text{-}H}$ = 2.4 Hz, pz-3), 5.66 (m, 1H, pz-4), 1.57 (br m, 4H, CH_2),1.23 (m, 18H, ^{t}Bu), 0.77 (m, 18H, ^{t}Bu). ^{31}P NMR (121.5 MHz, C_6D_6): δ = 67.4 (s). ^{13}C{^{1}H} NMR (75.5 MHz, C_6D_6): δ = 210 (CO), 147.6 (pz), 138.8 (Ph), 137.0 (Ph), 133.9 (pz), 126.5 (Ph), 108.6 (pz), 36.6 ($C(CH_3)_3$), 31.2 ($C(CH_3)_3$), 16.0 (br CH_2) . UV-vis (C_6H_6) λ_{max}, nm (ε): 350 (2900), 473 (2900), 946 (390), 1012 (400). IR (C_6H_6, KBr, cm^{-1}): 1983, 1923. Anal. Calcd. for $C_{29}H_{48}BCoN_2O_2P_2$: C, 59.20; H, 8.22; N, 4.76. Found: C, 59.14; H, 8.34; N, 4.72.

[PhBP$^{t\text{Bu}}_2$(pz)]Fe(CO)$_2$ (5.10). Solid **5.5** (0.0372 g, 0.0548 mmol) was dissolved in C_6H_6 (10 mL) and transferred to a Schlenk tube sealed with a Teflon stopcock. The solution was frozen, and the headspace was evacuated. Upon thawing, the headspace was refilled with CO(g). The resulting bright-red solution was stirred for one hour at room temperature. GC/MS of the crude solution revealed a single organic byproduct–(1-Ad)N=C=O (m/z = 177). The volatiles were removed in vacuo, and the remaining red solids were extracted with petroleum ether (8 mL) and filtered through Celite. This solution was cooled to -35 °C to afford analytically pure product as red crystals (0.0206 g, 64.1%). ^{1}H NMR (300 MHz, C_6D_6): δ = 9.5, 8.1, 7.5, 4.5 (br), 3.7 (br), 3.6, 3.4 (br), 2.7 (br), -11 (br). IR (C_6H_6 solution, cm^{-1}): 1890. IR (KBr pellet, cm^{-1}): 1953, 1887. UV-vis (C_6H_6) λ_{max}, nm (ε, $M^{-1}cm^{-1}$): 396 (2100), 522 (650), 781 (360). Evans method (C_6D_6,

295 K): 2.06 μ_B. Anal. Calcd. for $C_{29}H_{48}BFeN_2O_2P_2$: C, 59.51; H, 8.27; N, 4.79. Found: C, 59.46; H, 7.99; N, 4.78.

[PhBP$^{tBu}_2$(pz^{Me2})]Fe(CO)$_2$ (5.11). Solid **5.6** (0.0368 g, 0.0521 mmol) was dissolved in C_6H_6 (10 mL) and transferred to a Schlenk tube sealed with a Teflon stopcock. The solution was frozen, and the headspace was evacuated. Upon thawing, the headspace was refilled with CO(g). The resulting green solution was stirred for one hour at room temperature. GC/MS of the crude solution revealed a single organic byproduct–(1-Ad)N=C=O (m/z = 177). The volatiles were removed in vacuo, and the remaining green solids were extracted with petroleum ether (15 mL) and filtered through Celite. This solution was concentrated and cooled to -35 °C to afford analytically pure product as green crystals (0.0110 g, 34.3%). ^{1}H NMR (300 MHz, C_6D_6): δ = 9.5 (br), 8.1, 7.9, 7.3, 6.5 (br), 4.0 (br), 1.8, -3.1. IR (C_6H_6 solution, cm^{-1}): 1883. IR (KBr pellet, cm^{-1}): 1950, 1880. UV-vis (C_6H_6) λ_{max}, nm (ε, M^{-1}cm^{-1}): 322 (1900), 404 (1900), 572 (370), 756 (310), 1050 (200). Evans method (C_6D_6, 295 K): 2.07 μ_B. Anal. Calcd. for $C_{31}H_{52}BFeN_2O_2P_2$: C, 60.70; H, 8.55; N, 4.57. Found: C, 60.97; H, 8.48; N, 4.46.

[[PhBP$^{tBu}_2$(pz)]Fe≡N(1-Ad)][B(Ar$_F$)$_4$] (5.12). Solid **5.5** (0.0190 g, 0.0280 mmol) was dissolved in THF (2 mL) and cooled to -78 °C. To this was added a pre-cooled (-78 °C) solution of Fc[B(Ar$_F$)$_4$] (0.0294 g, 0.0280 mmol) in THF (0.5 mL). The solution immediately became intense green in color. Mixture was warmed to -50 °C and stirred for 30 minutes before collecting data. Crystals suitable for X-ray diffraction were grown by layering petroleum ether over a concentrated THF solution and cooling to -80 °C. Single crystalline samples were observed to decompose within 60 seconds at ambient temperature. Thus, crystals were kept at -80 °C until immediately before a single crystal

was chosen, mounted on a goniometer, and rapidly transferred to the cold nitrogen stream on the X-ray diffractometer. ^{1}H NMR (300 MHz, THF-d_8, 222 K): δ = 45 (br), 22.8, 12.3, 11.1, 10.6, 7.6 (br), 7.3, 6.8 (BAr_4), 6.6 (BAr_4), -14.0, -15.4, -24.6, -60.7. UV-vis (THF) λ_{max}, nm (ε, $M^{-1}cm^{-1}$): 677 (850), 580 (920). Evans method (THF-d_8, 222 K): 3.1 μ_B (av of four values).

[[PhBP$^{tBu}_2$(pz^{Me})]Fe≡N(1-Ad)][B(Ar$_F$)$_4$] (5.13). Solid **5.6** (0.0237 g, 0.0336 mmol) was dissolved in THF (2 mL) and cooled to -35 °C. To this was added a pre-cooled (-35 °C) solution of Fc[$B(Ar_F)_4$] (0.0352 g, 0.0336 mmol) in THF (0.5 mL). The solution immediately became intense green in color. Mixture was stirred for 30 minutes at -35 °C and then warmed to room temperature. Volatiles were removed from the resulting green solution in vacuo. The remaining solids were washed with petroleum ether (2 x 5 mL) and dried in vacuo to yield analytically pure product as a dark green powder (0.0462 g, 87.6%). Crystals suitable for X-ray diffraction were grown by layering petroleum ether over a concentrated THF solution and cooling to -35 °C. ^{1}H NMR (300 MHz, THF-d_8): δ = 130 (br), 40 (br), 35.6 (br), 22.7 (br), 18.7, 11.4, 9.6, 8.0, 7.8 (BAr_4), 7.5 (BAr_4), 6.2, -10.0, -17.7 (br), -20.0. UV-vis (THF) λ_{max}, nm (ε, $M^{-1}cm^{-1}$): 689 (1400), 604(sh), 443 (2400). Evans method (THF-d_8): 3.02 μ_B.

[[PhBP$^{tBu}_2$(pz^{Me})]Fe≡N(^{t}Bu)][B(Ar$_F$)$_4$] (5.14). Solid **5.8** (0.0169 g, 0.0269 mmol) was dissolved in THF (1 mL) and cooled to -35 °C. To this was added a pre-cooled (-35 °C) solution of Fc[$B(Ar_F)_4$] (0.0282 g, 0.0269 mmol) in THF (1 mL). The solution immediately became intense green in color. Mixture was stirred for 30 minutes at -35 °C and then warmed to room temperature. Volatiles were removed from the resulting green solution in vacuo. The remaining solids were washed with petroleum ether (2 x 5 mL)

and dried in vacuo to yield analytically pure product as a dark green powder (0.0276 g, 68.8%). ^{1}H NMR (300 MHz, THF-d_8): δ = 130 (br), 42 (br), 23.5 (br), 18.7, 11.3, 9.5, 7.8 (BAr_4), 7.5 (BAr_4), 0.8 (br), -10.0, -18.4. UV-vis (THF) λ_{max}, nm (ε, $M^{-1}cm^{-1}$): 446 (2200), 596 (sh), 682 (1200). Evans method (THF-d_8): 3.13 μ_B.

5.5.6 X-ray Experimental Data

Crystallographic procedures are outlined in Section 2.4.6. Crystallographic data are summarized in Table 5.2. The structure of **5.12** was refined isotropically, since satisfactory anisotropic refinement could not be achieved. The structure of **5.12** has three molecules of THF in each unit cell of the crystal lattice. The structure of **5.13** contains two molecules of THF in each unit cell of the crystal lattice. The structure of **5.14** contains a THF molecule and half a hydrocarbon molecule, best modeled as butane, per unit cell.

Table 5.2. Crystallographic data for [PhBP$^{t\text{Bu}}_2$(pz$^{\text{Me2}}$)]Fe(PMe$_3$), **5.3**; [PhBP$^{t\text{Bu}}_2$(pz)]Co≡N(*p*-tolyl), **5.4**; [PhBP$^{t\text{Bu}}_2$(pz)]Fe≡NAd, **5.5**; [PhBP$^{t\text{Bu}}_2$(pz$^{\text{Me2}}$)]Fe≡NAd, **5.6**; [PhBP$^{t\text{Bu}}_2$(pz)]Fe(CO)$_2$, **5.10**; [[PhBP$^{t\text{Bu}}_2$(pz)]Fe≡NAd][B(Ar$_F$)$_4$], **5.12**·3THF; [[PhBP$^{t\text{Bu}}_2$(pz$^{\text{Me}}$)]Fe≡NAd][B(Ar$_F$)$_4$], **5.13**·2THF; and [[PhBP$^{t\text{Bu}}_2$(pz$^{\text{Me}}$)]Fe≡N^{t}Bu][B(Ar$_F$)$_4$], **5.14**·THF,0.5C$_4$H$_{10}$.

	5.3	**5.4**	**5.5**
Chemical formula	$C_{32}H_{61}BFeN_2P_3$	$C_{34}H_{55}BCoN_3P_2$	$C_{37}H_{61}BFeN_3P_2$
Fw	633.40	637.49	676.49
T (°C)	-173	-173	-173
λ (Å)	0.71073	0.71073	0.71073
a (Å)	18.81(2)	10.0705(13)	10.8828(9)
b (Å)	18.822(20)	10.4533(14)	20.2565(17)
c (Å)	19.94(2)	16.508(2)	33.573(3)
α (°)	90	88.648(2)	90
β (°)	90	74.722(2)	94.412(2)
γ (°)	90	77.850(2)	90
V (Å^3)	7062(13)	1637.9(4)	7379.1(11)
space group	Pbca	P-1	C2/c
Z	10	2	8
D_{calc} (g/cm^3)	1.489	1.293	1.218
μ(cm^{-1})	7.32	6.50	5.25
R1, wR2[a] ($I > 2\sigma(I)$)	0.0497, 0.0736	0.0508, 0.0893	0.0893, 0.1237

[a] $R1 = \Sigma||F_o| - |F_c||/\Sigma|F_o|$, $wR2 = \{\Sigma[w(F_o^2 - F_c^2)^2]/\Sigma[w(F_o^2)^2]\}^{1/2}$

Table 5.2 (cont'd)

	5.6	**5.10**	**5.12**·3THF
chemical formula	$C_{39}H_{65}BFeN_3P_2$	$C_{29}H_{48}BFeN_2O_2P_2$	$C_{81}H_{121}BF_{24}FeN_3O_3P_2$
Fw	704.54	585.29	1769.41
T (°C)	-173	-173	-173
λ (Å)	0.71073	0.71073	0.71073
a (Å)	10.886(4)	18.581(5)	12.2246(19)
b (Å)	17.390(5)	10.259(3)	27.556(4)
c (Å)	21.104(6)	16.077(4)	12.862(2)
α (°)	83.777(11	90	90
β (°)	75.874(7)	97.040(7)	102.822(4)
γ (°)	85.190(8)	90	90
V (Å^3)	3845(2)	3041.5(15)	4224.7(11)
space group	P-1	P2(1)/c	P2(1)
Z	4	4	2
D_{calc} (g/cm^3)	1.217	1.278	1.391
μ(cm^{-1})	5.06	6.29	3.18
R1, wR2[a] ($I > 2\sigma(I)$)	0.0885, 0.1504	0.0654, 0.0973	0.1237, 0.1716

[a] $R1 = \Sigma||F_o| - |F_c||/\Sigma|F_o|$, $wR2 = \{\Sigma[w(F_o^2 - F_c^2)^2]/\Sigma[w(F_o^2)^2]\}^{1/2}$

Table 5.2 (cont'd)

	5.13·2THF	**5.14**·2THF,0.5C_4H_{10}
chemical formula	$C_{79}H_{93}B_2F_{24}FeN_3O_2P_2$	$C_{71}H_{74}BF_{24}FeN_3OP_2$
Fw	1711.97	1569.93
T (°C)	-173	-173
λ (Å)	0.71073	0.71073
a (Å)	19.438(17)	12.865(8)
b (Å)	18.86(2)	29.50(2)
c (Å)	22.418(17)	19.582(9)
α (°)	90	90
β (°)	99.66(5)	90.857(14)
γ (°)	90	90
V (Å^3)	8104(14)	7430(7)
space group	P2(1)/c	P2(1)/n
Z	6	6
D_{calc} (g/cm^3)	2.105	2.105
μ(cm^{-1})	4.92	5.25
R1, wR2[a] ($I > 2\sigma(I)$)	0.0607, 0.0871	0.0650, 0.1011

[a] $R1 = \Sigma||F_o| - |F_c||/\Sigma|F_o|$, $wR2 = \{\Sigma[w(F_o^2 - F_c^2)^2]/\Sigma[w(F_o^2)^2]\}^{1/2}$

References Cited

[1] (a) Einsle, O.; Tezcan, A.; Andrade, S. L. A.; Schmid, B.; Yoshida, M.; Howard, J. B.; Rees, D. C. *Science* **2002**, *297*, 1696. (b) Rees, D. C. *Annu. Rev. Biochem.* **2002**, *71*, 221. (c) Peters, J. W.; Lanzilotta, W. N.; Lennon, B. J.; Seefeldt, L. C. *Science* **1998**, *282*, 1853.

[2] (a) Kisko, J. L.; Hascall, T.; Parkin, G. *J. Am. Chem. Soc.* **1998**, *120*, 10561. (b) Smith, J. M.; Sadique, A. R.; Cundari, T. R.; Rodgers, K. R.; Lukat-Rodgers, G.; Lachicotte, R. J.; Flaschenriem, C. J.; Vela, J.; Holland, P. L. *J. Am. Chem. Soc.* **2006**, *128*, 756. (c)

Smith, J. M.; Lachicotte, R. J.; Pittard, K. A.; Cundari, T. R.; Lukat-Rodgers, G.; Rodgers, K. R.; Holland, P. L. *J. Am. Chen. Soc.* **2001**, *123*, 9222. (d) Stoian, S. A.; Yu, Y.; Smith, J. M.; Holland, P. L.; Bominaar, E. L.; Münck, E. *Inorg. Chem.* **2005**, *44*, 4915.

[3] (a) Li, Z.; Conser, K. R.; Jacobsen, E, N. *J. Am. Chem. Soc.* **1993**, *115*, 5326. (b)Evans, D. A.; Faul, M. M.; Bilodeau, M. T. *J. Am. Chem. Soc.* **1994**, *116*, 2742. (c) DuBois, J.; Tomooka, C. S.; Hong, J.; Carreira, E. M. *Acc. Chem. Res.* **1997**, *30*, 364. (d) Wigley, D. E. In *Progress in Inorganic Chemistry*; 1994; Vol. 42, pp 239-482. (e) Eikey, R. A.; Abu-Omar, M. M. *Coord. Chem. Rev.* **2003**, *243*, 83.

[4] For recent examples see: (a) Mindiola, D. J.; Hillhouse, G. L. *J. Am. Chem. Soc.* **2001**, *123*, 4623. (b) Jenkins, D. M.; Betley, T. A.; Peters, J. C. *J. Am. Chem. Soc.* **2002,** *124*, 5272. (c) Eikey, R. A.; Khan, S. I.; Abu-Omar, M. M. *Angew. Chem. Int. Ed.* **2002**, *41*, 3592. (d) Dai, X.; Kapoor, P.; Warren, T. H. *J. Am. Chem. Soc.* **2004**, *126*, 4798. (e) Hu, X.; Meyer, K. *J. Am. Chem. Soc.* **2004**, *126*, 16322.

[5] (a) Jenkins, D. M.; Betley, T. A.; Peters, J. C. *J. Am. Chem. Soc.* **2002,** *124*, 5272. (b) Hu, X.; Meyer, K. *J. Am. Chem. Soc.* **2004**, *126,* 16322. (c) Thyagarajan, S.; Shay, D. T.; Incarvito, D.; Rheingold, A. L.; Theopold, K. H. *J. Am. Chem. Soc.* **2003**, *125*, 4440. (d) Shay, D. T.; Yap, G. P. A.; Zakharov, L. N.; Rheingold, A. L.; Theopold, K. H. *Angew. Chem. Int. Ed.* **2005**, *44*, 1508. (e) Dai, X.; Kapoor, P.; Warren, T. H. *J. Am. Chem. Soc.* **2004**, *126*, 4798.

[6] Bart, S. C.; Lobkovsky, E.; Bill, E.; Chirik, P. J. *J. Am. Chem. Soc.* **2006**, *128*, 5302.

[7] (a) Brown, S. D.; Betley, T. A.; Peters, J. C. *J. Am. Chem. Soc.* **2003**, *125*, 322. (b) Betley, T. A.; Peters, J. C. *J. Am. Chem. Soc.* **2003**, *125*, 10782. (c) Brown, S. D.; Peters,

J. C. *J. Am. Chem. Soc.* **2004**, *126*, 4538. (d) Brown, S. D.; Peters, J. C. *J. Am. Chem. Soc.* **2005**, *127*, 1913.

[8] Fe(IV) imides have been implicated as intermediates in nitrene transfer reactions: (a) Lucas, R. L.; Powell, D. R.; Borovik, A. S. *J. Am. Chem. Soc.* **2005**, *127*, 11596. (b) Jensen, M. P.; Mehn, M. P.; Que, L., Jr. *Angew. Chem. Int. Ed.* **2003**, *42*, 4357.

[9] For recent non-heme iron examples see: (a) Rohde, J.-U.; In, J.-H.; Lim, M. H.; Brennessel, W. W.; Bukowski, M. R.; Stubna, A.; Münck, E.; Nam, W.; Que, L., Jr. *Science* **2003**, *299*, 1037. (b) Klinker, E. J.; Kaiser, J.; Brennessel, W. W.; Woodrum, N. L.; Cramer, C. J.; Que, L., Jr. *Angew. Chem. Int. Ed.* **2005**, *44*, 3690. (c) Bukowski, M. R.; Koehntop, K. D.; Stubna, A.; Bominaar, E. L.; Halfen, J. A.; Münck, E.; Nam, W.; Que, L., Jr. *Science* **2005**, *310*, 1000. (d) Grapperhaus, C. A.; Mienert, B.; Bill, E.; Weyhermuller, T.; Wieghardt, K. *Inorg. Chem*. **2000**, *39*, 5306.

[10] Verma, A. K.; Nazif, T. N.; Achim, C.; Lee, S. C. *J. Am. Chem. Soc.* **2000**, *122*, 11013.

[11] (a) Sur, S. K. *J. Magn. Reson.* **1989**, *82*, 169. (b) Evans, D. F. *J. Chem. Soc.* **1959**, 2003.

[12] Mindiola, D. J.; Hillhouse, G. L. *Chem. Commun.* **2002**, 1840.

[13] Betley, T. A.; Peters, J. C. *J. Am. Chem. Soc.* **2004**, *126*, 6252.

[14] (a) Calderazzo, F.; Pampaloni, G.; Rocchi, L.; Englert, U. *Organometallics* **1994**, *13*, 2592. (b) Chávez, I.; Alvarez-Carena, A.; Molins, E.; Roig, A.; Maniukiewicz, W.; Arancibia, A.; Brand, H.; Manríquez, J. M. *J. Organomet. Chem.* **2000**, *601*, 126.

[15] Smith, P. A. S.; Brown, B. B. *J. Am. Chem. Soc.* **1951,** *73,* 2438.

[16] Bottaro, J. C.; Penwell, P. E.; Schmitt, R. J. *Syn. Comm.* **1997,** *27,* 1465.

Appendix A: Comparative Studies with Zwitterionic Platinum(II) Bis(pyrazolyl)borate and 2,2'-Bipyridylborate Complexes

The text in this chapter is reproduced in part with permission from:

Thomas, C. M.; Peters, J. C. *Organometallics* **2005,** *24,* 5858.

A.1 Introduction

Motivated by the versatility of organometallic cations for processes such as polymerization, C-H bond activation, and C-E bond-forming reactions (E = H, C, Si), our group has studied various neutral, formally zwitterionic complexes to examine the effect of electrophilicity on the reactivity of late transition metal centers.[1,2] These zwitterions utilize ligands in which a borate moiety is incorporated within the ligand framework but is partially insulated from the coordinated metal center. Our goal has been to study the effect of the anionic borate unit on the reactivity of these complexes by comparison to cationic complexes supported by structurally similar neutral ligands. Accordingly, previous studies in our group have focused on monoanionic bidentate ligands such as bis(phosphino)borates and bis(amino)borates, in which a borate moiety is linked to tertiary phosphine or amine donors via a methylene linker.[3] We have found that zwitterionic complexes often display reactivity quite similar to their cationic congeners, but important reactivity and mechanistic differences can be prevalent. For example, bis(phosphino)borate rhodium catalysts show tolerance to relatively polar donor solvents such as acetonitrile, in contrast to their cationic bis(phosphine) relatives.[3e] Also, comparative structural, electronic, and mechanistic studies of zwitterionic and cationic bis(phosphine) platinum(II) complexes suggest that more electron-rich, platinum(II) zwitterions are equally, if not more, competent than their isostructural cations with respect to their propensities for benzene C-H activation. Subtle mechanistic differences distinguish the benzene solution chemistry of the two systems, leading to different overall reaction rates.[3c]

Square planar platinum(II) centers supported by nitrogen donor ligands have been more thoroughly examined with respect to alkane activation reactions than phosphine-supported systems.[4,5] One case pertinent to the present paper concerns various studies of the C-H activation reactivity of platinum tris(pyrazolyl)borate (Tp) complexes.[6] In this regard it is noteworthy that little attention has yet focused on bis(pyrazolyl)borate group 10 metal complexes, despite the fact that various platinum studies exploiting Tp ligands feature κ^2 Tp precursors and/or intermediates. The limited reports of platinum bis(pyrazolyl)borate systems have not described their utility for C-H activation chemistry.[7]

In addition to Tp platinum complexes, a range of Pt diimine species exhibit C-H activation activity. Amongst the more noteworthy diimine-type systems are the (2,2'-bipyrimidyl)platinum(II) complexes examined by Periana et al.[8] and a host of platinum diimine complexes that have proven particularly advantageous for careful mechanistic studies.[9] Platinum complexes of the 2,2'-bipyridine (bpy) ligand and its derivatives have also been investigated extensively, for example with respect to oxidative addition processes.[10,11] There are several reports that describe instances of C-H activation reactions mediated by platinum(II) bipyridyl complexes, though these reactions tend to involve intramolecular ligand C-H activation processes.[12]

In the present study, we report on platinum complexes supported by bidentate pyrazolyl and bipyridyl borate ligands. To extend borate-incorporation into the ubiquitous bipyridyl ligand class, we have synthesized the ligand 2,2'-bipyridylborate [(4-BPh_3)bpy]. This ligand and the bidentate borate [$Ph_2B(pz)_2$] comprise the specific ligands of interest herein (Figure A.1). We present a comparison of the structural and

electronic properties of their platinum derivatives as determined by X-ray crystallography, IR spectroscopy, and ^{1}H NMR spectroscopy. Also discussed is the proclivity of several platinum derivatives to undergo C-H bond activation processes. Most interesting in this context is the discovery of a double C-H bond activation reaction: it is observed that exposure of a coordination site of the precursor $\{[Ph_2B(pz)_2]Pt(Me)_2\}^-$ in benzene solution leads to the rapid production of $\{[Ph_2B(pz)_2]Pt(Ph)_2\}^-$ at ambient temperature. This reaction is reminiscent of Goldberg's earlier discovery of a $\{\kappa^2$-$[Tp^*]PtMe_2\}^-$ precursor that reacts with alkanes upon exposure of a coordination site to yield stable octahedral Pt(IV) products in which the Tp ligand is κ^3.[6,13]

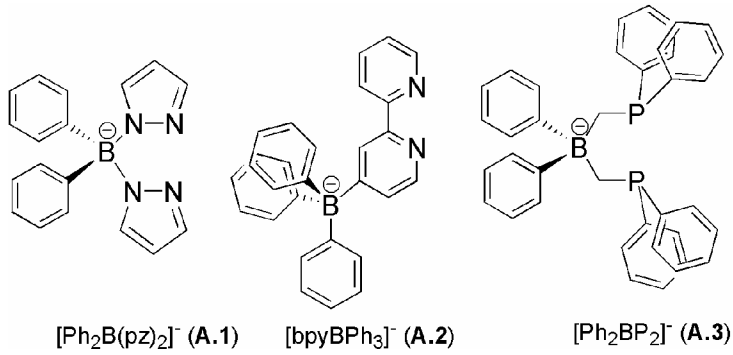

$[Ph_2B(pz)_2]^-$ (**A.1**) $[bpyBPh_3]^-$ (**A.2**) $[Ph_2BP_2]^-$ (**A.3**)

Figure A.1. The $[Ph_2B(pz)_2]$ (**A.1**), $[(4\text{-}BPh_3)bpy]$ (**A.2**), and $[Ph_2BP_2]$ (**A.3**) ligands each possess a borate anion incorporated within the ligand framework.

A.2 Results and Discussion

The $[Ph_2B(pz)_2][NBu_4]$ (**A.1**) ligand was synthesized using a modification of the procedure reported in the literature.[14] Excess pyrazole and sodium tetraphenylborate were heated to a melt (80-100 ˚C) for several hours. This was followed by salt metathesis with NBu_4Br in CH_2Cl_2 to generate **A.1** in 76% yield.

Scheme A.1:

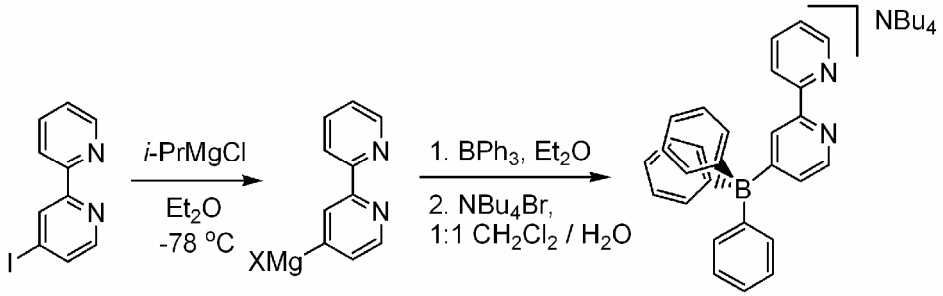

A.2

The [(4-BPh_3)bpy][NBu_4] (**A.2**) ligand was synthesized from 4-iodo-2,2'-bipyridine[15] via formation of a bipyridyl Grignard reagent (4-MgX)bpy using ^{i}PrMgCl at -78 ˚C in diethyl ether (Scheme A.1). The Grignard was then quenched with BPh_3, and the magnesium salt [(4-BPh_3)bpy]$_2$Mg was isolated as a red solid. It is noteworthy that traditional lithio reagents (i.e., ^{n}BuLi, ^{t}BuLi, etc.) and Mg^0 proved ineffective for the synthesis of this ligand. Strong chelation to magnesium made metallation of the magnesium derivative [(4-BPh_3)bpy]$_2$Mg difficult; however, salt metathesis with NBu_4Br in a 1:1 mixture of CH_2Cl_2 and H_2O generated a more useful reagent, **A.2**, in moderate overall yield (35%). The dimethyl platinum precursors [[$Ph_2B(pz)_2$]Pt(Me)$_2$][NBu_4] (**A.4**) and [[(4-BPh_3)bpy]Pt(Me)$_2$][NBu_4] (**A.5**) were prepared in good yield (76% and > 95%, respectively) by displacement of dimethyl sulfide from [(Me)$_2$Pt(μ-SMe_2)]$_2$ in THF solution. Substitution reactions with (COD)$PtMe_2$ (COD = cyclooctadiene) were ineffective.

Single crystals of **A.4** and **A.5** suitable for X-ray diffraction were grown by vapor diffusion of petroleum ether into concentrated THF solution. The resulting structures (Figure A.2) are to be compared with the structure previously reported for the bis(phosphino)borate dimethyl complex [[Ph_2BP_2]Pt(Me)$_2$][ASN] (**A.6**).[3] Relevant NMR data, interatomic distances, and bond angles are presented in Table A.1. All three

complexes adopt a typical square planar geometry but exhibit notable differences due to geometric constraints imposed by their respective donor ligands. Both N-donor complexes **A.4** and **A.5** have C-Pt-C angles near 90˚, while **A.6** has a slightly contracted C-Pt-C angle (86.6˚). A more significant difference is observed in the ligand bite angles. While both complexes **A.4** and **A.6** have ligand bite angles near 90˚ (90.64˚ and 89.73˚, respectively), the rigid bipyridine ligand leads to a much smaller N-Pt-N angle (77.96˚) in complex **A.5**.

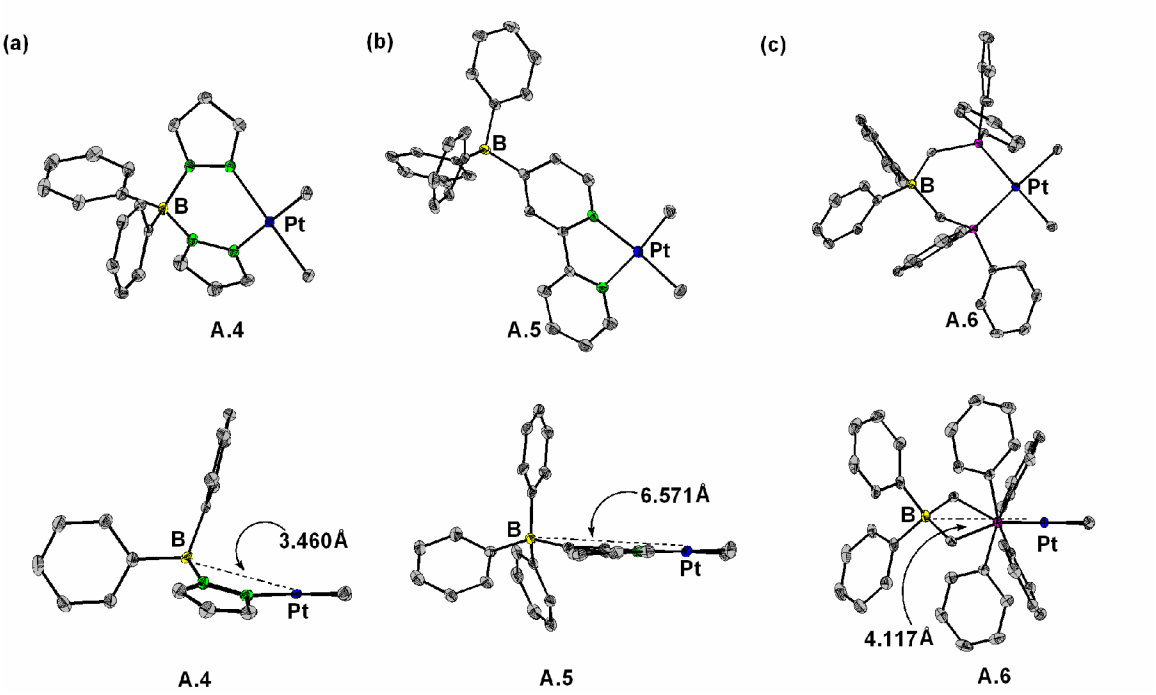

Figure A.2: Displacement ellipsoid representations (50%) of two different views of (a) [[$Ph_2B(pz)_2$]Pt$(Me)_2$][NBu_4] (**A.4**), (b) [[(4- BPh_3)bpy]Pt$(Me)_2$][NBu_4] (**A.5**), and (c) [[Ph_2BP_2]Pt$(Me)_2$][ASN] (**A.6**)[3a,c] displaying their geometries and Pt-B interatomic distances. The NBu_4 and ASN cations and hydrogen atoms have been omitted for clarity.

Table A.1: Relevant NMR and structural data for complexes **A.4**, **A.5**, and **A.6**.

Complex	$^2J_{Pt-H}$ (Hz)	Pt-B (Å)	Pt-C (Å)	C-Pt-C (deg)	P-Pt-P or N-Pt-N (deg)
$[[Ph_2B(pz)_2]Pt(Me)_2][NBu_4]$ (**A.4**)	83[a]	3.460	2.040[c]	89.30 (1)	89.73(9)
$[[(4\text{-}BPh_3)bpy]Pt(Me)_2][NBu_4]$ (**A.5**)	85, 86[a]	6.570	2.044(3), 2.036(3)	89.52(13)	77.96(10)
$[[Ph_2BP_2]Pt(Me)_2][ASN]$ (**A.6**)[b]	68[a]	4.117	2.133[c]	86.6(1)	90.64(2)

[a]NMR measurements were collected in d_6-acetone on a 300 MHz instrument. [b]Previously reported.[3a,c] [c]Average of both bond distances.

Another significant difference in ligand geometry is apparent upon looking into an edge of the square plane of each respective complex. While the $[(4\text{-}BPh_3)bpy]$ ligand is rigidly planar, the $[Ph_2B(pz)_2]$ ligand is canted out of the square plane, and the pyrazole rings eclipse one another. The $[Ph_2BP_2]$ ligand, on the other hand, has more flexible methylene connectors that allow it to maintain a staggered conformation that minimizes steric interactions. These differences in ligand geometry lead to variations in the distance between the Pt center and the negatively charged borated moiety. Complex **A.4** exhibits a Pt-B distance appreciably shorter than in **A.6** (3.460 Å compared to 4.117 Å), while complex **A.5** has a much longer Pt-B interatomic distance (6.570 Å).

A comparison of the average Pt-C bond lengths observed in these complexes is indicative of the relative *trans* influence of the borato ligands. Due to the strongly trans influencing nature of its phosphine donors, complex **A.6** exhibits an average Pt-C bond length significantly longer than either complex **A.4** or **A.5** (2.133 Å, compared to 2.040 (**A.4**) and 2.044 / 2.036 Å (**A.5**)). The NMR coupling constants are consistent with this description. For example, $^2J_{Pt-H}$ for **A.6** is much lower than that for either **A.4** or **A.5** (65 Hz, compared to 83 and 85 / 86 Hz). Evident from the NMR data and the observed Pt-C

bond lengths is that the [(4-BPh_3)bpy] ligand in **A.5** and the [$Ph_2B(pz)_2$] ligand in **A.4** exert comparable trans influences. In addition, neutral (bpy)$Pt(Me)_2$ has a nearly identical average Pt-C bond length and $^2J_{Pt\text{-}H}$ to **A.5**, indicating that the borate has negligible effect on the overall trans influence of the bipyridylborate ligand.

Although the [Ph_2BP_2] and [$Ph_2B(pz)_2$] complexes **A.4** and **A.6** are colorless, the [(4-BPh_3)bpy] complex **A.5** is intensely colored. This characteristic red-orange color can be attributed to a metal to ligand charge transfer (MLCT) {Pt d_{z^2} to ligand π^*} transition, as observed for similar bipyridine complexes.[10] Interestingly, the absorption maximum (λ_{max}) for **A.5** is blue shifted to 385 nm from the λ_{max} observed for the neutral (bpy)$Pt(Me)_2$ at 456 nm (Figure A.3). This large blue shift is likely a qualitative measure of the degree of destabilization of the bipyridyl centered LUMO upon incorporation of the anionic borate unit.

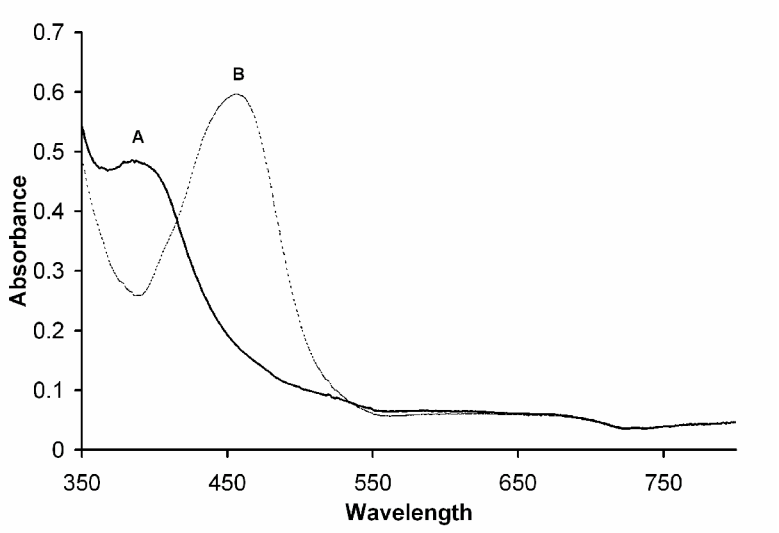

Figure A.3*:* Optical absorption spectra of (A) **A.5** (solid) and (B) (bpy)$Pt(Me)_2$ (dashed) in acetonitrile solution at 298 K.

As has been reported previously, protonation of **A.6** with an ammonium salt (e.g., $[HNR_3][BPh_4]$) in the presence of an L donor (L = THF, CO, $P(C_6F_5)_3$, etc.) leads to clean formation of neutral $[Ph_2BP_2]Pt(Me)(L)$ complexes.[3] Likewise, it is found that protonation of **A.4** with $[HN^{i}Pr_2Et][BPh_4]$ in THF in the presence of excess L cleanly generates several $[Ph_2B(pz)_2]Pt(Me)(L)$ complexes (L = $NCCH_3$, **A.7**; CO, **A.8**; $P(C_6F_5)_3$, **A.9**).

In the case of the unsymmetric complex **A.5**, protonolysis by $[HNEt_3][BPh_4]$ in acetonitrile solution led to formation of the two possible isomers of [(4-BPh_3)bpy]Pt(Me)($NCCH_3$) (**A.10**) in a 2.8:1 ratio (Scheme A.2). The major isomer formed in this reaction was determined to be that in which acetonitrile occupies the site *cis* to the borate-substituted pyridyl ring. This was established by NMR spectroscopy using a two-dimensional NOESY experiment. An identical ratio of products is observed when the reaction is performed at both high and low temperatures (-78 ˚C to 60 ˚C). The formation of appreciable amounts of both isomers in this reaction suggests that the *trans* effect of the pyridyl donor featuring a *p*-borate unit is quite similar to the unsubstituted donor ring. Similarly, protonation of **A.5** with $[HNEt_3][BPh_4]$ in THF followed by addition of excess carbon monoxide led to the formation of both isomers of [(4-BPh_3)bpy]Pt(Me)(CO) (**A.11**) in an identical 2.8:1 ratio.

Scheme A.2:

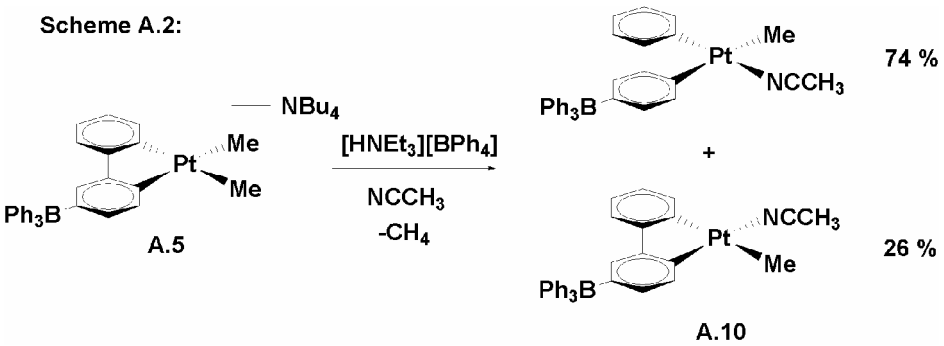

Table A.2: Infrared carbonyl frequencies for platinum methyl carbonyl complexes.

Complex	ν_{CO} (cm^{-1})
$[Ph_2B(pz)_2]Pt(Me)(CO)$ (**A.8**)	2078[a]
$[(4\text{-}BPh_3)bpy]Pt(Me)(CO)$ (**A.11**)	2098[a]
$[(bpy)Pt(Me)(CO)][BPh_4]$ (**A.12**)	2107[a]
$[Ph_2BP_2]Pt(Me)(CO)$[b]	2094[a]
$[[Ph_2SiP_2]Pt(Me)(CO)][B(C_6F_5)_4]$[b]	2118[a]

[a] KBr cell in CH_2Cl_2. [b] Previously reported.[3c,d 10b]

To probe the electronic differences between ligands **A.1**, **A.2**, and **A.3**, we have synthesized several neutral platinum methyl carbonyl complexes. The relative energies of the CO vibrations in these neutral complexes are effective indicators of the electronic environment around the platinum center. The relevant carbonyl stretching frequency data is reported in Table A.2. Bis(pyrazolyl)borate complex **A.8** possesses a CO stretching frequency 16 cm^{-1} lower than that of the $[Ph_2BP_2]Pt(Me)(CO)$ complex,[3d] indicating that, for the present square planar platinum system, the bidentate pyrazolyl ligand acts as a better electron donor than the bidentate phosphine. This result is surprising and contrasts other data from our group clearly suggesting that, in general, (phosphino)borate ligands are stronger field donors that (pyrazolyl)borates.[3c,16] The $[(4\text{-}BPh_3)bpy]$ complex **A.11** possesses the highest CO stretching frequency (2098 cm^{-1}), suggesting that the bipyridyl ligand is the poorest donor of the three monoanionic ligands. This trend can be correlated to the Pt-B interatomic distances established for complexes **A.4-A.6** via X-ray diffraction (Table A.1). The complex in which the borate is farthest removed from the platinum center (**A.5**, 6.570 Å) also corresponds to the methyl carbonyl complex with the highest

CO stretching frequency (**A.11**). Complex **A.4** has the shortest Pt-B distance (3.460 Å), and its methyl carbonyl complex (**A.8**) exhibits the lowest CO stretching frequency.

In addition to comparing the carbonyl data among the neutral methyl carbonyl complexes, comparisons can be made between the neutral complexes and structurally analogous cationic complexes lacking a borate moiety. It is important to note, however, that the absolute difference in CO stretching frequency, at least when comparing formally neutral complexes with formally cationic complexes, is strongly influenced by electrostatic factors.[17] The difference in CO stretching frequency ($\Delta\nu_{CO}$) between the neutral complex $[Ph_2BP_2]Pt(Me)(CO)$ and the cationic complex $[[Ph_2SiP_2]Pt(Me)(CO)][B(C_6F_5)_4]$ is reported to be 24 cm^{-1}, confirming that the $[Ph_2BP_2]$ ligand is more electron-releasing than its neutral silane analogue.[3] Although no data have been reported for a cationic analogue of **A.8**, the infrared data for **A.11** can be compared with the carbonyl stretch of 2107 cm^{-1} observed for the cationic complex $[(bpy)Pt(Me)(CO)][BPh_4]$ (**A.12**). Based on the $\Delta\nu_{CO}$ of 9 cm^{-1}, it can be concluded that the borate unit does effect the electronic environment of the platinum center, but to a much lesser extent than the borate of $[Ph_2BP_2]$. The aryl ring of the bipyridyl ligand serves as a much better insulator than the methylene linker of $[Ph_2BP_2]$.

Platinum complexes supported by ligands **A.1**, **A.2**, and **A.3** display varied solution chemistry in benzene. For example, we have previously reported that $[Ph_2BP_2]Pt(Me)(L)$ species are readily converted to their corresponding $[Ph_2BP_2]Pt(C_6D_5)(L)$ derivatives when gently heated in benzene-d_6 solution (where L = THF, $P(C_6F_5)_3$).[3c] For comparison we attempted to isolate the complex $[Ph_2B(pz)_2]Pt(Me)(THF)$ but found it is too reactive (vide infra). The complex

$[Ph_2B(pz)_2]Pt(Me)(P(C_6F_5)_3)$ (**A.9**) is conveniently accessible. Choice of the $P(C_6F_5)_3$ ligand is based on the presupposition that it provides a potentially labile donor ligand due to its high steric bulk and that it should feature relatively inert aryl rings. When **A.9** was subjected to the same reaction conditions as $[Ph_2BP_2]Pt(Me)(P(C_6F_5)_3)$ (80˚C, 24 h, C_6D_6), no reaction was observed, whereas we have previously observed that $[Ph_2BP_2]Pt(Me)(P(C_6F_5)_3)$ proceeds cleanly to the phenyl product $[Ph_2BP_2]Pt(C_6D_5)(P(C_6F_5)_3)$.[3c] The increased reactivity of $[Ph_2BP_2]Pt(Me)(P(C_6F_5)_3)$ might be attributable to the lability of the $P(C_6F_5)_3$ ligand because of a greater trans effect of the $[Ph_2BP_2]$ ligand, though it is equally likely that steric interactions between the $[Ph_2BP_2]$ ligand and the sterically bulky $P(C_6F_5)_3$ donor serve to more greatly labilize the latter than in the case of the bis(pyrazolyl)borate system.

Another interesting difference in reactivity between complexes **A.4-A.6** is observed upon attempts to protolytically cleave or abstract a methyl ligand by $B(C_6F_5)_3$ in benzene solution. Thus, protonation of **A.4** with *one* equivalent of $[HN^{i}Pr_2Et][BPh_4]$ in benzene solution leads to the rapid C-H activation of *two* equivalents of benzene leading to the formation of a single product, $[[Ph_2B(pz)_2]Pt(Ph)_2][NBu_4]$ (**A.13**), with concomitant loss of *two* equivalents of methane (Scheme A.3).

Scheme A.3:

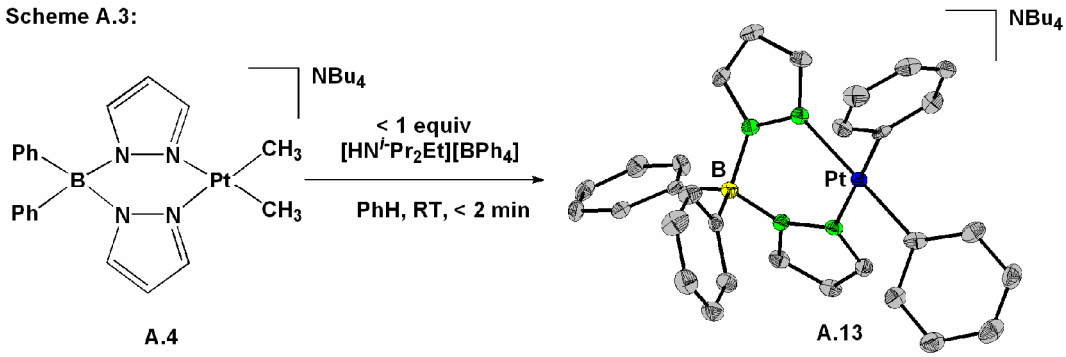

A.4 **A.13**

When a stronger and more soluble acid is used, such as $[H(OEt_2)_2][BAr_4]$ (Ar = $C_6H_3(CF_3)_2$), the reaction proceeds similarly but is more facile. The C-H activation process can be observed by ^{1}H NMR in toluene-d_8 at temperatures as low as –20 ˚C using the mild acid $[HN^{i}Pr_2Et][BPh_4]$. The reaction was monitored by the production of methane and the disappearance of starting material; however, due to the formation of multiple toluene activation products, the kinetics of this reaction could not be followed closely. Addition of substoichiometric amounts of $[HN^{i}Pr_2Et][BPh_4]$ or $[H(OEt_2)_2][BAr_4]$ (0.1 equiv) leads to much slower consumption of the starting precursor **A.4** (48 hrs), but nonetheless generates **A.13** quantitatively. This observation implies that acid catalyzes the double C-H activation process.

The above observations are consistent with several possible reaction mechanisms. Perhaps the simplest and most reasonable scenario, at least based upon literature precedent, concerns an associative oxidative addition/reductive elimination cycle (Scheme A.4).[6,9a] The first likely step of such a mechanism (a) is protonation at the metal center to form a six-coordinate platinum(IV) species (with the other axial site presumably occupied by a solvent molecule).[18] This is followed by reductive elimination of methane and coordination of benzene to form an η^2-benzene adduct (b). The benzene molecule is then oxidatively added to form another platinum(IV) hydride (c), from which another molecule of methane is reductively eliminated (d). Oxidative addition of another benzene molecule (e) would then lead to a platinum(IV) hydride species from which the $[HNR_3][BPh_4]$ salt could be regenerated (f), allowing the reaction to proceed via addition of catalytic acid. A related cycle to consider involves initial protonation and dissociation of one of the ligand pyrazole rings to open a metal coordination site, allowing benzene to

coordinate. Scenarios related to this have been previously suggested for Tp platinum(IV) complexes during acid-assisted reductive elimination processes.[6]

Scheme A.4:

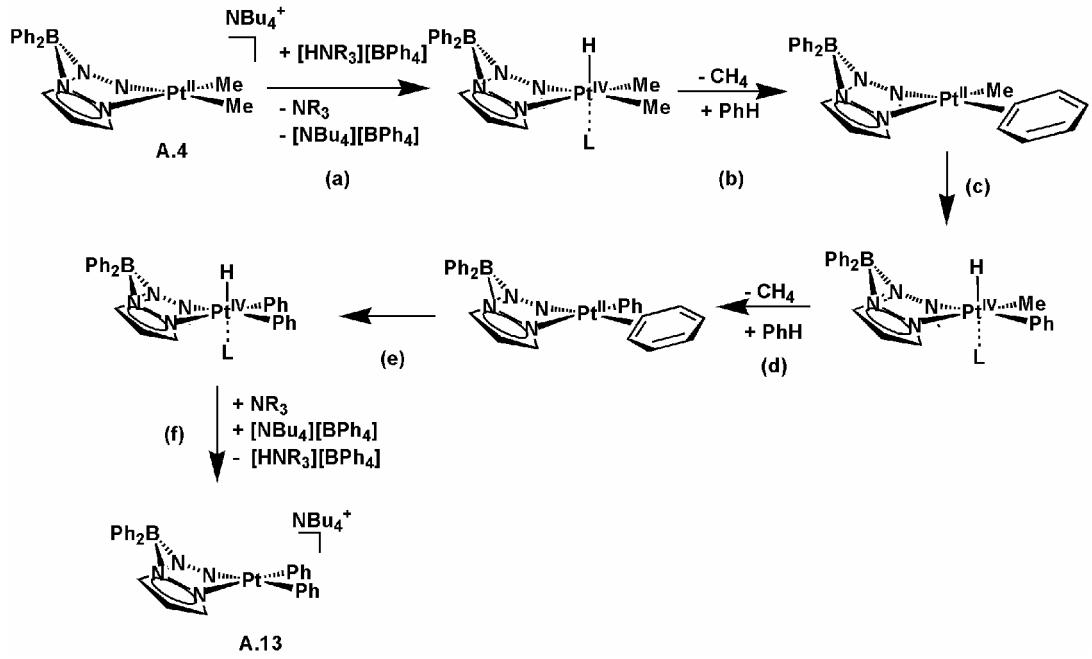

An interesting aspect of this benzene activation process is that the reaction proceeds rapidly in the presence of a labile two-electron donor such as tetrahydrofuran, but is quenched upon addition of a modestly stronger donor such as acetonitrile. Thus, protonation of **A.4** in benzene, followed by immediate addition of acetonitrile, leads to the formation of $[Ph_2B(pz)_2]Pt(Ph)(NCCH_3)$ (**A.14**) in high yield. Binding of acetonitrile to the platinum center apparently prohibits formation of the much more weakly coordinating η^2-benzene ligand (Scheme A.4(d)).[9a] Completion of the double C-H activation process in the presence of THF implies that benzene can compete with THF, to some extent, for the platinum binding site. This is also true of neutral $[Ph_2BP_2]PtMe(THF)$ complexes.[3a,c]

When the protonation reaction is monitored in benzene-d_6, CH_4, CH_3D, CH_2D_2, and CHD_3 are all observed by ^1H NMR. Even when a deuterated acid such as [$DN^{i}Pr_2Et$][BPh_4] is used, all of the mixed H/D isotopomers of methane, including CH_4, are observed. Since there is only one equivalent of H^+ in the reaction mixture, one equivalent each of CH_4 (where the acid is the proton source) and CH_3D (where benzene-d_6 is the proton source) might be expected. Observation of isotopic enrichment of the methane is indicative of the formation of an intermediate methane adduct that can be reversibly activated prior to dissociation.[5b,19] It is interesting to note that at -20˚C the ratio of deuterium-containing isotopomers of methane relative to CH_4 is greater, hinting that the relative rate of methane loss from the platinum methane adduct might be slowed considerably compared to the rate of H/D exchange at low temperature.

The observation that substoichiometric amounts of acid catalyze C-H activation is consistent with previous reports in which a catalytic amount of $B(C_6F_5)_3$ promotes C-H activation of solvent.[20] This extremely electrophilic Lewis acid has proven useful in abstracting a methide anion in a variety of other cases.[21] When either one or less than one equivalent of $B(C_6F_5)_3$ is added to **A.4**, the major product obtained is, indeed, the double benzene activation product **A.13**. The reaction rate is much faster than that of the acid-assisted reaction. Such a rapid reaction at room temperature makes this reaction pathway very promising; even more encouraging is that the reaction proceeds with $B(C_6F_5)_3$ at temperatures *as low as -64 ^oC in toluene-d_8*. Much like the acid-assisted case, all deuterium-containing isotopomers of methane (including CH_4) are observed in C_6D_6. Difficult to exclude is that the proton source for generating CH_4 in this reaction is adventitious water, similar to the result suggested by Goldberg.[6] As for the reaction with

$[HNR_3][BPh_4]$, the ratio of deuterium-containing isotopomers of methane to CH_4 is greater at -64 ^oC than at room temperature. One can envision similar mechanisms to those suggested for the protonation route with this Lewis acid, with the exception that the first step in this case is methide-abstraction rather than protonation (Scheme A.5).

Scheme A.5:

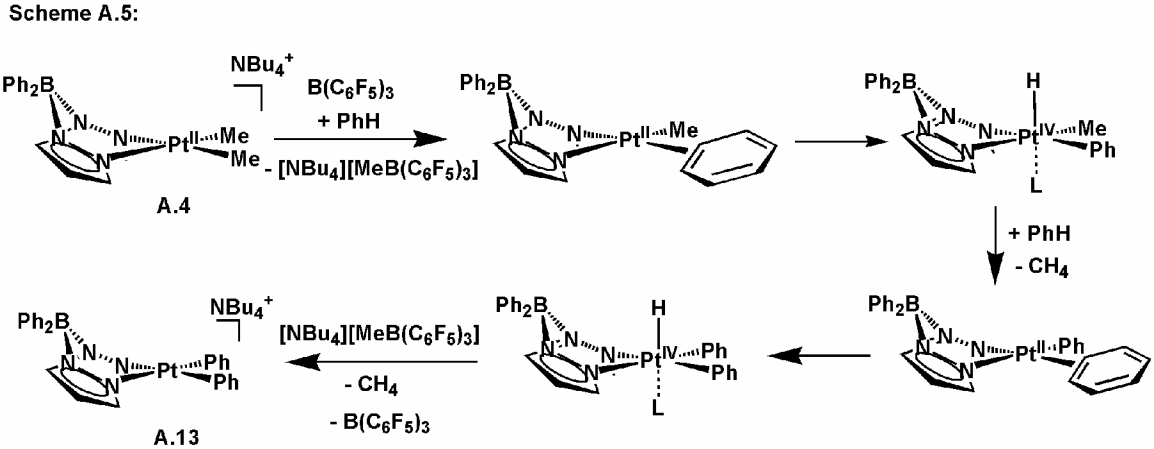

An estimate of the overall kinetic isotope effect for this reaction was obtained by performing the reaction with one equivalent of $[HNR_3][BPh_4]$ in a 1:1 C_6H_6 / C_6D_6 mixture. The resulting product was analyzed by ^1H NMR, and it was determined that 51% of the platinum phenyl groups in **A.13** were deuterated. This indicates that there is a negligible overall kinetic isotope effect ($k_H/k_D \sim 1.0$). Since there are likely multiple equilibria involved, the only conclusion that can be drawn from this data is that benzene C-H bond breaking is not significantly rate contributing.[22] We suspect that the rate-determining step is initial protonation based upon the acid concentration dependence of the overall reaction profile (i.e., the reaction slows when substoichiometric amounts of acid are added).

In contrast to complex **A.4**, bis(phosphino)borate complex **A.6** shows very different reactivity under both protonation and methide abstraction conditions in benzene. When **A.6** is exposed to either $B(C_6F_5)_3$ or $[HN^{i}Pr_2Et][BPh_4]$ in benzene-d_6 at room

temperature, the reaction is slower than that of **A.4** (~ 24 hrs), and a complex mixture of products is formed. In addition, only CH_4 and CH_3D are observed under these conditions, indicating there is a smaller barrier to methane loss relative to the bis(pyrazolyl)borate complex. This difference can be attributed to the strongly *trans* influence of the phosphine donors in **A.6**.

Complex **A.5** also shows limited reactivity with respect to C-H activation upon *in situ* protonation or methide abstraction in benzene-d_6. Under both sets of reaction conditions, the reaction proceeds much more slowly than the $[Ph_2B(pz)_2]$ case. An ill-defined mixture of products forms, but no evidence for C-H activation is observed. CH_4 is the only methane byproduct that can be detected under these conditions.

Upon further investigation we determined that $[Ph_2B(pz)_2]$ platinum complexes also show reactivity in the presence of acid and other aromatic substrates. Exposure of complex **A.4** to $[HN^{i}Pr_2Et][BPh_4]$ in toluene and *p*-xylene gives rise to a mixture of products that includes η^1-bound benzylic species.[9b,23] In contrast, when **A.4** is stirred with $[HN^{i}Pr_2Et][BPh_4]$ in mesitylene at room temperature for 18 hours, the major product isolated is $[Ph_2B(pz)_2]Pt(CH_2C_6H_3(CH_3)_2)(pzH)$ (**A.15**) (Scheme A.6). This product provides an interesting example of C-H activation of an sp^3-hybridized C-H bond position, but the relatively low yield (~ 50%) and the presence of a coordinated pyrazole ring establish that the formation of **A.15** is accompanied by undesired borate ligand degradation. The benzylic C-H activation process also occurs when the reaction is carried out in the presence of a donor ligand such as acetonitrile, THF, or pyridine, and an analogous product distribution is observed under such conditions. C-H activation was not observed with pentane, methylcyclohexane, or other non-aromatic hydrocarbons even at

elevated temperatures, indicating that sp^3-hybridized C-H bond activation is operative only for more reactive benzylic C-H bonds in this system.

Scheme A.6:

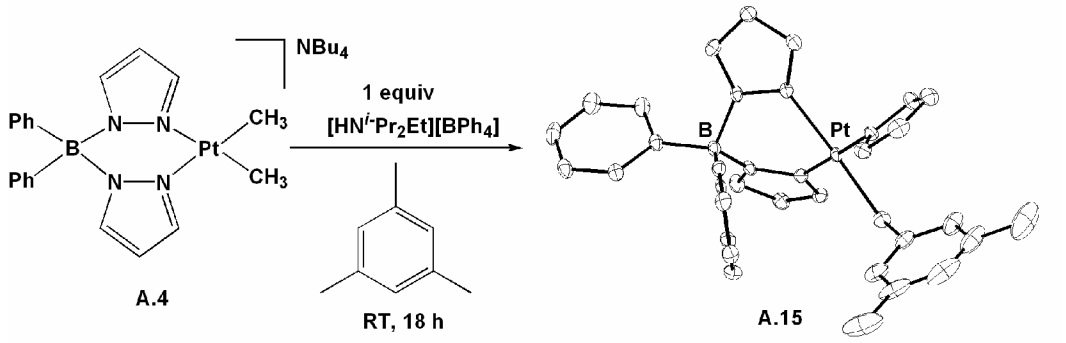

Platinum bis(pyrazolyl)borate and 2,2'-bipyridylborate complexes have been prepared and compared to previously reported bis(phosphino)borate complexes in an effort to better understand the extent of charge delocalization in structurally different borato ligands. NMR and structural data for the anionic dimethyl complexes **A.4**, **A.5**, and **A.6** indicate that the phosphine donors of the [Ph_2BP_2] ligand exert a stronger trans influence than the N-donor ligands; however, the [$Ph_2B(pz)_2$] ligand has been shown through IR carbonyl stretching frequency data to be the most electron-releasing of the three ligands. This may be a result of the closer proximity of the borate unit to the metal center in complex **A.4** in comparison to complexes **A.5** and **A.6**.

The structural and electronic differences between these ligands appear to have a substantial effect on the reactivity of their platinum complexes with respect to C-H activation. While [Ph_2BP_2]Pt(Me)(L) complexes are effective towards activation of aryl C-H bonds at elevated temperatures, analogous [$Ph_2B(pz)_2$] complexes are completely

unreactive under these conditions. [[$Ph_2B(pz)_2$]Pt$(Me)_2$][NR_4] complexes, however, are highly active with respect to C-H activation of aryl C-H bonds upon protonation or methide abstraction *in situ*, in the absence of a donor ligand poison. These reactions are facile at temperatures well below 0 ºC. Moreover, whereas coordination of a third pyrazolyl arm in the previously reported {κ^2-[Tp*]PtMe_2}$^-$ system occurs upon methide abstraction, thereby leading to {κ^3-[Tp*]Pt(Me)(H)(R)} Pt(IV) products in the presence of alkane substrate, for the present bis(pyrazolyl)borate system only Pt(II) species are observed. Destabilization of the Pt(IV) intermediate due to the lack of a third donor chelate arm enables the double C-H activation process to proceed efficiently. We have also observed that structurally related [Ph_2BP_2] and [(4-BPh_3)bpy] complexes are protonated much more slowly under analogous conditions, and these systems appear to lead to very different (and ill-defined) product distributions.

A.3 Experimental Section

A.3.1 General Considerations

All syntheses reported were carried out using standard glovebox and Schlenk techniques in the absence of water and dioxygen, unless otherwise noted. Acetonitrile, benzene, dichloromethane, diethyl ether, petroleum ether, tetrahydrofuran, and toluene were degassed and dried by sparging with N_2 gas followed by passage through an activated alumina column. Pentane, mesitylene, and *p*-xylene were deoxygenated via sparging with N_2, dried over CaH, and distilled prior to use. Ethanol was deoxygenated via sparging with N_2, dried over NaOEt, and distilled prior to use. All solvents were stored over 3-Å molecular sieves. Deuterated benzene, chloroform, acetonitrile, acetone, and toluene were purchased from Cambridge Isotope Laboratories, Inc., degassed via

repeated freeze-pump-thaw cycles, and dried over 3-Å molecular sieves. Nonhalogenated solvents were frequently tested using a standard solution of sodium benzophenone ketyl in tetrahydrofuran to confirm the absence of oxygen and moisture. NMR spectra were recorded at ambient temperature unless otherwise stated on Varian Mercury 300 MHz, Varian Inova 500 MHz, and JEOL 400 MHz spectrometers. ^{1}H and ^{13}C NMR chemical shifts were referenced to residual solvent. ^{31}P NMR chemical shifts were referenced to 85% H_3PO_4. IR spectra were recorded on a Bio-Rad Excalibur FTS 3000 spectrometer controlled by Win-IR Pro software. Elemental analyses were performed by Desert Analytics, Tuscon, AZ. X-ray diffraction experiments were carried out by the Beckman Institute Crystallographic Facility on a Bruker Smart 1000 CCD diffractometer.

A.3.2 Starting Materials and Reagents

. $[Me_2Pt(\mu\text{-}SMe_2)]_2$,[24] $[HN^{i}Pr_2Et][BPh_4]$,[3] $[HNEt_3][BPh_4]$,[25] $P(C_6F_5)_3$,[26] $[H(OEt_2)_2][B(C_6H_3(CF_3)_2)_4]$,[27] **A.3**,[3a] **A.6**,[3a,c,d] (bpy)Pt(Me)$_2$,[28] and 4-iodo-2,2'-bipyridine[15] were prepared using literature methods. $[DN^{i}Pr_2Et][BPh_4]$ was prepared by acidifying an aqueous solution of $N^{i}Pr_2Et$ and $NaBPh_4$ with aqueous DCl. $B(C_6F_5)_3$ was recrystallized from pentane at -35 ^{o}C prior to use. All other chemicals were purchased from Aldrich, Strem, Alfa Aesar, or Lancaster and used without further purification.

A.3.3 Synthesis of Compounds

$[Ph_2B(pz)_2][Na(pzH)_2]$. A mixture of solid $NaBPh_4$ (8.908 g, 26.03 mmol) and solid pyrazole (22.731 g, 333.9 mmol) was heated to a melt and stirred in a 50 mL flask fitted with a Dean-Stark trap and condenser to collect benzene as it distilled from the reaction mixture. The reaction was allowed to heat at 80-100 ˚C until a nearly stoichiometric amount of benzene (4.22 mL, 1.81 equiv) was collected (3 hr). The reaction was

extracted with boiling hexanes (4 x 200 mL). The solids were then dried under reduced pressure to yield a white powder (8.0090 g, 67.1%). *Note: This is a variation of the literature method,*[14] *which is reported to provide [$Ph_2B(pz)_2$][Na]. The literature method replaces the extraction with a distillation to remove the excess pyrazole.*

[$Ph_2B(pz)_2$][NBu_4] (A.1). Solid [$Ph_2B(pz)_2$][$Na(pzH)_2$] (3.7573 g, 8.1982 mmol) was dissolved in dichloromethane (80 mL) along with NBu_4Br (2.6733 g, 8.2924 mmol). The hazy solution was stirred for 10 minutes and filtered over Celite on a sintered glass frit. The filtrate was concentrated by rotary evaporation. Hexanes (80 mL) was added and stirred vigorously, forming white solids. The solids were collected by filtration and washed with toluene (3 x 20 mL) and hexanes (2 x 20 mL). The resulting solids were suspended in toluene (20 mL) and stirred for 5 min, and then collected by filtration and washed with hexanes (2 x 20 mL). The resulting white solids were dried under reduced pressure (4.2889 g, 96.6%). ^{1}H NMR (300 MHz acetone-d_6): δ = 7.40 (d, 2H, $^3J_{H\text{-}H}$ = 1.8 Hz, pz-3H), 7.21 (m, 4H, *o*-Ph), 7.15 (d, 2H, $^3J_{H\text{-}H}$ = 2.4 Hz, pz-5H), 6.97-7.05 (m, 6H, *m,p*-Ph), 5.95 (dd, 2H, $^3J_{H\text{-}H}$ = 1.8, 2.1 Hz, pz-4H), 3.70 (m, 8H, NBu_4), 1.77 (m, 8H, NBu_4), 1.40 (m, 8H, NBu_4), 0.97 (t, 12H, $^3J_{H\text{-}H}$ = 7.8 Hz, NBu_4).

[(4-BPh_3)bpy][NBu_4] (**A.2**). Solid 4-iodo-2,2'-bipyridine (1.3330 g, 4.72 mmol) was dissolved in Et_2O (50 mL) and cooled to -78 ˚C with stirring (upon cooling, the mixture becomes heterogeneous). To this suspension was added *i*-PrMgCl (2.36 mL, 2.0 M in Et_2O, 4.72 mmol) dropwise over 10 minutes. The suspension became deep red upon addition. After stirring for 1 hour, BPh_3 (1.1413 g, 4.72 mmol) in THF (10 mL) was added and the resulting solution was allowed to warm to room temperature over 3 hours. The resulting red solids were collected on a sintered glass frit and washed with Et_2O (3 x

10 mL). The solids were taken up in CH_2Cl_2 (20 mL), and solid NBu_4Br (1.5216 g, 4.72 mmol) was added. 40 mL of H_2O was added, and the mixture was stirred vigorously for 30 minutes. The CH_2Cl_2 layer was then collected and washed with additional H_2O (2 x 20 mL). The combined CH_2Cl_2 layers were collected, dried with Na_2SO_4, and evaporated in vacuo. The remaining solids were recrystallized via vapor diffusion of petroleum ether into THF to yield white needles (0.8187 g, 1.28 mmol, 27%). ^{1}H NMR (300 MHz, acetone-d_6): δ = 8.65 (br m, 1H, 3-bpy), 8.41-8.45 (m, 2H, 6,3'-bpy), 8.19 (d, 1H, $^3J_{H\text{-}H}$ = 5.1 Hz, 6'-bpy), 7.73 (ddd, 1H, $^3J_{H\text{-}H}$ = 8.4, 7.2, 2.1 Hz, 4'-bpy), 7.35 (m, 7H, *o*-Ph + 5-bpy), 7.18 (m, 1H, 4'-bpy), 6.96 (t, 6H, $^3J_{H\text{-}H}$ = 7.5 Hz, *m*-Ph), 6.81 (m, 3H, $^3J_{H\text{-}H}$ = 6.9 Hz, *p*-Ph), 3.44 (m, 8H, NBu_4), 1.82 (m, 8H, NBu_4), 1.42 (m, 8H, NBu_4), 0.98 (t, 12H, $^3J_{H\text{-}H}$ = 7.2 Hz, NBu_4). ^{13}C NMR (75.409 MHz, acetone-d_6): δ = 160.5, 149.9, 137.5, 137.4, 133.8, 131.9, 130.3, 126.8, 123.4, 123.2, 121.9, 59.8 (NBu_4), 24.9 (NBu_4), 20.8 (NBu_4), 14.4 (NBu_4). Anal. Calcd. for $C_{44}H_{58}BN_3$: C, 82.60; H, 9.14; N, 6.57. Found: C, 82.04; H, 9.24; N, 6.81.

[($Ph_2B(pz)_2$)$Pt(Me)_2$][NBu_4] (A.4). Solid $[Me_2Pt(\mu\text{-}SMe_2)]_2$ (0.3775 g, 1.215 mmol) and solid **A.1** (0.6573 g, 1.213 mmol) were suspended in tetrahydrofuran (10 mL). The resulting cloudy white mixture was stirred for three hours and then dried in vacuo. The resulting solids were collected on a sintered glass frit and washed with petroleum ether (3 x 5 mL) and benzene (3 x 5 mL). The off-white solids were dried further in vacuo to yield analytically pure **A.4** (0.7091 g, 76.1%). Crystals for X-ray diffraction were grown via vapor diffusion of petroleum ether into tetrahydrofuran. ^{1}H NMR (300 MHz acetone-d_6): δ = 7.76 (m, 2H, $^3J_{Pt\text{-}H}$ = 5.4 Hz, pz-3H), 7.12 (dd, 2H, $^3J_{H\text{-}H}$ = 2.3, 0.9 Hz, *p*-Ph), 7.08 (d, 2H, $^3J_{H\text{-}H}$ = 1.2 Hz, pz-5H), 7.06 (m, 4H, *o*-Ph), 6.83 (dd, 4H, $^3J_{H\text{-}H}$ = 6.9, 3.0 Hz,

m-Ph), 6.05 (t, 2H, $^{3}J_{H\text{-}H}$ = 1.8 Hz, pz-4H), 3.45 (m, 8H, NBu_4), 1.80 (m, 8H, NBu_4), 1.40 (m, 8H, NBu_4), 0.97 (t, 12H, $^{3}J_{H\text{-}H}$ = 7.8 Hz, NBu_4), 0.36 (s, 6H, $^{2}J_{Pt\text{-}H}$ = 83 Hz, Me). ^{13}C NMR (75.409 MHz, acetone-d_6): δ = 138.0, 135.6, 134.7, 126.9, 125.7, 103.0, 59.2 (s, NBu_4), 24.5 (s, NBu_4), 20.3 (s, NBu_4), 14.0 (s, NBu_4), -18.9 (s, Pt-Me). Anal. Calcd. for $C_{36}H_{58}BN_5Pt$: C, 56.39; H, 7.62; N, 9.13. Found: C, 56.68; H, 7.78; N, 9.28.

[((4-BPh_3)bpy)$Pt(Me)_2$][NBu_4] (A.5). Solid $[Me_2Pt(\mu\text{-}SMe_2)]_2$ (0.0267 g, 0.0466 mmol) was dissolved in THF (3 mL). To this stirring solution was added **A.2** (0.0596 g, 0.0933 mmol) in THF (5 mL), and the mixture was allowed to stir for 1 hour. The resulting red solution was dried in vacuo, and the remaining solids were washed with Et_2O (3 x 5 mL) to afford analytically pure product as a red-orange powder (0.0804 g, 0.0930 mmol, 99%). ^{1}H NMR (300 MHz, acetone-d_6): δ = 9.11 (d, 1H, $^{3}J_{H\text{-}H}$ = 7.5Hz, $^{3}J_{Pt\text{-}H}$ = 24 Hz, 6-bpy), 8.71 (d, 1H, $^{3}J_{H\text{-}H}$ = 5.4 Hz, $^{3}J_{Pt\text{-}H}$ = 21 Hz, 6'-bpy), 8.24 (br s, 1H, 3-bpy), 8.13 (ddd, 1H, $^{3}J_{H\text{-}H}$ = 9.6, 8.1, 0.3 Hz, 5'-bpy), 7.79 (d, 1H, $^{3}J_{H\text{-}H}$ = 7.8 Hz, 3'-bpy), 7.58 (br s, 1H, 5-bpy), 7.48 (m, 1H, 4'-bpy), 7.31 (br s, 6H, *o*-Ph), 7.01 (t, 6H, $^{3}J_{H\text{-}H}$ = 5.4 Hz, *m*-Ph), 6.87 (t, 3H, $^{3}J_{H\text{-}H}$ = 7.5 Hz, *p*-Ph), 3.41 (m, 8H, NBu_4), 1.79 (m, 8H, NBu_4), 1.39 (m, 8H, NBu_4), 0.96 (t, 12H, $^{3}J_{H\text{-}H}$ = 7.5 Hz, NBu_4), 0.92 (3H, $^{2}J_{Pt\text{-}H}$ = 86 Hz, Pt-Me), 0.82 (3H, $^{2}J_{Pt\text{-}H}$ = 85 Hz, Pt-Me). ^{13}C NMR (75.409 MHz, acetone-d_6): δ = 160.3, 159.7, 153.3, 147.3, 143.7, 137.6, 137.0, 136.0, 131.4, 127.1, 123.7, 123.2, 59.5 (NBu_4), 24.8 (NBu_4), 20.7 (NBu_4), 14.4 (NBu_4), -15.0 (Me), -15.3 (Me). Anal. Calcd. for $C_{46}H_{64}BN_3Pt$: C, 63.88; H, 7.46; N, 4.86. Found: C, 63.91; H, 7.80; N, 4.65.

($Ph_2B(pz)_2$)Pt(Me)($NCCH_3$) (A.7). Solid **A.4** (0.0595 g, 0.0775 mmol) and solid [$HN^{i\text{-}}Pr_2Et$][BPh_4] (0.0343 g, 0.0764 mmol) were combined in a mixture of tetrahydrofuran (2 mL) and acetonitrile (3 drops). The resulting clear solution was stirred for two hours at

room temperature and then dried in vacuo. The remaining solids were extracted with benzene and filtered through Celite to remove $[NBu_4][BPh_4]$. The filtrate was dried in vacuo to yield analytically pure product as an off-white solid (60%). ^{1}H NMR (300 MHz benzene-d_6): δ = 7.77 (d, 1H, $^3J_{H\text{-}H}$ = 2.1 Hz, $^3J_{Pt\text{-}H}$ = 25 Hz, pz-3'H), 7.59 (d, 1H, $^3J_{H\text{-}H}$ = 2.4 Hz, pz-3H), 7.49 (d, 1H, $^3J_{H\text{-}H}$ = 2.1 Hz, pz-5'H), 7.38 (d, 1H, $^3J_{H\text{-}H}$ = 2.7 Hz, pz-5H), 7.27 (m, 10H, Ph), 6.14 (t, 1H, $^3J_{H\text{-}H}$ = 2.1 Hz, pz-4H), 5.88 (m, 1H, $^3J_{H\text{-}H}$ = 2.1 Hz, pz-4'H), 1.09 (s, 3H, $^2J_{Pt\text{-}H}$ = 77.2 Hz, Pt-Me), 0.24 (s, 3H, $^4J_{Pt\text{-}H}$ = 6.9 Hz, NCC$\underline{H}_3$). ^{13}C NMR (75.409 MHz, benzene-d_6): δ = 140.8, 139.4, 138.5, 137.2, 135.1, 127.9, 127.1, 126.0, 104.9, 104.6, 30.7 (N$\underline{C}CH_3$), 1.56 (NC$\underline{C}H_3$), -18.8 (Pt-Me). ES-MS (m/z, negative) : 549 ($M - H^+$). Anal. Calcd. for $C_{21}H_{22}BN_5Pt$: C, 45.83; H, 4.03; N, 12.73. Found: C, 46.64; H, 3.99; N, 12.02.

$(Ph_2B(pz)_2)Pt(Me)(CO)$ (A.8). Solid **A.4** (0.0480 g, 0.0625 mmol) was dissolved in tetrahydrofuran (2 mL) under N_2 in a 25 mL Schlenk flask equipped with a rubber septum. CO was bubbled through the solution using a long needle for 2 minutes. To this was added a solution of $[HN^{i\text{-}}Pr_2Et][BPh_4]$ (0.278 g, 0.0619 mmol) in tetrahydrofuran (3 mL) via syringe. The solution immediately turned yellow upon addition of the ammonium salt, but slowly faded to a cloudy white slurry over a period of 5 minutes. Solvent was removed in vacuo. The resulting solids were extracted with benzene (3 x 2 mL) and filtered through Celite. Solvent was removed from the filtrate to yield white solids (85%). ^{1}H NMR (300 MHz benzene-d_6): δ = 7.44 (m, 2H, pz-3H), δ = 7.33 (m, 2H, pz-5H), δ = 7.24 (m, 4H, *o*-Ph), δ = 7.23 (m, 4H, *m*-Ph), 7.07 (m, 2H, *p*-Ph), 5.87 (m, 1H, $^3J_{H\text{-}H}$ = 2.1 Hz, pz-4H), 5.77 (t, 1H, $^3J_{H\text{-}H}$ = 1.5 Hz, pz-4H), 0.79 (s, 3H, $^2J_{Pt\text{-}H}$ = 70.2 Hz, Pt-Me). IR (cm^{-1}): 2087. Anal. Calcd. for $C_{20}H_{19}BN_4OPt$: C, 44.71; H, 3.56; N, 10.43.

Found: C, 46.59; H, 3.58; N, 11.02. Samples of this species repeatedly analyzed high in carbon content.

($Ph_2B(pz)_2$)Pt(Me)($P(C_6F_5)_3$) (A.9). Solid **A.4** (0.0347 g, 0.0452 mmol), solid [$HN^{i}Pr_2Et$][BPh_4] (0.0271 g, 0.0603 mmol), and solid $P(C_6F_5)_3$ (0.0449 g, 0.0844 mmol) were suspended in tetrahydrofuran (2 mL) and stirred for 30 minutes. The solvent was removed from the resulting mixture in vacuo. The remaining solids were extracted with benzene/petroleum ether (10:1) and filtered through Celite. These extracts were dried in vacuo, and the resulting off-white solids were extracted into petroleum ether and recrystallized at -35 ºC. The resulting white solids were washed with cold petroleum ether (1 mL) (42.4%). ^{1}H NMR (300 MHz, benzene-d_6): δ = 7.47 (d, 1H, $^3J_{H\text{-}H}$ = 2.1 Hz, pz-3H), 7.42 (d, 2H, $^3J_{H\text{-}H}$ = 2.1 Hz, pz-3H, pz-5H), 7.32 (m, 4H, *o*-Ph), 7.21-7.27 (m, 6H, *m,p*-Ph), 6.50 (d, 1H, $^3J_{H\text{-}H}$ = 1.8 Hz, pz-5H), 5.78 (m, 1H, pz-4H), 5.53 (t, 1H, $^3J_{H\text{-}H}$ = 2.4 Hz, pz-4H), 0.36 (d, 3H, $^2J_{Pt\text{-}H}$ = 72 Hz, $^3J_{P\text{-}H}$ = 6.0 Hz, Pt-Me). ^{31}P NMR (121.368 MHz, benzene-d_6): δ = -36.21 (s, $^1J_{Pt\text{-}P}$ = 5800 Hz). ^{13}C NMR (75.409 MHz, benzene-d_6): δ = 150.0 (m, $P(C_6F_5)_3$), 146.6 (m, $P(C_6F_5)_3$), 142.8 (m, $P(C_6F_5)_3$), 140.1, 139.8, 139.3, 138.9, 137.5, 133.4, 127.1, 105.4, 104.8, -14.9 (Pt-Me). Anal. Calcd. for $C_{37}H_{19}BF_{15}N_4PPt$: C, 42.67; H, 1.84; N. 5.38. Found: C, 42.50; H, 2.07; N, 5.06.

((4-BPh_3)bpy)Pt(Me)($NCCH_3$) (A.10). Solid **A.5** (0.0481 g, 0.0557 mmol) was stirred in THF with [$HNEt_3$][BPh_4] (0.0234 g, 0.0557 mmol). To this mixture was added 3 drops of acetonitrile. After 1 hour, the solvent was evaporated in vacuo. The resulting solids were extracted into benzene (2 x 10 mL). These extracts were dried in vacuo to yield both isomers in a 2.8:1 ratio (0.0286 g, 0.0440 mmol, 79%). ^{1}H NMR (300 MHz, acetone-d_6): δ = 8.91 (d, 1H, $^3J_{H\text{-}H}$ = 8.7 Hz, 6-bpy), 8.41 (d, 1H, $^3J_{H\text{-}H}$ = 5.4 Hz, 6'-bpy), 8.31 (br s,

1H, 3-bpy), 8.21 (ddd, 1H, $^{3}J_{H\text{-}H}$ = 8.4, 3.0, 1.2 Hz, 4'-bpy), 7.92 (d, 1H, $^{3}J_{H\text{-}H}$ = 9.0 Hz, 3'-bpy), 7.66 (m, 2H, 5-bpy, 5'-bpy), 7.32 (m, 6H, *o*-Ph), 7.03 (t, 6H, $^{3}J_{H\text{-}H}$ = 7.2 Hz, *m*-Ph), 6.90 (m, 3H, $^{3}J_{H\text{-}H}$ = 7.2 Hz, *p*-Ph), 2.79 (major) / 2.84 (minor) (s, 3H, $NCCH_3$, $^{4}J_{Pt\text{-}H}$ = 25 Hz), 0.94 (major) / 0.86 (minor) (s, 3H, Pt-Me, $^{2}J_{Pt\text{-}H}$ = 73 Hz). ^{13}C NMR for major isomer (75.409 MHz, acetone-d_6): δ = 161.7, 160.5 (br), 156.4, 148.8, 145.8, 141.3, 136.9, 135.9, 132.1, 128.1, 127.5, 124.1, 123.5, 41.4, 4.5, - 14.0 (Me). Anal. Calcd. for $C_{31}H_{28}BN_3Pt$: C, 57.42; H, 4.35; N. 6.48. Found: C, 57.17; H, 4.13; N, 5.99.

((4-BPh_3)bpy)Pt(Me)(CO) (A.11). Solid **A.5** (0.0356 g, 0.0412 mmol) was stirred in THF with $[HNEt_3][BPh_4]$ (0.0173 g, 0.0412 mmol). This mixture was placed under a blanket of CO and stirred for 1 hour. The solvent was evaporated in vacuo, and the resulting solids were extracted into benzene (2 x 10 mL). These extracts were dried *in vacuo* to yield both isomers in a 2.8:1 ratio (0.0227 g, 0.0357 mmol, 87%). ^{1}H NMR (300 MHz, CD_2Cl_2): δ = 8.65 (d, 1H, $^{3}J_{H\text{-}H}$ = 5.7 Hz, $^{3}J_{Pt\text{-}H}$ = 21 Hz, 6-bpy), 8.52 (br s, 1H, 3-bpy), 8.32 (d, 1H, $^{3}J_{H\text{-}H}$ = 5.7 Hz, $^{3}J_{Pt\text{-}H}$ = 33 Hz, 6'-bpy), 8.12 (ddd, 1H, $^{3}J_{H\text{-}H}$ = 8.3, 8.3, 1.5 Hz 4'-bpy), 8.01 (d, 1H, $^{3}J_{H\text{-}H}$ = 8.4 Hz, 3'-bpy), 7.56 (m, 1H, 5-bpy), 7.32 (m, 7H, *o*-Ph, 5'-bpy), δ = 7.13 (t, 6H, $^{3}J_{H\text{-}H}$ = 7.2 Hz, *m*-Ph), δ = 7.00 (m, 3H, $^{3}J_{H\text{-}H}$ = 7.2 Hz, *p*-Ph), (major) / (minor) 1.27 / 1.19 (s, 3H, Pt-Me, $^{2}J_{Pt\text{-}H}$ = 69 Hz). ^{13}C NMR for major isomer (75.409 MHz, CD_2Cl_2): δ = 192.0, 160.0 (br), 151.1, 143.1, 142.8, 141.5, 135.8, 135.4, 134.7, 131.6, 128.1, 127.1, 123.9, 123.7, - 12.3 (Me). IR (CH_2Cl_2) = 2098 cm^{-1}. Anal. Calcd. for $C_{30}H_{25}BN_2OPt$: C, 56.71; H, 3.97; N. 4.41. Found: C, 59.70; H, 4.02; N, 4.98. Samples of this species repeatedly analyzed high in carbon content.

[(bpy)Pt(Me)(CO)][BPh_4] (A.12). Solid (bpy)$Pt(Me)_2$ (0.0260 g, 0.0682 mmol) was stirred in THF, and CO was bubbled through the solution for 20 minutes. To this was

added a solution of $[HNEt_3][BPh_4]$ (0.0287 g, 0.0682 mmol) in THF. This mixture was allowed to stir under a blanket of CO for 1 hour. The solvent was evaporated in vacuo, and the resulting solids were washed with benzene (2 x 10 mL) and dried in vacuo to yield the yellow product (~80%). Spectroscopic data was similar to that reported previously for $[(bpy)Pt(Me)(CO)]^+$ cations.[10b] ^{1}H NMR (300 MHz, acetone-d_6): δ = 9.07 (d, 1H, $^3J_{H\text{-}H}$ = 9.0 Hz, 6-bpy), 8.98 (d, 1H, $^3J_{H\text{-}H}$ = 7.5 Hz, 6'-bpy), 8.66 (d, 1H, $^3J_{H\text{-}H}$ = 5.7 Hz, 3-bpy), 8.48 (m, 2H, 4'-bpy, 3'-bpy), 8.40 (m, 1H, 4'-bpy), 7.91 (m, 1H, 5-bpy), 7.40 (m, 1H, 5'-bpy), 7.33 (m, 8H, BPh_4), 6.92 (t, 8H, $^3J_{H\text{-}H}$ = 7.8 Hz, BPh_4), 6.77 (t, 4H, $^3J_{H\text{-}H}$ = 6.9 Hz, BPh_4), 1.28 (s, 3H, Pt-Me, $^2J_{Pt\text{-}H}$ = 68 Hz). ES-MS (*m/z)*: 394 $[M]^+$. IR (CH_2Cl_2) = 2107 cm^{-1}.

Generation of $[(Ph_2B(pz)_2)Pt(C_6D_5)_2][NBu_4]$ (A.13). Solid **A.4** (0.0345 g, 0.0449 mmol) and solid $[HN^{i}Pr_2Et][BPh_4]$ (0.0200 g, 0.0045 mmol) were stirred in benzene-d_6 (2 mL) for 30 minutes. The resulting reaction mixture was filtered through Celite. Upon standing for 1 hour, solids precipitated. These off-white solids were collected and washed with petroleum ether (3 x 2 mL) and benzene (2 x 2 mL). The remaining solids were dried further *in vacuo* to yield clean product (87% yield was detected by NMR using a ferrocene standard; however, only 40% was isolated). Crystals were grown for X-ray diffraction by dissolving product in benzene and layering with petroleum ether at room temperature. ^{1}H NMR (300 MHz, benzene-d_6): δ = 7.58 (d, 2H, $^3J_{H\text{-}H}$ = 2.7 Hz, pz-3H), 7.19 (m, 4H, $^3J_{H\text{-}H}$ = 6.6 Hz, *o*-BPh), 7.40 (t, 4H, $^3J_{H\text{-}H}$ = 7.2 Hz, *m*-BPh), 7.31 (m, 2H, *p*-BPh), 7.28 (d, 2H, $^3J_{H\text{-}H}$ = 1.2 Hz, pz-5H), 5.92 (t, 2H, $^3J_{H\text{-}H}$ = 2.1 Hz, pz-4H), 1.73 (br m, 8H, NBu_4), 0.89 (m, 8H, NBu_4), 0.77 (t, 12H, $^3J_{H\text{-}H}$ = 7.8 Hz, NBu_4), 0.66 (m, 8H, NBu_4). ^{13}C NMR (75.409 MHz, acetone-d_6): δ = 150 (br), 142(br), 141.3, 140(br), 136.4(br),

135.6, 134.9, 127.1, 126.1, 103.0, 59.2 (NBu_4), 24.4 (NBu_4), 20.4 (NBu_4), 13.9 (NBu_4). ES-MS(-) (*m/z)*: 648[M]. Anal. Calcd. for $C_{46}H_{52}D_{10}BN_5Pt$: C, 61.32; H, 8.05; N, 7.77. Found: C, 61.66; H, 6.84; N, 8.13. Alternatively, **5** can be prepared by (a) using 0.1 equivalents $[HN^{i}Pr_2Et][BPh_4]$, but reaction time must be lengthened from 30 minutes to 48 hrs; (b) using $[H(OEt_2)_2][B(C_6H_3(CF_3)_2)_4]$ in place of $[HN^{i}Pr_2Et][BPh_4]$; (c) using $B(C_6F_5)_3$ in place of $[HN^{i}Pr_2Et][BPh_4]$. Using 0.05 equivalents of $B(C_6F_5)_3$ and using 1.0 equivalents results in nearly identical reaction time and yield.

$(Ph_2B(pz)_2)Pt(C_6D_5)(NCCH_3)$ (A.14). Solid **A.4** (0.0366 g, 0.0477 mmol) and solid $[HN^{i}Pr_2Et][BPh_4]$ (0.0223 g, 0.0496 mmol) were dissolved in benzene-d_6 (2 mL). Three drops of acetonitrile were added, and the mixture was stirred for 1 hour. The resulting solution was filtered through Celite, and the filtrate was dried *in vacuo*. The resulting solids were extracted into petroleum ether and dried *in vacuo* to yield spectroscopically pure product as an off-white solid (~80%). ^{1}H NMR (300 MHz, benzene-d_6): δ = 7.58 (d, 1H, $^3J_{H\text{-}H}$ = 2.4 Hz, pz-3H), 7.45 (m, 2H, pz-3H, pz-5H), 7.28-7.36 (m, 5H, *o*-Ph, pz-5H), 7.18 (t, 4H, $^3J_{H\text{-}H}$ = 7.2 Hz, *m*-Ph), 7.06 (t, 2H, $^3J_{H\text{-}H}$ = 9.3 Hz, *p*-Ph), 6.09 (t, 1H, $^3J_{H\text{-}H}$ = 2.1 Hz, pz-4H), 5.63 (t, 1H, $^3J_{H\text{-}H}$ = 2.2 Hz, pz-4H), -0.02 (s, 3H, $^4J_{Pt\text{-}H}$ = 7.2 Hz, Pt-$NCCH_3$). ^{13}C NMR (75.409 MHz, benzene-d_6): δ = 144.2, 139.9, 138.5, 138.2, 137.7, 137.2, 135.0, 127.7, 127.3, 124.2, 104.8 (pz-4), 30.8 ($N\underline{C}CH_3$), 1.3 ($NC\underline{C}H_3$). Anal. Calcd. for $C_{26}H_{19}D_5BN_5Pt$: C, 50.58; H, 4.73; N, 11.34. Found: C, 50.72; H, 4.16; N, 11.17.

Reaction of complex A.4 with $[HNEt_3][BPh_4]$ in toluene and *p*-xylene. Solid **A.4** (0.0657 g, 0.0885 mmol) was stirred in toluene (or *p*-xylene) (10 mL) for 3 hours with $[HN^{i}PrEt_2][BPh_4]$ (0.0398 g, 0.0886 mmol). The resulting solution was filtered through

Celite, and the filtrate was then dried *in vacuo*. Solution NMR data revealed the following diagnostic signals: *toluene*: ^{1}H NMR (300 MHz, benzene-d_6): δ = 3.24 (s, $^{2}J_{Pt\text{-}H}$ = 99 Hz, benzylic activation), 2.36, 2.31, 2.24 (aryl activation products, *o*, *p*, *m*, respectively); *p-xylene*: ^{1}H NMR (300 MHz, acetone-d_6): δ = 2.90 (s, $^{2}J_{Pt\text{-}H}$ = 104 Hz, benzylic activation).

($Ph_2B(pz)_2$)Pt(pzH)($CH_2C_6H_3(CH_3)_2$) (A.15). Solid **A.4** (0.0115 g, 0.0149 mmol) was stirred in mesitylene (2 mL) for 18 hours with [$HNEt_3$][BPh_4] (0.0066 g, 0.0153 mmol). Volatiles were removed from the resulting solution *in vacuo*. The remaining solids were extracted with benzene (3 x 1 mL) and filtered through Celite. The filtrate was dried *in vacuo* to yield **A.15** as a white solid (~50%). Crystals of **A.15** suitable for X-ray diffraction were obtained by vapor diffusion of petroleum ether into a concentrated benzene solution. ^{1}H NMR (300 MHz, benzene-d_6): δ = 12.5 (br, 1H), 7.79 (d, 1H, $^{3}J_{H\text{-}H}$ = 1.8 Hz, pz-3H), 7.58 (d, 1H, $^{3}J_{H\text{-}H}$ = 2.4 Hz, pz-3H), 7.49 (d, $^{3}J_{H\text{-}H}$ = 2.1 Hz, 1H, pz-3H), 7.07-7.26 (m, 10H, BPh), 6.88 (m, 1H, Mes), 6.65 (m, 1H, pz-5H), 6.58 (m, 1H, pz-5H), 6.43 (m, 2H, Mes), 6.03 (m, 1H, pz-5H), 5.96 (t, 1H, $^{3}J_{H\text{-}H}$ = 2.1 Hz, pz-4H), 5.87 (t, $^{3}J_{H\text{-}H}$ = 2.1 Hz, 1H, pz-4H), 5.36 (m, 1H, pz-4H), 3.07 (s, 2H, C$\underline{H}_2$, $^{2}J_{Pt\text{-}H}$ = 104.9 Hz), 2.13 (s, 6H, CH_3). XRD analysis confirmed the identity of this degradation product. Further characterization of this material was not pursued.

A.3.4 X-ray Experimental Data

Crystallographic procedures are outlined in Section 2.4.6. Crystallographic data are summarized in Table A.3.

Table A.3. Crystallographic Data for [($Ph_2B(pz)_2$)Pt($Me)_2$][NBu_4], **A.4**; [((4-BPh_3)bpy)Pt($Me)_2$][NBu_4]**,** **A.5**; [($Ph_2B(pz)_2$)Pt($C_6D_5)_2$][NBu_4], **A.13;** and ($Ph_2B(pz)_2$)Pt(pzH)($CH_2C_6H_3(CH_3)_2$), **A.15.**

	A.4	**A.5**	**A.13**	**A.15**
chemical formula	$C_{36}H_{58}BN_5Pt$	$C_{46}H_{64}BN_3Pt$	$C_{46}H_{62}BN_5Pt$	$C_{33}H_{39}BN_4Pt$
Fw	766.77	864.90	890.91	697.58
T (˚C)	-177	-173	-177	-175
λ (Å)	0.71073	0.71073	0.71073	0.71073
a (Å)	9.7813(6)	9.0567(14)	14.8387(11)	8.2302(7)
b (Å)	23.2181(14)	11.888(3)	17.0287(13)	14.2054(11)
c (Å)	15.7888(9)	20.348(6)	17.1175(13)	14.6026(11)
α (deg)	90	87.714(14)	90	67.3000(10)
β (deg)	92.1140(10)	84.19(2)	103.0870(10)	74.0560(10)
γ (deg)	90	70.316	90	82.5650(10)
V (Å^3)	3583.2(4)	2052.2(8)	4213.0(6)	1513.9(2)
space group	$P2_1/c$	$P\bar{1}$	$P2_1/c$	$P\bar{1}$
Z	4	2	4	2
D_{calcd} (g/cm^3)	1.421	1.400	1.824	1.530
μ (cm^{-1})	3.947	3.453	3.368	4.662
R1, wR2[a] ($I > 2\sigma(I)$)	0.0299, 0.0721	0.0427, 0.0724	0.0306, 0.0509	0.0306, 0.0713

[a] $R1 = \Sigma \, ||F_o| - |F_o|| \, / \, \Sigma \, |F_o|$, $wR2 = \{\Sigma[w(F_o^2 - F_c^2)_2]/\Sigma[w(F_o^2)^2]\}^{1/2}$.

References Cited

[1] (a) Ittel, S. D.; Johnson, L. K.; Brookhart, M. *Chem. Rev.* **2000**, *100*, 1169-1203. (b) Beletskaya, I. P.; Cheprakov, A. V. *Chem. Rev.* **2000**, *100*, 3009-3066. (c) Crabtree, R. H. *Acc. Chem. Res.* **1979**, *12*, 331-337. (d) Schrock, R. R.; Osborn, J. A. *J. Am. Chem. Soc.* **1971**, *93*, 3089-3091.

[2] For recent discussions of C-H bond activation and functionalization mediated by cationic metal centers, see: (a) Lersch, M.; Tilset, M. *Chem. Rev.* **2005**, *105*, 2471-2526. (b) Arndtsen, B. A.; Bergman, R. G.; Mobley, T. A.; Peterson, T. H. *Acc. Chem. Res.*

1995, *28*, 154-162. (c) Sen, A. *Acc. Chem. Res.* **1998**, *31*, 550-557. (d) Stahl, S. S.; Labinger, J. A.; Bercaw, J. E. *Angew. Chem. Int. Ed.* **1998**, *37*, 2181-2192. (e) Crabtree, R. H. *J. Chem. Soc., Dalton Trans*. **2001**, 2437-2450. (f) Shilov, A. E.; Shul'pin, G. B. *Activation and Catalytic Reactions of Saturated Hydrocarbons in the Presence of Metal Complexes;* Kluwer: Boston, 2000.

[3] (a) Thomas, J. C.; Peters, J. C. *J. Am. Chem. Soc.* **2001,** *123*, 5100-5101. (b) Betley, T. A.; Peters, J. C. *Inorg. Chem.* **2002,** *41*, 6541-6543. (c) Thomas, J. C.; Peters, J. C. *J. Am. Chem. Soc.* **2003**, *125,* 8870-8888. (d) Thomas, J. C.; Peters, J. C. *Inorg. Chem.* **2003**, *42*, 5055-5073. (e) Betley, T. A.; Peters, J. C. *Angew. Chem., Int. Ed*. **2003**, *42*, 2385-2389. (f) Lu, C. C.; Peters, J. C. *J. Am. Chem. Soc.* **2002,** *124*, 5272-5273.

[4] See for example: (a) Rostovtsev, V. V.; Henling, L. M.; Labinger, J. A.; Bercaw, J. E. *Inorg. Chem.* **2002**, *41*, 3608-3619. (b) Rostovtsev, V. V.; Labinger, J. A.; Bercaw, J. E. *Organometallics* **1998**, *17*, 4530-4531. (c) Rendina, L. M.; Puddephatt, R. J. *Chem. Rev.* **1997**, *97*, 1735-1754.

[5] See for example: (a) Fekl, U.; Goldberg, K. I. *J. Am. Chem. Soc.* **2002**, *124*, 6804-6805. (b) Stahl, S. S.; Labinger, J. A.; Bercaw, J. E. *J. Am. Chem. Soc.* **1996**, *118*, 5961-5976.

[6] (a) Reinartz, S.; White, P. S.; Brookhart, M.; Templeton, J. L. *J. Am. Chem. Soc.* **2001**, *123*, 12724-12725. (b) Lo, H. C.; Haskel, A.; Kapon, M.; Keinan, E. *J. Am. Chem. Soc.* **2002,** *124*, 3226-3228. (c) Reinartz, S.; White, P. S.; Brookhart, M.; Templeton, J. L. *J. Am. Chem. Soc.* **2001**, *123*, 6425-6426. (d) Reinartz, S.; White, P. S.; Brookhart, M.; Templeton, J. L. *Organometallics* **2000,** *19*, 3854-3866. (e) Wick, D. D.; Goldberg, K. I. *J. Am. Chem. Soc.* **1997**, *119*, 10235-10236. (f) Haskel, A.; Keinan, E. *Organometallics*

1999, *41*, 2808-2810. (f) Jensen, M. P.; Wick, D. D.; Reinartz, S.; White, P. S.; Templeton, J. L.; Goldberg, K. I. *J. Am. Chem. Soc.* **2003**, *125*, 8614.

[7] (a) Onishi, M.; Hiraki, K. *Inorganica Chimica Acta* **1994**, *224*, 131-135. (b) Clark, H. C.; von Werner, K. *J. Organometallic Chemistry* **1975**, *101*, 347-358. (c) Reger, D. L.; Baxter, J. C.; Lebioda, L. *Inorganica Chimica Acta* **1989**, *165*, 201-205.

[8] Periana, R. A.; Taube, D. J.; Gamble, S.; Taube, H.; Satoh, T.; Fujii, H. *Science* **1998**, *280*, 560-564.

[9] (a) Johansson, L.; Tilset, M.; Labinger, J. A.; Bercaw, J. E. *J. Am. Chem. Soc.* **2000**, *122*, 10846-10855. (b) Johansson, L.; Ryan, O. B.; Romming, C.; Tilset, M. *J. Am. Chem. Soc.* **2001**, *123*, 6579-6590. (c) Johansson, L.; Tilset, M. *J. Am. Chem. Soc.* **2001**, *123*, 739-740. (d) Zhong, H. A.; Labinger, J. A.; Bercaw, J. E. *J. Am. Chem. Soc.* **2002**, *124*, 1378-1399.

[10] See for example : (a) Klein, A.; van Slageren, J.; Zalis, S. *Eur. J. Inorg. Chem.* **2003**, 1927-1938. (b) Doppiu, A.; Cinellu, M. A.; Minghetti, G.; Stoccoro, S.; Zucca, A.; Manassero, M.; Sansoni, M. *Eur. J. Inorg. Chem.* **2000**, 2555-2563. (c) Bayler, A.; Canty, A. J.; Skelton, B. W.; White, A. H. *J. Organomet. Chem.* **2000**, *595*, 296-299. (d) Hill, G. S.; Rendina, L. M.; Puddephatt, R. J. *Organometallics* **1995**, *14*, 4966-4968. (e) Chaudhury, N.; Puddephatt, R. J. *J. Organomet. Chem.* **1975**, *84*, 105-115. (f) Achar, S.; Catalano, V. J. *Polyhedron*, **1997**, *16*, 1555-1561. (g) Hill, G. S.; Manojlovic-Muir, L.; Muir, K.; Puddephatt, R. J. *Organometallics*, **1997**, *16*, 525-530.

[11] (a) Hill, R. H.; Puddephatt, R. J. *J. Am. Chem. Soc.* **1985***, 107*, 1218-1225. (b) Crespo, M.; Puddephatt, R. J. *Organometallics* **1987**, *6*, 2548-2550. (c) Kuyper, J. *Inorg. Chem.* **1978**, *17*, 1458-1463. (d) Kuyper, J. *Inorg. Chem.* **1977**, *16*, 2171-2176. (e) Kuyper, J. *Inorg. Chem.* **1978**, *17*, 77-81. (f) Levy, C. J.; Puddephatt, R. J. *J. Am. Chem. Soc.* **1997**, *119*, 10127-10136.

[12] (a) Minghetti, G.; Stoccoro, S.; Cinellu, M. A.; Soro, B.; Zucca, A. *Organometallics* **2003**, *22*, 4770-4777. (b) Zucca, A.; Stoccoro, S.; Cinellu, M. A.; Minghetti, G.; Manassero, M.; Sansoni, M. *Eur. J. Inorg. Chem.* **2002**, 3336-3346. (c) Zucca, A.; Doppiu, A.; Cinellu, M. A.; Stoccoro, S.; Minghetti, G.; Manassero, M. *Organometallics* **2002**, *21*, 783-785. (d) Minghetti, G.; Cinellu, M. A.; Stoccoro, S.; Zucca, A.; Manassero, M. *J. Chem. Soc., Dalton Trans.* **1995**, *5*, 777-781.

[13] Aspects of this work have been briefly described in an ACS Symposium Series contribution: Peters, J. C.; Thomas, J. C.; Thomas, C. M.; Betley, T. A. *Activation and Functionalization of C-H Bonds*; K. Goldberg and A. Goldman, eds.; ACS Symposium Series No. 885, **2004**, Ch. 20, 334-354.

[14] Trofimenko, S. *J. Am. Chem. Soc.* **1967**, *89*, 6288-6293.

[15] (a) Wenkert, D.; Woodward, R. B. *J. Org. Chem.* **1983**, *48*, 283-289. (b) Sprecher, M.; Breslow, R.; Uziel, O.; Link, T. M. *OPPI Briefs* **1994**, *26*, 696-701.

[16] Jenkins, D. M.; DiBilio, A. J.; Allen, M. J.; Betley, T. A.; Peters, J. C. *J. Am. Chem. Soc.* **2002**, *124*, 15336-15350.

[17] (a) Goldman, A. S.; Krogh-Jespersen, K. *J. Am. Chem. Soc.* **1996**, *118*, 12159-12166. (b) Caulton, K. G.; Fenske, R. F. *Inorg. Chem.* **1968**, *7*, 1273-1284. (c) Hush, N. S.; Williams, M. I. *J. Mol. Spectrosc.* **1974**, *50,* 349-368.

[18] Wik, B. J.; Lersch, M.; Tilset, M. *J. Am. Chem. Soc.* **2002**, *124*, 12116-12117.

[19] Johannson, L.; Tilset, M. *J. Am. Chem. Soc.* **2001**, *123*, 739-740.

[20] Reinhartz, S.; White, P. S.; Brookhart, M.; Templeton, J. L. *Organometallics* **2001**, *20,* 1709-1712.

[21] (a) Hill, G. S.; Manojlovic-Muir, L.; Muir, K. W.; Puddephatt, R. J. *Organometallics* **1997**, *16*, 525-540. (b) Hill, G. S.; Rendina, L. M.; Puddephatt. R. J. *J. Chem. Soc., Dalton Trans.* **1996,** 1809.

[22] Jones, W. D. *Acc. Chem. Res.* **2003**, *36,* 140-146.

[23] (a) Heyduk, A. F.; Driver, T. G.; Labinger, J. A.; Bercaw, J. E. *J. Am. Chem. Soc.* **2004**, *126*(46), 15034-15035. (b) Heyduk, A. F.; Zhong, A. H.; Labinger, J. A.; Bercaw, J. E. *Activation and Functionalization of C-H Bonds*; K. Goldberg and A. Goldman, eds.; ACS Symposium Series No. 885, **2004**, 250-263.

[24] Scott, J. D.; Puddephatt, R. J. *Organometallics* **1983**, *2*, 1643-1648.

[25] Rodima, T.; Kaljurand, I.; Pihl, A.; Maeemets, V.; Leito, I.; Koppel, I. A. *J. Org. Chem.* **2002**, *67*(6), 1873-1881.

[26] Kemmitt, R. D. W.; Nichols, D. I.; Peacock, R. D. *J. Am. Chem. Soc. A.* **1968**, 2149-2152.

[27] Brookhart, M.; Grant, B.; Volpe, A. F., Jr. *Organometallics* **1992**, *11,* 3920.

[28] Monaghan, P. K.; Puddephatt, R. J. *Organometallics* **1984**, *3*, 444-449.

Appendix B: Coordinating Anions: (Phosphino)tetraphenylborate Ligands as New Reagents for Synthesis

The text in this chapter is reproduced in part with permission from:

Thomas, C. M.; Peters, J. C. *Inorg. Chem.* **2004,** *43,* 8.

B.1 Introduction

Whereas monodentate neutral phosphine ligands find utility in nearly all areas of chemical synthesis,[1] comparatively little attention has been devoted to structurally related anionic derivatives. The diphenylphosphidoboratabenzene ligand of Fu provides one of the noteworthy exceptions.[2] This system features a triphenylphosphine-type ligand rendered anionic by a boratabenzene subunit, the latter of which has itself been offered as an intriguing cyclopentadienyl alternative.[3] Given the growing interest in sterically demanding, electron-releasing phosphines (and carbenes) for homogeneous catalysis,[4] access to electron-rich, anionic phosphines would provide a timely complement to these increasingly popular ligands. One conceptual way to generate such species, while at the same time preserving desirable properties inherent to tertiary phosphines, is to embed a borate counteranion within the phosphine donor framework. This approach has already found utility with respect to developing catalytically active, zwitterionic organometallic species.[5] In this chapter, we introduce a new series of monodentate phosphines templated upon the tetraphenylborate anion and briefly discuss aspects of their stability, their transition-metal binding affinity, their comparative electron-releasing character, and their potential as reagents for organic synthesis.

B.2 Results and Discussion

The delivery of lithiated carbanions of methyldiarylphosphines (i.e., $LiCH_2PAr_2$) and methyldialkylphosphines (i.e., $LiCH_2PR_2$) to borane electrophiles in the preparation of tri- and bidentate (phosphino)borates has been explored.[6] For example, addition of 3 equiv of $LiCH_2P^iPr_2$ to $PhBCl_2$ provides the tridentate anion $[PhB(CH_2P^iPr_2)_3]^-$,[6a] whereas addition of 2 equiv of $LiCH_2P^iPr_2$ to Ph_2BCl provides the bidentate anion

$[Ph_2B(CH_2P^iPr_2)_2]^-$.[6b] A similar protocol exploiting triphenylborane as the electrophile of choice provides related monodentate ligands. For example, the addition of $(TMEDA)LiCH_2PPh_2$ to BPh_3 generates $[(TMEDA)Li][Ph_2PCH_2BPh_3]$ (**B.1**) in good yield.

An alternative and potentially more general strategy is to exchange the methylene linker for an aryl linker. This latter approach in effect provides a tetraarylborate counteranion featuring a coordinating phosphine donor. As a number of known halo-substituted arylphosphines are precursors to lithio arylcarbanions,[7] a diverse family of anionic phosphines can be envisioned. Several *meta*- and *para*-substituted bromoarylphosphines (**B.2-B.5**) were prepared to examine this approach (Scheme B.1).

Scheme B.1:

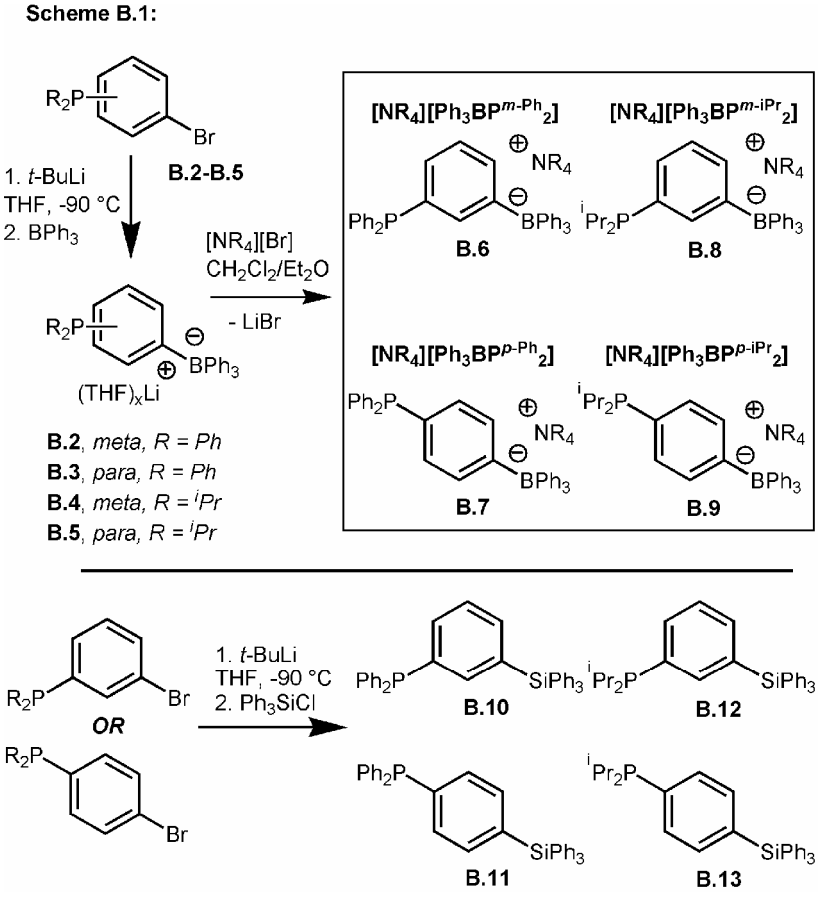

Reaction of the para- and meta-substituted bromoarylphosphines with a single equivalent of *t*-BuLi (-90 °C, THF) generated the required arylcarbanions. The solutions were subsequently quenched by low temperature addition of triphenylborane. This protocol afforded reasonably high crude yields (>70%) of the desired (phosphino)borate species, as ascertained by ^{11}B and ^{31}P NMR spectroscopy. These lithium species were converted *in situ* to their more conveniently isolated ammonium salt derivatives, **B.6**-**B.9**, by salt exchange with $[NR_4][Br]$ in dichloromethane solution (NR_4 = NBu_4, NEt_4, and ASN = 5-azonia-spiro[4.4]nonane). The solid-state structures of the ammonium salts of **B.6** and **B.8** (Figure B.1) establish the structural integrity of these borates and compare well with structural data for related neutral phosphines (e.g., PPh_3 and Ph^iPr_2P).[8] For comparative purposes, the isostructural neutral silane ligands were also prepared (Scheme B.1) via low temperature generation of the arylcarbanion (as above) and subsequent quenching with triphenylsilyl chloride. This procedure afforded consistently high crude yields (> 90% by ^{31}P NMR) of the desired (phosphino)silanes (**B.10**-**B.13**).

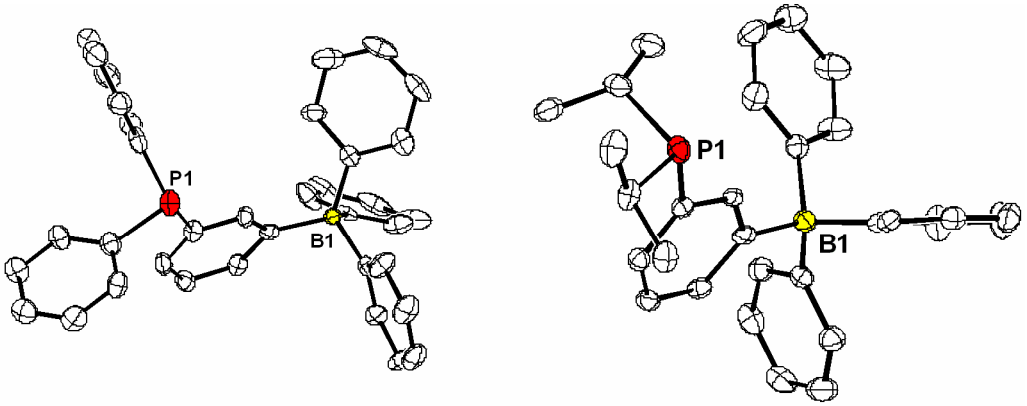

Figure B.1. Displacement ellipsoid representations (50%) of **B.6** (left) and **B.8** (right). Both phosphines were crystallized as ammonium salt derivatives (cations omitted).

The anionic phosphine salts **B.6**-**B.9** are appreciably soluble in alcohols (e.g., EtOH), acetonitrile, tetrahydrofuran, chlorinated solvents, and acetone.[9] Their stability in $CHCl_3$ and CH_2Cl_2 is distinct from those of **B.1** and related methylene-bridged (phosphino)borates, which tend to degrade rather rapidly in such solvents.[6b] Moreover, ligands **B.6**-**B.9** proved very stable to both air oxidation and hydrolysis. For example, **B.6**-**B.9** afforded no discernible oxidation products (^{31}P NMR) over a period of 2 weeks under an atmosphere of air in acetone solution. This stability again contrasts that of methylene-bridged **B.1**, which was oxidized very rapidly by air in acetone solution, and also underwent gradual hydrolysis to release $MePPh_2$ upon exposure to water.

To benchmark the binding affinity of ligands **B.6**-**B.9**, their reactivity with $\{(NBD)RhCl\}_2$ and $(COD)PtMe_2$ (COD = cyclooctadiene, NBD = norbornadiene) was surveyed. Addition of **B.9** as a tetra-*n*-butylammonium salt to $\{(NBD)RhCl\}_2$ provided the molecular salt $\{^nBu_4N\}\{[Ph_3BP^{p\text{-}i\text{Pr}}{}_2]RhCl(NBD)\}$ (**B.14**), whose solid-state structure is shown in Figure B.2. This anion is a promising precursor to zwitterionic rhodium species upon formal release of $[^nBu_4N][Cl]$. Indeed, addition of $[Tl][PF_6]$ precipitates TlCl instantly to give a benzene soluble species with a single resonance in the ^{31}P NMR ($^1J_{Rh\text{-}P}$ = 166 Hz). The ligands **B.6**, **B.7**, and **B.8** also reacted with $\{(NBD)RhCl\}_2$ to give analogous salt products. With respect to platinum, addition of 2 equiv of an ammonium salt of **B.6**-**B.9** to $(COD)PtMe_2$ afforded in each case disubstitution and the *cis* isomer exclusively: $\{ASN\}_2\{(Ph_3BP^{m\text{-}Ph}{}_2)_2\text{-}PtMe_2\}$ (**B.15**), $\{NBu_4\}_2\{[Ph_3BP^{p\text{-}Ph}{}_2]_2PtMe_2\}$ (**B.16**), $\{NBu_4\}_2\{[Ph_3BP^{m\text{-}i\text{Pr}}{}_2]_2PtMe_2\}$ (**B.17**), and $\{NBu_4\}_2\{[Ph_3BP^{p\text{-}i\text{Pr}}{}_2]_2PtMe_2\}$ (**B.18**).[11] The ^{31}P NMR shifts and coupling constants of complexes **B.15** and **B.16** (28.63, ppm, $^1J_{Pt\text{-}P}$ = 1947 Hz; and 27.47 ppm, $^1J_{Pt\text{-}P}$ = 1935 Hz, respectively) compare well with

literature values for *cis*-$(PPh_3)_2PtMe_2$ (27.7 ppm, $^1J_{Pt\text{-}P}$ = 1900 Hz).[10,11] The isopropyl derivatives **B.17** and **B.18** are shifted further downfield in their ^{31}P NMR spectra (38.11 ppm, $^1J_{Pt\text{-}P}$ = 1900 Hz and 36.53 ppm, $^1J_{Pt\text{-}P}$ = 1917 Hz, respectively). An XRD study of crystals of **B.15** confirmed its *cis* coordination (Figure B.2).

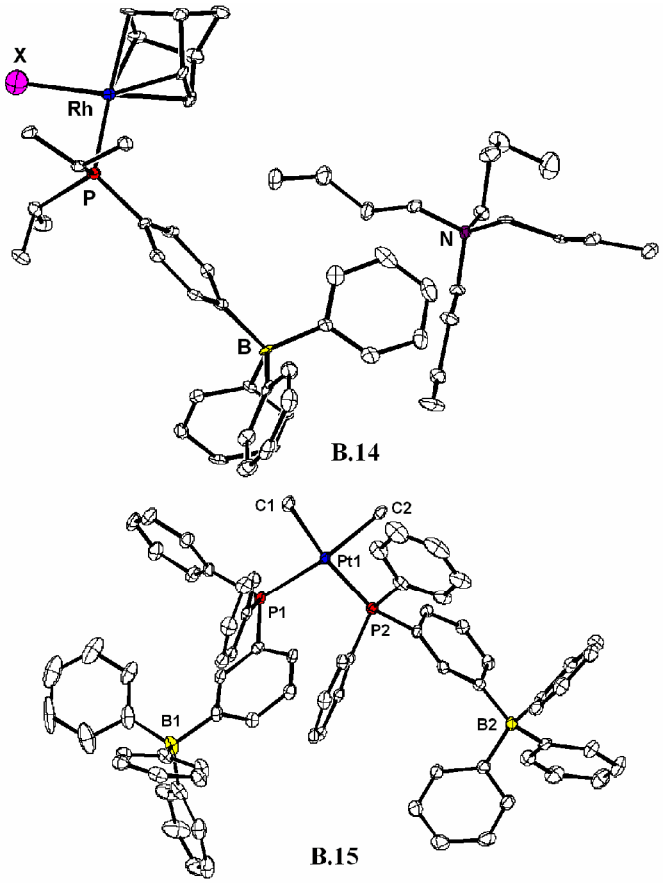

Figure B.2. Displacement ellipsoid representations (50%) of **B.14** (top) and **B.15** (bottom). The two ASN countercations of **B.15** have been omitted for clarity.

The dianionic species **B.15-B.18** are highly reactive toward both Brønsted and Lewis acids in THF and acetonitrile solution. For example, stoichiometric addition of $B(C_6F_5)_3$ effected the rapid release of 1 equiv of $[NR_4][Me(B(C_6F_5)_3)]$ (^1H, ^{19}F NMR) to produce the corresponding *trans*, monoanionic solvento species $\{NR_4\}\{trans\text{-}[Ph_3BP']_2Pt(Me)(solv)\}$. *trans*-Disposition of the phosphine ligands was inferred from

the dramatic increase in the $^{1}J_{Pt\text{-}P}$ coupling constants and the single resonance observed in the ^{31}P NMR spectra. The isostructural but neutral dimethyl complexes ($Ph_3SiP^{p\text{-}iPr}{}_2)_2PtMe_2$ (**B.19**) and ($Ph_3SiP^{p\text{-}Ph}{}_2)_2PtMe_2$ (**B.20**) displayed quite distinct reactivity. For example, in the case of **B.19**, methide abstraction by $B(C_6F_5)_3$ required ca. 12 h and led to the *cis*-mono(solvento) species [*cis*-($Ph_3SiP^{p\text{-}Ph}{}_2)_2PtMe(solv)][$Me(B(C_6F_5)_3$] (**B.21**) exclusively as the kinetic product at RT. Slow isomerization of **B.21** to its thermodynamic *trans* isomer occurred over a period of days in solution. Given the steric similarity between ligands **B.9** and **B.13**, the apparently substantial rate difference displayed with respect to *cis* → *trans* isomerization in these mono-solvento adducts is striking and most likely electronic in origin. One plausible explanation is to suggest that the anionic ligand **B.9** exerts a greater *trans*-influence and thus labilizes solvent molecules in the *trans* position of the kinetic *cis*-phosphine product to a larger extent than for the neutral ligand **B.13**, thereby facilitating rapid isomerization.

As a final point of interest, we have briefly examined the ability of **B.6**-**B.9** to promote Suzuki cross-coupling reactions. Each ligand proved generally effective for the coupling of $PhB(OH)_2$ with typical aryliodide and arylbromide substrates. More interesting was the ability of these ligands to facilitate the cross-coupling of aryl chlorides since such substrates typically require electron-rich phosphine promoters.[12] Under conditions recently reported by Fu,[13] we found that [$^{n}Bu_4N$][$Ph_3BP^{m\text{-}iPr}{}_2$] (**B.8**) promoted the cross-coupling of the three substrates shown in Table B.1 in modestly good yield. For comparison, the isostructural but neutral ligand **B.12**, as well as the more conventional phosphine $P^{i}Pr_2Ph$, were screened and also found to give the cross-coupled products, albeit in yields that were reproducibly ~20% lower than the yields obtained

using **B.8**.[14] The appreciable difference in yields likely reflects the greater electron-releasing character of **B.8**. Assuming oxidative addition of the aryl chloride to be rate-limiting, an anionic $[LPd^0]^-$ fragment would be expected to undergo oxidative addition more rapidly than a neutral LPd^0 fragment.

Table B.1. Examination of the efficiency of ligands **B.8**, **B.12**, and $(i\text{-Pr})_2PPh$ to facilitate Suzuki cross-coupling between phenylboronic acid and *p*-chlorotoluene, *p*-chloroacetophenone, or 1,4-dichlorobenzene.

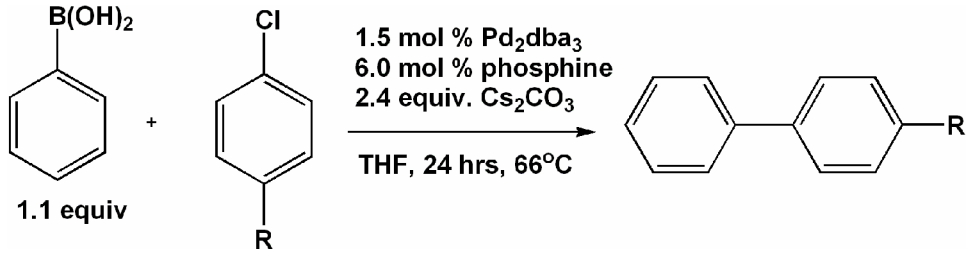

	Yield (%)[a]		
R	**L = B.8**	**L = B.12**	**L = $(i\text{-Pr})_2PPh$**
Me	71	56	49
Cl	68	43	43
COMe	74	38	49

[a] Isolated yields reported as the average of two runs.

Infrared model studies of ligands **B.8** and **B.12** are consistent with this latter suggestion. For example, refluxing a solution of either **B.8** or **B.12** in a THF solution of $Mo(CO)_6$ led, respectively, to the anionic pentacarbonyl complex $\{^nBu_4N\}\{[Ph_3BP^{m\text{-}i\text{Pr}}{}_2]Mo(CO)_5\}$ (**B.22**) and the neutral pentacarbonyl $(Ph_3SiP^{m\text{-}i\text{Pr}}{}_2)Mo(CO)_5$ (**B.23**), as confirmed by IR and ^{31}P NMR spectroscopy, as well as ES/MS. Infrared carbonyl vibrations for **B.22** were recorded at 2065 and 1925 cm^{-1}, whereas those for **B.23** were recorded at 2070 and 1942 cm^{-1}.[15,16] Both the high and low energy vibrations thus shift to

lower energy in the anionic system **B.22**, likely reflecting an appreciable increase in electron-releasing character of anionic **B.8** versus neutral **B.12**.

B.3 Experimental Section

B.3.1 General Considerations

Experimental procedures were carried out as described in 2.4.1.

B.3.2 Starting Materials and Reagents

(COD)$PtMe_2$,[1] (TMEDA)$LiCH_2PPh_2$,[2] and ASNBr[3] were prepared using literature methods. P(i-Pr)$_2$Ph was prepared by reaction of (i-Pr)$_2$PCl with PhMgBr in THF at -90 °C. (Bromophenyl)diphenylphosphine was prepared using a modification of the literature procedure as described below.[4] $B(C_6F_5)_3$ was purchased from Strem and recrystallized from pentane at -35 °C prior to use. All other chemicals were purchased from Aldrich, Strem, Alfa Aesar, or Lancaster and used without further purification.

B.3.3 Synthesis of Compounds

[(TMEDA)Li][$Ph_2PCH_2BPh_3$] (B.1). [Li(TMEDA)][CH_2PPh_2] (1.0364 g, 3.215 mmol) was dissolved in toluene (18 mL) and placed under an N_2 atmosphere. To this solution was added BPh_3 (0.778 g, 3.21 mmol) in toluene (10 mL) at -78 °C. Mixture was stirred and allowed to warm to room temperature slowly over a period of 2.5 hours. Volatiles were then removed in vacuo. Solids were re-dissolved in toluene (30 mL) followed by filtration through a Celite plug. Volatiles were removed from the filtrate in vacuo (~ 90 % crude yield by ^{31}P NMR). The product was recrystallized via vapor diffusion of petroleum ether into THF (~ 50 %). ^{1}H NMR (300 MHz, d_6-acetone): δ = 7.38 (m, 6H), 7.17 (m, 4H), 7.02 (m, 4H), 7.00 (m, 2H), 6.83 (m, 6H), 6.69 (m, 3H), 3.63 (m, 8H, THF), 1.89 (m, 2H, CH_2), 1.79 (m, 8H, THF). ^{13}C NMR (75.397 MHz, CH_3CN): δ =

135.13, 132.99, 132.78, 127.71, 126.62, 125.91, 122.18, 67.83, 25.80. ^{31}P NMR (121.475 MHz, d_6-acetone): -10.34 (s).

(3-Bromophenyl)diphenylphosphine (B.2). 1,3-dibromobenzene (11.0 g, 47.01 mmol) was dissolved in 150 mL dry, degassed THF and cooled to -95 ºC under nitrogen using an acetone/liquid nitrogen bath. ^{n}BuLi (1.6 M in hexane, 29.4 mL, 47.04 mmol) was added dropwise and the resulting cloudy solution was stirred at -95 ºC. After 1 hour chlorodiphenylphosphine (8.43 mL, 46.98 mmol) was added dropwise. The solution was allowed to warm to room temperature over the course of 2 hours and was then filtered through Celite in air. The resulting filtrate was dried in vacuo. The solids were then extracted with hexanes followed by filtration through a silica plug. Volatiles were removed in vacuo to afford a spectroscopically pure, moderately air-stable viscous oil (11.70 g, 74.0 %). ^{1}H NMR (300 MHz, d_6-acetone): δ = 7.56 (m, 1H), 7.41 (m, 4H), 7.25-7.40 (m, 9H), 7.35. ^{13}C NMR (75.397 MHz, CH_3CN): δ = 137.45, 136.55, 134.74, 133.25, 132.78, 131.61, 130.37, 129.92, 123.87. ^{31}P NMR (121.475 MHz, d_6-acetone): δ = -4.22 (s).

(4-Bromophenyl)diphenylphosphine (B.3). 1,4-dibromobenzene (3.05 g, 13.0 mmol) was dissolved in 75 mL dry, degassed THF and cooled to -95 ºC under nitrogen using an acetone/liquid nitrogen bath. ^{n}BuLi (1.6 M in hexane, 8.2 mL, 13.0 mmol) was added dropwise, and the resulting cloudy solution was stirred at -95 ºC. After 1 hour, chlorodiphenylphosphine (2.88 g, 13.0 mmol) was added dropwise. The solution was allowed to warm to room temperature over the course of 2 hours and was then filtered through Celite under air. The filtrate was then dried in vacuo. The resulting solids were extracted with hexanes followed by filtration through a silica plug. Volatiles were then

removed in vacuo to afford a spectroscopically pure, moderately air-stable viscous oil (3.060 g, 69 %). ^{1}H NMR (300 MHz, d_6-acetone): δ = 7.52 (m, 2H), 7.33-7.37 (m, 6H), 7.26 (m, 4H), 7.16 (m, 2H). ^{13}C NMR (75.397 MHz, THF): δ = 137.28, 137.04, 135.38, 133.72, 131.67, 128.66, 128.94, 123.26. ^{31}P NMR (121.475 MHz, d_6-acetone): δ = -5.70 (s).

(3-Bromophenyl)diisopropylphosphine (B.4). 1,3-dibromobenzene (4.2 g, 17.95 mmol) was dissolved in 150 mL dry, degassed THF and cooled to -95 ºC under nitrogen using an acetone/liquid nitrogen bath. ^{n}BuLi (1.6 M in hexane, 11.2 mL, 17.95 mmol) was added dropwise, and the resulting cloudy solution was stirred at -95 ºC. After 1 hour, chlorodiisopropylphosphine (2.8 mL, 17.7 mmol) was added dropwise. The solution was allowed to warm to room temperature over the course of 2 hours and was then filtered through Celite under a nitrogen atmosphere. The resulting filtrate was dried in vacuo and the remaining solids were extracted with petroleum ether followed by filtration through a silica plug. The volatiles were then removed in vacuo to afford the spectroscopically pure product as a viscous oil (2.95 g, 60.6 %). ^{1}H NMR (300 MHz, d_6-acetone): δ = 7.63 (m, 1H), 7.57 (m, 1H), 7.50 (m, 1H), 7.35 (t, 1H, J = 7.6Hz), 2.15 (m, 2H), 1.07 (m, 6H), 0.90 (m, 6H). ^{13}C NMR (75.397 MHz, THF): δ = 137.31, 134.95, 133.55, 132.24, 129.98, 122.87, 23.55, 20.20, 19.17. ^{31}P NMR (121.475 MHz, d_6-acetone): δ = 13.54 (s).

(4-Bromophenyl)diisopropylphosphine (B.5). 1,4-dibromobenzene (12.5 g, 53.42 mmol) was dissolved in 150 mL dry, degassed THF and cooled to -95 ºC under nitrogen using an acetone/liquid nitrogen bath. ^{n}BuLi (1.6 M in hexane, 33.3 mL, 53.28 mmol) was added dropwise, and the resulting cloudy solution was stirred at -95 ºC. After 1 hour, chlorodiisopropylphosphine (8.5 mL, 53.45 mmol) was added dropwise. The solution

was allowed to warm to room temperature over the course of 2 hours and was then filtered through Celite under a nitrogen atmosphere. The remaining filtrate was dried in vacuo, and the solids were extracted with petroleum ether followed by filtration through a silica plug. Solvent was removed in vacuo yielding the spectroscopically pure product as a viscous oil (12.03 g, 83.0 %). ^{1}H NMR (300 MHz, d_6-acetone): δ = 7.51 (m, 2H), 7.36 (m, 2H), 2.07 (m, 2H), 1.02 (m, 6H), 0.84 (m, 6H). ^{13}C NMR (75.397 MHz, THF): δ = 136.63, 134.92, 134.19, 131.42, 24.45, 20.23, 19.12. ^{31}P NMR (121.475 MHz, d_6-acetonitrile): δ = 15.75 (s).

[ASN][Ph$_3$BP$^{m\text{-Ph}}{}_2$] (B.6). *m*-Br$C_6H_4PPh_2$ (**B.2)** (0.734 g, 2.15 mmol) was dissolved in 75 mL of dry, degassed THF, and the stirring solution was cooled to -90 ºC. To this solution was added *tert*-BuLi (1.50 M in pentane, 1.43 mL, 2.15 mmol), and the resulting yellow solution was stirred for 1 hour at -90 ºC. Triphenylborane (0.520 g, 2.15 mmol) was then added to the reaction pot as a THF solution. The mixture was then stirred and allowed to warm to room temperature. Volatiles were then removed in vacuo, and the remaining solids were taken up in CH_2Cl_2. A solution of [ASN][Br] (0.443 g, 2.15 mmol) in CH_2Cl_2 was added dropwise. After stirring for 1 hour, copious amounts of Et_2O were added to precipitate the product. The resulting solids were collected on a sintered glass frit, washed with Et_2O, and dried thoroughly to afford analytically pure **B.6** (1.175 g, 87 %). Crystals suitable for an X-ray diffraction study were grown by vapor diffusion of Et_2O into acetonitrile. ^{1}H NMR (300 MHz, d_3-acetonitrile): δ = 7.50 (m, 1H), 7.20-7.32 (m, 19H), 6.98 (m, 6H), 6.83 (m, 3H), 3.83 (m, 8H), 2.10 (m, 8H). ^{13}C NMR (75.396 MHz, CH_3CN): δ = 163, 142.51, 139.36, 136.96, 135.94, 133.62, 132.38, 128.68, 128.55,

127.98, 126.04, 122.24, 65.10, 22.19. ^{31}P NMR (121.475 MHz, d_3-acetonitrile): δ = -0.829(s). ^{11}B NMR (400 MHz, d_3-acetonitrile): δ = -10.99 (s). Anal. Calcd. for $C_{44}H_{45}BNP$: C, 83.93; H, 6.84; N, 2.61. Found: C, 83.64; H, 7.03; N, 2.41.

[NBu$_4$][Ph$_3$BP$^{p\text{-Ph}}{}_2$] (B.7). *p*-$BrC_6H_4PPh_2$ (**B.3**) (1.254 g, 3.68 mmol) was dissolved in 75 mL of dry, degassed THF, and the stirring solution was then cooled to -90 ºC. To this solution was added *tert*-BuLi (1.50 M in pentane, 2.45 mL, 3.68 mmol) to form a yellow solution that was stirred for 1 hour at -90 ºC. Triphenylborane (0.890 g, 3.68 mmol) was added as a THF solution after 1 hour, and the resulting solution was stirred while warming gradually to room temperature. The reaction volatiles were then removed in vacuo, and the remaining solids were taken up in CH_2Cl_2. A solution of [NBu_4][Br] (1.186 g, 3.68 mmol) in CH_2Cl_2 was added dropwise. After 1 hour, copious amounts of Et_2O were added, and the solution was cooled to -35 ^oC to precipitate the product, which was isolated and dried to afford spectroscopically pure **B.7** (1.584 g, 57.8 %). ^{1}H NMR (300 MHz, d_3-acetonitrile): δ = 7.37 (m, 4H), 7.20-7.33 (m, 12H), 7.04 (m, 2H), 7.00 (m, 6H), 6.85 (m, 3H), 3.07 (m, 8H, NBu_4), 1.56 (m, 8H, NBu_4), 1.33 (m, 8H, NBu_4), 0.96 (m, 12H, NBu_4). ^{13}C NMR (75.397 MHz, CH_3CN): δ = 162, 139.30, 136.52, 135.95, 133.49, 131.72, 128.69, 128.58, 126.01, 125.97, 122.23, 58.69, 23.79, 19.81, 13.36. ^{31}P NMR (121.475 MHz, d_3-acetonitrile): δ = -3.23(s). ^{11}B NMR (400 MHz, d_3-acetonitrile): δ = -11.08. Anal. Calcd. for $C_{52}H_{65}BNP$: C, 83.74; H, 8.78; N, 1.88. Found: C, 83.52; H, 8.01; N, 2.32.

[NBu$_4$][Ph$_3$BP$^{m\text{-}i\text{Pr}}{}_2$] (B.8). *m*-$BrC_6H_4P^iPr_2$ (**B.3**) (0.671 g, 2.46 mmol) was dissolved in 75 mL dry, degassed THF, and the stirring solution was cooled to -90 ºC. To this solution

was added *tert*-BuLi (1.50 M in pentane, 1.64 mL, 2.46 mmol), and the yellow solution was stirred for 1 hour at -90 ºC. Triphenylborane (0.595 g, 2.46 mmol) was added as a THF solution, and the solution was allowed to stir and warm to room temperature. Volatiles were removed in vacuo, and the remaining solids were taken up in CH_2Cl_2. A solution of NBu_4Br (0.793 g, 2.46 mmol) in CH_2Cl_2 was added. The solution was allowed to stir for 3 hours and was then filtered through Celite. Solvent was removed in vacuo, and solids were washed with copious amounts of petroleum ether and diethyl ether to afford **B.8** (0.802 g, 48 %). This borate ligand is more difficult to crystallize than the others described, and its combustion analysis proved consequently high in carbon and low in nitrogen (two attempts). Crystals suitable for an X-ray diffraction study were grown via vapor diffusion of Et_2O into THF. ^{1}H NMR (300 MHz, d_3-acetonitrile): δ = 7.51(m, 3H), 7.37 (m, 6H), 7.01 (m, 1H), 6.94 (m, 6H), 6.81 (m, 3H), 3.43 (m, 8H, NBu_4), 1.95 (m, 2H), 1.82 (m, 8H, NBu_4), 1.45 (m, 8H), 1.12 (m, 6H), 0.99 (m, 12H, NBu_4), 0.84 (m, 6H). ^{13}C NMR (75.397 MHz, acetonitrile): δ = 162, 136.40, 135.96, 133.70, 128.77, 126.45, 125.85, 125.46, 122.08, 58.70, 23.80, 22.85, 20.06, 19.81, 18.76, 13.33. ^{31}P NMR (121.475 MHz, d_3-acetonitrile): δ = 13.99 (s). ^{11}B NMR (400 MHz, d_3-acetonitrile): δ = -11.02 (s). Anal. Calcd. for $C_{46}H_{69}BNP$: C, 81.51; H, 10.26; N, 2.07. Found: C, 83.07; H, 11.26; N, 1.32.

[NBu_4][$Ph_3BP^{p\text{-}i\text{Pr}_2}$] (B.9). *p*-$BrC_6H_4P^iPr_2$ (**B.4**) (1.391 g, 5.11 mmol) was dissolved in 75 mL dry, degassed THF, and the stirring solution was cooled to -90 ºC. To this solution was added *tert*-BuLi (1.50 M in pentane, 3.41 mL, 5.11 mmol), providing a yellow solution that was stirred for 1 hour at -90 ºC. Triphenylborane (1.235 g, 5.11 mmol) was added as a THF solution, and the solution was stirred and allowed to warm to room

temperature. Volatiles were removed in vacuo, and the remaining solids were taken up in CH_2Cl_2. A solution of [NBu_4][Br] (1.647 g, 5.11 mmol) in CH_2Cl_2 was then added. The resulting solution was then allowed to stir for 3 hours, followed by filtration through Celite. Solvent was removed in vacuo, and the solids were washed with copious amounts of petroleum ether and ether to afford **B.9** (2.895 g, 84 %). ^{1}H NMR (300 MHz, d_3-acetonitrile): δ = 7.26 (m, 8H), 7.13 (m, 2H), 7.00 (m, 6H), 6.85 (m, 3H), 3.07 (m, 8H, NBu_4), 2.05 (m, 2H), 1.59 (m, 8H, NBu_4), 1.34 (m, 8H), 1.03 (m, 6H), 0.96 (m, 12H, NBu_4), 0.88 (m, 6H). ^{13}C NMR (75.397 MHz, acetonitrile): δ = 162, 135.98, 135.69, 132.36, 126.45, 125.89, 122.16, 58.70, 23.80, 22.90, 20.13, 19.81, 18.91, 13.33. ^{31}P NMR (121.475 MHz, d_3-acetonitrile): δ = 12.42 (s). ^{11}B NMR (400 MHz, d_3-acetonitrile): -11.13 (s). Anal. Calcd. for $C_{46}H_{69}BNP$: C, 81.51; H, 10.26; N, 2.07. Found: C, 81.71; H, 10.58; N, 2.26.

(**$Ph_3SiP^{m\text{-}Ph}_2$) (B.10)**. *m*-$BrC_6H_4P^iPr_2$ (**B.2**) (1.391 g, 5.11 mmol) was dissolved in 75 mL of dry, degassed Et_2O and stirred at -90 ºC. To this solution was added *tert*-BuLi (1.50 M in pentane, 3.41 mL, 5.11 mmol) to form a yellow solution that was stirred for 1 hour at -90 ºC. Triphenylsilylchloride (1.235 g, 5.11 mmol) was then added as an Et_2O solution, and the reaction mixture was stirred while allowing it to warm to room temperature. The final solution was filtered through Celite to remove LiCl, and the volatiles were removed from the filtrate in vacuo. The remaining oil was taken up in toluene and refluxed for 6 hours to precipitate the remaining LiCl salts. The supernatant was filtered through a pad of Celite, and the volatiles were again removed to yield the product **B.10** (70 %). ^{1}H NMR (300 MHz, d_6-benzene): δ = 7.96 (m, 1H), 7.64-7.77 (m, 2H), 7.58 (m, 6H), 7.49

(m, 1H), 7.35 (m, 4H), 7.20 (m, 4H), 7.11 (m, 6H), 7.04 (m, 2H), 7.00 (m, 3H). ^{31}P NMR (121.475 MHz, d_6-benzene): δ = -7.29 (s). ES-MS^{+} (m/z) = 521.2

(**$Ph_3SiP^{p\text{-}Ph}{}_2$) (B.11)**. *m*-$BrC_6H_4P^iPr_2$ (**B.3**) (1.391 g, 5.11 mmol) was dissolved in 75 mL of dry, degassed Et_2O and stirred at -90 ºC. To this solution was added *tert*-BuLi (1.50 M in pentane, 3.41 mL, 5.11 mmol) to form a yellow solution that was stirred for 1 hour at -90 ºC. Triphenylsilylchloride (1.235 g, 5.11 mmol) was then added as an Et_2O solution, and the reaction mixture was then stirred while being allowed to warm to room temperature. The resulting suspension was filtered through Celite to remove LiCl, and the volatiles were removed from the filtrate in vacuo. The remaining oil was then extracted into toluene and refluxed for 6 hours to further precipitate the remaining LiCl salts. The supernatant was filtered through a pad of Celite, and the volatiles were again removed to afford product **B.11** (68 %). ^{1}H NMR (300 MHz, d_6-benzene): δ = 7.46 (m, 8H), 7.34 (m, 4H), 7.30 (m, 6H), 7.26 (m, 6H), 7.19 (m, 3H). ^{31}P NMR (121.475 MHz, d_6-benzene): δ = -9.21 (s). ES-MS^{+} (m/z) = 521.2

(**$Ph_3SiP^{m\text{-}i\text{Pr}}{}_2$) (B.12)**. *m*-$BrC_6H_4P^iPr_2$ (**B.4**) (1.391 g, 5.11 mmol) was dissolved in 75 mL of dry, degassed Et_2O and stirred at -90 ºC. To this solution was added *tert*-BuLi (1.50 M in pentane, 3.41 mL, 5.11 mmol) to form a yellow solution that was stirred for 1 hour at -90 ºC. Triphenylsilylchloride (1.235 g, 5.11 mmol) was added as an Et_2O solution, and the resulting suspension was allowed to warm to room temperature while stirring. The mixture was filtered through Celite to remove LiCl, and the volatiles were then removed in vacuo from the filtrate. The remaining oil was taken up in toluene and refluxed for 6 hours to further precipitate the remaining LiCl salts. The solution was then filtered

through a pad of Celite, and the solvent was removed to afford product **B.12** (51 %). ^{1}H NMR (300 MHz, d_6-benzene): δ = 7.98 (m, 1H), 7.69 (m, 6H), 7.65 (m, 1H), 7.57 (m, 1H), 7.17 (m, 9H), 7.10 (m, 1H), 1.88 (m, 2H), 0.99 (m, 6H), 0.87 (m, 6H). ^{31}P NMR (121.475 MHz, d_6-benzene): δ = 8.41 (s). ES-MS^{+} (m/z) = 453.1

(**$Ph_3SiP^{p\text{-}i\text{Pr}_2}$) (B.13)**. *m*-$BrC_6H_4P^{i}Pr_2$ (**B.5**) (1.391 g, 5.11 mmol) was dissolved in 75 mL of dry, degassed Et_2O and stirred at -90 ºC. To this solution was added *tert*-BuLi (1.50 M in pentane, 3.41 mL, 5.11 mmol) to form a yellow solution that was stirred for 1 hour at -90 ºC. Triphenylsilylchloride (1.235 g, 5.11 mmol) was added as an Et_2O solution, and the mixture was stirred and warmed gradually to room temperature. The resulting suspension was filtered through Celite to remove LiCl, and the volatiles were then removed from the filtrate in vacuo. The remaining oil was extracted into toluene and refluxed for 6 hours to further precipitate the remaining LiCl salts. The solution was then filtered through a pad of Celite, and the filtrate was dried in vacuo to provide product **B.13** (56 %). ^{1}H NMR (300 MHz, d_6-benzene): δ = 7.71 (m, 2H), 7.67 (m, 6H), 7.47 (m, 2H), 7.16 (m, 6H), 7.11 (m, 3H), 1.95 (m, 2H), 1.02 (m, 6H), 0.90 (m, 6H). ^{31}P NMR (121.475 MHz, d_6-benzene): δ = 11.36 (s). ESI-MS^{+} (m/z) = 453.1.

{(NBD)RhCl][$Ph_3BP^{m\text{-}i\text{Pr}_2}$]}{$NBu_4$} (B.14). Solid $[(NBD)RhCl]_2$ (0.0144 g, 0.0224 mmol) was dissolved in THF. To this solution was added **B.9** (0.0302 g, 0.0461 mmol) as a THF solution. The reaction solution immediately changed from yellow to orange. Volatiles were removed in vacuo to yield product that was spectroscopically pure (yield ~ quantitative). ^{1}H NMR (300 MHz, d_6-acetone): δ = 7.33 (m, 8H, *o*-BPh_3), 7.04 (m, 2H), 6.96 (m, 6H, *m*-BPh_3), 6.82 (m, 3H, *p*-BPh_3), 3.62 (m, 4H, NBD), 3.52 (br, 2H, NBD),

3.42 (m, 8H, NBu_4), 2.43 (m, 2H, ^{i}Pr), 1.82 (m, 8H, NBu_4), 1.44 (m, 8H, NBu_4), 1.22 (m, 6H, ^{i}Pr), 1.08 (m, 6H, ^{i}Pr), 0.99 (m, 12H, NBu_4), 0.85 (m, 2H, NBD). ^{13}C NMR (75.397 MHz, acetonitrile): δ = 163.6, 138.25, 136.07, 135.72, 130.89, 128.60, 126.06, 122.35, 67.78, 58.86, 51.63, 50.98, 50.00, 23.91, 23.02, 19.11, 19.94, 18.91, 13.45. ^{31}P NMR (121.475 MHz, d_6-acetone): δ =44.88 (d, $^{1}J_{Rh\text{-}P}$ = 166.4 Hz). Anal. Calcd. for $C_{53}H_{77}BClNPRh$: C, 70.08; H, 8.54; N, 1.54. Found: C, 69.76; H, 8.49; N, 1.72. Note: A crystallographic study was performed on crystals of **B.14** generated from a separate experiment that showed significant bromide incorporation at the halide site. The batch of ligand **B.9** used in that preparation had not been thoroughly freed of $[NBu_4][Br]$.

{ASN}$_2${[Ph$_3$BP$^{m\text{-}Ph}_2$]$_2$PtMe$_2$} (**B.15).** Solid **(**COD)$PtMe_2$ (0.0276 g, 0.083 mmol) and **B.3** (0.1024 g, 0.169 mmol) were dissolved and stirred in THF at room temperature for one hour. White precipitate was collected on a fine frit and washed first with petroleum ether (2 x 2 mL) and then with copious amounts of Et_2O. Thorough drying provided the desired white product **B.15** (isolated yield = 80 %). Crystals suitable for an X-ray diffraction study were grown from a crude product sample by vapor diffusion of Et_2O into acetonitrile. ^{1}H NMR (300 MHz, d_6-acetone): δ = 8.03 (m, 1H), 7.66 (m, 1H), 7.38 (m, 1H), 7.30 (m, 6H, *o*-BPh_3), 7.22 (m, 1H), 7.15 (m, 4H, PPh_2), 7.00 (m, 4H, PPh_2), 6.86-6.96 (m, 8H, PPh_2, *m*-BPh_3), 6.80 (m, 3H, *p*-BPh_3), 3.48 (m, 16H, ASN), 2.09 (m, 16H, ASN), 0.32 (m, 6H, Pt-Me, $^{2}J_{Pt\text{-}H}$ = 72.0 Hz). ^{13}C NMR (75.396 MHz, acetonitrile): δ = 163, 138.8, 136.94, 134.64, 133.4, 129.28, 128.32, 127.05, 123.19, 65.10, 23.30, -19.5. ^{31}P NMR (121.475 MHz, d_6-acetone): δ =28.63 (s, $^{1}J_{Pt\text{-}P}$ = 1947 Hz). Anal. Calcd. for $C_{90}H_{96}B_2N_2P_2Pt$: C, 72.82; H, 6.52; N, 1.89. Found: C, 72.45; H, 6.75; N, 2.20.

$\{NBu_4\}_2\{[Ph_3BP^{p\text{-}Ph}{}_2]_2PtMe_2\}$ (B.16). Solid **(**COD)$PtMe_2$ (0.0756 g, 0.226 mmol) and **B.7** (0.3372 g, 0.453 mmol) were stirred in THF at room temperature for one hour. Volatiles were then removed in vacuo, and the remaining solids were washed first with petroleum ether (2 x 2 mL) and then with a copious amount of Et_2O to provide, after drying, the desired product **B.16** (yield ~ quantitative). The product was readily recrystallized from THF/Et_2O. ^{1}H NMR (300 MHz, d_6-acetone): δ = 7.43 (m, 2H), 7.38 (m, 4H, PPh_2), 7.36 (m, 6H, *o*-BPh_3), 7.28 (m, 4H, PPh_2), 7.08 (m, 2H), 6.94-7.01 (m, 8H, PPh_2, *m*-BPh_3), 6.81 (m, 3H, *p*-BPh_3), 3.38 (m, 16H, NBu_4), 1.78 (m, 16H, NBu_4), 1.40 (m, 16H, NBu_4), 0.96 (m, 24H, NBu_4), 0.33 (m, 6H, Pt-Me, $^2J_{Pt\text{-}H}$ = 69.5 Hz). ^{13}C NMR (75.397 MHz, acetonitrile): δ = 164, 136.30, 135.68, 134.32, 133.66, 129.08, 128.91, 127.60, 126.20, 122.50, 122.23, 58.87, 23.87, 19.91, 13.44. ^{31}P NMR (121.475 MHz, d_6-acetone): δ = 27.47 (s, $^1J_{Pt\text{-}P}$ = 1935 Hz). Anal. Calcd. for $C_{106}H_{136}B_2N_2P_2Pt$: C, 74.15; H, 7.56; N, 1.63. Found: C, 73.77; H, 8.18; N, 1.90.

$\{NEt_4\}_2\{(Ph_3BP^{m\text{-}i\text{Pr}}{}_2)_2PtMe_2\}$ (B.17). **(**COD)$PtMe_2$ (0.0840 g, 0.252 mmol) and **B.8** (0.1681 g, 0.298 mmol) were stirred in THF at room temperature for one hour. The reaction volatiles were then removed in vacuo, and the resulting solids were washed with petroleum ether (2 x 2 mL) and then copious amounts of Et_2O to yield, after drying, the desired product **B.17** (yield ~ quantitative). The product was easily recrystallized from THF/Et_2O. ^{1}H NMR (300 MHz, d_6-acetone): δ = 7.51 (m, 1H), 7.44 (m, 1H), 7.31 (m, 6H, *o*-BPh_3), 7.23 (m, 1H), 7.14 (m, 1H), 7.02 (m, 6H, *m*-BPh_3), 6.88 (m, 3H, *p*-BPh_3), 3.05 (m, 16H, NEt_4), 2.21 (m, 2H, ^{i}Pr), 1.42 (m, 24H, NEt_4), 0.98 (m, 6H, ^{i}Pr), 0.88 (m, 6H, ^{i}Pr), 0.17 (m, 6H, Pt-Me, $^2J_{Pt\text{-}H}$ = 67.5 Hz). ^{13}C NMR (75.396 MHz, acetonitrile): δ =

165 (*ipso*-B), 140.33, 137.17, 136.36, 133.65, 128.86, 126.48, 126.11, 123.48, 122.32, 52.61, 23.91, 20.70, 18.73, 7.27, -10.93. ^{31}P NMR (121.475 MHz, d_6-acetone): 38.11 (s, $^1J_{Pt\text{-}P}$ = 1910 Hz). Anal. Calcd. for $C_{78}H_{112}B_2N_2P_2Pt$: C, 69.07; H, 8.32; N, 2.07. Found: C, 69.29; H, 8.17; N, 1.36.

$[NBu_4]_2[(Ph_3BP^{p\text{-}i\text{Pr}}{}_2)_2PtMe_2]$ (B.18). **(**COD)$PtMe_2$ (0.0840 g, 0.252 mmol) and **B.9** (0.1681 g, 0.298 mmol) were stirred in THF at room temperature for one hour. The reaction volatiles were then removed in vacuo, and the resulting solids were washed with petroleum ether (2 x 2 mL) and then copious amounts of Et_2O to provide the desired white product (yield ~ quantitative). Product was recrystallized from THF/Et_2O. ^{1}H NMR (300 MHz, d_6-acetone): δ = 7.25-7.34 (m, 12H), 7.18-7.24 (m, 4H), 7.07 (m, 4H), 6.93 (m, 12H), 6.79 (m, 6H), 3.41 (m, 16H, NBu_4), 2.20 (m, 4H, ^{i}Pr), 1.78 (m, 16H, NBu_4), 1.41 (m, 16H, NBu_4), 1.14 (m, 12H, ^{i}Pr), 1.04 (m, 12H, ^{i}Pr), 0.97 (m, 24H, NBu_4), 0.30 (m, 6H, Pt-Me, $^2J_{Pt\text{-}H}$ = 66.0 Hz). ^{13}C NMR (75.396 MHz, acetonitrile): δ = 164 (*ipso*-B), 138.17, 136.05, 134.86, 131.13, 125.93, 122.19, 67.75, 58.78, 23.85, 20.58, 19.88, 18.92, 13.41, -9.8. ^{31}P NMR (121.475 MHz, d_6-acetone): δ = 31.53 (s, $^1J_{Pt\text{-}P}$ = 1907 Hz). Anal. Calcd. for $C_{94}H_{144}B_2N_2P_2Pt$: C, 71.42; H, 9.18; N, 1.77. Found: C, 71.29; H, 9.21; N, 2.25.

$(Ph_3SiP^{p\text{-}i\text{Pr}}{}_2)_2PtMe_2$ (B.19). (COD)$PtMe_2$ (0.0840 g, 0.252 mmol) was stirred in the presence of **B.13** (0.1681 g, 0.298 mmol) in THF at room temperature for one hour. The reaction volatiles were then removed in vacuo, and the remaining solids were washed with petroleum ether (2 x 2 mL) and Et_2O (2 x 2 mL) to provide the desired white product quantitatively. ^{1}H NMR (300 MHz, d_6-acetone): δ = 7.34-7.64 (m, 38H), 2.42

(m, 4H, ^{i}Pr), 1.13 (m, 12H, ^{i}Pr), 1.01 (m, 12H, ^{i}Pr), 0.30 (m, 6H, Pt-Me, $^{2}J_{\text{Pt-H}}$ = 63.0 Hz). ^{31}P NMR (121.475 MHz, d_6-acetone): δ = 36.94 (s, $^{1}J_{\text{Pt-P}}$ = 1883 Hz).

($Ph_3SiP^{p\text{-}Ph}$)$_2$PtMe$_2$ (B.20). Prepared as for the case of **B.19**. ^{1}H NMR (300 MHz, d_6-acetone): δ = 7.45 (m, 12H), 7.16-7.45 (m, 46H), 0.39 (m, 6H, Pt-Me, $^{2}J_{\text{Pt-H}}$ = 60.0 Hz). ^{31}P NMR (121.475 MHz, d_6-acetone): δ = 30.45 (s, $^{1}J_{\text{Pt-P}}$ = 1900 Hz).

[*cis*-($Ph_3SiP^{p\text{-}Ph}$)$_2$PtMe(solv)][Me(B(C_6F_5)$_3$] (B.21). Complex **B.20** (0.0195 g, 0.0154 mmol) was stirred in a THF solution containing B(C_6F_5)$_3$ (0.0079 g, 0.0154 mmol) for 12 hours. The ^{31}P NMR spectrum verified clean generation of a single *cis* mono-solvento, mono-methyl species (**B.21**). ^{1}H NMR (300 MHz, d_6-acetone): δ = 6.98-8.02 (m, 58H), 0.52 (br s, 3H, Me(B(C_6F_5)$_3$), 0.61 (m, 3H, Pt-Me, $^{2}J_{\text{Pt-H}}$ = 54.0 Hz). ^{31}P NMR (121.475 MHz, d_6-acetone): δ = 24.4 (d, $^{1}J_{\text{Pt-P}}$ = 1942 Hz, $^{2}J_{\text{P-P}}$ = 396 Hz).

{NBu_4}{Mo(CO)$_5$[$Ph_3BP^{m\text{-}i\text{Pr}_2}$]} (B.22). Solid Mo($CO_6$) (0.0078 g, 0.030 mmol) and solid **B.8** (0.0204 g, 0.0301 mmol) were combined in THF and refluxed for 12 hours to provide a yellow solution. Volatiles were then removed in vacuo. The solid product was recrystallized from THF/Et_2O to provide **B.22**. ^{1}H NMR (300 MHz, d_6-acetonitrile): δ = 7.42 (m, 3H), 7.34 (m, 6H), 7.11 (m, 1H), 6.95 (m, 6H), 6.80 (m, 3H), 3.43 (m, 8H, NBu_4), 2.32 (m, 2H), 1.81 (m, 8H, NBu_4), 1.42 (m, 8H), 1.07 (m, 6H, ^{i}Pr), 0.97 (m, 12H, NBu_4), 0.91 (m, 6H, ^{i}Pr). ^{31}P NMR (121.475 MHz, d_6-acetone): δ = 52.33 (s). IR: (KBr/CH_2Cl_2): 2065, 1925 cm^{-1}. ES-MS^{-} (m/z) = 671, 643, 615.

[NBu_4][Mo(CO)$_5$($Ph_3SiP^{m\text{-}i\text{Pr}_2}$)] (B.23). Solid Mo($CO_6$) (0.0078 g, 0.030 mmol) and solid **B.12** (0.0204 g, 0.0301 mmol) were combined in THF and refluxed for 12 hours to provide a yellow solution. The reaction volatiles were removed in vacuo, and the

remaining solid product was recrystallized from THF/Et_2O. ^1H NMR (300 MHz, d_6-benzene): δ = 7.68 (m, 1H), 7.59 (m, 6H), 7.47 (m, 1H), 7.29 (m, 1H), 7.16 (m, 9H), 7.10 (m, 1H), 2.03 (m, 2H), 1.04 (m, 6H), 0.89 (m, 6H). ^{31}P NMR (121.475 MHz, d_6-benzene): δ = 51.86 (s). IR: (KBr/CH_2Cl_2): 2070, 1942 cm^{-1}.

General Procedure for Suzuki coupling reactions. $Pd_2(dba)_3$ (0.0046 g, 1.5 mol %), **B.8** (0.0135 g, 6.0 mol %), $PhB(OH)_2$ (0.0446 g, 0.367 mmol), and Cs_2CO_3 (0.2606 g, 0.800 mmol) were combined under air in a 5 mL screw-cap vial equipped with a stir bar. The vial was then sealed with a septum and flushed thoroughly with nitrogen, after which time one equivalent of the appropriate aryl halide was added as a THF solution (dry, 1.5 mL). While under nitrogen, the septum was quickly replaced with a Teflon-lined cap. The reaction mixture was then refluxed with stirring for 24 hours. The mixture was then diluted with copious amounts of ether and filtered through a silica plug. Volatiles were removed in vacuo, and the product was purified by flash chromatography.

4-chlorobiphenyl. Aryl halide: 1,4-dichlorobenzene (0.0489 g, 0.333 mmol). Product was isolated via column chromatography (hexanes). ^1H NMR (300 MHz, $CDCl_3$): δ = 7.37-7.58 (m, 9H).

4-methylbiphenyl. Aryl halide: 4-chlorotoluene (39.4 μL, 0.333 mmol). Product was isolated via column chromatography (hexanes). ^1H (NMR (300 MHz, $CDCl_3$): δ = 7.57 (m, 2H), 7.49 (m, 2H), 7.42 (m, 2H), 7.32 (m, 1H), 7.35 (m, 2H), 2.39 (s, 3H).

4-phenylacetophenone. Aryl halide: 4-chloroacetophenone (43.2 μL, 0.333 mmol). Product was isolated via column chromatography (1% EtOAc/hexanes). ^1H NMR (300

MHz, $CDCl_3$): δ = 8.03 (m, 2H), 7.69 (m, 2H), 7.63 (m, 2H), 7.47 (m, 2H), 7.40 (m, 1H), 2.64 (s, 3H).

Note on Suzuki coupling reactions: A point of concern pertains to whether the tetraarylborate unit of ligand **B.8** is transferred during the cross-coupling reactions. While we cannot rule out this possibility altogether, we note that (i) tolylboronic acids were also screened and found to give comparable yields of cross-coupled products. Also, the yield of cross-coupled product far exceeds the molar ratio of the (phosphino)borate ligand, which was used in catalytic quantity. Thus, aryl transfer from the ligand is not critical to cross-coupling of the chloride substrates shown in Table B.1.

B.3.4 X-ray Experimental Data

Crystallographic procedures are outlined in Section 2.4.6. In the case of **B.14,** halide occupancy was modeled reasonably as 60% bromide and 40% chloride. The structure was otherwise unremarkable. Crystallographic data are summarized in Table B.2.

Table B.2. Crystallographic data for $[NEt_4][Ph_3BP^{m\text{-}Ph}{}_2]$, **B.6**; $[NBu_4][Ph_3BP^{m\text{-}i\text{Pr}}{}_2]$, **B.8**; $\{(NBD)RhCl][Ph_3BP^{p\text{-}i\text{Pr}}{}_2]\}\{NBu_4\}$, **B.14**; and $\{ASN\}_2\{[Ph_3BP^{m\text{-}Ph}{}_2]_2PtMe_2\}$, **B.15**.

	B.6	**B.8**	**B.14**
chemical formula	$C_{44}H_{49}BNP$	$C_{38}H_{53}BNP$	$C_{53}H_{77}BBr_{0.6}Cl_{0.4}NPRh$
Fw	633.62	565.59	988.21
T (°C)	-175	-175	-175
λ (Å)	0.71073	0.71073	0.71073
a (Å)	18.0519(13)	9.8900(8)	15.8487(10)
b (Å)	10.4941(8)	20.1253(16)	15.6527(10)
c (Å)	38.060(3)	16.7970(14)	20.3787(13)
α (°)	90	90	90
β (°)	90.4990(10)	92.835(2)	102.6390(10)
γ (°)	90	90	90
V (Å^3)	7209.7(9)	3339.2(5)	4932.9(5)
space group	$P2_1$	$P2_1$	$P2_1$
Z	8	4	4
D_{calc} (g/cm^3)	1.167	1.125	1.331
μ(cm^{-1})	1.08	1.09	12.78
R1, wR2[a] ($I > 2\sigma(I)$)	0.0903, 0.1242	0.0659, 0.0917	0.0432, 0.0646

[a] $R1 = \Sigma||F_o| - |F_c||/\Sigma|F_o|$, $wR2 = \{\Sigma[w(F_o^2 - F_c^2)^2]/\Sigma[w(F_o^2)^2]\}^{1/2}$

Table B.2 cont.

	B.15·Et_2O
chemical formula	$C_{102}H_{122}B_2BrN_3OP_2Pt$
Fw	1764.59
T (°C)	-175
λ (Å)	0.71073
a (Å)	10.1511(18)
b (Å)	17.534(3)
c (Å)	24.912(4)
α (°)	76.949(3)
β (°)	85.774(3)
γ (°)	83.253(3)
V (Å^3)	4284.4(13)
space group	P-1
Z	2
D_{calc} (g/cm^3)	1.368
μ(cm^{-1})	21.93
R1, wR2[a] ($I > 2\sigma(I)$)	0.0413, 0.0947

[a] $R1 = \Sigma||F_o| - |F_c||/\Sigma|F_o|$, $wR2 = \{\Sigma[w(F_o^2 - F_c^2)^2]/\Sigma[w(F_o^2)^2]\}^{1/2}$

References Cited

[1] Dias, P. B.; de Piedade, M. E. M.; Simões, J. A. M. *Coord. Chem.Rev.* **1994**, *135*, 737.

[2] (a) Qiao, S.; Hoic, D. A.; Fu, G. C. *J. Am. Chem. Soc.* **1996**, *118*, 6329. (b) Hoic, D. A.; Davis, W. M.; Fu, G. C. *J. Am. Chem. Soc.* **1996**, *118*, 8176. (c) Hoic, D. A.; DiMare, M.; Fu, G. C. *J. Am. Chem. Soc.* **1997**, *119*, 7155.

[3] (a) Ashe, A. J., III; Shu, P. J. *J. Am. Chem. Soc*. **1971**, *93*, 1804. (b) Putzer, M. A.; Rogers, J. S.; Bazan, G. C. *J. Am. Chem. Soc*. **1999**, *121*, 8112.

[4] (a) Kirchhoff, J. H.; Dai, C.; Fu, G. C. *Angew. Chem., Int. Ed.* **2002**, *41*, 1945. (b) Yin, J.; Rainka, M. P.; Zhang, X.; Buchwald, S. L. *J. Am. Chem. Soc*. **2002**, *124*, 1162. (c) Stambuli, J. P.; Kuwano, R.; Hartwig, J. F. *Angew. Chem., Int. Ed.* **2002**, *41*, 4746.

[5] (a) Lu, C. C.; Peters, J. C. *J. Am. Chem. Soc.* **2002**, *124*, 5272. (b) Betley, T. A.; Peters, J. C. *Angew. Chem., Int. Ed.* **2003**, *42*, 2003.

[6] (a) Betley, T. A.; Peters, J. C. *Inorg. Chem.* **2003**, *42*, 5074. (b) Thomas, J. C.; Peters, J. C. *Inorg. Chem.* **2003**, *42,* 5055.

[7] See for example: Lustenberger, P.; Diedrich, F. *Helv. Chim. Acta* **2000**, *83*, 2865.

[8] (a) Daly, J. J. *J. Chem. Soc.* **1964**, 3799. (b) Bruckmann, J.; Kruger, C.; Lutz, F. *Z. Naturforsch., B: Chem. Sci.* **1995**, *50*, 351.

[9] Ligand solubility is highly dependent on the ammonium salt used. For example, the ASN salt of **B.6** is sparingly soluble in THF, while the $^{n}Bu_4N$ salts of **B.7**-**B.9** and the $Li(TMEDA)_2$ salt of **1** are highly soluble in THF.

[10] Nolan, S. P.; Haar, C. M.; Marshall, W. J.; Moloy, K. G.; Prock, A.; Giering, W. P. *Organometallics* **1999**, *18*, 474.

[11] (a) Konze, W. V.; Scott, B. L.; Kubas, G. J. *Chem. Commun.* **1999**, 1807. (b) Alibrandi, G.; Minniti, D.; Scolaro, M.; Romeo, R. *Inorg. Chem.* **1988**, *27*, 318. (c) Alibrandi, G.; Romeo, R. *Inorg. Chem.* **1997**, *36*, 4822.

[12] (a) Miyaura, N.; Suzuki, A. *Chem. Rev.* **1995**, *95*, 2457. (b) Suzuki, A. *J. Organomet. Chem.* **1999**, *576*, 147.

[13] (a) Littke, A. F.; Fu, G. C. *Angew. Chem., Int. Ed.* **1998**, *37*, 3387. (b) Littke, A. F.; Dai, C.; Fu, G. C. *J. Am. Chem. Soc.* **2000**, *122*, 4020.

[14] The phenyl-substituted ligands **B.6** and **B.7** were much less effective in the Suzuki coupling of aryl chlorides. Ligand **B.9** showed comparable activity to **B.8** in several model studies. Also, a point of concern pertains to whether the tetraarylborate unit of ligand **B.8** is transferred during the cross-coupling reactions. While we cannot rule out this possibility altogether, we note that tolylboronic acids were also screened briefly and found to give comparable yields.

[15] Although three IR active vibrations are predicted, only the A_1^2 and E stretches are resolved. The A_1^1 stretch is weak and presumably coincident with the E vibration.

[16] (a) Cotton, F. A.; Darensbourg, D. J.; Ilsley, W. H. *Inorg. Chem.* **1981**, *20*, 578. (b) Cotton, F. A.; Kraihanzel, C. S. *J. Am. Chem. Soc.* **1962**, *84*, 4432. (c) Magee, T. A.; Matthews, C. N.; Wang, T. S.; Wotiz, J. H. *J. Am. Chem. Soc.* **1961**, *83*, 3200.

Appendix C: X-ray Data for Structures Not Discussed in the Text

Table C.1 Crystallographic parameters for [[Ph_2BP_2]Ru(=CHPh)Cl_2][$^nBu_4N$] (**C.1**·2C_5H_{10}), [κ^2-PhB($CH_2P(^tBu)_2)_2(CH_2S^tBu)$]$FeCl_2$ (**C.2**), [$PhBP^{iPr}_3$]$Fe^{III}(N_2CMes_2)$ (**C.3**), [$PhBP^{iPr}_3$]Fe^{II}(C≡CPh) (**C.4**), [$PhBP^{iPr}_3$]Co-O-Co($SiPhH_2$)($PhBP^{iPr}_2$) (**C.5**), [$PhBP^{tBu}_2$(pz)]Co(N_2CPh_2) (**C.6**), and {[$PhBP^{iPr}_3$]Fe}(μ-O) (**C.7**).

	C.1·2C_5H_{10}	**C.2**	**C.3**
chemical formula	$C_{71}H_{96}BCl_2NP_2Ru$	$C_{29}H_{56}BCl_2FeP_2S$	$C_{46}H_{75}BFeN_2P_3$
Fw	1207.07	635.92	815.65
T (°C)	-173	-173	-173
λ (Å)	0.71073	0.71073	0.71073
a (Å)	12.3810(12)	22.1991(12)	51.788(8)
b (Å)	15.4701(15)	22.1991(12)	9.8632(14)
c (Å)	17.3608(17)	15.3562(12)	18.246(3)
α (°)	89.306(2)	90	90
β (°)	73.674(2)°.	90	104.971(3)
γ (°)	78.855(2)°.	120	90
V (Å^3)	3127.8(5)	6553.7(7)	9004(2)
space group	P-1	P6(5)	C2/c
Z	2	410	8
D_{calc} (g/cm^3)	1.577	1.451	1.203
μ(cm^{-1})	4.46	9.03	4.75
R1, wR2[a] ($I > 2\sigma(I)$)	0.0530, 0.0853	0.1410, 0.2382	0.0634, 0.0843

[a] $R1 = \Sigma||F_o| - |F_c||/\Sigma|F_o|$, $wR2 = \{\Sigma[w(F_o^2 - F_c^2)^2]/\Sigma[w(F_o^2)^2]\}^{1/2}$

Table C.1 (cont'd)

	C.4	**C.5**	**C.6**
chemical formula	$C_{34}H_{58}BFeP_3$	$C_{53}H_{97}B_2Co_2OP_5Si$	$C_{44}H_{68}BCoN_4OP_2$
fw	626.37	1062.53	800.70
T (°C)	-173	-173	-173
λ (Å)	0.71073	0.71073	0.71073
a (Å)	13.226(2)	11.600(3)	9.865(3)
b (Å)	14.562(2)	12.827(3)	20.145(5)
c (Å)	18.857(3)	21.376(5)	11.087(3)
α (°)	90	95.195(4)	90
β (°)	98.641(3)	96.831(4)	105.036(4)
γ (°)	90	107.262(4)	90
V (Å^3)	3590.5(10)	2989.0(12)	2127.9(9)
space group	P2(1)/c	P-1	P2(1)
Z	5	3	2
D_{calc} (g/cm^3)	1.448	1.312	1.250
μ(cm^{-1})	7.18	6.15	5.17
R1, wR2[a] ($I > 2\sigma(I)$)	0.0923, 0.1837	0.1089, 0.1898	0.1000, 0.2467

[a] $R1 = \Sigma||F_o| - |F_c||/\Sigma|F_o|$, $wR2 = \{\Sigma[w(F_o^2 - F_c^2)^2]/\Sigma[w(F_o^2)^2]\}^{1/2}$

Table C.1 (cont'd)

	C.7
chemical formula	$C_{54}H_{106}B_2Fe_2OP_6$
fw	1090.53
T (°C)	-173
λ (Å)	0.71073
a (Å)	14.086(7)
b (Å)	14.948(7)
c (Å)	14.835(7)
α (°)	90
β (°)	103.090(7)°.
γ (°)	90
V (Å^3)	3042(2)
space group	P2(1)
Z	3
D_{calc} (g/cm^3)	1.786
μ(cm^{-1})	10.03
R1, wR2[a] ($I > 2\sigma(I)$)	0.1013, 0.1732

[a] $R1 = \Sigma||F_o| - |F_c||/\Sigma|F_o|$, $wR2 = \{\Sigma[w(F_o^2 - F_c^2)^2]/\Sigma[w(F_o^2)^2]\}^{1/2}$

[[Ph_2BP_2]Ru(=CHPh)Cl_2][^{n}Bu_4N] (**C.1**)- cmt13

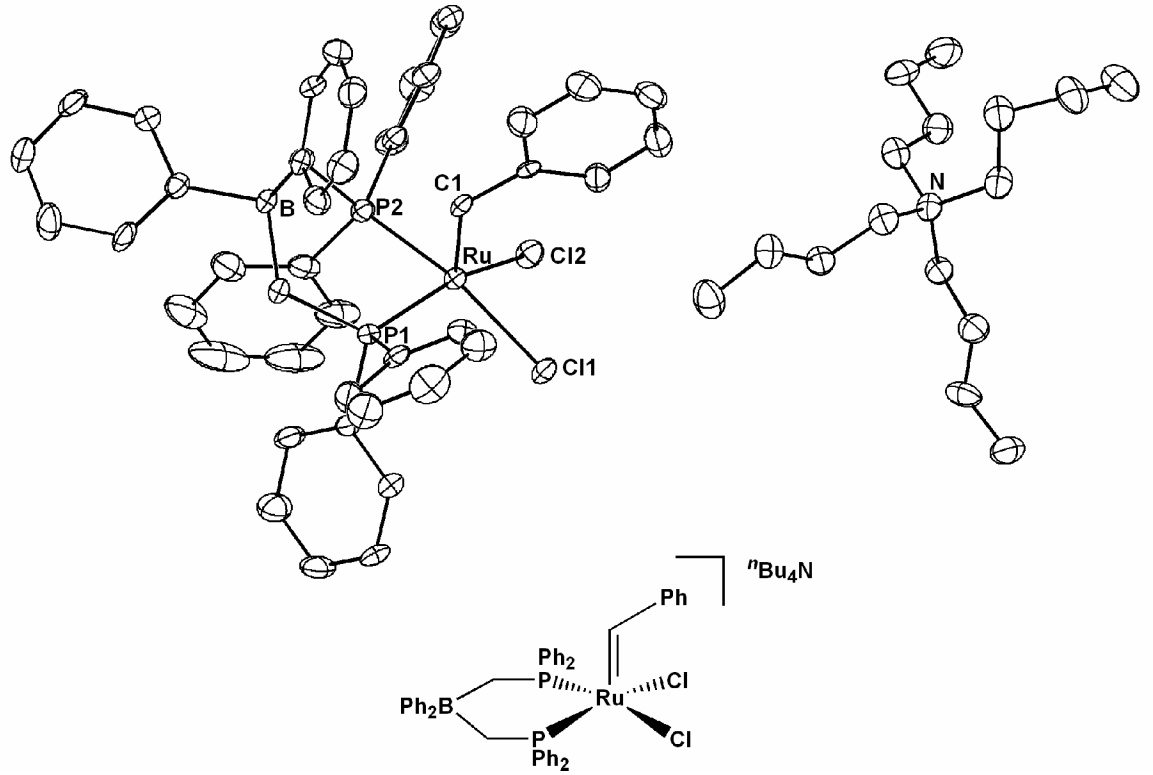

Relevant Interatomic Distances and Angles

Ru-C1	1.854(2) Å
Ru-P1	2.279(3) Å
Ru-P2	2.286(3) Å
Ru-Cl1	2.418(3) Å
Ru-Cl2	2.407(2) Å
Ru-B	4.024(2) Å
P2-Ru-P1	88.46°

[κ^2-PhB($CH_2P(^tBu)_2$)$_2$(CH_2S^tBu)]$FeCl_2$] (**C.2**)- cmt18

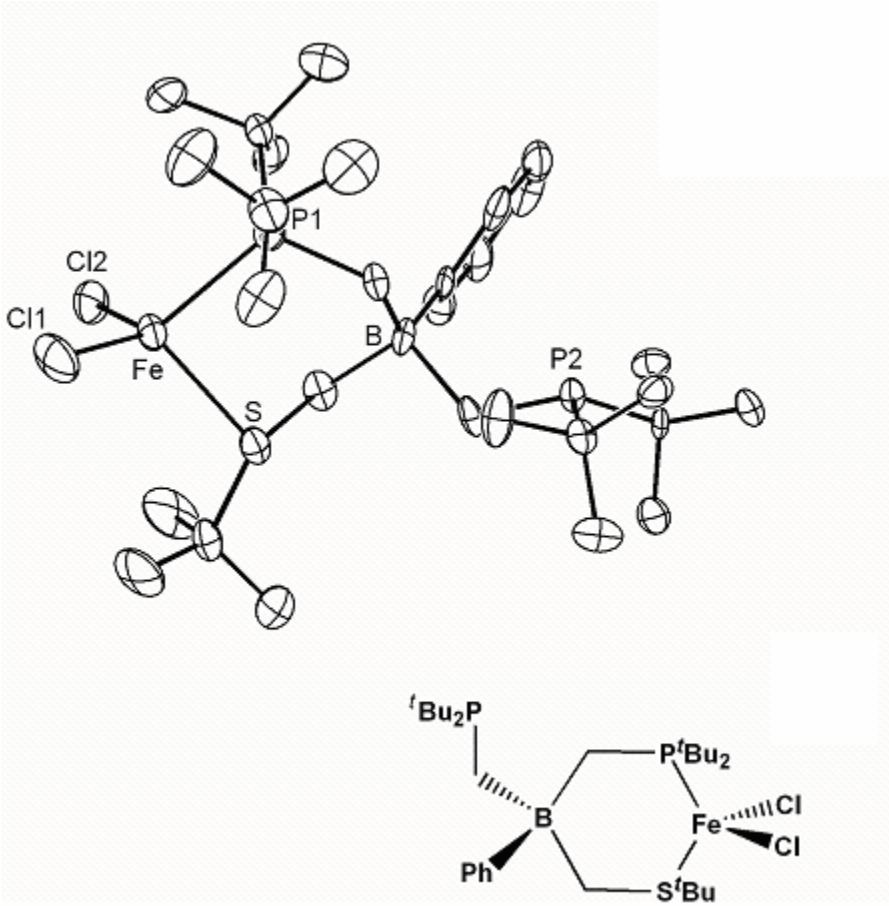

Relevant Interatomic Distances and Angles

Fe-S	2.419 Å
Fe-P1	2.461 Å
Fe-B	4.046 Å
Fe-Cl2	2.264 Å
Fe-Cl1	2.23 Å
P1-Fe-S	90.41°
Cl2-Fe-Cl1	113.65°

$[PhBP^{iPr}_3]Fe^{III}(N_2CMes_2)$ (**C.3**) – cmt22

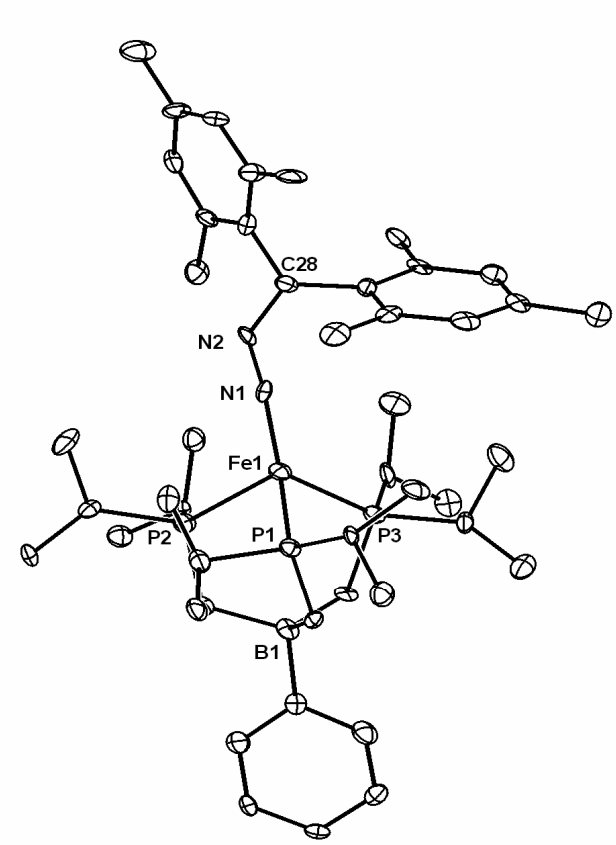

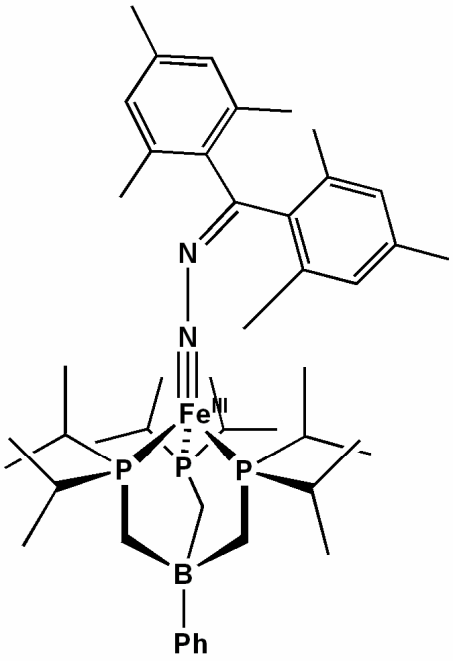

Relevant Interatomic Distances and Angles

C28-N2	1.331(2) Å
N2-N1	1.241 Å
N1-Fe1	1.751(1) Å
Fe1-P3	2.382 Å
Fe1-P1	2.421(2) Å
Fe1-P2	2.338(4) Å
Fe1-N1-N2	169.87(1)°
N1-N2-C28	131.67(1)°
P3-Fe1-P2	94.53(1)°
P2-Fe1-P1	94.85(1)°
P1-Fe1-P3	95.85(1)°

[PhBP$^{i\text{Pr}}_3$]Fe^{II}(C≡CPh) (**C.4**) – cmt24

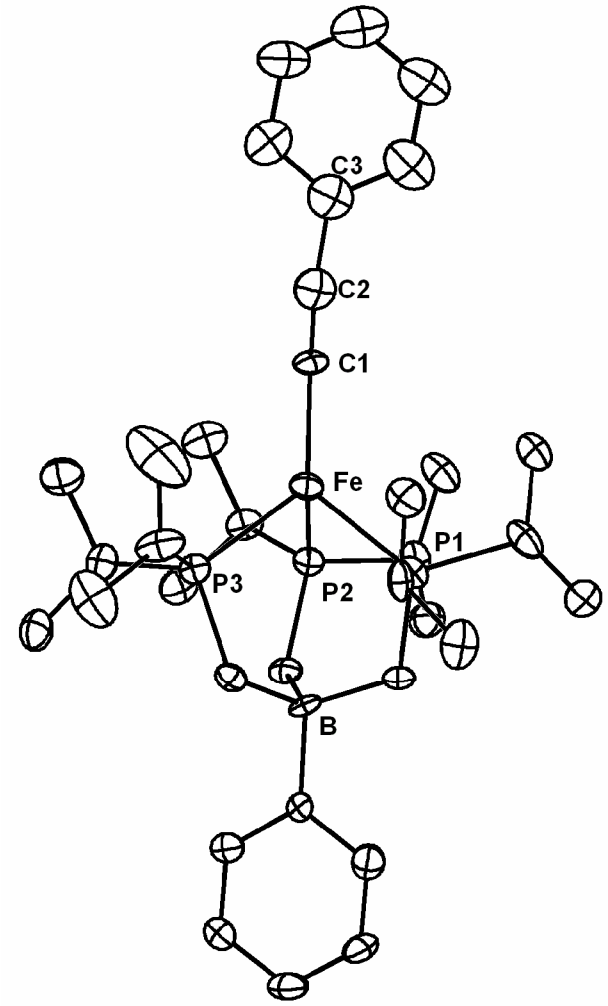

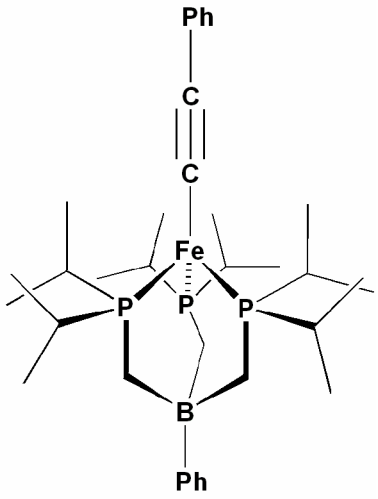

Relevant Interatomic Distances and Angles

Fe-C1	1.989(5) Å
C1-C2	1.184(8) Å
C2-C3	1.495(9) Å
P3-Fe	2.408(2) Å
Fe-P2	2.428(2) Å
P1-Fe	2.406(2) Å
Fe-C1-C2	177.73(42)
C1-C2-C3	170.63(58)
P3-Fe-P1	93.20(6)°
P1-Fe-P2	93.53(5)°
P2-Fe-P3	93.40(5)°

[PhBP$^{i\text{Pr}}_3$]Co-O-Co(SiPhH$_2$)(PhBP$^{i\text{Pr}}_2$) (**C.5**)– cmt32

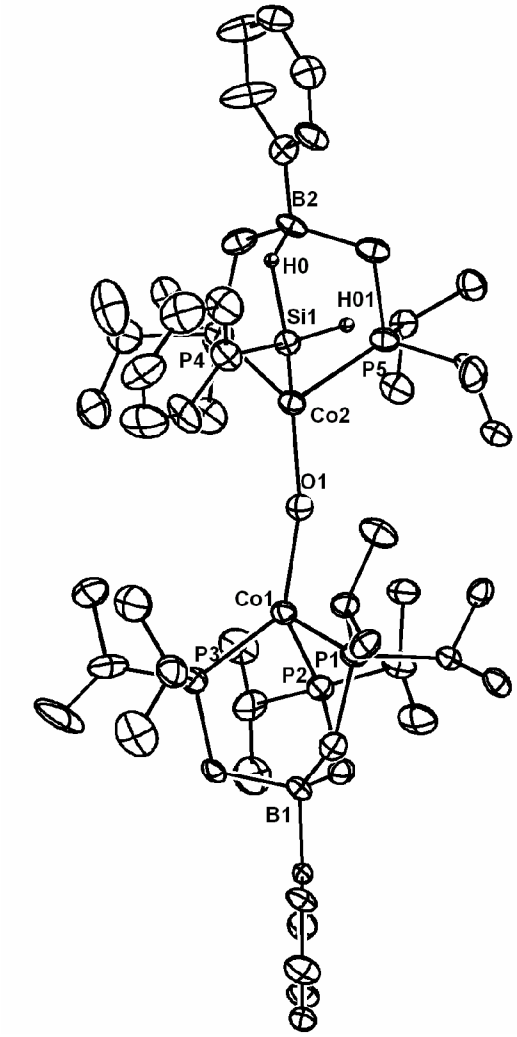

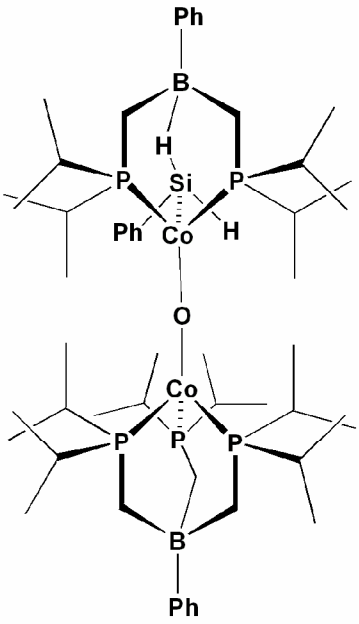

Relevant Interatomic Distances and Angles

Co1-P3	2.263(7) Å
Co1-P2	2.234(4) Å
Co1-P1	2.220(4) Å
Co1-O1	2.089(5) Å
O1-Co2	2.082(5) Å
Co2-Si1	2.203(3) Å
P4-Co2	2.223(3) Å
Co2-P5	2.211(7) Å
H0-B2	1.599(1) Å
H0-Si1	1.619(4) Å
Si1-H01	1.430(4) Å
Co2-O1-Co1	166.63(1)°

[PhBP$^{t\text{Bu}}_2$(pz)]Co(N_2CPh_2) (**C.6**)– cmt43

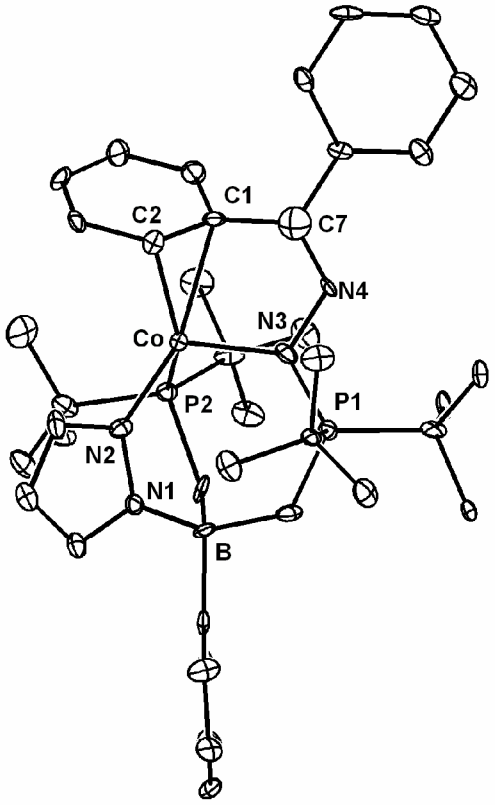

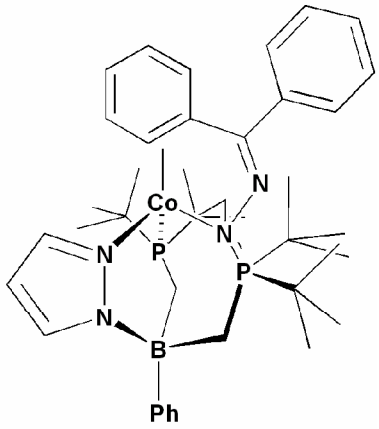

Relevant Interatomic Distances and Angles

Co-N2	1.996(1) Å
Co-P2	2.317(2) Å
Co-N3	1.997(5) Å
N3-N4	1.384(1) Å
C7-N4	1.295(1) Å
C1-Co	2.218(2) Å
C2-Co	2.030(3) Å
N3-N4-C7	115.84(2)°
C1-C7-N4	123.53(2)°
Co-N3-P1	128.66(1)°

{[PhBP$^{i\text{Pr}}_3$]Fe}(μ-O) (**C.7**) – cmt20

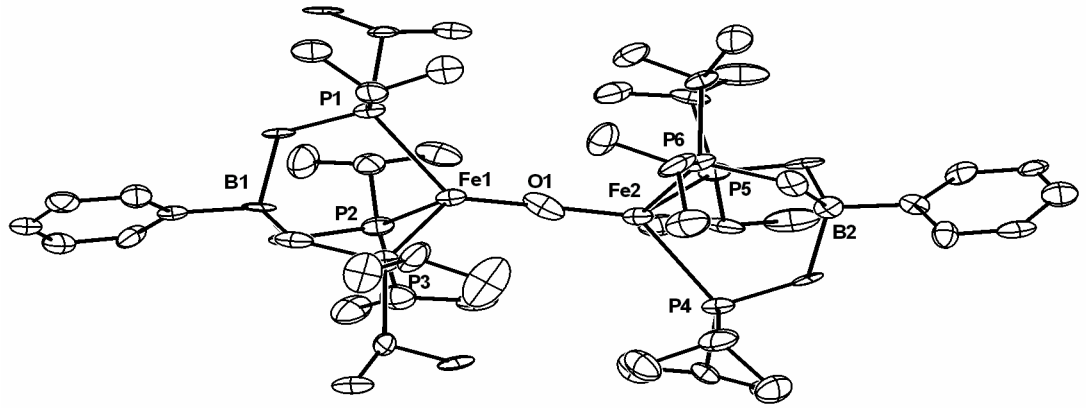

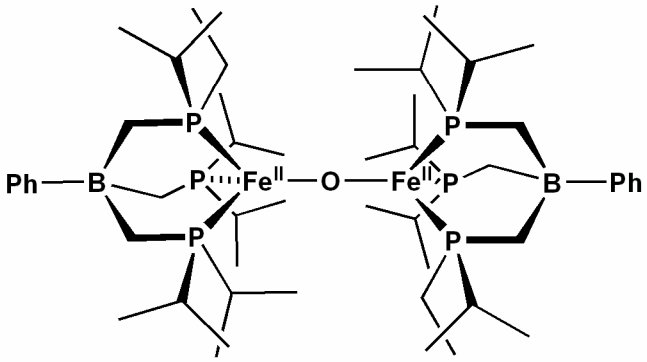

Relevant Interatomic Distances and Angles

Fe1-O1	1.764(9) Å
Fe2-O1	1.793(9) Å
Fe1-P1	2.518(4) Å
Fe1-P2	2.420(4) Å
Fe1-P3	2.448(3)Å
Fe2-P4	2.515(4) Å
Fe2-P5	2.457(3) Å
Fe2-P6	2.437(4) Å
Fe1-O1-Fe2	173.6(4)°